Mapping the therapy resistance landscapes of acute leukemias using *in vivo* functional genomics

by

Azucena Ramos

B.A., Chemistry and Neuroscience
Smith College, 2009

Submitted to the Department of Biology
in Partial Fulfillment of the Requirements for the Degree of

DOCTOR OF PHILOSOPHY

at the

MASSACHUSETTS INSTITUTE OF TECHNOLOGY

September 2020

Signature of Author: _____

Azucena Ramos
Department of Biology
June 8, 2020

Certified by: _____

Michael T. Hemann
Associate Professor of Biology
Thesis Supervisor

Accepted by: _____

Stephen P. Bell
Uncas and Helen Whitaker Professor of Biology
Investigator, Howard Hughes Medical Institute
Co-Director, Biology Graduate Committee

Mapping the therapy resistance landscapes of acute leukemias using *in vivo* functional genomics

by
Azucena Ramos

Submitted to the Department of Biology on June 8, 2020 in Partial Fulfillment of the Requirements for the Degree of Doctor of Philosophy in Biology

ABSTRACT

The recurrence of therapy resistant disease remains an intractable problem in oncology clinical care. To address this issue, investigators have traditionally focused on elucidating cell-intrinsic mechanisms that render tumors refractory to both classical chemotherapeutics and targeted agents. However, cancers resident in organs throughout the body do not develop in isolation. Instead, tumors arise in the context of the non-malignant components of a tissue, defined as the tumor microenvironement (TME). While the importance of cell-extrinsic factors in cancer biology is well established, our understanding of the TME's influence on therapeutic outcome is in its infancy. Pooled *in vivo* screens offer an unbiased strategy for identifying novel resistance mediators in the context of a normal immune system and microenvironment.

In the first part of this thesis, I describe the results of an *in vivo* RNAi screen in a treatment naïve mouse model of acute myeloid leukemia (AML) completed in the context of combination chemotherapy. Using this approach and a new mouse model of AML chemoresistance generated in our lab, I identified and validated the tricarboxylic acid cycle gene Succinate-CoA Ligase GDP-Forming Beta Subunit (*SUCLG2*) as an *in vivo*-specific mediator of therapy resistance. Additional experiments indicate that proper function of the Succinate-CoA Synthetase (SCS) complex, in which SUCLG2 functions, is critical for AML LSCs to survive therapy. Our data suggest that depletion of SCS members may lead to altered tumor energetic features that ultimately sensitize AML blasts to combination chemotherapy.

In the second part of my thesis, I describe a genome-wide CRISPR-Cas9 screen to investigate mechanisms of resistance to chimeric antigen receptor T cell therapy in a mouse model of B-cell acute lymphoblastic leukemia both *in vitro* and *in vivo*. Here, we describe preliminary results from an *in vivo* pilot screen and results from *in vitro* genome-wide screens. Preliminary analyses indicate the screen is robust, with genes previously reported to be important for T cell mediated killing showing expected phenotypes. Ultimately, completion of these screens will provide the field with a critically necessary data set that can guide efforts to uncover highly synergistic agents that potentiate the effects of this promising treatment modality.

Thesis Supervisor: Michael T. Hemann
Title: Associate Professor of Biology

BIOGRAPHICAL NOTE

Azucena Ramos

Education

2012 – 2022: MD, Harvard Medical School, Boston, MA
2014 – 2020: Ph.D. (Biology), Massachusetts Institute of Technology, Cambridge, MA
2005 – 2009: BA (Chemistry and Neuroscience), Smith College, Northampton, MA

Relevant research experience

2015 – 2020
Graduate Student, Hemann Lab, Massachusetts Institute of Technology
Completed *in vivo* screens using RNAi and CRISPR-Cas9 technologies to uncover novel mediators of resistance to frontline and immunotherapies in acute leukemia.

2013 – 2014
Pursuing Inquiry in Medicine (PIM) Student, Dr. Warf, Children's Hospital Boston
Investigated the developmental sequelae of two different neurosurgical approaches, shunting versus endoscopic third ventriculostomy with choroid plexus cauterization, in hydrocephalous patients.

2009 – 2012
Research Assistant, Camargo Lab, Harvard Stem Cell Institute
Developed a cellular barcoding system and novel paradigm for the study of hematopoietic stem cell dynamics in the adult mouse.

2008 – 2009
Thesis Student, Barresi Lab, Smith College
Studied the roles of Roundabout receptors 1 – 4 and their Slit ligands during post-optic commissure development in zebrafish.

Teaching experience

Fall 2019: Teaching Associate, Biological and Engineering principles Underlying Novel Biotherapeutics (7.371), MIT

- Chosen by Professors Harvey Lodish and Jianzhu Chen from a competitive pool of 12 postdoctoral fellows and graduate students
- I co-lead the course, along with Professors Harvey Lodish and Jianzhu Chen. I made curriculum decisions, chose topics to cover, and designed my own lectures and assignments for students.

Spring 2018 and 2019: Guest lecturer for Introduction to Experimental Biology & Communication (7.02/10.702) course, MIT

Spring 2017: Teaching Assistant, Introduction to Experimental Biology & Communication (7.02/10.702), MIT

Spring 2016: Teaching Assistant, Introduction to Biology (7.013), MIT

2007 – 2008: Master Tutor of Chemistry, Smith College

Awards

2020	Margaret A. Cunningham Immune Mechanisms of Cancer Research Fellowship, MIT
2019	MIT Graduate Women of Excellence, Leadership Award
2018 – 2022	F31 Individual Predoctoral M.D./Ph.D. Fellowship, Award # 1F31CA213902-01A1
2018	AACR Minority Scholar in Cancer Research Award
2017 – 2018	MIT School of Science Fellowship in Cancer Research Award
2014 – 2016	Paul and Daisy Soros Fellowship for New Americans
2008 – 2009	Beckman Scholar Award
2009	Highest Honors in Neuroscience for a Senior Thesis, Smith College
2009	Hause-Sheffer Memorial Prize for the best academic record in Chemistry, Smith College
2009	Cum Laude, Smith College
2009	Sigma Xi
2006 – 2009	First Group Scholar (top 5% of all students, academically), Smith College

Research articles

Christodoulou C, Spencer JA, Yeh SCA, Turcotte R, Kokkaliaris KD, Panero R, Ramos A, Guo G, Seyedhassantehrani N, Esipova TV, Vinogradov SA, Rudzinskas S, Zhang Y, Perkins AS, Orkin SH, Calogero RA, Schroeder T, Lin CP, Camargo FD. (2020) Live-animal imaging of native hematopoietic stem and progenitor cells. **Nature**, 578: 278-283

Wojtaszek JL*, Chatterjee N*, Najeeb J*, Ramos A, Lee M, Bian K, Xue Y, Li D, Hemann MT, Hong J, Walker GC, Zhou P. (2019) Small molecule adjuvant disrupting mutagenic translesion synthesis enhances chemotherapy. **Cell**, 178: 152-159

Fenouille N, Bassil CF, Ben-Sahra I, Benajiba L, Alexe G, Ramos A, Pikman Y, Conway AS, Burgess MR, Li Q, Luciano F, Auberger P, Galinsky I, DeAngelo DJ, Stone RM, Zhang Y, Perkins AS, Shannon K, Hemann MT, Puissant A, Stegmaier K. (2017) The creatine kinase pathway is a metabolic vulnerability in EVI1-positive acute myeloid leukemia. **Nat Med**, 23: 301-313

Pikman Y, Puissant A, Alexe G, Furman A, Chen LM, Frumm SM, Ross L, Fenouille N, Bassil CF, Lewis CA, Ramos A, Gould J, Stone RM, DeAngelo DJ, Galinsky I, Clish CB, Kung AL, Hemann MT, Vander Heiden MG, Banerji V, Stegmaier K. (2016) Targeting MTHFD2 in acute myeloid leukemia. **J Exp Med**, 213: 1285-1306

Lindblad O, Cordero E, Puissant A, Macaulay L, Ramos A, Kabir NN, Sun J, Vallon-Christersson J, Haraldsson K, Hemann MT, Borg Å, Levander F, Stegmaier K, Pietras K, Rönnstrand L, Kazi JU. (2016) Aberrant activation of the PI3K/mTOR pathway promotes resistance to sorafenib in AML. **Oncogene**, 35: 5119-5131

Sun J, Ramos A, Chapman B, Johnnidis JB, Le L, Ho YJ, Klein A, Hofmann O, Camargo F. (2014) Clonal dynamics of native haematopoiesis. **Nature**, 514: 322-327

Reviews and commentaries

Ramos A and Hemann MT. (2017) Drugs, Bugs, and Cancer: *Fusobacterium nucleatum* Promotes Chemoresistance in Colorectal Cancer. **Cell**, 170: 411–413

Ramos A and Camargo F. (2012) The Hippo signaling pathway and stem cell biology. **Trends Cell Biol**, 22: 339-346

Presentations

Poster	Using *In vivo* genome-wide screens to understand mechanisms of resistance to Chimeric Antigen Receptor T-cell (CAR-T) therapy, Co-presented with Catherine Koch and Yunpeng Liu, Koch Institute Annual Fall Retreat, North Falmouth, MA, November 14, 2019
Talk	Suclg2 is a novel mediator of resistance in AML, Koch Institute Annual Fall Retreat, North Falmouth, MA, October 29, 2018
Poster	Suclg2 is a novel mediator of resistance in AML, MD-PhD Annual Retreat, South Yarmouth, MA, September 30, 2018
Poster	Uncovering novel mechanisms of resistance in AML using integrative functional genomics, AACR Annual Meeting, Chicago, IL, April 16, 2018
Poster	Uncovering novel mechanisms of resistance in AML using integrative functional genomics, Koch Institute Annual Fall Retreat, North Falmouth, MA, November 6, 2017
Poster	Investigating mechanisms of therapy resistance in AML using *in vivo* screens, Koch Institute Annual Fall Retreat, North Falmouth, MA, October 6, 2016

ACKNOWLEDGEMENTS

Para mi madre, mi abuela, y mi familia que me dieron todo el amor del mundo, mis raízes, y las alas para volar.

First and foremost, this thesis is dedicated to all of the strong and trailblazing women in my life who have helped shape me into the person I am today. To my wita (my grandmother), mom, and aunts (especially my Tia Lucy) who immigrated to the U.S. so that my generation could have a better life, thank you. You left everything you knew behind, sacrificing your own dreams and aspirations in the hopes that moving to this country would afford our family greater opportunities than those our little rancho could ever allow. I hope you find that promise at least partially realized in my work. This Ph.D. would have been impossible without you and your sacrifices, and I am forever grateful to you all. To my sisters, biological (Lita, Lala, Kika) and chosen (PB, Albara, Norma, CeeCee, Jenn, Layla, Lauren, Rosie, Tova, Hannah, Kate, Christina, and Karin), thank you for all of your support and pep talks throughout this entire process. Our conversations, laughs (on Marco Polo, especially), cries, and vacations together kept me sane and grounded, especially after hard days in the lab. I deeply love and appreciate you all. To Ms. Rachel Bronwyn, my high school AVID and honors English teacher who opened up a whole new educational world for me and empowered me to dream bigger than I could have ever imagined, thank you. I know that teaching at a high poverty school with high failure rates like Orange Glen can't be easy. Your strength and commitment to educational equity has always left me in awe and I often wonder if you are even capable of thinking about anything outside of your students' needs. Please know that your mentorship and support has made all the difference in my life. I am certain that without your help, I would not be where I am today.

This thesis is also dedicated to my husband, Giovany. Gio, thank you for all of your patience, love, and support. These last few years have encompassed of some of our highest highs and also, some of our lowest lows as a couple. But we always seem to come out on the other side stronger and more committed to each other than before. You are the perfect teammate. I love you and can't imagine a better life partner. You are truly the best part of me and the example you set, just by being you, makes me want to be a better person. Thank you for all that you do for me and our family. This Ph.D. is as much mine as it is yours. Te adoro mi amor.

I'd like to thank my advisor Michael Hemann. Mike, you have been a constant support throughout this entire process, always letting me have the freedom to explore my own ideas and projects, even when they seem impossible or overly difficult. Your trust in my scientific instincts has fostered a sense of confidence that I will carry with me for the rest of my career. Beyond your scientific mentorship however, I'd like to thank you for always treating me with respect and kindness. You always made me feel like I was more than just your grad student. By taking the time to get to know me on a deeply personal level and by spending time with my family, it always felt like you were invested in me as a whole person and for that, I can't thank you enough. Thank you for empowering me to bring all of myself to the lab. And thank you for making our lab feel more like a family than anything else. Many grad students told me that by the end of my Ph.D., I should expect to dislike my dissertation advisor. On the contrary, at the end of this process I find myself wanting to spend more time in lab and in your office, chatting about weird science (like squids with fluorescent bacteria in their guts), funny pranks (credit to Kate Koch for some of the best ideas), and future project/company ideas. Thank you for a fantastic experience. I will miss you and the lab deeply.

I'd also like to thank our collaborator Kim Stegmaier and her lab. I have learned a lot from Kim's approach to science and I am grateful to her and her group for their willingness to share their resources and expertise in support of our joint AML projects. I am also grateful to all of my other scientific collaborators for the stimulating conversations and productive scientific interactions I've had the pleasure of sharing with you all. This Includes folks in the Birnbaum lab (Tayeoon), the Vander Heiden lab (Zhaoqi, Peggy, Ahmed, and Keene), the Koehler lab (Becky), the Amon lab (Jette), the Maus lab, and the Walker lab.

I am grateful to Tyler jacks, Jackie Lees, and Ömer Yilmaz, who have taken the time to serve on my thesis committee. In addition to their thoughtful contributions and suggestions during our discussions of my research, Tyler, Jackie and Ömer have also given me great advice and perspective on the scientific training road ahead. I am grateful for all of their support and input, which has undoubtedly improved my research and contributed to my development as a scientist. I also thank Ben Ebert for serving as the outside member of my thesis defense committee. Thank you all for your time and effort. I truly appreciate it.

I would also like to thank all of the wonderful scientists at MIT who have spent time mentoring me more informally. I would especially like to thank Harvey Lodish and Hojun Li who have been so supportive and always willing to help me think through everything from career decisions, issues with my research, and general life things that have popped up. Also, you both seem to have a keen sixth sense about when I am feeling the most unsure or insecure. Your encouraging emails and kind words always seem to come right when I need them and they always make my day. Thank you for your time and effort. You have no idea how much it means to me to feel like I have such close mentors and friends at MIT.

I'd also like to thank Jianzhu Chen, Alan Grossman, Matt Vander Heiden, and Michael Birnbaum. I will forever think back fondly on the offline conversations that I was lucky enough to have with each of you. With Jianzhu, conversations about his experience raising children or about CAR-T cells and collaborations; with Alan Grossman, chats about racial and gender equity gaps in academia and what we at MIT can do to address this issue; with Matt Vander Heiden, random, unplanned chats about the TCA cycle and mtGTP; and with Michael Birnbaum, conversations about how difficult it can be when you feel like you have to succeed on behalf of your entire family. Thank you all for making me feel welcomed and supported at MIT.

I am thankful for Kate Koch and Yunpeng Liu, my closest friends and collaborators in the Hemann lab. You two have become so much more to me than I could ever express in words. You are truly my family. In our conversations, I find solace, peace, and joy. I know that no matter what any of us is going through, you both will always be there. It has been so comforting to know that I can always count on you two to listen, to help me talk things out (scientific or otherwise), to make me laugh when I need it, and to remind me to love and take care of myself when I am feeling particularly down. Some of my fondest memories from grad school have been formed with you two: our trip to AACR (shout out to Hannah and Jason too!), our late night pranks on Mike, our crazy clandestine social events (TT & HONG KONG!!), our late night (and technically illegal) pizza consumption, and the endless hours we spent together completing our crazy joint endeavors. It has been an absolute honor to be able to work with such brilliant and hard-working people. In some near future, I imagine us all living near each other and our kids growing up together because at this point, it's SKY team for life.

To my technician Riley, thank you for all of the hard work you're always willing to put in for the team. You are so smart and so talented that I often wonder how you can be so humble. (It must be that Midwest thing.) Your humility and kindness make me so proud to call you my friend, and your indefatigable work ethic and ability to pick things up quickly has made you indispensable in lab. I have no doubt that you will go far in medicine, science, and life. You are a rare kind of person and it was been an absolute pleasure to work with you.

I am grateful to the rest of the Hemann lab, new and old, for always being willing to discuss science with me and for all of the great moments we've shared together. In particular, I'd like to thank James, Julia, Faye, Peter, Bo, and Christian for all of their help, pep talks, and unwavering support throughout this process. I will always remember our precision drinking games, our Friday hang outs in the nook/lab, and our late night conversations about everything from generational wealth, our favorite podcasts, and iron monks, to our frustrations in lab, our dreams for our careers, and the random bits of fascinating science we'd found that week. Thank you all for making the lab feel fun, welcoming, and intellectually stimulating. Also, special thanks to Julia, Ayantu, and Dan for providing feedback on parts of my thesis. I truly appreciate the time and effort you spent looking over my writing.

I'd like to thank all of the friends and family that I have not had the space to mention yet. This includes Sergio, Black Alex, Big Alex, Elsa, Erik, Eileen, Monica, Jaime, Max and Ally, Victor and Diana Rodriguez, Diana Lu, Sana, Kenton, Juan, Oscar, Patricia, Peter K., Mr. and Mrs. Sloan, Mr. and Mrs. Clarke, Melanie, Audra, and Jamila (just to name a few) for their unwavering support. I love and cherish you all.

Lastly, I'd like to thank my mentor Fidencio Saldaña for always reminding me that the world is full of hope and possibility, and for empowering me to feel like I can do anything I set my mind to. I often wonder how Fidencio has enough time in the day to be a brilliant cardiologist, a deeply empathetic and effective mentor to many of us POC in medicine, and a kickass Dean of Students at HMS, all while taking care of his own family. I imagine he does not sleep enough. Thank you for all that you do.

TABLE OF CONTENTS

TITLE PAGE 1

ABSTRACT 3

BIOGRAPHICAL NOTE 4

ACKNOWLEDGEMENTS 7

TABLE OF CONTENTS 9

CHAPTER ONE: Introduction 10
References 89

CHAPTER TWO: A targeted *in vivo* RNAi screen identifies Suclg2 as a novel mediator of resistance in acute myeloid leukemia 109
References 169

CHAPTER THREE: Investigating *in vivo* mechanisms of resistance to chimeric antigen receptor T (CAR-T) cells using genome-wide CRISPR-Cas9 genetic screens 174
References 229

CHAPTER FOUR: Discussion and future directions 231
References 254

CHAPTER 1—Introduction

The last 100 years have witnessed a radical change in the way cancer, an affliction known to humanity for thousands of years, is understood, studied and treated. Groundbreaking discoveries that came about in the 20th century firmly established cancer as a disease of the genome, driven by chromosomal abnormalities (Boveri, 2008) and inherited and somatic mutations (Stehelin et al., 1976; Tabin et al., 1982). Accordingly, the emphasis of modern cancer research has largely centered on the characterization of malignant cells with little regard for the non-transformed tissues on which they expand. The advent of massively parallel sequencing technologies significantly facilitated this cell-autonomous approach to cancer biology, allowing us to gain unprecedented insight into the molecular processes governing oncogenesis (Ding et al., 2018). Despite a dramatic increase in our knowledge of genes that are mutated, amplified or deleted in many malignancies, our understanding of how these changes conspire to orchestrate various aspects of tumor biology is still preliminary, especially as it relates to treatment failure. As such, many cancer patients ultimately relapse even after treatment with the most successful regimens (Inaba et al., 2013; Roschewski et al., 2014; Paul et al., 2016; Döhner et al., 2015). Relapse driven by therapy resistant cells that persist in the body after treatment is the principal source of fatality in cancer patients today, with over 50,000 patients dying from treatment refractory hematopoietic tumors each year in the United States alone (Borst, 2012; Wu et al., 2017; Siegel et al., 2020). This fact underlies the motivation for my work in this thesis.

Today, human carcinogenesis is known to be a multistep process in which normal cells progressively acquire discrete genetic and epigenetic alterations as they are transformed from normal cells into malignant tumors (Hanahan and Weinberg, 2011). This complex process however, occurs in the context of a whole organism where normal environmental factors can be recruited to either hamper or aid in the malignant progression of a tumor cell. These factors include a range of players, from an intact immune system and stromal fibroblasts to a sophisticated series of whole body metabolic reactions and organ site-specific nutrient repertoires. Jointly, these normal cellular and non-cellular factors are defined as the tumor microenvironment (TME). Classic experiments performed by Mintz and Illmensee demonstrated the power of tissue context to modify a cancer cell's malignant potential (Mintz & Illmensee, 1975). Here, injection of teratocarcinoma cells into mouse blastocysts suppressed the tumorigenicity of this cancer, allowing these malignant cells to contribute to various functional

tissues in cancer-free adult mice. A similar example was later discovered in chickens, where the highly oncogenic Rous sarcoma virus (RSV) potently transformed cells into aggressive tumors in chickens but failed to do so when injected into developing chick embryos, even though v-Src (the oncogene responsible for RSV-based transformation) was both expressed and active (Dolberg & Bissell, 1984). On the other end of the spectrum, microenvironmental factors have also been shown to promote the emergence of cancerous cells. The observation that tumors preferentially emerged at the site of RSV injection in RSV-infected chickens led to the discovery that TGF-β release at the wound site was pro-tumorigenic (Sieweke et al., 1990). In mice, the expression of an activating mutation of β-catenin in osteoblasts, not in hematopoietic stem cells (HSCs), induced the development of AML (Kode et al., 2014; Kode et al., 2016). Similarly, deletion of the TGF-β receptor in stromal cells results in lethally aggressive malignancies that arise from the prostate and forestomach epithelium (Bhowmick et al., 2004). In humans, chronic inflammation caused by pathogens like *Helicobacter pylori* or autoimmune diseases like ulcerative colitis and Crohn's disease, is a major risk factor for the development of intestinal tumors (Ungaro et al., 2017; Torres et al., 2017; Alfarouk et al., 2019). The examples described here constitute only a small subset of such studies, illustrating that as in healthy organs, the TME is now appreciated as having significant regulatory functions in tumorigenesis (Klemm & Joyce, 2015; Fiedler & Hemann, 2009).

While the importance of cell-extrinsic factors in cancer initiation and progression, including contributions from the TME, is well established, our understanding of the TME's influence on therapeutic outcome is in its infancy. The goal of my research has been to further explore TME-mediated mechanisms of resistance to various treatment modalities in acute leukemias. Using mouse models of acute myeloid and B-cell acute lymphoblastic leukemias (AML and B-ALL, respectively), and a functional genomics approach, we examined the mechanisms by which acute leukemias become resistant frontline and immunotherapies. Critical to our approach was the examination of these therapeutic responses in an *in vivo* setting, in the context of an intact immune system and microenvironment. In this thesis, I describe the results of two such *in vivo* screens. First, I describe the results of a targeted RNAi screen revealing the citric acid cycle protein SCS-G as an *in vivo* specific mediator of resistance to frontline combination chemotherapy in MLL-rearranged acute myeloid leukemia (AML). Second, I describe our efforts to establish parallel genome-wide *in vitro* and *in vivo* CRISPR-Cas9 screens for chimeric antigen receptor T (CAR-T) cell therapy resistance in a BCR-ABL+ mouse model of precursor B-cell acute lymphoblastic leukemia (B-ALL) and discuss the results from both the *in*

vitro arm of the study and the preliminary pilot screen completed *in vivo*. To put these results into context, I first provide relevant background on both AML and B-ALL, including current treatment strategies and known mechanisms of resistance in these diseases. Embedded in these individual sections, I describe the successes, failures, and challenges of examining resistance to frontline therapy in AML and to CAR-T therapy by sequencing and examining human tumor samples. Finally, I review the arguably much more powerful approach of studying tumorigenesis, including mechanisms of therapeutic resistance, in *in vivo* settings using functional genetic screening. Here, I focus more extensively on the results of targeted mutational techniques while still providing a brief overview of the genetic toolkit available to biologists today.

Part I: Acute leukemias

Normal hematopoiesis requires an exquisite balance between self-renewal and differentiation of hematopoietic stem cells (HSCs) to successfully generate the full repertoire of mature peripheral blood cells for the duration of an organism's lifetime (Figure 1.1). In acute leukemia, a series of mutational events occurring in early HSCs or progenitor cells (HSPCs) gives rise to leukemic blast cells that exhibit uncontrolled proliferation but are unable to terminally differentiate. This results in the rapid clonal outgrowth of an immature, non-functional population of precursor cells that replace the bone marrow (BM) pulp, leading to hematopoietic insufficiency after healthy progenitors are depleted. Ultimately, leukemic blasts spill out of the marrow into the periphery, accumulating in the spleen, lymph nodes, blood, and other organs (Arber et al., 2016). Clinically, the diagnosis of acute leukemia can be made when blast forms account for more than 20% of all cells in the BM or peripheral blood, or in some cases, if specific genetic abnormalities known to occur in acute leukemia subtypes are detected (Horton et al., 2019; Schiffer & Gurbuxani, 2019).

The first step in the categorization of acute leukemias is to assign a lineage based on the resemblance of blast cells to normal progenitor cells (Appelbaum, 2020). This is primarily accomplished by examining surface expression of lineage markers on blasts using flow cytometry (FC), but can also involve immunohistochemistry (IHC) and enzyme cytochemistry (EC). This initial description is useful for monitoring the leukemia as patients undergo treatment, provides preliminary hints about the pathways that may be involved in disease pathogenesis, and can be helpful in determining the most effective therapeutic approach. Although they encompass a heterogeneous range of hematopoietic malignancies, acute leukemias can be subdivided into 3 main lineages: myeloid (AML), B cell lymphoblastic (B-ALL), and T cell

lymphoblastic (T-ALL). Rarely, malignancies displaying multilineage protein expression on individual blasts or those exhibiting of an admixture of discrete myeloid and lymphoid populations (mixed-phenotype acute leukemias or MPALs) can also arise, accounting for 2-5% of all acute leukemias (Charles Boyer, 2017). Here, I briefly review the biology of AML and ALL, focusing most heavily on MLL-rearranged AML and BCR-ABL+ B-cell acute lymphoblastic leukemia (B-ALL).

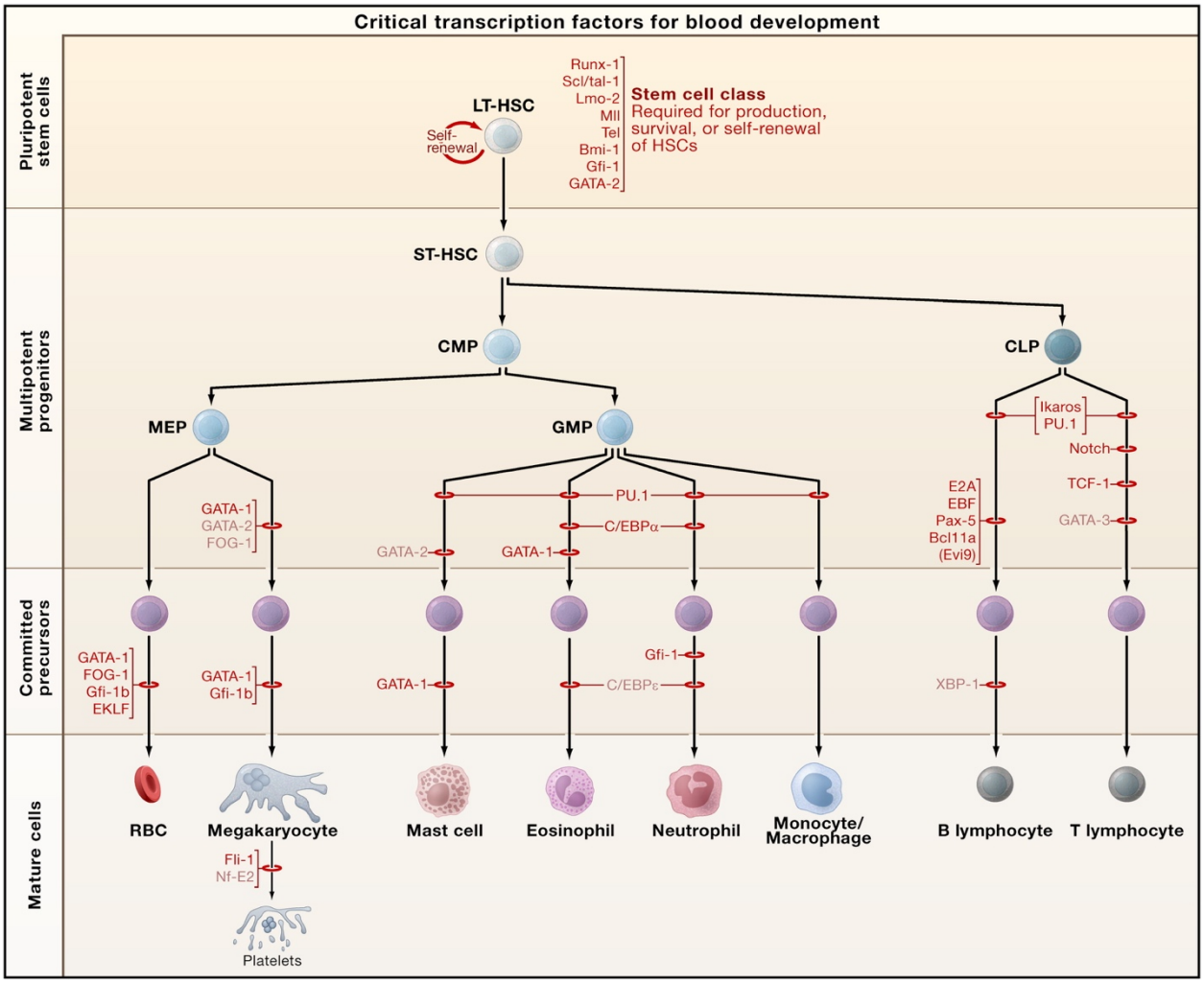

Figure 1.1. Critical transcription factors in hematopoiesis. The stages at which hematopoietic development is blocked in the absence of a given transcription factor, as determined through conventional gene knockouts, are indicated by red bars. The factors depicted in black have been associated with oncogenesis. Those factors in light font have not yet been found translocated or mutated in human/mouse hematologic malignancies. Abbreviations: LT-HSC, long-term hematopoietic stem cell; ST-HSC, short-term hematopoietic stem cell; CMP, common myeloid progenitor; CLP, common lymphoid progenitor; MEP, megakaryocyte/erythroid progenitor; GMP, granulocyte/macrophage progenitor; RBCs, red blood cells.
Reprinted from Cell, 132, Orkin, S. H. & Zon, L. I. Hematopoiesis: An Evolving Paradigm for Stem Cell Biology, 631–644, 2008, with permission from Elsevier.

1. Acute myeloid leukemias

1.1. Epidemiology of AML

AML, the most common acute leukemia in adults, is a highly heterogeneous collection of aggressive blood cancers driven by the uncontrolled growth of poorly differentiated myeloid progenitor cells. In the United States, approximately 21,000 people are diagnosed with AML and over 10,000 deaths due to AML are reported annually, accounting for 1.2% of all new cancer cases but 1.8% of all cancer related deaths (Siegel et al., 2020; SEER, 2020a). The incidence of AML increases with age, growing from 2 cases per 100,000 population before the age of 65, to 20 cases per 100,000 population after the age of 65, while the median age at diagnosis is approximately 68 (Döhner et al., 2015). Thus, while AML can arise at any age, it is largely a disease of the elderly.

1.2. Disease characteristics and classification in AML

Morphologically, AML blasts vary in size from approximately 6-18μm and have a high nuclear-to-cytoplasmic ratio. They express surface proteins that are also found on normal immature myeloid cells, including cluster of differentiation (CD) markers CD13, CD33, and CD34. The remainder of the surface phenotype depends on the specific lineage subtype and degree of blast differentiation, such as monocyte differentiation proteins (CD14, CD11b, CD4), megakaryocyte (CD41a, CD61), and erythrocyte markers (CD36, CD71). Occasionally, AML blasts will also express lymphocyte-specific surface proteins such as CD19, CD7, Terminal deoxynucleotidyl transferase (TdT), and human leukocyte antigen-DR (HLA-DR).

Subtypes of AML are classified using the World Health Organization (WHO) system, which relies on blast morphology, karyotype, immunophenotype, molecular features, and clinical presentation to define six major disease entities in AML: AML with recurrent genetic abnormalities; AML with myelodysplasia-related changes (without a history of prior cytotoxic therapy exposure); therapy-related myeloid neoplasms; AML, not otherwise specified, which does not meet the criteria for the categories described above; myeloid sarcoma; and myeloid proliferation related to Down Syndrome (Table 1.1) (Arber et al., 2016). Among the WHO criteria used to categorize AML cases, genetic lesions continue to constitute the strongest prognostic factors for AML survivability (De Kouchkovsky & Abdul-Hay, 2016; Döhner et al., 2015). Accordingly, AML cases can be further stratified by prognostic impact into favorable, intermediate, or adverse risk groups (also summarized in Table 1.1) (Döhner et al., 2017).

Table 1.2. Summary of the six AML subtypes defined by the World Health Organization (WHO) stratified by risk according to the European LeukemiaNet guidelines (where available). Adapted from data in both Arber et al., 2016 and Döhner et al., 2017.

Classification	Genetic Abnormality/Phenotype	Risk
Recurrent Genetic Abnormalities	t(8;21)(q22;q22.1);RUNX1-RUNX1T1	Favorable
	inv(16)(p13.1q22) or t(16;16)(p13.1;q22);CBFB-MYH11	Favorable
	PML-RARA	Favorable
	t(9;11)(p21.3;q23.3);MLLT3-KMT2A	Adverse
	t(6;9)(p23;q34.1);DEK-NUP214	Adverse
	inv(3)(q21.3q26.2) or t(3;3)(q21.3;q26.2); GATA2, MECOM	Adverse
	Megakaryoblastic AML with t(1;22)(p13.3;q13.3);RBM15-MKL1	Intermediate
	Provisional entity: BCR-ABL1	Adverse
	Mutated NPM1	Favorable
	Biallelic mutations of CEBPA	Favorable
	Provisional entity: Mutated RUNX1	Adverse
Myelodysplasia-related changes		Adverse
Therapy-related myeloid neoplasms		Adverse
Not Otherwise Specified	Minimal differentiation	Mixed
	Without maturation	
	With maturation	
	Acute myelomonocytic leukemia	
	Acute monoblastic/monocytic leukemia	
	Pure erythroid leukemia	
	Acute megakaryoblastic leukemia	
	Acute basophilic leukemia	
	Acute panmyelosis with myelofibrosis	
Myeloid sarcoma		
Myeloid proliferations related to Down syndrome	Transient abnormal myelopoiesis (TAM)	
	Myeloid leukemia associated with Down syndrome	

1.3. Pathobiology of AML

In normal hematopoiesis, growth signals control proliferation while transcription factors (TFs) function as intrinsic determinants of cellular identity by activating genetic programs that ultimately push cells to terminally differentiate into cells of a particular lineage (reviewed in Orkin & Zon, 2008). A remarkable feature of the regulatory growth factors and TFs in the blood system is that the majority are involved in chromosomal translocations or somatic mutations in human hematopoietic cancers (Figure 1.1). For example, germ line inheritance of mutations in the myeloid TF genes *RUNX1*, *GATA2,* and *CEBPA* lead to autosomal dominant, familial predispositions to AML that are well described in the literature (reviewed in Sood et al., 2017; Crispino & Horwitz, 2017; Tawana et al., 2017; Churpek & Bresnick, 2019) and are now outlined

in the 2016 WHO classification guidelines for AML (Arber et al., 2016). Further, experimental evidence in mice has shown that manipulation of the genes encoding these factors often promotes the emergence of malignancies. Hence, the origin of leukemia is intimately linked to hematopoietic cell fate.

1.3.1. The two-hit model of leukemogenesis

The aforementioned studies in animal models led to the proposal of the two-hit model of leukemogenesis by Gilliland and Griffin (Gilliland & Griffin, 2002). This model postulates that genetic lesions that increase proliferation (class I mutations) must occur with mutations that impair normal hematopoietic differentiation and apoptosis (class II mutations) in order for AML to develop. Class I mutations commonly affect members of signal transduction pathways, involving mutations in NRAS, KRAS, c-KIT, PTPN11, and FLT3 tyrosine kinase domain mutations (TKD) or internal tandem duplications (ITD). Mutations within this class are often identified in subclonal populations, indicating that they occur late in disease evolution, arising after class II mutations (Papaemmanuil et al., 2016). Class II mutations are thought to be the initiating lesions in AML and primarily affect transcription factors. Examples of class II mutations include PML/RARα and RUNX1 rearrangements, and mutations in genes encoding other master myeloid TFs such as *CEBPA* and *GATA2*. However, the acquisition of mutations in AML doesn't always follow a strict order and examples of 'early' mutations lost at relapse and 'late' mutations that are acquired first have been described in human studies comparing matched primary tumors (Krönke et al. 2013; Shlush et al., 2014; Anderson et al. 2011). Recently, sequencing studies in human tumor samples identified mutations in epigenetic modifiers such as *TET2*, *IDH1*/2, and *DNMT3A* that impinge on both proliferation and differentiation (Delhommeau et al., 2009; Mardis et al., 2009; Ley et al., 2010; Shih et al., 2012). Additionally, rearrangements involving the histone methyl transferase gene *MLL1* located on chromosome 11q23 had long been appreciated. Although they do not neatly fit into one of the two classes described above, these mutations are thought to synergistically induce the same effects. This model has proven to be a useful framework for conceptualizing the pathogenesis of AML. However the identification and validation of driver mutations and the additional genetic changes that cooperate with those lesions to induce AML is an active area of research.

1.4. The leukemia cell of origin (LCO) in AML

Arguably as important as determining the genetic lesions that lead to transformation is the identification of the cell type in which those changes occurred to initiate leukemia, otherwise known as the leukemia cell of origin (LCO). Mounting evidence suggests that the cellular context in which mutations arise can contribute to the emergence of distinct tumor subtypes with unique biological and clinical behavior (Thomas & Majeti, 2017; Visvader et al., 2011). Indeed, the discovery that expression signatures resembling those found in normal HSCs are associated with adverse outcomes in human AML suggests that transcriptional programs specified during normal blood development can have a profound impact on clinical outcomes in AML patients (Eppert et al., 2011; Gentles et al., 2010; Valk et al., 2004). It is important to note that the LCO refers to the normal hematopoietic cell that acquires the first cancer-promoting lesion(s) and should not be confused with leukemia stem cells (LSCs, also known as leukemia initiating cells or LICs). LSCs constitute a specific subset of cells within the leukemia that sustain malignant growth through their unlimited potential for self-renewal and are functionally able to initiate leukemia when transplanted into immunodeficient mice (reviewed in Thomas & Majeti, 2017). Thus, LSCs and LCOs are closely related, but are not identical.

1.4.1. Examining the AML LCO in mouse models

A number of human and mouse studies have examined the LCO in AML. Mouse studies have traditionally employed the use of retroviral oncogene transduction and knock-in models to investigate this question and have generally concluded that both HSCs and more committed progenitor cells can serve as cellular targets of transformation. In one such study, the oncogene MN-1 was shown to induce AML when it was used to transduce common myeloid progenitors (CMP), but not the more differentiated granulocyte-macrophage progenitor (GMP) or HSCs. This suggests that there is a tight developmental window in which MN-1 can transform cells (Heuser et al., 2011). Conversely, studies using the MLL-AF9, MLL-ENL, and MOZ-TIF2 fusion proteins all induced AML irrespective of the cell type being transduced, and MLL-AF9 was shown to reactivate a self-renewal program in more differentiated cells during leukemogensis (Krivtsov et al., 2006; Drynan et al., 2005; Cozzio et al., 2003; Huntly et al., 2004). In a follow up study again using a retroviral mouse model of MLL-AF9, Krivtsov and colleagues provided direct evidence that the cell of origin influenced the gene expression program, epigenetic landscape and drug response of the resulting leukemia and LSCs (Krivtsov et al., 2013). Here, LSCs derived from either HSCs or GMPs had identical immunophenotypes but HSC-induced AMLs expressed a

more extensive stem cell-derived transcriptional program, were significantly more aggressive *in vivo*, and were less sensitive to frontline chemotherapy. However, as with any contrived experimental system, models derived from retroviral oncogene transduction appear to have limitations—especially when it comes to oncogene dosage expressed in the resulting leukemia. The importance of utilizing models with genetic lesions that more closely approximate those seen in the human disease was exemplified when the expression of MLL-AF9 was placed under the control of endogenous regulatory elements to induce AML (Chen et al., 2008). In this knock-in model, MLL-AF9 was highly expressed in HSCs, leading to high transformation susceptibility in this cellular compartment. GMPs from this model were shown to express lower levels of the fusion product and could only be efficiently transformed by higher doses of MLL-AF9 after retroviral transduction. Thus, oncogene dosage affects transformation susceptibility.

1.4.2. Examining the AML LCO in human studies

Attempts to identify the LCO human leukemia have proven significantly more difficult. These studies have generally relied on pathological features of the disease only *after* it has emerged to infer the LCO identity. Experiments using immunophenotyping and gene expression analysis suggested that AML LSCs can arise from HSCs or from more committed progenitors, including lymphoid-primed multipotent progenitors (L-MPP) and GMPs (Goardon et al., 2011; Kreso & Dick, 2014). These results were corroborated by a later study that generated DNA methylation and gene expression profiles for early HSPCs from healthy individuals that were then used to interrogate human AML data from the Cancer Genome Atlas project (TCGA) (TCGA, 2013; Jung et al., 2015). As before, the authors found that the LCO is variable and can arise from HSCs, MPPs, L-MPPs , or GMPs. Strikingly, patient prognosis could be stratified based on the developmental origin of the leukemia, where leukemias derived from more premature HSCs or MPPs appeared to be more aggressive *in vivo* than GMP-derived AML (Jung et al., 2015; Goardon et al., 2011; George et al., 2016). The most direct evidence that the LCO in human AML can arise from an ancestral HSC came when researchers isolated HSCs and T-cells from AML patients at various time points and found that they carried *DNMT3A* mutations, but not the concurrent NPM1 mutations detected in AML blasts (Shlush et al., 2014). Similar results were later recapitulated in another human study (Thol et al., 2017). Together, these data corroborated and extended findings from other groups who used various *in vitro* and *in vivo* assays to show that leukemogenic mutations can originate in pre-leukemic HSCs (Corces-Zimmerman et al., 2014; Jan et al., 2012). In order for AML to occur however, pre-leukemic HSCs must then

undergo further clonal evolution to give rise to AML LSCs. Here, cooperating events that help drive transformation likely occur in downstream myeloid progenitor cells, as has been demonstrated in studies examining blast lineage and maturation status at various disease phases in chronic myeloid leukemia (CML) patients (Jamieson et al., 2004).

The clinical consequences of the existence of pre-leukemic HSCs is significant, especially when considering the basis of relapse in this disease. Populations of pre-leukemic HSCs with a predisposition for transformation could serve as a reservoir for relapse, making this disease even more difficult to cure and suggesting that allogenic HSC transplant (allo-HSCT) could be a better treatment strategy in patients found to harbor such cells. In this scenario, a non-transformed pre-leukemic HSC resident in the BM during therapy would acquire new mutations, resulting in the emergence of a genetically divergent leukemia at disease recurrence. Indeed, studies examining relapsed AML genomes have already begun to uncover patterns like this in clinical patient samples. These studies will be discussed in detail in section 1.7 of my introduction (Krönke et al., 2013; Corces-Zimmerman et al., 2014; Tawana et al., 2015; Hirsch et al., 2016).

1.4.2.1. Discovery of clonal hematopoiesis of indeterminant potential (CHIP)

Recent sequencing studies examining the blood of individuals with no history of blood cancers revealed the existence of clonally driven hematopoiesis harboring leukemia-associated mutations in epigenetic modifiers such as *DNMT3A* and *TET2* (Jaiswal et al., 2014; Genovese et al., 2014; Xie et al., 2014). This new clinical entity, referred to as clonal hematopoiesis of indeterminate potential (or CHIP) was shown to be associated with an increased (albeit, overall still relatively small) risk hematological malignancies, along with various other maladies (e.g. cardiovascular disease). Most of the blood cancers that arise from CHIP are of the myeloid lineage, however the development of lymphoid malignancies has also been described in a small subset of these patients. Thus, mutations likely occur in HSCs or early multipotent progenitors (reviewed in Bowman et al., 2018). This raises the possibility that in some instances, CHIP might represent an AML precursor state akin to those observed in and screened for in solid malignancies, such as adenomatous colon polyps or high-grade cervical dysplasia (reviewed in Wacholder, 2013). Indeed, early evidence supporting this idea has started to emerge for at least *DNMT3A* driven-leukemia (Shlush et al., 2014; Bowman et al., 2018). Consequently, CHIP provides researchers with an opportunity to examine AML at early stages of development—an

opportunity that could also allow for a broader characterization of the LCO in some AML subtypes.

Although by no means comprehensive, the studies summarized in this section clearly paint a picture of AML as a disease driven by genetic lesions in oncogenes and tumor suppressors, which function within, and interact with the underlying (epi)genetic network in a cell to give rise to a fulminant leukemia with unique biological and clinical characteristics. Identifying the cellular origin of AML subtypes and examining how LCO properties impinge on the biology of LSCs will be critical for a better understanding and characterization of this heterogeneous disease, and the design of more effective treatments.

1.5. The AML leukemia stem cell (LSC)

Analogous to normal hematopoiesis, examination of primary patient tumors has revealed that many leukemias, including AML are organized in a hierarchical fashion, with LSCs that can self-renew and partially differentiate to generate bulk, non-LSCs, sitting at the apex of the hierarchy (Figure 1.2). Initial studies aimed at identifying colony-forming progenitors *in vitro* from both normal HSCs and patients with myeloid cancers provided the first clues that leukemias could be organized in a hierarchical manner (Metcalf et al., 1969; Moore et al., 1973). Around the same time, studies in AML patients injected with titrated thymidine showed that leukemic stem cells varied significantly in their ability to proliferate, providing the first conclusive *in vivo* evidence of functional intraleukemic heterogeneity (Clarkson et al., 1967). This observation also hinted at the existence of rare populations of AML blasts within tumors that cycled slowly and were resistant to antiproliferative drugs (Clarkson, 1969). Continued exploration of the *in vitro* properties of myeloid blast cells led to the theoretical framework that AML represented a corrupted version of hematopoiesis, similarly organized in hierarchical fashion (Buick et al., 1977; McCulloch, 1982). More than a decade later, John Dick's group provided conclusive evidence that AML is driven by LSCs that sit atop a developmental hierarchy. This was done by showing that primary human AML cells could maintain the disease over serial xenotransplantation experiments in immunocompromised mice (Lapidot et al., 1994; Bonnet and Dick, 1997).

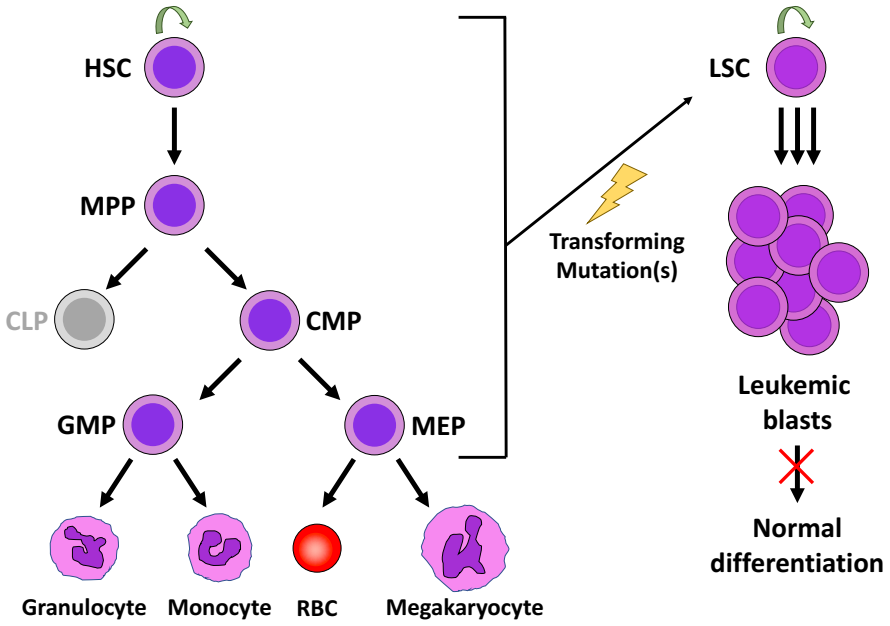

Figure 1.2. AML follows a cancer stem cell model. Acute myeloid leukemia (right) arises from mutations in hematopoietic stem and progenitor cells and follows a cancer stem cell model, akin to normal hematopoiesis (left). As with HSCs in normal blood formation, self-renewal abilities in AML (indicated by the green arrow) are restricted to LSCs that proliferate uncontrollably but are unable to differentiate (right). Abbreviations: LSC (leukemia stem cells), HSC (hematopoietic stem cell), MPP (multipotent progenitor), CMP (common myeloid progenitor), CLP (common lymphoid progenitor), GMP (granulocyte-monocyte progenitor), MEP (megakaryocyte-erythroid progenitor), RBC (red blood cell).

The gold standard assay for identifying LSCs today is still the establishment of leukemia in secondary recipients. Here "establishment" is defined as the presence of >0.1% human cells relative to murine BM cells, a remarkably low bar compared to clinical disease (Thomas & Majeti, 2017). However, it is now apparent that immunocompromised models that were initially used for transplant studies, such as SCID and NOD-SCID, posed a high xenographic barrier to AML engraftment. As immunodeficient mouse models have improved, so has the number of AML subtypes that can be successfully transplanted. These include less aggressive AMLs that have historically shown little to no engraftment in mice, such as acute promyelocytic leukemia (APML, commonly associated with the PML-RARA translocation) and core binding factor AML (CBF-AML, commonly associated with t(8;21) translocations and inv16; Goyama et al., 2015; Reinisch et al., 2016). However, even with more transplant-receptive mouse models, engraftment rates are still highly variable (reported anywhere from 40-80% using a cut off of >0.1% human leukemic chimerism in the mouse BM). Indeed, many primary AML samples fail to engraft when transplanted into animals—a fact that is often not reported (Thomas & Majeti, 2017). Recent

studies have also shown that engraftment is often limited to a single subclone within a given AML sample, and that the choice of recipient mouse model dictates which subclone reproducibly engrafts (Klco et al., 2014; Quek et al., 2016). Beyond engraftment rates, choice of mouse model also seems to impact LSC frequency. LSC frequency was initially thought to be on the order of 1:100,000 (Lapidot et al., 1994; Bonnet and Dick, 1997) but has recently been reported as being substantially higher, sometimes by as much as two orders of magnitude (Sarry et al., 2011; Eppert et al., 2011; Goardon et al., 2011; Reinisch et al., 2016). Together, these data demonstrate that interspecies differences in cytokines, microenvironment and immune interactions present in xenograft experiments are central determinants of the observed properties of LSCs. As LSCs are known to rely heavily on signals and interactions with surrounding non-transformed cells for their identity and function, this is perhaps unsurprising.

1.5.1. AML LSCs co-opt developmental programs and characteristics of normal HSPCs to promote leukemic transformation and fuel relapse

Based largely on transplantation studies, it is now well accepted that leukemias follow a cancer stem cell model. Currently, CD34+CD38- is the most commonly used immunophenotype used to isolate AML LSCs, as previous xenotransplantation studies suggested that AML LSCs are enriched in this fraction. It is important to note however, that about 25% of AML cases (typically enriched for *NPM1* and *TET2* mutations) lack expression of CD34. In these cases, most LSCs are found to reside in CD34- compartments, further highlighting the complex heterogeneity of this disease (Falini et al., 2005; Taussig et al., 2010; Quek et al., 2016). Efforts in the field to examine LSC properties has revealed that in AML, LSCs are in fact self-renewing, fairly quiescent, resistant to apoptosis (partially through interactions with the TME), have low levels of reactive oxygens species (ROS), have high rates of oxidative phosphorylation, and express high levels of drug efflux pumps (Bendall et al., 1993; Bendall et al., 1998; and reviewed in Thomas & Majeti, 2017). Together, these properties conspire to make LSCs less susceptible to frontline therapies that effectively eliminate the bulk proliferative tumor. Further evidence that these LSC features have clinical ramifications for patients has come from recent studies that have shown that LSCs are predictive of patient survival. Both a higher LSC frequency (measured by either CD34+CD38- surface phenotype or ALDH expression) and greater engraftment rates of LSCs at the time of AML diagnosis were shown to be associated high leukemic persistence after chemotherapy and a significantly shorter overall survival rate (van Rhenen et al., 2005; Pearce et al., 2006; Ran et al., 2009). This suggests that traditional LSC assays can have prognostic value.

Additionally, the identification of LSC gene expression programs resembling those normally found in HSPCs has also been shown to predict poor outcomes in AML patients (Valk et al., 2004; Gentles et al., 2010; Eppert et al., 2011).

That (most) AMLs should follow a cancer stem cell model has therapeutic implications for patients, as this conceptual framework posits that drug resistance is driven by LSCs. Clinically, this implies that in order to fully eradicate the disease, therapy must be able to eliminate LSC populations that persist during therapy and fuel subsequent relapse. Recent studies have begun to confirm this idea, showing that LSCs survive after therapy (even in patients who achieved remission) and increase in frequency by 1-2 orders of magnitude at relapse. These surviving LSCs populations demonstrate expanded immunophenotypes, such that after therapy, functional LSCs could be isolated from immunophenotypic compartments that initially lacked transplantation potential (Craddock et al., 2013; Ho et al., 2016, Shlush et al., 2017). In the end, the best validation of the cancer stem cell model in AML will require evidence that selective elimination of LSCs leads to superior outcomes and increased survival in patients. Interestingly enough, such studies have already begun to emerge in elderly AML patents treated with LSC-targeting therapy (Pollyea et al., 2018).

1.6. AML Genetics

Genetic lesions have been appreciated as key players in AML pathogenesis for over three decades, with cytogenetic aberrations still forming the backbone of current AML classification schemes (Arber et al., 2016). Recently, advances in –omics based technologies, particularly in next-generation sequencing (NGS) have greatly expanded our knowledge of the molecular genetics and pathophysiology of this aggressive malignancy. (The Cancer Genome Atlas Research Network, 2013; Döhner et al., 2015). Although it makes up only about 1.2% of all cancers, AML remains one of the most studied and best understood malignancies. In fact, it was one of the first cancers to be profiled by novel technologies of the time, such as high throughput microarray analysis and NGS (Shivarov & Bullinger, 2014; Ley, T. J., et al., 2008).

The first AML genome was published in 2008, and since then, the number of primary AMLs sequenced has grown exponentially (Ley et al., 2008, TCGA, 2013). In one of the largest systematic analysis of the (epi)genetic landscape of AML to date, whole-genome sequencing (n = 50) or whole-exome sequencing (n = 150) of 200 cases of *de novo* AML revealed a genomic profile that is notably heterogeneous (TCGA, 2013). While nearly 300 genes were found to be affected in two or more patients, most were found to be infrequently mutated between cases.

Only 23 of the 260 genes identified were recurrently mutated and almost half of those were already known to be associated with AML, such as *NPM1*, *FLT3*, *CEBPA*, *DNMT3A*, *IDH1/2*, and *EZH2*. Notably, only 3 genes are mutated in more than a quarter of AML patients (*FLT3*, *NPM1*, and *DNMT3A*). Overall, the average number of coding mutations per person was also strikingly low at 13, which includes an average of 3 driver mutations. Additionally, little genomic instability was noted (with the exception of *TP53*-mutated AMLs), with a median of one copy-number variant per genome and an average of less than one translocation. Before these data and the advent of NGS, nearly half of all AML patients presented with cytogenetically normal leukemias which were deemed as 'intermediate risk,' but could be stratified no further (Döhner et al., 2015). Using current technology, at least one somatic mutation can be confirmed in more than 95% of all AML cases, providing particularly useful prognostic information in this heterogeneous group of patients (DiNardo & Cortes, 2016). Later, studies investigating both larger sets of AML patient samples and mutation rates across cancer types confrimed TCGA findings and revealed that overall, AML is a disease of low mutational burden (Lawrence et al., 2013; Lawrence et al., 2014; Tyner et al., 2018).

Additional insights from TCGA data such as the temporal order of mutations, clonal composition, and clonal evolution could be gleaned by analyzing variant allele frequencies. Using this approach, more than half of all patients were found to harbor at least one founding clone and one subclone, confirming results from previous studies that described leukemogenesis as a Darwinian process of branching, multi-clonal evolution (Ding et al., 2012; Jan et al., 2012; Krönke et al., 2013; Shlush et al., 2014; Corces-Zimmerman et al., 2014). Additionally, alterations in epigenetic regulators (*DNMT3A*, *TET2*, and *ASXL1*) were found to be amongst the earliest mutations that occur in AML, with evidence that they can appear in pre-leukemic HSCs and are often associated with CHIP (Bowman et al., 2018). Together, these data reinforce the opinion that AML is not a single disease, but rather that this clinical diagnosis represents a diverse group of genetically distinct leukemias.

1.6.1. MLL-AF9-driven AML

The mixed lineage leukemia 1 (*MLL1*) gene located on chromosome 11q23.3 (now re-named as Lysine Methyltransferase 2A or *KMT2A*) was discovered in 1992 after leukemia-associated rearrangements in this region were found to affect the same unique locus at 11q23 (Figure 1.3; Gu et al., 1992; Tkachuk et al., 1992; Djabali et al., 1992). Associated with both ALL and AML, reciprocal translocations of this locus create a new chimeric protein encoded by the

5’ region of the *KMT2A* gene and the 3’ region of one of more than 80 different reported partner genes (reviewed in Winters & Bernt, 2017). The number of different loci involved in translocations with *KMT2A* exceeds those known to affect the immunoglobulin loci, suggesting that this breakpoint cluster region (BCR) (an 8.3kb region, from exon 8 to 14) contains genetically unstable sequences that are highly susceptible to recombination events. Indeed, topoisomerase II cleavage sites are found throughout the *KMT2A* BCR and cleavage of this region by unknown proteases in response to other genotoxic agents has also been reported, likely explaining the association between prior therapy and the emergence of AML (Broeker et al., 1996; Betti et al., 2005; Zhang & Rowley, 2006). The majority of MLL-rearranged (MLL-r) leukemias arise from translocations with one of 6 common partners (AF4 [t(4,11)], AF9 [t(9,11)], ENL [t(11,19)(q23,p13.3)], AF10 [t(10,11)], ELL [t(11,19)(q23,p13.1), or AF6 [t(6,11)]), and *MLLT3* gene encoding the AF9 protein (located on chromosome 9p21.3) is the second most prevalent fusion partner of *KMT2A* (Winters & Bernt, 2017). This balanced translocation results in the t(9,11)(p21.3,q23.3) lesion that encodes the oncogenic MLL-AF9 protein and is most frequently associated with AML of intermediate risk (Stock & Thirman, 2020).

Overall, rearrangements in the *KMT2A* gene are detected in 6% of adults (most often in young-middle aged patients) and 12% of children with AML, and are generally associated with an aggressive disease course and a poor prognosis (Stock & Thirman, 2020). Interestingly and possibly concordant with this observation, MLL rearrangements appear to be among the most potent oncogenic lesions in AML. TCGA data reveals an average of 2.09 driver lesions in this AML subtype, as compared to an average of 5.24 for all 200 samples (TCGA, 2013). The incidence of MLL rearrangements in infant leukemias and in therapy-related leukemias, two particularly aggressive subtypes, can reach upwards of 70-80% (Chowdhury & Brady, 2008; Blanco et al., 2001). In fact, of all patients treated with chemotherapeutics targeting topoisomerase II, 2-12% will go on to develop leukemia, with most cases developing into AML and a much smaller fraction resulting in ALL (Winters & Bernt, 2017). Rearrangements specifically resulting in MLL-AF9 are seen in 1% of all AML patients, yet, AML driven by this fusion oncogene is the most studied and best understood in the field (Bullinger et al., 2017).

The normal *KMT2A* gene encodes a histone methyltransferase protein (430kDa) that is structurally and functionally homologous to the *Drosophila* protein trithorax, a protein that plays a critical role in body plan specification by epigenetically regulating defined developmental genes, including the *homeobox* (*Hox) genes* (reviewed in Schuettengruber et al., 2011). The *N*-terminal region of the wildtype MLL1 protein contains a domain for binding Menin which then

links MLL1 to lens-epithelium derived growth factor (LEDGF), a chromatin binder that specifically recognizes H3K36 marks placed by ASH1L. This Menin/LEDGF association has been shown to be required for both the wild-type functions of MLL1 and for transformation by MLL1 fusion proteins (Yokoyama et al., 2005; Chen et al., 2006; Caslini et al., 2007; Yokoyama & Cleary, 2008; Zhu et al., 2016). The *N*-terminus also contains DNA-binding domains (AT-hook motifs), two speckled nuclear localization domains (SNL-1/2), and two repression domains (RD1/2), the first of which also contains a CxxC domain that binds and methylates CpG DNA islands (Winters & Bernt, 2017). Novel fusion proteins retain all of these domains. The remainder of the protein, including four plant homeodomain (PHD) fingers (important for protein-protein interactions), a bromodomain (binds acetylated lysine residues on histones), a transcriptional activation domain (TAD), and a SET domain (methylates H3K4) are all lost in most chimeric proteins. After translation, wild-type MLL1 is cleaved by taspase-1, downstream of the BCR, into MLL-N and MLL-C that bind together and form part of a multiprotein complex responsible for regulating chromatin modifications and gene expression (Yokoyama et al., 2011). Fusion proteins that contain the *N*-terminal region of MLL1 lose the ability to associate with MLL-C, though the functional consequence of this in leukemogenesis has not been worked out.

1.6.1.1. Physiologic functions of MLL1 and AF9

The physiologic functions of normal MLL1 and AF9 were elucidated in mouse studies. Mice with homozygous deletions of *KMT2A* die at embryonic day 10.5-12.5 and display facial abnormalities, aberrant innervation, and defects in hematopoiesis (Yu et al., 1995; Yagi et al., 1998; Yokoyama et al., 2011). Heterozygote embryos are haploinsufficient and show abnormal body segmentation phenotypes and decreased cell numbers in various hematopoietic lineages. The developmental defects noted in these mice resemble those noted in mice with knockouts in *Hox* genes, many of which (eg. *Hoxa7, Hoxc8,* and *Hoxa9*) are known targets of both wild-type MLL1 and MLL1 fusion proteins. Additional studies later demonstrated that MLL1 plays an essential and non-redundant role in development and hematopoiesis by maintaining expression of specific genes through epigenetic mechanisms (Jones et al., 2012; Shilatifard, 2012). Like to MLL1, normal AF9 protein is also an important player in the epigenetic and transcriptional control of various developmental pathways, specifically those that govern cell fate decisions in the erythrocyte and megakaryocyte lineages during human and murine hematopoiesis (Pina et al., 2008). The *C*-terminus of AF9 contains regions with functions that are critical for the transformation properties of MLL-AF9, including a transactivating coiled-coil domain and regions

that allow AF9 to bind to AF4 protein (Yokoyama, 2010; Li et al., 2014). AF4 binding is critical, as this protein forms a bridge between AF9 and the "super elongation complex" (SEC) that regulates transcription by interacting with the positive transcription elongation factor b (pTEFb) complex (reviewed in Luo et al., 2012). The pTEFb complex promotes transcriptional elongation through gene bodies by phosphorylating RNA Pol II (necessary to release paused Pol II) and either directly or indirectly recruits DOT1L (and its associated binding partners), a histone methyltransferase that lays down the activating histone mark H3K79me2 to increase transcription at specific loci.

1.6.1.2. Mechanisms of MLL-AF9 mediated leukemic transformation: Hijacking transcriptional control to induce cellular transformation

In leukemogenesis, the normally highly regulated processes regulated by MLL1 and its binding partners are co-opted to promote transformation in HSPCs. Although the more than 80 possible fusion partners all appear to have assorted structures and functions, two unifying features that are critical for transformation have emerged. First, MLL1 fusion proteins regulate transcriptional elongation by interacting with SEC members in the nucleus and by recruiting DOT1L to specific loci (Thoms et al., 2019). Various studies have shown that DOT1L recruitment is necessary for transformation in MLL-r AML, with MLL-fusion target loci displaying increases in H3K79me2 marks (Chang et al., 2010; Bernt et al., 2011; Nguyen et al., 2011; Krivtsov et al., 2008). Additionally, pinometostat, a small molecule inhibitor of DOT1L has already begun to show moderate efficacy as a single agent in both preclinical and clinical trials targeting this AML subtype (Daigle et al., 2013; Stein et al., 2018). The second unifying feature of many MLL1 binding partners, including cytoplasmic proteins, is their ability to form complexes in the nucleus when they are fused to MLL1. Fusion of the *N*-terminus of MLL1 to LacZ, which forms tetramers was enough to induce leukemia in mice, as was the induced dimerization of MLL1-FKBP12 (Dobson et al., 2000; Martin et al., 2003).

These observations have led to the hypothesis that the fusion of MLL1's chromatin-targeting domains to partners of the SEC that recruit DOT1L containing complexes results in aberrant recruitment of these proteins to MLL target loci, leading to loss of the transcriptional elongation checkpoint (Thoms et al., 2019). This then leads to the deposition of strongly activating epigenetic marks that sustain and enhance the expression of stem cell promoting genes and lead to increased proliferation and defects in differentiation. Indeed, MLL-r AMLs have consistently been found to differ from other subtypes in their transcriptional programs, with the

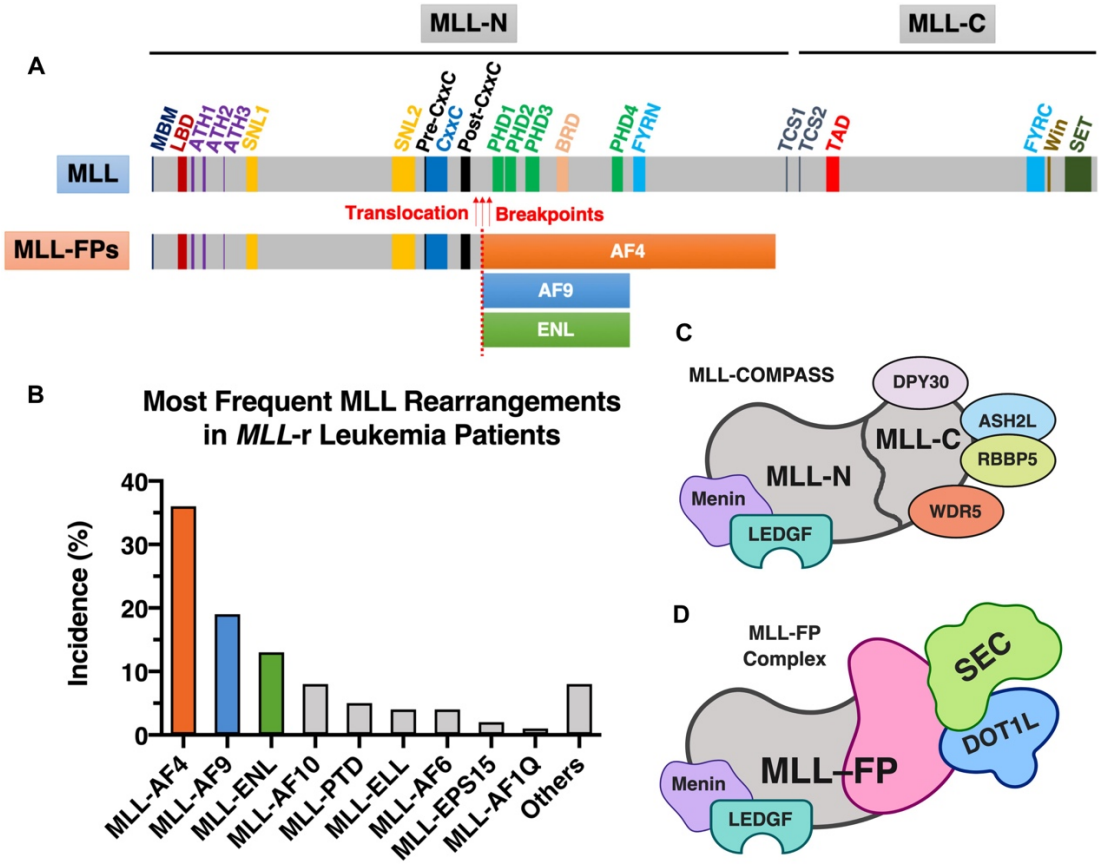

Figure 1.3. Wild-type and aberrant MLL proteins. (A) Schematic of domain architecture of wild-type (WT) MLL and MLL-fusion proteins (MLL-FP). The WT canonical form of human MLL protein (UniProt ID: Q03164) has a total of 3,969 amino acids in length and contains several functional domains and important sites (drawn to scale): high-affinity Menin-binding motif (MBM, residue 6–10), LEDGF-binding domain (LBD, residue 109–153), AT-Hook1/2/3 (ATH1, residue 169–180; ATH2, residue 217–227; ATH3, residue 301–309; UniProt annotations of Q03164); nuclear-localization signal 1/2 (SNL1, residue 400–443; SNL2, 1008–1106), pre-CxxC region (residue 1149–1154), CxxC domain (residue 1147–1242), post-CxxC (residue 1298–1337), plant homology domain 1/2/3/4 (PHD1, residue 1431–1482; PHD2, residue 1479–1533, PHD3, residue 1566–1627; PHD4, residue 1931–1978; UniProt annotations of Q03164), bromodomain (BRD, residue 1703–1748; UniProt annotations of Q03164), FY-rich N-terminal domain (FYRN, residue 2018–2074; UniProt annotations of Q03164), FY-rich C-terminal domain (FYRC, residue 3666–3747; UniProt annotations of Q03164), taspase1 cleavage site 1/2 (TCS1, residue 2666–2670, D/GADD; TCS2, residue 2718–2722, D/GVDD), transactivator domain (TAD, residue 2829–2883), WDR5 interaction motif (Win; residue 3762–3773), and Su(Var)3-9, enhancer-of-zeste, trithorax domain (SET, residue 3829–2945; UniProt annotations of Q03164). The most frequently observed translocation breakpoints (shown by red arrows) are located in the region between CxxC and PHDs. The three most common MLL-FPs (MLL-AF4, MLL-AF9, and MLL-ENL) are shown (the translocation breakpoints and the size of FPs are partially drawn to scale). (B) The most frequent MLL rearrangements identified in MLL-r leukemia patients. The statistics shown in this figure was obtained from a study of 2,345 MLL-r leukemia patients dated from 2003 to 2016 (Meyer et al., 2018). (C) Components of complexes formed by WT MLL, complexes that are also known as MLL-COMPASS (complex of proteins associated with Set1; named for the single yeast homolog). (D) MLL-FP (e.g., MLL-AF4, MLL-AF9, or MLL-ENL) in complex with DOT1L and SEC.

Reprinted from Front. Cell Dev. Biol., 7, Chan, A. K. N. & Chen, C. W. Rewiring the epigenetic networks in MLL-rearranged leukemias: Epigenetic dysregulation and pharmacological interventions, 1-15, 2019, with permission from Frontiers Media SA.

most frequently overexpressed genes being *HOXA7-HOXA10* and their dimerization partner *MEIS1* (Armstrong et al., 2002; Li et al., 2009). During normal hematopoiesis, *HOX* genes and *MEIS1* are most highly expressed in HSCs and early progenitor cells, and expression of these genes is downregulated as cells differentiate (Lawrence et al., 1997; So et al., 2004). In AML, *MEIS1* expression has been shown to be critical for leukemic cell proliferation and the level of expression of this gene is inversely correlated with disease latency (Wong et al., 2007). Similarly, *HOX* gene expression has been shown to be indispensable for transformation in the context of several MLL-rearrangements, with *HOXA9* (in cooperation with *MEIS1*) altering the epigenetic landscape of the LCO to activate an ectopic embryonic gene program that drives leukemogenesis (Sun et al., 2018). Clinically, *HOXA9* overexpression is prevalent amongst the most aggressive acute leukemias and is still one of the strongest predictors for poor prognosis in this disease (Collins & Hess, 2016). Interestingly, the isolation of a large SEC in MLL-r leukemias has proven elusive and structural analyses of protein binding sites have suggested that binding of several of these members is mutually exclusive (Thoms et al., 2019; Biswas et al., 2011; He et al., 2011). Still, it is likely that chimeric proteins form several smaller complexes (rather than one large SEC) that regulate transcription in MLL-r leukemia. This would then have the same result of dysregulating transcriptional programs that critically contribute to the stem-like properties of MLL-r leukemias by conferring and/or maintaining self-renewal properties, growth, and survival advantages that define the oncogenicity of these cells.

1.6.1.3. MLL-AF9-driven mouse model of AML

To study mechanisms of chemoresistance in this disease, we took advantage of an established transplantable mouse model of dsRed+ MLL-AF9-driven AML developed by the Ebert lab (Puram et al., 2016). Briefly, GMP cells isolated from *Actin-dsRed* mice were transduced with retroviruses carrying the *MLL-AF9* translocation and subsequently injected into lethally irradiated recipients. Leukemic cells were then isolated from moribund mice and serially re-transplanted for three additional rounds into sub-lethally irradiated recipients. The resulting model produces a transplantable, highly penetrant leukemia in sub-lethally irradiated hosts after 2 weeks. Importantly, this model has already been used to perform pooled *in vivo* RNAi screens, demonstrating the tractability of this approach (Miller et al., 2013; Puram et al., 2016).

1.6.2. *IDH1*/2 and *TET2*-mutated AML—Discovery of oncometabolites

Isocitrate dehydrogenase 1 (IDH1) and 2 (IDH2) are homodimeric isoenzymes that catalyze the oxidative decarboxylation of isocitrate (Figure 1.4). This results in the formation of α-ketoglutarate (αKG), NADPH, and CO_2 which are required for the tricarboxylic acid (TCA) cycle and, in the case of αKG, for the function of αKG-dependent dioxygenases (αKG-DDs) to complete their enzymatic reactions (Golub et al., 2019). In normal cells, IDH1 is localized to the cytoplasm and peroxisomes, while IDH2 is found in mitochondria. Recently, human sequencing studies in glioma and AML, identified recurring driver mutations in *IDH1* (found in 7-14% of AML cases) and *IDH2* (found in 8-19% of AML cases) (Mardis et al., 2009; Dang et al., 2009; Ward et al., 2010). Mutations in these genes are typically mutually exclusive and heterozygous, suggesting that retention of a wild-type copy is necessary for either normal metabolism, transformation, or for both. These alterations are also neomorphic, affecting key residues in the catalytic domain of these enzymes, namely R132 in IDH1 and R140/R172 in IDH2. When present, these mutations eliminate the wild-type function of IDH1/2 and instead, allow mutIDH1/*2* to generate 2-hydroxyglutarate (R-2HG) from αKG in an NADPH-dependent manner (Dang et al., 2009). Together, these observations suggested that lesions in *IDH1/2* are selected for their gain of function (GOF) in novel enzymatic activity (rather than a loss of function (LOF)) and that the critical role of mutIDH1/2 in leukemogenesis is likely related its production and the accumulation of R-2HG in cells.

Hints in the literature that the transforming properties of mutIDH1/2 might arise from elevated levels of R-2HG came from metabolic profiling studies in patients bearing mutIDH1/*2* tumors. Using this approach, AML patients carrying *IDH1*/2 mutations were shown to have significant increases of R-2HG in their sera, a physical property that was later shown to be predictive of these mutations and of clinical outcome in AML patients (Gross et al., 2010; DiNardo et al., 2013). In a landmark study from the Kaelin lab, R-2HG was finally established as a bona fide 'oncometabolite' when its accumulation in hematopoietic cells was shown to promote cytokine independence and induce a block in differentiation, hallmarks of leukemic transformation (Losman et al., 2013). This study also showed that the effects of R-2HG were reversible upon removal of this oncometabolite, suggesting that pharmacological inhibition of mutIDH1/2 to drive down R-2HG levels represents a promising therapeutic avenue in this AML subtype. As expected, highly selective inhibition of mutIDH1/2 by small molecule compounds was subsequently shown to effectively diminish R-2HG levels and induce differentiation of AML

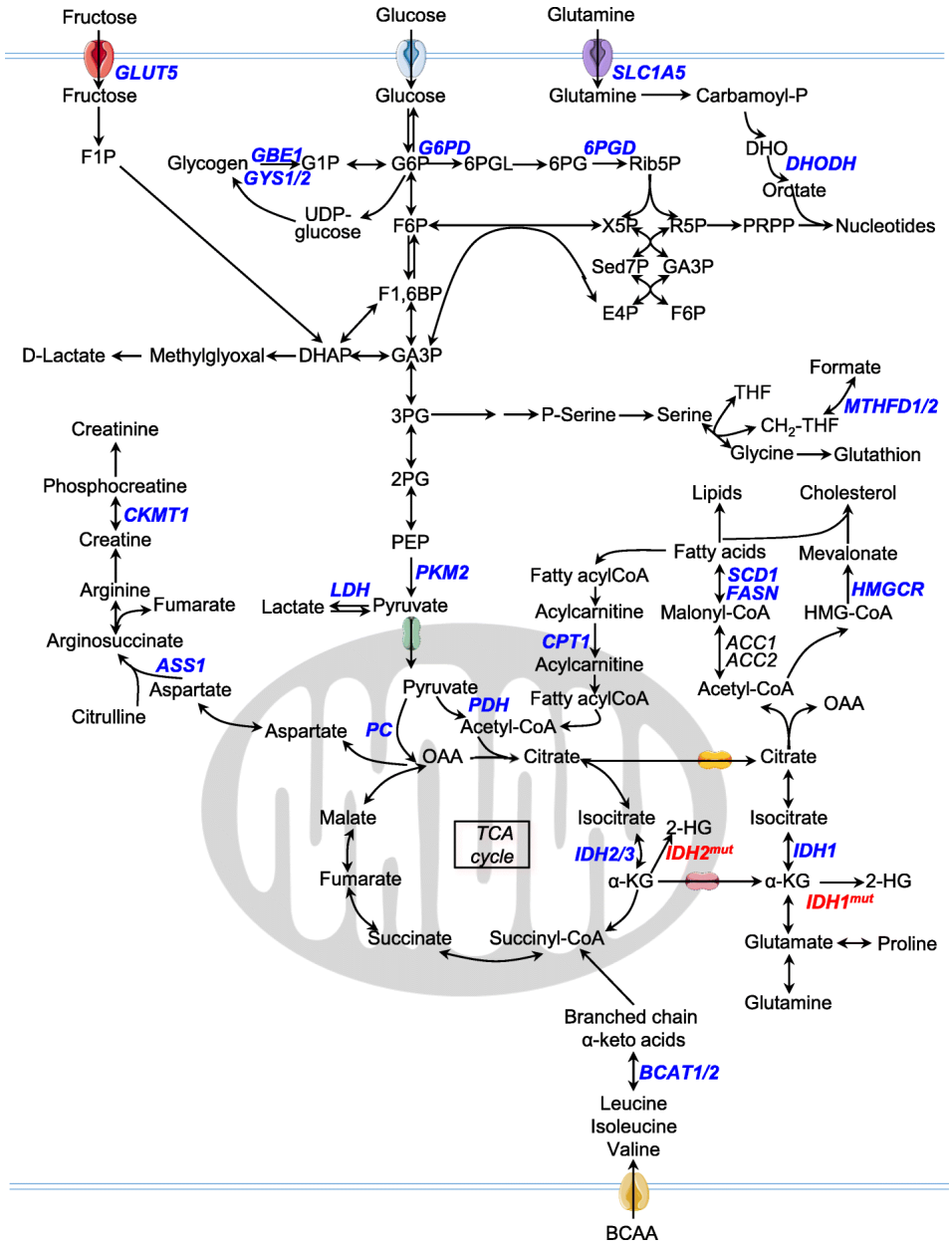

Figure 1.4. Metabolic pathways and deregulated reactions in AML. Enzymes known to be deregulated in AML are shown in blue. Driver mutations in isocitrate dehydrogenase 1 and 2 ($IDH1^{mut}$ and $IDH2^{mut}$) have also been found in AML and are shown in red. Compound abbreviations: *F1P* fructose-1-phosphate, *G1P* glucose-1-phosphate, *G6P* glucose-6-phosphate, *F6P* fructose-6-phosphate, *F1,6BP* fructose-1,6-biphosphate, *GA3P* glyceraldehyde 3-phosphate, *DHAP* dihydroxyacetone phosphate, *3PG* 3-phosphoglycerate, *P-Serine* phosphoserine, *2PG* 2-phosphoglycerate, *PEP* phosphoenolpyruvate, *6PGL* 6-phosphogluconolactone, *6PG* 6-phosphogluconic acid, *Rib5P* ribulose-5-phosphate, *X5P* xylulose-5-phosphate, *R5P* ribose-5-phosphate, *Sed7P* sedoheptulose-7-phosphate, *E4P* erythrose-4-phosphate, *PRPP* phosphoribosyl pyrophosphate, *Carbamoyl-P* carbamoyl phosphate, *DHO* dihydroorotate, *THF* tetrahydrofolate, *OAA* oxaloacetate, *α-KG* α-ketoglutarate, *2-HG* 2-hydroxyglutarate, *BCAA* branched-chain amino acid.
Reprinted from BMC Biol., 17, Stuani, L., Sabatier, M. & Sarry, J. E., Exploiting metabolic vulnerabilities for personalized therapy in acute myeloid leukemia, 1-17, 2019, with permission from BMC and Springer Nature.

blasts, culminating in the FDA approval of two mutIDH inhibitors for use in AML: Enasidenib (2017) and Ivosidenib (2018) (Kim, 2017; Dhillon, 2018; Golub et al., 2019).

Mechanistically, R-2HG is structurally similar to αKG and has been shown to act as a competitive inhibitor of this metabolite, occupying the same binding pocket as αKG in αKG-DDs to effectively block their enzymatic functions (Xu et al., 2011). Over 60 αKG-DDs with functional roles in chromatin remodeling, DNA/RNA methylation, collagen maturation, DNA damage, cellular signaling, and hypoxia responses have been reported in humans (Gagné et al., 2017). In AML, R-2HG-induced inhibition of αKG-DDs that epigenetically regulate transcription has emerged as a key mechanism by which *IDH1/2* mutations promote leukemogenesis. Epigenetic analysis of large cohorts of patients revealed that AMLs with mutIDH1/2 consistently demonstrated DNA hypermethylation phenotypes and a specific epigenetic signature that could differentiate them from leukemias harboring alterations in other transcriptional or epigenetic regulators (Figueroa et al., 2010a). Interestingly, this epigenetic signature was also shown to overlap with that of AMLs harboring LOF mutations in *TET2* (Figueroa et al., 2010b). As a member of the ten-eleven translocation (TET) family of 5-methylcytosine (5mC) hydroxylases, TET2 is an αKG-DDs responsible for catalyzing the formation of 5-hydroxymethylcystine (5hmC) from 5mC, ultimately resulting in demethylated DNA (reviewed in Bowman & Levine; 2017). These observations hinted at a unifying mechanism involving both enzymes, prompting researchers to examine the co-occurrence of these mutations in AML. Strikingly, *TET2* and *IDH1/2* alterations were mutually exclusive, suggesting that these lesions functioned within the same pathway and were thus biologically redundant (Abdel-Wahab et al., 2010). Concrete evidence of this came soon thereafter when mutIDH1/2 derived R-2HG was shown to competitively inhibit TET2 and block differentiation in AML cells *(*Figueroa et al., 2010b; Xu et al., 2011).

That altered metabolism, a long appreciated hallmark of cancer (Hanahan & Weinberg, 2011) could functionally modify the epigenetic landscapes of cells was exceptionally surprising. Here, the identification and characterization of *IDH1/2* mutations had the broader consequence of linking aberrant cellular metabolism to the age of genomics in cancer research. Today, other metabolites that structurally resemble αKG, such as succinate and fumarate have also been implicated in cancer and have also been shown to competitively inhibit αKG-DDs (reviewed in Sciacovelli & Frezza, 2016). As expected, cancers associated with these three oncometabolites demonstrate overlapping features that include hypermethylation phenotypes and other effects not reviewed here (e.g. pseudohypoxia and increased ROS formation). However, this converging oncometabolic signature, mediated mostly by αKG-DD inhibition, likely does not fully explain the

transformation properties of these metabolites. The complete compendium of cellular sequelae due to oncometabolite accumulation, either through genetic or non-genetic mechanisms, is vast and is only now starting to be appreciated (Raffel et al., 2017). Hence, while the full impact of these defects remains incompletely understood, cancer metabolomics have emerged as critical nodes in cancer initiation and as exciting targets in the treatment of various tumor types.

1.7. AML therapy

The emergence of resistant disease poses a formidable challenge to the clinical management of AML, taking an already difficult disease and transforming it into a uncontrollable one with increasingly limited treatment options. Today, the overwhelming majority of cures in this disease (excluding APML) come from the administration of intensive therapy using traditional cytotoxic agents (+/- allo-HSCT). In fact, improvements in AML death rates over the decades have not been linked to the advent of novel therapeutics, but rather, are a result of better supportive care, better management of allo-HSCT complications, advancements in blood banking, improved antimicrobial agents, and to the optimization of dosing schedules for the traditional chemotherapeutics used to treat AML (Fernandez et al., 2009; Löwenberg et al., 2011; Othus et al., 2014). In the 1970's, cytarabine (ara-C) and anthracyclines were found to be effective and were later combined into the "7 + 3" regimen that still constitutes the backbone of AML therapy today. Clinically, AML therapy is split up into an induction phase, which aims to debulk the majority of the tumor to reinstate normal hematopoiesis, and a subsequent consolidation phase aimed at eliminating persistent leukemic cells. While induction therapy is standardized and includes repeated cycles of the 7 + 3 schedule, consolidation therapy varies depending on the prognostic risk associated with genetic lesions present in specific cases. In patients with lower risk AMLs, additional cycles of chemotherapy are preferred while allo-HSCT is preferred in eligible patients with intermediate to high risk AML. Together, this combination of chemotherapeutics (+/- allo-HSCT) results in high initial response rates and complete remissions (CRs) in 40 to >90% of cases, depending on the AML subtype and patient age (Hackl et al., 2017). However, the majority of patients, even those in remission, harbor residual AML that leads to relapse within 3-5 years of diagnosis. Interestingly, AMLs that recur after treatment failure(s) will often still be responsive to the same frontline therapies, with many patients achieving second and even third remissions. Nevertheless, as treatment cycles are repeated, any additional remissions become progressively shorter as AMLs become increasingly resistant and more difficult to treat, leading to dismal survival rates in this disease.

Excluding APML where targeted therapy has significantly bettered prognosis, AML has a 5-year overall survival (OS) of about 28% and a median age of 68 at diagnosis. Elderly patient demographics in AML contribute to the difficulty of treating the disease, often precluding the use of intensive therapy in this population. In fact, only about half of all patients over the age of 60 will qualify for treatment with intensive induction therapy, while the remainder are placed on alternate treatments (such as hypomethylating agents, histone deacetylase inhibitors, cell cycle inhibitors, and others) that are often palliative. The estimated 5-year OS for older patients, patients with secondary AMLs, or those with relapsed or refractory disease (R/R) is only 5-10%. Even in younger patients, the prognosis of this disease remains grim, with only 35-40% of patients under the age of 60 achieving a cure.

These bleak clinical outcomes stand in stark contrast to the astounding progress that has been made in characterizing the molecular underpinnings of AML in the past few decades, as reviewed in the antecedent sections of my thesis. The long lead-time needed to integrate basic research efforts into clinical practice is likely partially to blame. Still, the last few years have witnessed a burst of FDA approvals for AML therapies, representing the first major additions to the armamentarium against this disease in nearly five decades (excluding APML therapy) (Lai et al., 2019). In the year 2000, the FDA approved the use of the anti-CD-33 antibody-drug conjugate, gemtuzumab ozogamicin (GO) for older AML patients with CD33+ relapsed AML. GO was subsequently withdrawn from the market in 2010 when concerns about its safety and efficacy were raised. Most recently (from 2017-2018) a total of eight drugs for AML were approved, including GO with an adjusted schedule/dose, the mutIDH1/2 inhibitors ivosidenib and enasidenib, a liposomal formulation of daunorubicin and cytarabine (CPX-351), the FLT3-ITD inhibitors midostaurin and gilteritinib, the BCL2 inhibitor venetoclax, and a hedgehog pathway inhibitor (glasdegib). With this new array of options available to patients and their providers, it is clear that the paradigm by which AML is treated is likely to change soon. However, whether these drugs will lead to significantly better patient outcomes once they are applied on a population level is yet to be determined, especially given the fact that relapse was still highly prevalent in all of the clinical trials examining these compounds. One thing is clear—chemotherapy will continue to play a leading role in the way the vast majority of patients are treated and cured. Hence, understanding the mechanisms by which AML cells become resistant to frontline therapy is paramount if we are to significantly extend the lives of AML patients.

1.7.1. Mechanisms of resistance to AML therapy

The population of leukemic cells that survive therapy represent minimal residual disease (MRD) and drug resistance in this population can either exist prior to chemotherapeutic exposure (primary resistance) or may develop or be enhanced during drug treatment (acquired resistance). MRD-derived relapse is the foremost source of fatality in AML patients receiving frontline treatment (Schuurhuis et al., 2018; Jongen-Lavrencic, et al., 2018). Chemotherapy can fail to kill MRD cells for numerous reasons, as demonstrated by various recent studies. Impaired drug effectiveness can, for instance, be due to reduced levels of active chemo agents in target cells as a consequence of decreased uptake, increased efflux, or decreased delivery of drug to target tissues (reviewed in Shaffer et al., 2012; Marin et al., 2016). Other cell intrinsic processes, such as deregulation of apoptosis (Vo et al., 2012; Cassier et al., 2017), amplification or modification of drug targets (Tyner et al., 2018; Yuan et al., 2019), increased capacity for DNA damage repair (Bouwman & Jonkers, 2012), and the activation of prosurvival signaling (Holohan et al., 2013) have also been shown to render tumors insensitive to therapy. Previous reports have also hypothesized that therapy refractory cells are enriched in immature LSC populations. Overall, LSCs are thought to be intrinsically more resistant to conventional chemotherapy by virtue of their properties of self-renewal, resistance to apoptosis, relative quiescence, and increased expression of drug efflux pumps (Thomas & Majeti, 2017). Indeed, quiescent $CD34^{+}CD38^{-}$ LSCs have been shown to home to, engraft in, and expand at the endosteal niche of the BM (Ishikawa et al., 2007). Cells resident in this osteoblast-rich niche were specifically shown to be chemoresistant and could be sensitized to therapy when induced to cycle using the growth factor G-CSF (granulocyte-colony stimulating factor) (Ishikawa et al., 2007; Saito et al., 2010). However, human studies investigating the use of G-CSF in combination with chemotherapy in AML showed disappointing results (reviewed in Bendall & Bradstock, 2014). Other therapeutic strategies aimed at targeting LSCs resident in HSC niches are described below.

In addition to the plethora of cell-intrinsic factors implicated in AML chemoresistance, the TME has also recently been shown to be a major determinant of therapeutic response in this disease (reviewed in Behrmann et al., 2018). Here, the TME has been shown to promote drug resistance either by secreting protective factors (soluble factor-mediated drug resistance [SM-DR]) or by directly interacting with leukemic cells (cell adhesion-mediated drug resistance [CAM-DR]). In the best described form of SM-DR, stromal derived factor (SDF)-1 (also known as CXCL12) secreted in the BM protects AML cells expressing chemokine receptor 4 (CXCR4, the SDF-1 receptor) from apoptosis induced by cytarabine treatment (Möhle et al., 1998; Chen et

al., 2013). Mechanistically, the overexpression of CXCR4 on AML cells allowed them to sense CXCL12 chemoattractant signals secreted by BM stromal cells, causing them to migrate to a protective niche that is normally reserved and critical for HSC survival. Accordingly, administration of a CXCR4 inhibitor (AMD3465, an analog of the FDA approved drug plerixafor) re-sensitized AML cells to both chemotherapy and kinase inhibitors by dislodging them from these niches and thereby inhibiting SDF-1-induced activation of prosurvival pathways [PI3K/AKT and MAPK] (Zeng et al., 2009; Nervi et al., 2009). On a clinical level, overexpression of CXCR4 on AML blasts at diagnosis was also found to portend a poor prognosis and shorter overall survival (Konoplev et al., 2007). Together, these data have led to the clinical development and testing of various CXCR4 inhibitors that are now beginning to show promising results in both relapsed and *de novo* AML (reviewed in Walenkamp et al., 2017). As in preclinical studies, administration of CXCR4 inhibitors in patients was also shown to mobilize AML cells to the periphery, leading to increased granulocyte differentiation, increased leukemic sensitivity to frontline therapy, and to a significant increase in CRs rates, as reported by an ongoing phase II trial (Borthakur et al., 2014). Interestingly, CXCR4 has also been shown to be induced by chemotherapy, perhaps explaining why these inhibitors have been successful in relapsed AML (Behrmann et al., 2018). Many well described examples of CAM-DR that render AML cells refractory to treatment by similar TME-derived mechanisms (albeit, via direct cell-cell interactions) can also be found in the literature (e.g. the VCAM1/VLA4 axis) (Matsunga et al., 2003; Poulos et al., 2014; reviewed in Behrmann et al., 2018). However, as with SM-DR inhibitors, the ultimate therapeutic goal remains the same: to potentiate the effects of frontline therapy by dissociating blasts away from protective anatomical sites where these cells co-opt pre-existing or therapy-induced signaling networks, normally reserved for HSPCs, to promote their own survival. Hence, TME-leukemia interactions have now emerged as one major, non-genetic method by which AML cells can become resistant to therapy.

1.7.1.1. Metabolic rewiring to an OXPHOS high status can promote broadly drug resistant states across various cancer types and treatment modalities

Recently, mitochondrial metabolism has also emerged as a key player in the development of chemoresistant AML and as a viable therapeutic target in this disease (reviewed in Chapuis et al., 2019). A study by Lagadinou and colleagues demonstrated that depending on the expression of the oncogene *BCL-2*, AML LSCs displayed increased reliance on oxidative phosphorylation (OXPHOS) (Lagadinou et al., 2013). Here, inhibition of BCL-2 reduced OXPHOS and selectively

eradicated chemotherapy-resistant AML LSCs. Similarly, experiments utilizing patient derived xenografts (PDXs) treated *in vivo* with cytarabine demonstrated that chemotherapy spared preexisting and persisting AML cells that displayed high rates of OXPHOS as shown by increased expression of OXPHOS gene sets, increased mitochondrial mass, retention of active polarized mitochondria, high levels of ROS, and greater mitochondrial respiration (Farge et al., 2017). This increase in OXPHOS was at least partially dependent on increased fatty acid oxidation (FAO), as chemoresistant AML cells displayed an upregulation of FA metabolism genes (including FA translocase/receptor, CD36) and pharmacological inhibition of FAO with etomoxir induce energetic shifts toward OXPHOS low states (also known as the Pasteur effect), ultimately sensitizing cells to Ara-C. Additionally, the high OXPHOS gene signature generated from therapy refractory AML cells was predictive for treatment response in both PDXs and patients, indicating that increased OXPHOS might indeed be a clinically relevant determinant of AML cell survival, at least in the context of Ara-C treatment (Farge et al., 2017; Yan et al., 2017). Similar results in AML were later achieved by other groups using *in vitro* systems (Yucel & Sonmez, 2017; Ashton et al., 2018).

Interestingly, recent studies have also shown that while bulk AML cells have an increased mitochondrial mass and oxygen consumption rate, they also have a lower spare reserve capacity of the respiratory chain and appear to be less efficient in employing glycolysis. This renders AML cells more reliant on OXPHOS for survival, as compared with normal hematopoietic cells (Škrtić et al., 2011; Lagadinou et al., 2013; Sriskanthadevan et al., 2015). Thus, there might be a therapeutic window for the targeted inhibition of OXPHOS in AML, especially in the context of cytarabine treatment. Accordingly, inhibiting ClpP (a mitochondrial protease that interacts with respiratory chain proteins), mitochondrial biogenesis, mitochondrial protein synthesis, mitochondrial DNA replication, electron transfer, or mitochondrial FA transport/oxidation have all been show to activate the Pasteur effect and re-sensitize AML blasts to Ara-C treatment (Samudio et al., 2010; Škrtić et al., 2011; Cole et al., 2015; Farge et al., 2017). The intriguing possibility that cancer resistance is more generally associated with a high OXPHOS status has recently been suggested by data from various groups. Inhibition of OXPHOS has now been shown to suppress resistance to taxanes in prostate cancer, 5-fluorouracil (5-FU) in colon and Myc/PGC-1α-driven pancreatic adenocarcinoma, and protein kinase inhibitors in lung adenocarcinoma, melanoma and chronic myeloid leukemia (CML) (Vazquez et al., 2013; De Rosa et al., 2015; Ippolito et al., 2016; Kuntz et al., 2017; Bosc et al., 2017; Lee et al., 2017; Ashton et al., 2018).

As resistance occurs in the context of the TME, it is tempting to speculate that by virtue of their unique metabolic features, various anatomical sites might also serve as better "soil" for the protection of residual cells with altered metabolism—especially in the context of drug exposure. In the case of AML, a nutrient-supportive catabolic niche that provides oxidizable substrates to leukemic cells could have the effect of fueling OXPHOS to ultimately sustain chemoresistant phenotypes in surviving cells. A similar idea has proven true in a related malignancy where work from the Jordan lab showed that CD36+ CML LSCs migrate to adipose tissue niches where they induce lipolysis and fuel FAO to survive chemotherapy (Ye et al., 2016). When FAO was reduced via KO of CD36, CML cells were deprotected and re-sensitized to combination chemotherapy. Data from Farge and colleagues, combined with the observations that adipocytes colonize the BM after Ara-C treatment and that expression of CD36 is a predictor of poor outcomes in AML patients, raise the possibility that a similar biology to that described in CML is also at play in AML resistance (Perea et al., 2005; Farge et al., 2017). Here, CD36 upregulation could be promoting FA uptake from adipocytes in the BM, thereby fueling FA metabolism that maintains OXPHOS and promotes leukemic survival upon cytarabine exposure. While this has yet to be conclusively shown, it is well known that AML cells induce a pro-tumorigenic niche in the BM. This occurs partially through the induction of lipolysis in normal BM adipocytes that then provide FAs for blast survival (Shafat et al., 2017; Tabe et al., 2017). Together, these examples highlight the idea that tumor bioenergetic features, acquired either through genetic or non-genetic changes, can be major determinants of therapeutic outcome in both classical and targeted AML therapy.

Accordingly, the scientific rationale of targeting mitochondrial biology to exploit this metabolic synthetic lethality and potentiate the effects of therapy in AML has already begun to yield clinical progress. Venetoclax, a BCL-2 inhibitor previously shown to exert its antileukemic effects via the inhibition of OXPHOS in AML, was recently shown to have clinical efficacy in elderly AML patients ineligible for intensive therapy. Here, patients were treated with either low-dose ara-C or hypomethylating agents and venetoclax, a combination that led to more, and faster, CRs (Konopleva et al., 2016). Due to the success of this and other studies, venetoclax for use in elderly AML populations was approved by the FDA in 2018 (Lagadinou et al., 2013; Pollyea et al., 2018; DiNardo et al., 2018; Jones et al., 2018; DiNardo et al., 2019). As relapse was still a frequent occurrence in these studies, it will be interesting to see if venetoclax will be even more effective in the context of intensive combination chemotherapy. Interestingly, at relapse, LSCs that were shown to be more resistant to venetoclax treatment also had upregulated FAO. Thus

resistance against these combinations may occur via the acquisition of additional metabolic plasticity (Jones et al., 2018). Further clinical translation of the finding that mitochondrial biology seems critical for resistance across various treatment modalities and tumor types is currently underway. Other new drugs, including CPI-613 (an putative inhibitor of pyruvate dehydrogenase and α-KG dehydrogenase) and mitochondrial electron transport chain (ETC) complex I inhibitors (phenformin and IACS-010759) are also being investigated and have already begun showing promising results in both clinical and preclinical testing (Molina et al., 2018; Pardee et al., 2018; Kreitz et al., 2019).

1.7.1.2. Genomic landscapes of relapsed AML suggest the emergence multidrug resistant cell states driven by non-genetic or complex multigenic mechanisms

That AML cells can become resistant to therapy through non-genetic mechanisms (e.g. through alterations of metabolic, epigenetic, apoptotic, and developmental cell states) is an idea that is currently supported by the repeated failure of sequencing studies to identify gene candidates with recurring mutations in matched AML patient samples (taken at diagnosis and relapse). In total, 13 studies have used NGS modalities (including whole genome sequencing [WGS], whole exome sequencing [WES], and targeted deep sequencing [TDS]) to examine pre- and post-treatment matched samples from a total of 180 patients diagnosed with various AML subtypes, including 31 patients with APML (Ding et al., 2012; Corces-Zimmerman et al., 2014; Garg et al., 2015; Tawana et al., 2015; Sood et al., 2016; Kim et al., 2016; Madan et al., 2016; Farrar et al., 2016; Masetti et al., 2016; Shiba et al., 2016; Hirsch et al., 2016; Shlush et al., 2017; Buelow et al., 2019). For any particular genetic alteration to qualify as a candidate driver of relapse, it should be gained at relapse across multiple patients, should not be recurrently lost at relapse in other patients (although it is possible that in a small subset of cases, cells with pre-existing relapse drivers at diagnosis could be outcompeted by the expansion of an undetected minor clone with a preexisting or acquired driver that is even stronger), and either not be detected in diagnosis samples, or if detected, be associated with poor therapeutic response.

The first landmark study to use this approach in AML was published by Ding et al. and uncovered several key concepts concerning leukemic evolution after therapy exposure (Ding et al., 2012). Using WGS followed by validation with deep sequencing of captured variants, matched somatic (skin), diagnostic, and relapse samples from 8 AML patients (n=7 normal karyotype AML, n=1 APML) were examined. This analysis revealed an average of 539 somatic

mutations and structural variants (detected in non-repetitive genomic areas) per case, of which, 21 affected protein coding regions. Most of these mutations could be detected at both diagnosis and relapse, with only a small proportion of these occurring specifically at disease recurrence. Patients were also found to harbor 1-4 genetically distinct clones at diagnosis, and all patients accumulated additional mutations at relapse, though surprisingly in three cases, none of these mutations were non-synonymous. Here, two main patterns of clonal evolution were described: 1. three patients gained additional mutations in the dominant clone as it evolved into the relapse clone, and 2. five patients gained additional mutations in minor subclones that expanded at relapse, including a loss of some of the initial lesions present at diagnosis. Transversions were also found to be enriched in among relapse-specific mutations, highlighting the mutagenic effects of chemotherapy and suggesting that through this property, therapy may have contributed to resistance, though no clear or direct mechanism could be found. In fact, when the authors searched for recurring mutations in biological pathways that could potentially underlie the relapse phenotype (e.g. metabolism, efflux pumps), strikingly, none could be identified.

The inability of the Ding et al. study to identify candidate relapse drivers could have been due to the small, heterogeneous sample size analyzed. However, this does not appear to be the case. Additional reports using larger or more homogeneous patient subsets were recently published, and uniformly, the data from all of these studies confirm the initial findings by Ding and colleagues (Corces-Zimmerman et al., 2014; Garg et al., 2015; Tawana et al., 2015; Sood et al., 2016; Kim et al., 2016; Farrar et al., 2016; Masetti et al., 2016; Shiba et al., 2016; Hirsch et al., 2016; Shlush et al., 2017; Buelow et al., 2019). In an extension to the clonal evolution patterns described by the Ding report, some of these newer studies have suggested an additional pattern. Specifically, these studies describe cases in both familial and sporadic AML in which the relapse clone(s) evolved from pre-leukemic HSPCs, generating a genetically discordant leukemia at relapse (Corces-Zimmerman et al., 2014; Tawana et al., 2015; Hirsch et al., 2016). Interestingly, this pattern had also been suggested in a previous study using single-nucleotide polymorphism (SNP) microarray profiling in 53 patients with *NPM1*-mutated AML (Krönke et al., 2013). Additionally, four studies examining matched pediatric AML samples by WES (n=35 patients in total) described findings that mirrored those in adult AML (Farrar et al., 2016; Masetti et al., 2016; Shiba et al., 2016; Buelow et al., 2019). One new interesting discovery from these data, however, came from Farrar and colleagues (Farrar et al., 2016). Here, analysis of 20 pediatric AML cases revealed an average of 3.5 non-synonymous mutations in patients less than 2 years of age, while older patients (2-17) had an average of 8 such lesions. This finding directly supports the notion

that most genetic lesions detected in AML are non-causal “passenger” mutations resulting from aging-induced changes.

Together, the aforementioned studies have revealed important concepts about tumor evolution in AML. However, they have also repeatedly failed to identify putative candidate genes that when mutated, could drive resistance in AML treated with combination chemotherapy. Possible exceptions to this statement include mutations in the splicing factor ZRSR2 and in the epigenetic proteins *ASXL1* and *SETBP1*. However, while these lesions fit all three criteria of a relapse driver outlined above, the actual number of patients in which they occurred was small (2-4 cases) (Garg et al., 2015; Hirsch et al., 2016; Papaemmanuil et al., 2016). Taken together, these data indicate that in AML treated with combination therapy, resistance is dominated by the emergence of multidrug resistant (MDR) cell states. Here, these phenotypes arise by either non-genetic or complicated multigenic changes, resulting in developmental, epigenetic, apoptotic, metabolic, and possibly other alterations that then promote blast survival and fuel resistance.

The abovementioned results stand in stark contrast to the clinical resistance mechanisms frequently observed in targeted AML therapies like arsenic trioxide, *all trans* retinoic acid, and FLT3 inhibitors. Here, resistance overwhelmingly occurs via direct mutations in drug targets (de Thé et al., 2017; Madan et al., 2016; Perl, 2017; Tyner et al., 2018). On the surface, this may seem like a property attributable to the agents themselves, as traditional chemotherapeutics are thought to be non-specific. While this might hold true for some chemotherapeutics, anthracyclines have been shown to kill cells partially though a direct interaction with topoisomerase II (topo II) that poisons this enzyme (Nitiss, 2009; Pommier et al., 2010). In fact, an RNAi screen completed in our lab using a mouse model of lymphoma directly showed that knockdown of topo II induced resistance to doxorubicin monotherapy both *in vivo* and *in vitro* (Burgess et al., 2008). Additionally, a recent screen in the near-haploid CML cell line KBM7 identified factors that promoted doxorubicin resistance by attenuating either the expression or function of topo II (Wijdeven et al., 2015). In the case of Ara-C, a nucleoside analog that induces DNA damage after it is incorporated into the genomes of replicating cells, broad non-targeted effects *are* expected. However, specific mutations in the proteins that transport (ENT1-2), metabolically activate (DCK), or detoxify (5’-nucleotidases [5-NT]) this pro-drug have been described *in vitro* (Marin et al., 2016). Clinically though, recurrent mutations in these Ara-C-related genes or in the gene encoding topo II have never been detected.

It is tempting to speculate that changes in drug-target interactions do not underlie resistance in AML because they are not easily selected for in the context of the multi-drug frontline therapy regimens used to treat it. Further, this seems to be a direct consequence of combining specific drugs in this specific disease, and not to the properties of the drugs themselves. Indeed, recent NGS studies in matched diagnosis and relapsed ALL (T-ALL and B-ALL) samples identified mutations in the 5-NT gene *NT5C2* (known to inactivate nucleoside analogs frequently used in ALL, including Ara-C) in almost 20% of all patients analyzed (17 of 126 B-ALL patients and 27 of 103 T-ALL patients) (Tzoneva et al., 2013; Meyer et al., 2013; Ma et al., 2015). Here, it is possible that either: A. the specific combination and/or timing of agents used in ALL more readily allows for the emergence of resistance driven by alterations in drug-target interactions. B. that ALL serves as a more permissive substrate on which these mutations might arise (i.e. ALL might be more dependent than AML on the specific pathways impacted by nucleoside analogs such that drug-target mutations would be more strongly selected for in ALL). or C. that characteristics of both the treatment regimen and the disease are at play here. Along the same lines, in sarcoma, topo II-dependent resistance mechanisms have been shown to re-emerge if the MDR phenotype that is normally selected for is simultaneously inhibited with cyclosporine, a substrate and modulator of efflux pump p-glycoprotein (PGP, encoded by MDR1) (Beketic-Oreskovic et al., 1995; Qadir et al., 2005). Either way, it is clear that in AML, single genetic changes that alter primary protein structures are not the underlying determinants of chemotherapeutic outcome. It is possible, of course, that additional sequencing studies examining larger, more homogeneous populations of AML patients will lead to the discovery of new candidate drivers. However, the observation that AML can relapse without the acquisition of any new non-synonymous mutations argues against this (Ding et al., 2012; Shiba et al., 2016; Kim et al., 2016). Thus, mutations in uncharacterized regulatory regions that lead to, for example, transcriptional changes, along with other non-genetic or complex multigenic changes likely underlie the biology of resistance in AML.

Together, the data summarized in part 1 of my thesis directly argue a need for new methodologies and suggest that at least in AML, a functional dissection of therapy-refractory phenotypes in the context of an intact TME is likely to be a more effectual approach. This underlies the rationale for the work in my thesis—specifically, for the completion of an *in vivo* RNAi screen in AML, in the context of frontline therapy. A brief review of some of these functional

approaches to examine drug resistance, particularly focused on hematological malignancies or CAR-T therapy, is provided later in part 3 of my introduction.

2. B-cell acute lymphoblastic leukemia (B-ALL)

In this section, I provide a brief overview of B-ALL as a disease entity with a focus on BCR-ABL+ B-ALL. This disease served as our cancer model for investigating *in vivo* specific mechanisms of CAR-T resistance, as outlined in chapter 3 of my thesis.

2.1. Epidemiology of B-ALL

Acute lymphoblastic leukemia is a disease driven by the clonal outgrowth of somatically transformed lymphoid progenitor cells that can emerge at any age, with approximately half of all cases occurring in children and teenagers (Hunger & Mulligan, 2015). In the United States, approximately 6,100 new ALL cases and more 1,500 deaths attributable to this disease occur annually (Siegel et al., 2020; SEER, 2020b). ALLs demonstrate a bimodal incidence, with the first and most significant peak occurring between the ages of 3 to 5 and a second peak occurring in elderly populations around the age of 60 (Appelbaum, 2020). ALL can be further sub-divided by the resemblance of leukemic blasts to normal hematopoietic lineages. B-cell-driven disease (B-ALL) accounts for more than 80% of all ALL cases, while disease driven by transformed cells from the T-lineage (T-ALL) comprise the remainder (Schwab et al., 2018). The median age of diagnosis in ALL overall is 17 years and today, it remains the leading cause of cancer-related death in children and adolescents under the age of 20, accounting for approximately 30% of all childhood cancers (Hunger & Mulligan, 2015; Mohseni et al., 2018; SEER, 2020b).

2.2. Disease characteristics and classification of B-ALL

ALL blasts are typically smaller than those seen in AML, are completely devoid of granules, and display a high nuclear to cytoplasmic ratio (Appelbaum, 2020). The surface immunophenotype of ALL blasts largely reflects a leukemic cell's level of maturation, and this feature provides prognostic information about the clinical course of the disease. In general, B-ALL blasts display a surface immunotype of CD19+ CD10+, CD24+ TdT+ surface-Ig-, with variable expression of other lymphoid markers such as CD20, CD22, and CD45. Additionally, up to 30% of precursor B-ALLs have been found to express some myeloid lineage markers (Campos-Sanchez et al., 2011). The specific surface phenotype of any specific ALL case

depends on the developmental stage at which it is paused and the underlying genetic lesions driving the disease.

Table 2.1. Summary of the B-ALL subtypes defined by the World Health Organization (WHO). Adapted from data in Arber et al., 2016.

Classification	Genetic Abnormality
B-lymphoblastic leukemia/lymphoma, Not Otherwise Specified	
B-lymphoblastic leukemia/lymphoma with recurrent genetic abnormalities	t(9;22)(q34.1;q11.2);BCR-ABL1
	t(v;11q23.3);KMT2A rearranged
	t(12;21)(p13/2;q22.1); ETV6-RUNX1
	Hyperdiploidy
	Hypodiploidy
	t(5;14)(q31.1;q32.3) IL3-IGH
	t(1;19)(q23;p13.3);TCF3-PBX1
	Provisional entity: BCR-ABL1-like
	Provisional entity: iAMP21

Like all acute leukemias, subtypes of ALL are classified using the WHO system which incorporates information on blast morphology, transcriptional profiles, immunophenotype, molecular genetic features, cytogenetic features, and clinical presentation to stratify the disease into subtypes (Arber et al., 2016). Using this approach, the WHO has divided B-ALL into two diseases: B-ALL with recurrent genetic abnormalities and B-ALL not otherwise specified (Table 2.1). Overall, the strongest prognostic factors in ALL are age and white blood cell count at diagnosis, with increases in either indicating a worsening prognosis. However, cytogenetic alterations also play a substantial role when risk stratifying B-ALL cases, as indicated by the inclusion of recurrent genetic abnormalities in the WHO classification scheme (Arber et al., 2016; Terwilliger & Abdul-Hay, 2017).

2.3. Pathobiology of B-ALL

The transformation process that leads to the emergence of fulminant leukemia in ALL is thought to occur in a step-wise fashion in HSPCs, with acquired mutations cooperating to fuel the emergence, maintenance and progression of the disease (Campos-Sanchez, 2011). The mutations that arise in ALL vary with age and ultimately define a heterogeneous collection of diseases. However, the mechanisms involved in leukemogenesis converge on similar properties: increased proliferation via translocations or genetic lesions that activate these pathways, an

inability to differentiate along with increased self-renewal via alterations to developmental TFs (losses or gains), and increased resistance to apoptotic signals (Inaba et al., 2013; Bernt & Hunger, 2014). Mutations in genes that are critical for B-cell development are a hallmark of ALL, highlighting the critical role that aberrant differentiation programs play in this disease (Somasundaram et al., 2015). In fact, more than 40% of B-ALL patients harbor lesions involving developmental transcription factors critical for lymphopoiesis, such as: PAX5, a known master regulator of B-cell development that enforces B-cell specific expression programs while suppressing B-lineage inappropriate gene expression at B cell commitment; EBF1, which acts in concert with other TFs like PAX5 to modulate epigenetic landscapes and specify B-cell fate; the gene encoding the IKAROS TFs (*IKZF1*), a critical regulator of lymphoid differentiation that is involved in at multiple levels of B-cell differentiation via various mechanisms, including chromatin modification through its interactions with epigenetic machinery in the cell; and TFC3, which collaborates with the developmental TFs IKZF1 and PU.1 to prime cells towards the lymphoid lineage (Zhang et al., 2017; Somasundaram et al., 2015). Additionally, inherited mutations in some of these developmental genes, including *PAX5* and the transcriptional repressor *ETV6* (also known as *TEL*) are associated with familial ALL (Hunger & Mulligan, 2015).

2.4. B-ALL does not follow a cancer stem cell model

Unlike other hematological malignancies, like AML where cancer is thought to follow a cancer stem cell model, countless studies have repeatedly failed to identify LSCs in ALL. Rather, various leukemic subpopulations across multiple stages of maturation that display disparate surface immunophenotypes have been shown to exhibit the characteristic features of an LSC, including the ability to initiate and maintain leukemia in secondary recipients (le Viseur et al., 2008; Bernt & Armstrong, 2009). In fact, studies using limiting dilution experiments in NSG mice (NOD/SCID/IL2R$\gamma^{-/-}$, a severely immunocompromised mouse model bearing a targeted deletion in the common interleukin receptor γ chain which eliminates the residual NK cell function of NOD/SCID predecessor mice) have shown that the frequency of LSCs in B-ALL is as high as one in 40. This number is likely to be an underestimate, given that these cells have to overcome xenotransplantation barriers to be defined as an LSC (McClellan & Majeti, 2013). Other studies have also repeatedly shown that ALL does not follow a hierarchical pattern of organization similar to that seen in normal hematopoiesis and consistent with a cancer stem cell model. For example, using PDXs, multiple studies have shown that both more immunophenotypically mature CD34- and more immature CD34+ blasts can each give rise to both CD34- and CD34+ cells in NSG

mice (le Viseur et al., 2008; Kong et al., 2008; Rehe et al., 2013). Additionally, both of these populations showed no differences in their transcriptional signatures with regard to stemness genes (Rehe et al., 2013). One mechanism by which stemness properties, such as dormancy and chemoresistance *have* been shown to be induced in this disease is through the interaction of B-ALL cells with their microenvironment (Ebinger et al., 2016). Interestingly, this stem-like phenotype was shown to be reversible, as dissociation from the *in vivo* environment sensitized cells to therapy and induced them to proliferate. Together, these data demonstrate that in ALL, stemness appears to be a ubiquitous or inducible feature of all blast cells present in the tumor, and that interactions with the TME appear to be critical for the induction and maintenance of this property in this disease. Overall, B-ALL appears to be a highly mutable cancer with a high level of intrinsic plasticity (Figure 2.1).

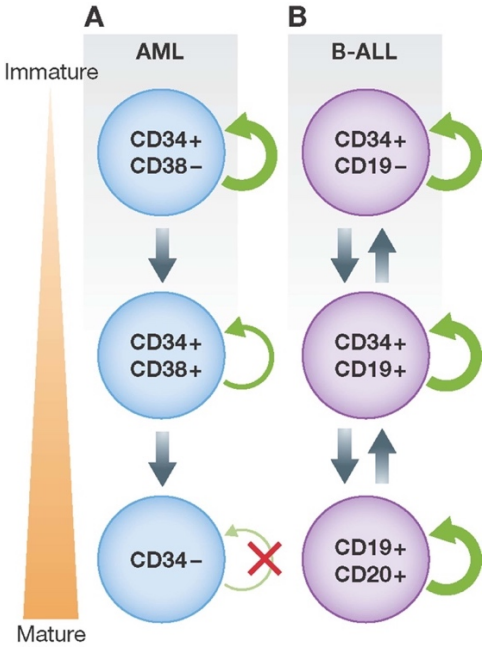

Figure 2.1. Unlike AML, B-ALL does not follow a cancer stem cell model.
(A) As discussed above, AML follows a traditional cancer stem cell model where self-proliferation capacity (indicated by the size of the green arrow) is largely restricted to the most immature blasts and become progressively lost as blasts mature.

(B) B-ALL does not follow a cancer stem cell model and instead, appears to follow a stochastic model. Here, most blasts display significant self-renewal capacity and are equally able to propagate disease in xenograft studies. Blasts also do not appear to be organized in a strict hierarchy.

Reprinted from McClellan, J. S. & Majeti, R. The cancer stem cell model: B cell acute lymphoblastic leukaemia breaks the mould. EMBO Mol. Med. ***5****, 7–9 (2013), with permission from John Wiley and Sons, Ltd on behalf of EMBO.*

2.5. B-ALL genetics

Cytogenetic aberrations are hallmark of B-ALL that also define various subtypes of the disease and provide prognostic information when they are detected clinically. The full list of recurrent genetic abnormalities delineated by the WHO is shown in Table 2.1 and includes hypodiploidy (with less than 44 chromosomes), hyperdiploidy (with a gain of at least 5 chromosomes), intrachromosomal amplification of chromosome 21 (iAMP21), and 6 translocations (Arber et al., 2016). Chromosomal rearrangements are thought to occur early in

the disease, possibly serving as initiating lesions, as these can often be detected in blood spots taken at birth, years before children present to the clinic with ALL (Hunger & Mullighan, 2015). Sequencing studies have also uncovered a number of secondary cooperative mutations that are associated with specific chromosomal aberrations and affect a myriad of cellular processes (Mullighan et al., 2007; Iacobucci & Mullighan, 2017). These include mutations in lymphoid-lineage TFs (*IKZF1*, *PAX5*, *EBF1*), apoptosis regulators, epigenetic factors, cell-cycle regulators and tumor suppressors (*CDKN2A/B*, *RB1*), and mutations that impart growth factor independence (*JAK1/2*). Overall, most, if not all B-ALLs are thought to harbor multiple cooperating lesions. The only exception to this rule seems to be in infant MLL-r ALL, a high-risk subtype where disease latency is remarkably short (with some patients presenting at birth with full-blown ALL). Here, the average number of driver mutations is exceedingly low at approximately 1.3, indicating that few, if any additional mutations (detectable by current technologies) are needed to transform cells (Krivtsov & Armstrong, 2007; Andersson et al., 2015).

2.5.1. BCR-ABL+ B-ALL

The Philadelphia (Ph) chromosome arises from a reciprocal translocation between chromosomes 9 and 22 [t(9;22)(q34;q11)], resulting in the formation of a chimeric oncogenic protein encoded by the 5' region of the *BCR* gene and almost the entire coding region (exons 2-11) of the *c-ABL* gene (Iacobucci & Mullighan, 2017). Named after the city in which it was first identified in the leukemic cells of a CML patient by Nowelll and Hungerford in 1960, the Ph chromosome can exist as two major isoforms that are named based on their molecular size and are each associated with different diseases (Nowell & Hungerford, 1960). The longest of these results from a translocation between the major "CML" breakpoint region of the *BCR* gene (between exons 12 and 16) and *cABL*, generating the p210 isoform found in most CML patients, although this isoform has also been found in 25-50% of adult Ph^+ ALL cases (Bernt & Hunger, 2014; Mohseni et al., 2018). Translocations that occur in the minor "ALL" breakpoint region located in intron 1 generate the smaller p190 isoform that retains only the first exon of the *BCR* gene and is commonly detected in Ph+ B-ALL. In ALL, the incidence of this BCR-ABL lesions increases with age, occurring in 2-5% of all pediatric cases (90% will be due to p190), in 20% of all young adult cases, and in up to 40% of cases affecting the elderly (50-75% will be due to p190) (Jain et al., 2017; Mohseni et al., 2018).

Early pivotal studies showed that expression of either isoform in BM cells was sufficient to induce either a CML-like disease (p210) or acute leukemias (p190) in mice, providing

conclusive evidence of this genetic lesion's role as an oncogenic driver (Daley et al., 1990; Heisterkamp et al., 1990). Shortly thereafter, another landmark study used a mutant version of BCR-ABL with an inactive tyrosine kinase domain to show that it was unable to transform cells (Lugo et al., 1990). This indicated that ABL1's enzymatic activity was indispensable for the fusion protein's oncogenic properties. Indeed, the recent discovery of Ph-like B-ALL with translocations that do not include *BCR* but often involve ABL kinases (along with other protein kinases, like JAK-STAT pathway members) support this idea (Jain et al., 2017; Roberts et al. 2017). That BCR-ABL's oncogenic properties resided in ABL's tyrosine kinase activity suggested that targeted inhibition of this domain would be an effective therapeutic strategy in this disease. Through work spearheaded by Brian Druker, the first tyrosine kinase inhibitor (TKI), Imatinib, was developed and later approved by FDA in the year 2000 (Druker et al., 1996; Druker et al., 2001a; Druker et al., 2001b; O'Brien et al., 2003). While monotherapy with imatinib or other second and third generation TKIs can prevent CML from progressing to terminal stages of the disease (i.e. blast crisis), monotherapy in Ph^+ B-ALL does not show long-term effectiveness, with initial responses rapidly progressing to TKI-resistant disease through mutations in the ABL1 kinase domain that are now well-described in the literature (Bernt & Hunger, 2014). A better approach has been to incorporate these TKIs into combinations with traditional therapeutics, a strategy has revolutionized the treatment of Ph+ B-ALL, leading to significantly better rates of overall survival in these patients. Still, outcomes in this disease lag behind those of other B-ALL subtypes, particularly in older adult populations where the overall 5 year survival rate is only 20% (Geyer et al., 2017).

Mechanistically, fusing BCR to ABL results in the loss of ABL's N-terminus autoinhibitory domain along with homodimerization and autophosphorylation of the chimeric protein (Bernt & Hunger, 2014). Ultimately this leads to the constitutive activation of ABL's tyrosine kinase activity. Aberrant phosphorylation of an assortment of targets activates multiple downstream pathways, including MAPK, EGFR, Ras, c-Myc, PI3K, AKT, MTOR, SRC family kinases, NF-kB, and JAK-STAT, while also altering apoptotic signaling to promote proliferation (Sattler & Griffin, 2003; Mohseni et al., 2018). Unlike in CML where BCR-ABL is sufficient to drive disease, Ph+ B-ALL has been shown to harbor additional alterations that contribute to leukemogenesis, the commonest of these being LOF mutations in *IKZF1* (found in 70-80% of cases), *PAX5* (lost in 50% of cases), and *CDKN2A/B* (lost in 50% of cases) (Bernt & Hunger, 2014; Liu et al., 2016). Loss of Ikaros and Pax5 have been shown to lead directly to blocks in differentiation, whereas loss of the *CDKN2A/B* has been linked in HSC self-renewal. Together, the *CDKN2A* and

CDKN2B genes encode three tumor suppressors, two of which inhibit cyclin-dependent kinases ($p16^{INK4A}$ from *CDKN2A* and $p15^{INK4B}$ from *CDKN2B*) and one of which directly inhibits the ubiquitin ligase, HDM2 (Mdm2 in mice) to stabilize TP53 ($p14^{ARF}$, or $p19^{Arf}$ in mice, [also known as just ARF] from *CDKN2A*) (Bernt & Hunger, 2014) (Figure 2.2).

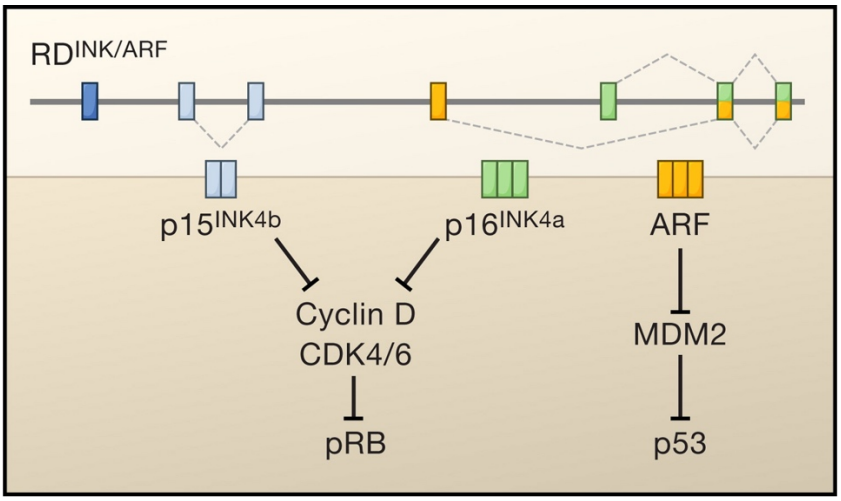

Figure 2.2. The INK4a/ARF/INK4b locus encodes three tumor suppressor genes within 35 kilobases. The gene *CDKN2B* (blue) encodes *p15INK4b* while *CDKN2A* (green and yellow) encodes *p16INK4a* and *p14ARF* (in humans, shown above as ARF; *p19Arf* in mouse). Together, these genes suppress tumor formation via the RB and TP53 pathways.
Reprinted from Cell, 127, Kim, W. & Sharpless, N. The Regulation of INK4/ARF in Cancer and Aging, 265–275, 2006, with permission from Elsevier.

2.5.1.1. BCR-ABL+ B-ALL mouse model

In chapter three of my thesis, I describe the set up and preliminary results of parallel genome-wide *in vitro* and *in vivo* screens for CAR-T resistance. For these experiments, we use a transplantable C57BL/6 mouse model of Ph+ $Arf^{-/-}$ B-ALL developed by the Sherr lab (Williams et al., 2006; Williams et al., 2007). Briefly, cells from whole BM were isolated from C57BL/6 $Arf^{-/-}$ mice, retrovirally infected with human p190 BCR-ABL, and plated on IL-7 secreting stroma which selects for the outgrowth of pre-B cell cultures. One week later, leukemic cells with a uniform immunophenotype of $B220^{+}$ $CD19^{+}$ $CD24^{+}$ $Sca1^{-}$ $cKit^{-}$ $Gr1^{-}$ $Mac1^{-}$ IgM^{-} that proliferated in an IL-7 independent manner emerged. Cytokine independent growth is a direct result of BCR-ABL signaling, while loss of the Arf tumor suppressor is necessary to destabilize p53 protein, thus allowing cells to evade apoptosis due to excessive oncogenic signaling (Williams et al., 2006; Bernt & Hunger, 2014). When these cells were transplanted into immunocompetent, syngeneic, non-irradiated 12-week-old mice, a highly penetrant leukemia that closely resembles human B-

ALL and has a predictable 2 week latency emerged. Limiting dilution experiments performed in non-irradiated hosts showed that as few as 20 cells can induce fulminant B-ALL with a latency of 3 weeks, indicating an exceedingly high LSC frequency that was estimated to be one in every two cells (Williams et al., 2007).

2.6. B-ALL therapy

Frontline therapy for B-ALL is given over 2.5 to 3 years and is generally split up into remission-induction, consolidation (or intensification), and continuation (or maintenance) phases (Hunger & Mulligan, 2015; Inaba et al., 2013). Induction therapy is intended to reinstate normal hematopoiesis and induce remission. This therapy lasts 6 to 8 weeks and includes treatment with a glucocorticoid, vincristine, asparaginase, an anthracycline (though this is optional), and intrathecal chemotherapy to eliminate CNS disease. Six to eight months of intensive combination chemotherapy then follows in the consolidation phase and is intended to eliminate residual leukemic cells in the body. Therapy here normally includes drugs used in induction therapy along with the addition of various antimetabolites, including repeated cycles of methotrexate and a nucleoside analog (such as Ara-C or 6-mercaptopurine [6-MP]). Finally, the maintenance phase includes 18 to 30 months of low-intensity antimetabolite therapy consisting of daily oral 6-MP or thioguanine and weekly oral methotrexate along with weekly glucocorticoids and vincristine. Using this therapeutic approach, the overall 5-year survival rate in Ph+ B-ALL stood at less than 20% (Short et al., 2016). Today, the addition of BCR-ABL inhibitors to combination chemotherapy regimens in this genetic subtype has more than doubled this figure, with long-term survival seen in 30-50% of all patients (Inaba et al., 2013). However, compared to a survival rate of nearly 70% in ALL as a whole, outcomes in Ph^+ B-ALL clearly still lag behind despite amazing progress in the last few decades. When outcomes are stratified by age, this discrepancy is even more obvious. B-ALL is associated with high cure rates of nearly 90% when it is diagnosed in children. In adults, outcomes have remained steady over the last two decades and are much more modest, with only about 30-40% of all adult ALL patients achieving a cure despite high rates of CRs in this population (Ronson et al., 2016). Additionally, patients who manage to survive B-ALL, including children, must often endure long-term side-effects of the intensive cytotoxic therapy regimes used to cure them.

2.6.1. Chimeric antigen receptor T-cell (CAR-T) therapy—a brief history

The idea that a patient's immune system can be deliberately (re-)mobilized against an encroaching tumor in order to eradicate it from the body, known today as cancer immunotherapy (CI), is one that dates back to the mid 19th century. In the 1880s, German physicians Fehleisen and Busch independently observed tumor reductions in cancer patients who had accidentally developed skin infections, a phenomenon that had been described in the literature as early as 3000 years prior in ancient Egypt (Oiseth & Aziz, 2017). Their subsequent attempts to recapitulate these effects by purposefully inoculating cancer patients with pathologic bacteria marked the first attempt at CI and produced a limited amount of mixed, but overall, disappointing results. Similarly, the American surgeon William Coley, today considered the Father of Immunotherapy, began injecting mixtures of live and heat-inactivated pathogenic bacteria directly into the tumors of patients with inoperable bone cancers in 1891 (Dobosz & Dzieciątkowski, 2019). "Coley's toxins," as they came to be known, were subsequently reported to result in over 1,000 cures and regressions. However, inconsistent results and patient deaths from the infectious agents themselves ultimately caused this approach to fall out of favor amongst physicians, casting CI back into obscurity. Nonetheless, after more than 100 years of staggering scientific discovery and at least five major shifts in the stance toward CI, these early concepts have finally found their home amongst the modern oncologist's armamentarium, with immunotherapy now constituting the "fifth pillar" of cancer treatment.

One of the most promising CI approaches in cancer care today is the adoptive cell transfer (ACT) of autologous T lymphocytes engineered to express chimeric antigen receptors (CARs) that redirect them towards a patient's tumor (Figure 2.3). Despite only obtaining approval by the FDA in 2017, CAR-T cells represent more six decades of research aimed at understanding and harnessing the mechanisms of cellular immunity for the fight against cancer (Singh & McGuirk, 2020). The first indication that anti-tumor cellular components could be successfully grafted onto a recipient's immune system came in 1955. Here, the transfer of cancer-adjacent lymph nodes from donor mice was shown to induce tumor regressions in recipient animals, but only if viable cells were transplanted (Mitchison, 1955). By the 1980s, the discovery of thymic function and T cells by Miller, along with advancements in inbred mouse models allowed researchers to establish that T lymphocytes possessed potent anti-tumor properties via similar transplantation studies (Miller, 1961; Rosenberg & Terry, 1977). Inspired by these data, Rosenberg and colleagues began exploring the therapeutic applications of ACT by treating solid tumor patients with autologous infusions of IL-2-activated cytotoxic T cells and tumor infiltrating

T lymphocytes (TILs) after lymphodepleting chemotherapy, a critical step that creates an environment conducive to T cell proliferation (Rosenberg et al., 1986; Rosenberg et al., 1988). Notably, patients treated on these protocols are already highly refractory to chemotherapy, and in this context, lymphodepleting therapy was thought to have minimal direct effect on tumor cell killing. Major limitations of TIL therapy soon emerged however, including its reliance on the presence, isolation, and expansion of tumor-specific T cells. This tedious protocol, when possible, is used to produce TILs on the order of tens to hundreds of billions per patient, on average (Rosenberg & Restifo, 2015). Additionally, this approach is further hampered by the propensity of cancer cells to downregulate antigen-processing and presentation pathways (i.e. major histocompatibility complex (MHC) class I molecules), a known mechanism deployed by malignancies to avoid T-cell-mediated killing (Vinay et al., 2015). Around the same time, independent investigations from the BM transplantation field began reporting that hematological malignancies could sometimes be eradicated by allogeneic donor T cells via graft-versus-leukemia (GVL) effects (Horowitz et al., 1990). However GVL can also extend to other native cells resident in the recipient's body, leading to the devastating pathology of graft-versus-host disease (GVHD) (Ferrara et al., 2009). Together, these early pivotal studies highlighted the double-edged roles that T lymphocytes can play in human disease and pointed to a need for better therapeutic T cell products that were enriched for anti-tumor components and depleted of potentially harmful cells.

In a landmark study published in 1989, Eshhar and colleagues provided one clear path towards necessary improvements in therapeutic T cells when they successfully grafted the antigen-recognizing domains of an antibody onto the constant α-/β- chains of the T cell receptor (TCR) and transfected this construct into T cell hybridomas (generating T bodies) (Gross et al., 1989). The creation of this first T cell-based CAR represented the earliest proof-of-concept that lymphocytes could be genetically redirected towards tumor cells and provided the initial design from which modern CAR-T constructs evolved. More broadly, the development of this synthetic biology approach, along with the concurrent generation and application of replication-defective viral vectors by Baltimore, Miller and Sadelain, revolutionized the nascent field of cell engineering and ultimately established therapeutic T-cell engineering as its own, novel field of study (Mann et al., 1983; Miller, 1990; Sadelain & Mulligan, 1992). Today, CAR designs have changed significantly, representing critical advancements in many disciplines, such as protein engineering, cell manufacturing sciences, viral biology, immunology, and synthetic biology. Exciting new data has shown that novel CAR design strategies can also be used to generate

these “living therapies” from other immune cell types (e.g. macrophages and natural killer cells) (Shimasaki et al., 2020; Klichinsky et al., 2020). Additionally, significant efforts to generate allogeneic “off-the-shelf” CAR-T cells are also underway (reviewed in Depil et al., 2020). However, the remainder of this section is primarily focused on autologous 2nd generation αβ CAR-T cells, as these are currently the most widely used CAR-T products in oncology and because we use 2nd generation CARs in our experiments.

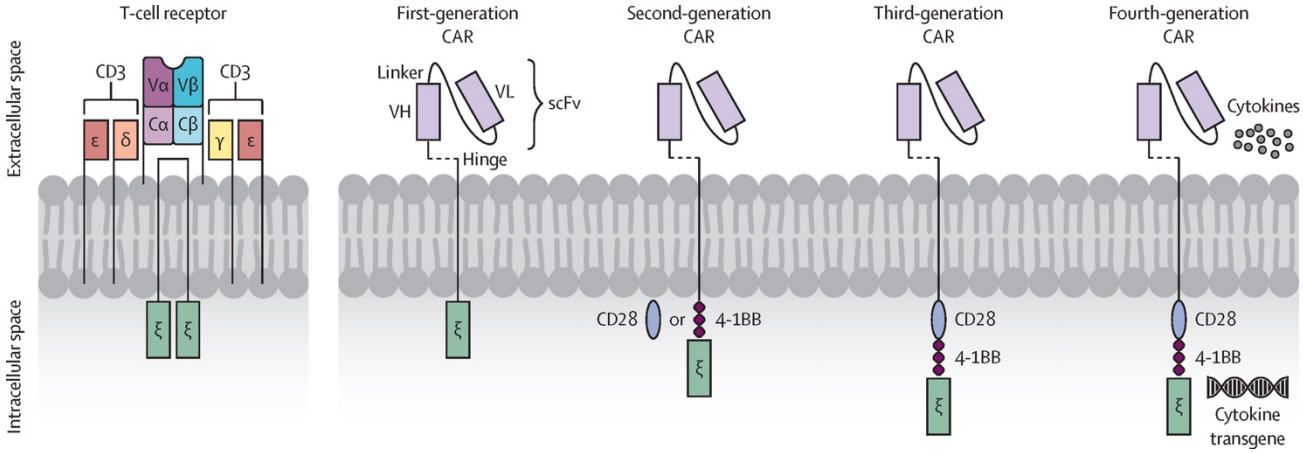

Figure 2.3. Engineered T cells: Structure of the T-cell receptor (TCR) versus chimeric antigen receptors (CAR). T-cells can be genetically re-directed towards a malignant cell via the expression of synthetic CARs that target a specific tumor associated antigen. Different generations of CARs vary in terms of the number of intracellular costimulatory domains present and the incorporation of additional cytokine genes or cytokine receptor signaling domains, either in *trans* (as shown) or on the CAR itself (not shown). *Reprinted from The Lancet Oncology, 21, Singh, A. K. & McGuirk, J. P. CAR T cells: continuation in a revolution of immunotherapy. e168–e178, 2020, with permission from Elsevier.*

2.6.1.1. The biology of T cell-mediated killing

In order to understand the rationale behind the CAR alterations that eventually gave us modern CAR-T cell therapy, an appreciation of normal TCR-based killing is required (reviewed in Broere & Eden, 2019). Normally, tumor-specific T lymphocytes are primed to eliminate malignant cells after they interact with and are stimulated by antigen presenting cells (APCs), the most common of which are dendritic cells (DCs). The interface between the T cell and APC is intricate, involving the interaction of receptors on either cell with their cognate ligands on the other. Proper activation of T cells has been shown to require at least 2 specific types of receptor-ligand interactions, leading to the co-stimulatory, or 2-signal model of T cell activation. The first signal is antigen/TCR specific and is delivered to the T cell through the interaction of its clonal TCR-CD3 complex, including its CD8 or CD4 accessory molecule (depending on the type of T cell), with its cognate peptide-MHC (pMHC) complex (formed when an antigen is processed and

bound to either an MHC-I or MHC-II molecule) present on the surface of an APC. This interaction initiates signals downstream of the TCR, through CD3 members and CD8 or CD4, depending on whether the cell is a cytotoxic (CTL) or helper T cell, respectively. On its own, signal 1 is not sufficient to activate a T cell and when given without signal 2, can lead to activation induced cell death (AICD) (an important mechanism of immune tolerance and homeostasis) and/or anergy (a type of unresponsive cell state) (Chen & Flies, 2013). Delivery of the second signal to the T cell Is also accomplished by the APC. The main receptor families on T cells that are involved in this co-stimulatory event are: 1. The CD28 family, including CD28 and ICOS which interact with their APC-bound cognate ligands CD80/CD86 and B7-H2, respectively; and 2. The tumor necrosis factor receptor superfamily (TNFRSF), including 4-1BB, CD27, and OX40L which interact with their own APC-bound ligands 4-1BBL, CD27L, and OX40L, respectively. While signal 1 ensures the potential activation of an antigen-specific T lymphocyte by an APC, signal 2 can have varying effects on T cell fate, including subsequent effector functions, the establishment of memory, and survival (Chen & Flies, 2013). After receiving both signals, the T cell is primed and activated, leading to the release of cytokines (i.e. interferon [INF]-**γ**, granulocyte-macrophage colony-stimulating factor [GM-CSF], IL-2) that, among other things, promote its subsequent proliferation and induce apoptosis in target cells. After a cancer-specific $CD8^+$ T cell finds its way into the tumor and uses its TCR complex to bind its cognate antigen displayed within an MHC-I molecule, the T lymphocyte unleashes a cytolytic cascade that kills the target cell via two distinct mechanisms: 1. exocytosis of cytotoxic granules containing perforin and granzymes, and 2. the secretion or surface expression of ligands that induce target cell apoptosis upon binding their cognate receptor (Halle et al., 2017). These include membrane bound molecules such as TNF-related apoptosis-inducing ligand (TRAIL) and Fas ligand (FasL), and cytokines such as INF**γ**.

2.6.1.2. CAR anatomy and clinical efficacy

The first major alteration to the T-body CAR was the integration of the antibody targeting region with signaling domains from the TCR-CD3 complex into one single polypeptide chain, yielding first generation CARs (Daniyan & Bertjens, 2016). Here, the V_L and V_H chains of an antibody are combined using a flexible linker to generate an scFv (single chain variable fragment) which is then attached in line to a hinge (or spacer) region derived from the membrane proximal portion of CD8. Finally, the hinge is fused in frame with the most powerful activating component of the TCR-CD3 complex, the ζ chain, a molecule that normally exists as a homodimer. When transduced into T lymphocytes, the resulting CAR-T cells could recognize antigens and kill target

cells in an MHC-independent fashion (Moritz et al., 1994). Other CARs that substitute scFvs for ligand domains or the antigen binding region of a TCR that can engage specific pMHC complexes (allowing CAR-T cells to detect intracellular proteins) have also been reported (Frigault & Maus, 2020). Preclinical *in vitro* studies using first generation CAR-T cells demonstrated that they were functional, as they were able to specifically kill target cells, secrete growth promoting/immunomodulatory cytokines, and proliferate in response to CAR stimulation. In subsequent *in vivo* experiments, single infusions of first generation CAR-T cells were shown to be able infiltrate solid tumors derived from transformed NIH3T3 cells and slow their growth (Altenschmidt et al., 1997). However, unless they were repeatedly injected directly into cancer sites over many days, these first-generation CAR-T cells were unable to eradicate tumors. Properly activated T or CAR-T cells will continue to expand in response to repeated antigen exposure (Maher et al., 2002; Chen & Flies, 2013). First generation CAR-T cells did not exhibit this property and instead became anergic both *in vivo* and *in vitro*. Hence, no substantial clinical responses could ever be achieved in patients treated with this first iteration of CAR-T therapy (Kershaw et al., 2006; Pule et al., 2008; Till et al., 2008; Savoldo et al., 2011).

In order to incorporate a second signal into first generation CARs while still maintaining them as a single chain receptors, the Sadelain lab devised an unnatural receptor design that combined multiple signaling domains (Maher et al., 2002). Here, researchers introduced a CD28 costimulatory domain between the transmembrane and T-cell activating domains of the CD3ζ chain. In an elegant set of experiments, Maher and colleagues showed that unlike first generation constructs, these second-generation CARs were able to induce human primary T cells to proliferate and expand in number upon serial exposure to antigen *in vitro*. Soon thereafter, other groups published similar constructs containing alternate costimulatory molecules that were later shown to each induce distinct cytokine secretion profiles, persistence potential, killing kinetics, and other functional properties (reviewed in Daniyan & Brentjens, 2016). The most commonly used costimulatory molecules used at the time were CD28 and 4-1BB, as these proteins had already been established as important mediators of 2nd signal stimuli. As in the Maher report, subsequent studies repeatedly demonstrated that 2nd generation CARs outperformed 1st generation CARs both *in vitro* and *in vivo* (Savoldo et al., 2011; Daniyan & Brentjens, 2016). One notable exception, however, came from Carl June's lab where researchers directly compared CD28, 4-1BB, or 1st generation CARs both *in vitro* and *in vivo* (Milone et al., 2009). Interestingly, multiple lines of data from *in vitro* experiments completed in this study suggested that the CD28-CAR was more efficacious, with these CARs showing significantly more proliferation and

cytokine release in response to target antigen exposure. Surprisingly, however, when both of these constructs were tested in NSG mice bearing human CLL tumors, CAR-T cells generated with the 4-1BB molecule substantially outperformed those generated with CD28. Here, 4-1BB CAR-T cells showed increased persistence over at least the 6 months in which they were studied and displayed a more central memory differentiation state. These CAR-T cells also induced more significant life extensions in animals—a change that could not be appreciated in cell-based studies. Indeed, the CAR-T field continues to be challenged by an inability to effectively detect differences in CAR-T cell efficacy using only *in vitro* approaches. Based on these preclinical results, the June lab decided to pursue 4-1BB based CARs (Kymirah, or tisagenlecleucel [tisa-cel]) for subsequent clinical trials. Strangely, this study also showed that the specific CD28-based CAR tested could not outperform 1st generation constructs, results that directly contradicted previous data generated in the June lab itself and data that were emerging from the Rosenberg lab at the NIH's NCI around the same time (Carpenito et al., 2009, Kochenderfer et al., 2009).

Concurrent preclinical efforts by the Rosenberg group led researchers there to compare a 2nd generation CD28-CAR and a 3rd generation CD28-4-1BB-CAR, based on previous experiments that demonstrated the superiority of these two vectors over a 2nd generation 4-1BB-CAR independently cloned in the lab (although these results were not shown) (Kochenderfer et al., 2009). Here, researchers showed that the CD28-CAR construct was superior in its ability to infect and produce CAR-T cells, leading to more robust cytokine release and greater expansion after *in vitro* antigen exposure using human CLL cells. For these reasons, the Rosenberg group decided to pursue the 2nd generation CD28-CAR (Yescarta, or axucabtagene ciloleucel [axi-cel]) for subsequent clinical trials. Significant differences between the methods employed in the June and Rosenberg studies, including CAR design, transduction, and expansion methods made a head to head comparison of 4-1BB versus CD28 impossible. Later, more robust comparisons were made, finding that CD28-based CARs promote rapid T cell proliferation, a shift towards glycolytic metabolism through activation of the PI3K-AKT pathway, and self-limited CAR-T persistence based on a more effector T cell differentiation phenotype. Conversely, 4-1BB-based CARs induced a less potent effector T cell but stimulated greater oxidative metabolism, greater frequency of central memory T cell phenotypes, less CAR-T cell exhaustion, and greater CAR-T persistence (Kawalekar et al., 2016; Daniyan & Brentjens, 2016). The clinical ramifications of these differences are still being investigated, however some early studies have shown that CAR-T cell persistence is correlated with remissions in 4-1BB-CAR therapy, while peak *in vivo* CAR-

T expansion and pretreatment disease burden are the best predictors of short term responses, remission duration, and OS in CD28-CAR therapy (Maude et al., 2014; Turtle et al., 2016; Park et al., 2018). Together, these results demonstrate the plasticity inherent in T cell reprogramming by CAR constructs and show that T cell fate is substantially impacted by the specific signaling molecules used in this process. Importantly, these results also indicate that clinicians could end up having a choice of administering either short-lived (CD28) or long-lived (4-1BB) CAR-T cells, depending on the cancer type and the risk of ongoing on-target, off-tumor toxicity. Finally, in the absence of direct evidence, it is tempting to speculate that a mix of both 4-1BB and CD28 CAR-T cells will ultimately be more efficacious than either CAR alone. Here, I would expect that combining CARs would more closely recapitulate normal immune responses which are initially dominated by effector T cell function (mediated by CD28 CARs) but also establish long term immunity via the formation of memory T cells (accomplished with 4-1BB CARs). This approach would likely require significant optimization, including the determination of ideal 4-1BB:CD28 CAR ratios, best T cell types or populations to transduce with either/both CAR constructs, and which diseases are best targeted with this approach.

The key to the initial successful use of CAR-T therapy involved understanding how to achieve optimal CAR-T cell function as well as selection of optimal tumor cell surface antigens (Sadelain, 2015). Situations in which target antigens are expressed on both tumor cells and healthy tissue cells (even if expression is very different between cell types) can quickly turn deadly, as reported with an ERBB-targeted CAR-T cell used in a recent clinical trial (Morgan et al., 2010). Here, a metastatic colon cancer patient died after CAR-T cells began lysing normal lung epithelial cells expressing low levels of ERBB, exemplifying the danger of on-target, off-tumor toxicity inherently associated with this treatment modality. Fortunately, by the time these toxicities began to emerge in the literature, rituximab, an anti-CD20 therapeutic antibody developed to treat B-cell-driven malignancies had already found broad use in the clinic (Storz, 2014). Data from rituximab treated patients indicated that acute loss of normal B cells was well tolerated and did not lead to an increase in infection rates. Additionally, eliminating normal B cells in the context of this treatment modality may actually have been beneficial, as it could prevent the generation of antibodies against the CARs themselves. This anti-CAR phenomenon had already been reported to occur in patients treated with non-CD19 CARs that also contain murine components (Lamers et al., 2011; Maus et al., 2013). The clinical success of rituximab led to the idea of CARs targeting CD19. Like CD20, CD19 expression is almost exclusively restricted to B-cells (with the only exception being some populations of follicular dendritic cells)

and is not expressed in hematopoietic stem cells (Sadelain, 2015). Additionally, CD19 was known to be expressed on most B-cell driven hematopoietic malignancies, including those resembling the earliest pro-B cell progenitor. Together, these characteristics suggested that CD19 was an ideal tumor associated antigen (TAA) to target, and that testing new 2nd generation CARs in B-cell driven human hematopoietic malignancies would likely provide the best chance of success.

Remarkably, when tested clinically, both the Rosenberg and June CD19-targeting CAR-T cells unexpectedly induced unprecedented rates of complete remissions in patients bearing therapy-refractory and multiply relapsed B cell malignancies of various origins that were uniformly associated with poor outcomes. These included cases of relapsed B-ALL, CLL, and diffuse large B cell lymphoma (DLBCL, the most common type of non-Hodgkin lymphoma [NHL]) (Kochenderfer et al., 2010; Brentjens et al., 2011; Porter at al., 2011). Subsequently, three pivotal clinical trials showed CR rates of 57% in DLBCL patients treated with CD28-based CARs, 81% in pediatric B-ALL patients treated with 4-1BB-based CARs, and 40% in DLBCL patients treated with 4-1BB-based CARs, responses that were shown to persist in at least half of all patients over 12 months of follow up (Locke et al., 2017; Maude et al., 2018; Schuster et al., 2019). Early stellar results from these trials led to FDA and European Medicines Agency approvals for both the 4-1BB-containing tisa-cel and the CD28-containing axi-cel CAR-T cell products in 2017, representing the first approved gene therapies in the U.S. This approval solidified CAR-T therapy as one of the greatest breakthroughs in cancer care since chemotherapy and established a robust CAR-T cell therapy market in biopharma/biotechnology, with over 300 clinical trials approved world-wide.

Today, numerous ongoing or completed CAR-T trails in hematological malignancies are corroborating the results of these early studies, including the fact that of all blood cancers, B-ALL appears to respond best to this treatment modality (June et al., 2018). However, significant differences in manufacturing processes, T cell sources (allogenic vs. autologous), expansion protocols, chosen patient populations, and CD19 malignancies targeted have also led to substantial fluctuations in CR rates, making direct efficacy comparisons between diseases or between CAR-T cells used (axi-cel vs. tisa-cel) difficult. Overall, overwhelmingly positive results continue to emerge in hematological malignancies, with various large studies showing CR rates of 30 to 70%, or sometimes, more than 90%, a particularly shocking result given the overwhelming amount of untreatable therapy-refractory cases represented in this figure (Singh & McGuirk, 2020). With more data amassing over time, success with CAR-T cells also seems to be different among hematopoietic disease types. In NHL, overall response rates (ORRs) of 50-

84% and CR rates of 40-59% have been reported, with long term response rates of 30-40% (follow up time of 6-27 months) and a median overall survival of 12 months (Chavez et al., 2019). These results are significant given data from a historical cohort of 600 relapsed NHL patients where ORRs of 26% and CR rates of 7% were reported, along with a mean overall survival of only 6.3 months (Neelapu et al., 2017). In B-ALL, ORRs of 81% to >90% and CRs of 68% to >93% have been reported, with long term response rates of 55-79% (follow up time of 12-29 months) and a median overall survival of 12.9 to 20.1 months, depending on the severity of the initial disease (Park et al., 2018; DiNofia & Maude, 2019). Here, these results are also striking, given that the mean overall survival for relapsed B-ALL has been reported to be as low as 4.6 months (Ronson & Rowe, 2016).

Efforts to continue to optimize CAR constructs and expand them to non-$CD19^+$ cancers, a feat that has been particularly difficult in solid tumors, are currently ongoing (reviewed in Tokarew et al., 2019 and Frigault & Maus, 2020). BCMA (B-cell maturation antigen) and CD22 have recently emerged as promising targets in $CD19^-$ B-cell malignancies such as multiple myeloma, while EGFRvIII, a mutant protein that arises from an in-frame deletion of exons 2-7 in wild-type EGFR, is starting to generate promising results in glioblastoma multiforme (GBM) (Brown et al., 2016; Raje et al., 2019; Akhavan et al., 2019). A plethora of 4^{th} and 5^{th} generation CAR constructs based on alterations to 2^{nd} generation CARs have also entered the field (Tokarew et al., 2019; Frigault & Maus, 2020). These generations incorporate changes that induce CAR-T cells to secrete cytokines (e.g. IL-12, IL-15) or that allow them engage cytokine signaling pathways by including signaling domains of cytokine receptors in CARs themselves (e.g. IL-2Rβ chain fragments), greatly promoting tumor killing. Still other groups have focused on broad array of other approaches, such as modulating the affinity of antigen binding, utilizing specific T cell subsets for transduction, combining CARs with checkpoint inhibitors or incorporating changes that antagonize the inhibitory effects of PD-1/Fas/TGFβ, and using, for example, CRISPR-Cas9 mediated genome engineering to express CAR constructs from endogenous TCR loci. This last approach is especially worth noting. Here, direct targeting of CAR constructs to the native TCR α chain (*TRAC*) locus induced few appreciable improvements *in vitro* (except for a reduction in the amount of exhaustion markers expressed on CAR-T cells, a phenotype that has not been predictive for CAR-T success across clinical trials), but produced strikingly superior life extension *in vivo*, as compared to CAR-T cells generated via normal viral transduction protocols (Eyquem et al., 2017; Shah & Fry, 2019). This study highlights the TME-based dependency that this treatment modality exhibits, arguing that any CAR-T study aimed at improving their efficacy

should include *in vivo* assays. This study also emphasizes a need to better understand the intricacies of TCR biology so as to incorporate the most important regulatory aspects of TCR signaling/transcriptional dynamics into CAR-T cell design. Critically, Carl June recently reported the successful use of this same approach in three patients, indicating that genome engineering of human CAR-T cells using CRISPR-Cas9 is safe and effective, while concomitantly opening the door for future applications of this editing technology in this treatment modality (Stadtmauer, 2020). Undoubtedly, further development of this new immunotherapy approach will continue to transform the way in which we treat cancers, likely getting us one large step closer to victory in the fight against cancer.

2.6.1.3. Mechanisms of resistance to CAR-T therapy

A complete appreciation of the true efficacy of any cancer treatment requires the existence and collection of long term follow up data. As a young therapy, such data for CAR-T cells have only recently begun to emerge but suggest that the problem of relapse is likely to be significant. Current studies have reported that as many as 60% of all patients will eventually relapse after CD19-directed therapy, the majority of which will occur within just 1 year of CAR-T cell infusion (Shah & Fry, 2019; Cheng et al., 2019). The best data available to date is also showing that durable responses following CAR-T therapy is highly variable between cancer types, with long term response rates of 30-40% and 55-79% reported in NHL and B-ALL, respectively (Park et al., 2018; DiNofia & Maude, 2019; Chavez et al., 2019). Additionally, 10-20% of all blood cancer patients treated with CAR-T cells will fail to experience any benefit at all. Moreover, in solid malignancies, CAR-T cells have been shown to have very limited effects, save for several notable patients (Majzner & Mackall, 2019; Bagley & O'Rourke, 2020). Importantly, relapse does not appear to be an exclusive feature of CD19-directed therapies, as early clinical data from other targeted TAAs, such as EGFRvIII and CD22, indicate that disease recurrence will be a frequent and ongoing challenge in this treatment modality (Fry et al., 2018; Majzner & Mackall, 2018; O'Rourke et al., 2017). As CAR-T cells become increasingly integrated into cancer care, a better understanding the biological basis of response and relapse in this treatment modality will be needed if we are to overcome these limitations and potentiate the effects of this nearly $500k treatment. In this section, I will briefly cover some of the most commonly described mechanisms of CAR-T resistance observed in patients to date. Broadly speaking, resistance can be driven by suboptimal CAR-T cell properties/function, by alterations

in tumor cells, by TME-based factors that can limit CAR-T efficacy, or by a combination of any or all of these factors in any given patient.

CAR-T cell dysfunction can contribute to resistance

Characteristics of harvested apheresis products have been shown impact the quality of the final manufactured CAR-T product (Shah & Fry, 2019). Here, prior treatment with clofarabine and doxorubicin has been shown to result in quantitatively inadequate or poor quality CAR-T cells, while previous cyclophosphamide or cytarabine exposure is associated with the depletion of early lineage T cells that are linked to productive CAR-T cell proliferation *in vivo*. Presently, CAR-T cells are indicated in people with relapsed and therapy-refractory blood cancers. This population is enriched for heavily pre-treated patients whose inherent T cell function might be reduced, thereby potentially leading to decreased anti-leukemic functionality and greater rates of relapse. Hence, efforts to develop allogenic CAR-T cells are currently underway (Depil et al., 2020). T cells from some cancer patients have also been shown to have diminished inherent cytotoxicity or expansion capabilities for reasons that remain poorly understood (Turtle et al., 2016). Reduced CAR-T cell engraftment and expansion is also associated with reduced depth and duration of clinical response, however the mechanisms that underlie differential engraftment rates are also incompletely understood (Maude et al., 2015; Porter et al., 2015; Kochenderfer et al., 2017). Aside from expansion and engraftment, CAR-T lineage phenotypes and their associated transcriptional programs have also been shown to impact the efficacy of this treatment modality. Expression analysis experiments demonstrated that in 4-1BB-containing CARs administered to CLL patients, aerobic glycolysis pathways, effector T cell differentiation programs, T cell exhaustion, and apoptosis programs were strongly upregulated in the CAR-T products of non-responders (Fraietta et al., 2018). As human T cell populations are known to shift from more undifferentiated naïve T cells to more differentiated effector and memory T cells that also have decreased proliferation potential with age, data from the CLL study indicate that older patients might be at much higher risk of relapse by virtue of the inherent differentiation phenotypes of their initial T cell pools (Chou & Effros, 2013; Van Deursen, 2014). However, this phenomenon has not yet been systematically studied. Prolonged *ex vivo* expansion of CAR-T cells can also result in a more differentiated product and in one preclinical study, *in vivo* CAR-T efficacy was inversely correlated with *in vitro* culture time (Ghassemi et al., 2018).

Finally, CAR-T cell exhaustion has also been shown to significantly contribute to relapse in this treatment modality. Characterized as a state of dysfunction in which T cells demonstrate

poor effector function, persistent expression of inhibitory receptors, and unique transcriptional programs that are distinct from functional memory/effector cells, T cell exhaustion is usually induced by chronic antigen stimulation, a phenomenon that is common in cancer (Wherry et al., 2011). Overall, markers of T cell exhaustion have generally failed to predict the clinical efficacy of CAR-T therapy (Shah & Fry, 2019). However, in DLBCL, a large proportion of LAG3+ CAR-T cells (a canonical marker of T cell exhaustion) did correlate with an increased chance of therapeutic failure (Schuster et al., 2019). Similarly, studies in CLL patients have shown that a specific subset of $CD8^+$ CAR-T cells that were also PD-1^- (programmed death 1, another canonical marker of T cell exhaustion) and $CD27^+$ (a molecule known to be important for generating T memory phenotypes) present before manufacturing predicted better therapeutic response in 4-1BB treated patients. Subsequent murine studies demonstrated that this $CD27^+$ population was directly responsible for tumor control (Fraietta et al., 2018). The mechanisms by which CAR-T cells exhaust are still poorly characterized. However, one recent study found that tonic CAR-CD3ζ signaling resulting from spontaneous, antigen-independent clustering of CARs on the surface of CAR-T cells induced exhaustion phenotypes in these cells (Long et al., 2015). Similarly, strong T cell activation has been known to lead to exhaustion phenotypes. In an elegant set of experiments, the Sadelain lab showed that excessive activation via all three of the immunereceptor tyrosise-based activation motifs (ITAMs) normally responsible for signaling in the CD3ζ chain overactivated CD28-CAR-T cells upon target antigen exposure and led to their exhaustion (Feucht et al., 2019). Here, more balanced activation could be achieved if only one ITAM in the most membrane proximal location was left functional. Resulting CAR-T cells showed increased replicative and anti-leukemic capacities *in vivo*, as compared to CARs with normal ITAM configurations. Hence, suboptimal CAR design can also likely contribute to relapse. Lastly, one final mechanism by which CAR-T cell exhaustion has been shown to arise is via engagement of, and subsequent signaling through, the endogenous TCR of a CAR-T cell (Yang et al., 2017). Here, antigen stimulation of the TCR, either alone or in combination with CAR stimulation lead to increased T cell exhaustion and apoptosis, severely limiting the antileukemic properties of $CD8^+$ CAR-T cells (Yang et al., 2017). However, the relevance of this phenomenon to CAR-T recipients remains unclear.

Alterations in tumor cells can promote resistance to CAR-T therapy

A major mechanism of CAR-T cell therapy resistance that has emerged from examining the tumor samples of relapsed patients is loss of the epitope targeted by the CAR-T cell (Majzner

& Mackall, 2018). In CD19-targeted therapy at least, antigen loss was an unexpected event, as this protein has been shown to be critical for B-lineage development (Del Nagro et al, 2005; Chung et al., 2012). Yet, available data from 7 CAR-T clinical trials targeting either CD19 or CD22 in B-ALL revealed that out of 267 patients who initially responded to therapy, 53 (49% of all relapses and 16% of all patients) had antigen-negative disease (summarized in table 2.2). In DLBCL the rate of antigen loss at relapse is even higher at 33% of all cases. However this information is based on a limited number of patients and more data is needed (Locke et al., 2019). Multiple genetic and non-genetic mechanisms have been shown to lead to the emergence of target-negative disease. Frameshift mutations and splice variants that result in the deletion or exclusion (respectively) of CD19's transmembrane domain have been identified in patients who had $CD19^{+}$ disease before CAR-T therapy, but ultimately relapsed with $CD19^{-}$ disease (Cheng et al., 2019). Similarly, cancer cells have also been shown to express a CD19 splice variant that excludes exon 2, which encodes the epitope targeted by the FMC63 scFv used in both axi-cel and tisa-cel (Frigault & Maus, 2020). Aside from changes in the CD19 protein itself, lineage switching phenotypes that lead to antigen loss in MLL-rearranged and MLL-mutated B-ALL have also recently been described in patients. In all cases reported to date, immune escape was mediated by the emergence of $CD19^{-}$ disease that had switched to a myeloid lineage, resulting in genetically related AMLs that were impervious to killing by CD19-directed CAR-T cells (Jacoby et al., 2015; Gardner et al., 2016; Lucero et al., 2019). One of these patients was also shown to have mutation in the gene encoding PHF6, a transcription factor that our lab has recently shown to be important for lineage plasticity in Ph^{+} B-ALL (Soto-Feliciano et al., 2017; Lucero et al., 2019). However, how this mutation contributed, if at all, to the switching phenotype was not explored. Another report showed a peculiar tumor-driven mechanism by which antigen loss can occur. Here, CD19 molecules were bound and masked by CD-19 directed CARs co-expressed on the cell surface of CAR-transduced leukemic cells (Ruella et al., 2018). While many CAR-T products were later found to also contain accidentally transduced B-ALL cells, this mechanism of resistance was only identified in one patient, indicating that this is likely to be a rare occurrence (Frigault & Maus, 2020). Finally, research conducted in mouse models of leukemia has found that CAR-T cells can decrease the density of CD19 molecules on the surface of target cells via trogocytosis, a process where lymphocytes engaged in an immune synapse can extract membrane associated proteins from the cell with which it is interacting in order to express them on their own surface (Hamieh et al., 2019). This study also showed that target antigen transfer to CAR-T cells resulted in increased rates of fratricide and subsequent CAR-T cell exhaustion.

While interesting, this resistance mechanism has not been conclusively shown to occur in patients. Efforts to overcome antigen loss via targeting of multiple antigens are currently ongoing in the CAR-T field, and early studies suggest that this might be an effective approach in some cases (reviewed in Frigault & Maus, 2020).

Compared to antigen loss, significantly less is known about mechanisms by which tumor cell alterations lead to antigen-positive resistance. Ostensibly, this type of relapse may seem to be driven largely by defects in the CAR-T cells themselves. However, as chronic antigen exposure is known to lead to T cell exhaustion, changes that spare CD19 but render leukemic cells impervious to CAR-T mediated killing would be expected to contribute to the recurrence of $CD19^{+}$ disease via two mechanisms: 1. By the proliferation of antigen-positive leukemic cells themselves, and 2. by inducing CAR-T cells to exhaust, thereby potentially hastening relapse (Wherry et al., 2011). Hence, in CAR-T therapy, resistance is probably multifactorial, with different mechanisms likely conspiring together to promote relapse. CAR-T cells are known to kill target cells via the same mechanisms employed by normal T cells: by the release of cytotoxic granules and by activating the extrinsic apoptosis pathway (e.g. by providing apoptosis-inducing molecules like TRAIL, FasL, and INF$\boldsymbol{\gamma}$) (Benmebarek et al., 2019). Experiments completed *in vitro* have shown that the addition of a TRAIL inhibitor to CAR-T cells co-cultured with susceptible target cells can significantly suppress the cytotoxic effects of this therapy, even when CAR-T cells are functioning normally, as assayed by cytokine release assays (Torres-Collado & Jazirehi, 2018). Similarly, a recent genome-wide *in vitro* screen completed in a human model of B-ALL demonstrated that alterations in a tumor cell's extrinsic apoptosis pathway can result in antigen-positive relapses with concomitant CAR-T cell dysfunction (Singh et al., 2020). There is some precedent in the literature for these types of resistance mechanisms to occur in patients, as LOF mutations in the Janus kinase (*JAK*) 1 or 2 genes are known to render melanomas refractory to inhibitors of the immune checkpoint molecule PD-1 by blocking apoptosis-inducing INF$\boldsymbol{\gamma}$ signals (Herbst et al., 2014; Zaretsky et al., 2016). However, whether or not these apoptosis-based mechanisms contribute to antigen-positive resistance in patients is yet to be determined. Outside of these few examples, no additional studies examining the relationship between tumor mutations and CAR-T therapy have been published.

Table 2.2. Summary of antigen negative relapse rates in published CAR-T cell clinical trials. Abbreviations: Antigen⁻ (antigen negative), CSM (costimulatory molecule), CR (complete response), scFv (single chain variable fragment), MFU (median follow-up), BCL (B-cell lymphoma).

Trial	Patient population	Target antigen (scFv)	CSM used	Disease treated	CR rate	Relapse rate	Antigen⁻ relapse rate	MFU	ClinicalTrials.gov identifier	Reference
Children's Hospital of Philadelphia phase I	Pediatric	CD19 (FMC63)	4-1BB	B-ALL (n=58) CD19+ T-ALL (n=1)	93% (55/59)	36% (20/55)	24% (13/55)	12 months	NCT01626495	Maude et al., 2014 Maude et al., 2016
Novartis phase II (ELIANA)	Pediatric & Young adult	CD19 (FMC63)	4-1BB	B-ALL (n=75)	81% (61/75)	33% (20/61)	25% (15/61)	13.1 months	NCT02435849	Maude et al., 2018
Seattle Children's Research Institute phase I	Pediatric	CD19 (FMC63)	4-1BB	B-ALL (n=43)	93% (40/43)	45% (18/40)	18% (7/4)	12.2 months	NCT02028455	Gardner at al., 2016 Gardner et al., 2017
NCI phase I	Pediatric & Young adult	CD19 (FMC63)	CD28	B-ALL (n=51) BCL (n=2)	53% (28/53)	29% (8/28)	18% (5/28)	18.7 months	NCT01593696	Lee et al., 2015 Lee et al., 2016
Memorial Sloan Kettering phase I	Adult	CD19 (SJ25C1)	CD28	B-ALL (n=53)	83% (44/53)	57% (25/44)	9% (4/44)	29 months	NCT01044069	Park et al., 2018
Fred Hutchinson Cancer Center phase I	Adult	CD19 (FMC63)	4-1BB	B-ALL (n=29)	93% (27/29)	33% (9/27)	7% (2/27)	9.7 months	NCT01865617	Turtle et al., 2016
Stanford University/ NCI phase I	Pediatric & Adult	CD22 (humani-zed)	4-1BB	B-ALL (n=21)	57% (12/21)	75% (9/12)	58% (7/12)	Range: 6-21 months	NCT02315612	Fry et al., 2018 Xiao et al., 2009

Tumor microenvironmental factors can be determinants of CAR-T response

Although studies on the TME's role in CAR-T therapy are uncommon in the literature, early data from some CAR-T clinical trials and TME studies in other CIs used in solid malignancies have led to the conclusion that the TME likely plays a critical role in CAR-T response. It is now well established that one of the most potent drivers of CI failure in solid tumors is the existence of an immunosuppressive TME. In CAR-T therapy specifically, one major concern is that patients will reject these modified cells altogether. Indeed, CARs often contain murine components, such as the FMC63 scFv, and various studies have now shown that both CTLs and antibodies directed against this and other immunogenic molecules can sometimes result in the clearance of CAR-T cells from the body (Kershaw et al., 2006; Maus et al., 2013; Turtle et al., 2016). In the study by Turtle and colleagues, reinfusion of additional CAR-T cells had no effect on the relapsed leukemia, even in patients with antigen-positive disease (Turtle et al., 2016). However, another study reported that while 85% of all patients developed anti-tisa-cel antibodies after infusion, the presence of these molecules did not affect CAR-T cell expansion, killing kinetics, response rates (CR = 89%), or relapse rates (Mueller et al., 2018). Thus, the occurrence of an immunologic reaction against CAR domains and the clinical implications of this response remain presently unclear.

Cancer cells themselves, along with non-transformed cells in the TME can also contribute to the established of an immunosuppressive environment. The ability of tumor cells to both secrete and upregulate cell surface expression of PD-L1 (a PD-1 ligand) in order to induce apoptosis of immune effector cells or to inactivate them is now a well-known mechanism by which cancer cells can evade the immune system (reviewed in Alsaab et al., 2017; Chen et al., 2018). Similarly, prostaglandins (PGE2) secreted by tumor cells, along with TME produced IL-6, hypoxia, and a low pH due to excessive lactic acid production by glycolytic tumor cells have all been shown to suppress the cytotoxic function of T cells, partially by reducing their ability to secrete key cytokines (IL-2 and INF$\boldsymbol{\gamma}$) (Fischer et al., 2007; Alfarouk et al., 2014). Non-transformed cells in TME, such as cancer associated fibroblasts (CAFs), myeloid-derived suppressor cells (MDSCs), and subtypes of tumor associated macrophages (TAMs), have also been shown to limit the infiltration of T (and other) effector cells into the tumor (Joyce & Fearon, 2015). While these and other TME-based resistance mechanisms are already thought to contribute to the failure of CAR- T therapy in solid malignancies, it is unclear whether they will ultimately contribute to CAR-T resistance in hematologic malignancies. In fact, in B-ALL, several lines of evidence suggest that leukemic cells resident in the BM are actually more accessible

and/or more susceptible to CAR- T-mediated killing, potentially indicating that this TME is less immunosuppressive than the TMEs of solid tumors. Studies tracking tumor regression in leukemia patients who had both lymphomatous masses and BM disease have shown that leukemic cells resident in the BM are rapidly cleared by CAR-T cells, while lymphomatous masses are cleared more slowly and sometimes, less effectively (Turtle et al., 2017; Fry et al., 2018). Additionally, CAR-T therapy has induced CRs in two patients with neuroblastoma involving the BM and in one patient with rhabdomyosarcoma limited to the BM (the only patient in this sarcoma trial who achieved a CR) (Pule et al., 2008; Louis et al., 2011; Hegde et al., 2017; Straathof et al., 2018). Hence, hematological malignancies appear to be amenable to CAR-T therapy partially by virtue of their association with the BM. It will be interesting to determine if other non-hematological cancers that involve the marrow will also be uniquely susceptible to CAR-T-mediated killing. If true, CAR-T therapy could prove to be effective in disseminated solid tumors that have metastasized to the marrow, a disease state that is usually incurable with frontline therapies.

In 2018, CAR-T therapy was named the “advancement of the year” by the American Society of Clinical Oncology (ASCO) after tisa-cel and axi-cel were approved by the FDA. Together, the data summarized in this section clearly illustrate why. Once better optimized, CAR-T therapy has the potential to revolutionize the way oncologists tackle cancer. After all, the use of early chemotherapeutics, developed in the late 1940s and early 1950s by visionaries like Gertrude Elion (antimetabolites), George Hitchings (antimetabolites), Sidney Farber (antifolates) and Charles Heidelberg (5-FU), was initially dismissed and even ridiculed due to the severely limited success of these agents as monotherapies (DeVita & Chu, 2008). Additional ongoing studies aimed at both improving current CAR designs and at uncovering the determinants of therapeutic response in this modality are poised to improve upon the already impressive results achieved with CAR-T therapy in blood cancers. Further, these investigations will also likely aid in the ultimate goal of enhancing CAR-T efficacy in other cancers outside of the hematopoietic system, especially in solid tumors where early studies are starting to show limited, but promising results (Bagley & O’Rouke, 2020). In all of these endeavors, it is clear that *in vivo*-based approaches that most closely recapitulate the native TME (including an intact immune system) will be critical, as the actual preclinical and clinical efficacy of CAR-T cells clearly cannot be determined in a dish. This is perhaps best exemplified by the clinical failure of first generation CAR-T cells. For these reasons, we decided to complete parallel *in vivo* and *in vitro* genome-

wide CRISPR-Cas9 screens using a mouse model of one of the most aggressive B-cell leukemia subtypes, Ph+ B-ALL. Here, an *in vivo* approach is also justified by the properties of the disease itself, as B-ALL has also been shown to be significantly dependent on the TME for survival in the context of traditional therapy. While this study is not yet fully completed, I describe the results from the *in vitro* arm of the screen, along with the results of a small *in vivo* pilot screen in chapter three of my thesis. Broadly speaking, these screens have the potential to uncover critical and as of yet, largely unexplored mechanisms of CAR-T resistance driven by alterations in tumor cells that could subsequently be targeted to potentiate the effects of this therapeutic approach.

Part II: Functional genomics in cancer research

One of the most powerful tools in the biologist's toolbox is the ability to genetically alter cells in order to determine the functional roles that genes play in specific physical processes, a concept first developed by H. Muller in the late 1920s. In a reverse genetic or 'genotype-to-phenotype' approach, prior knowledge about the specific alteration induced is available. Here, researchers examine the phenotypic ramifications of known changes in order to establish a functional role for the affected gene in cellular pathways regulating those specific phenotypes. This approach has been critical in many biological fields, including hematopoiesis where it has helped establish the fundamental core of genetic features indispensable for normal blood formation. For example, characterization of the hematopoietic systems of mice with *Pax5* or *Cebpa* gene knockouts (KOs) allowed researchers to establish these transcription factors as master regulators of cell identity and differentiation in B lymphocytes and myeloid cells, respectively (Figure 1.1) (Nutt & Kee, 2007; Rosenbauer & Tenen, 2007).

By contrast, forward genetic screens are an unbiased approach for identifying gene mutations that underlie a phenotype of interest, encompassing a 'phenotype-to-genotype' methodology. Generally speaking, forward genetics involves the generation of a large collection of mutant organisms that have been induced to acquire changes or deletions in their genomes. Classically, mutagenesis could be accomplished by several means, including chemical, biological, and physical agents that each display their own characteristics in terms of the types of mutations they produce, the efficacy of mutagenesis, and the breadth of their genomic target regions. As a cornerstone method in biology, this powerful approach has been extensively utilized throughout history and has led to landmark discoveries in model organisms, well before their genomes had been sequenced. For example, in pivotal studies that ultimately uncovered a fundamental mechanism of biology, Lee Hartwell and Paul Nurse performed forward genetic

screens in yeast that identified of a large proportion of the genes now known to regulate the cell cycle (Hartwell et al., 1974; Nurse, 1975). Before the advent of NGS, identifying causal mutations was often labor and resource intensive, requiring linkage studies through crosses with established lines. Additionally, classical mutagenesis approaches usually generate heterozygote alterations that can obscure recessive phenotypes. In diploid model organisms, this issue can be circumvented by inbreeding the progeny of the initial heterozygote in order to generate homozygote mutants. However this process is also often costly and tedious, reducing the tractability of this approach in mammals. As a result, recessive screens in mammalian systems had largely been limited to embryonic cells, to near haploid cell lines, or to cells that lack Bloom helicase (BLM) and subsequently have increased rates of mitotic recombination (Shalem et al., 2015). Recently however, the discovery of RNA interference (RNAi) and CRISPR has resulted in a rapidly expanding set of tools that have revolutionized genetic screening approaches in mammalian systems. Using these methodologies in conjunction with NGS, researchers can now systematically alter all of the genes in the genome and subsequently characterize the functional repercussions of each perturbation in a massively paralleled fashion, an approach known today as functional genomics screening.

The application of high-throughput screening approaches is particularly timely in cancer, as the end of major genome-wide sequencing projects (e.g. TCGA, the Pediatric Genome Project, the International Cancer Genome Consortium [ICGC] project) in the late 2010's marks the field's emergence from the first phase of its genomics era (Ding et al., 2018; Campbell et al., 2020). Here, more than a decade of world-wide coordinated sequencing efforts in over 50,000 tumors from more than 30 cancer types has created a broad census of the mutations that underlie the biology of this disease. Looking back from the close of this period, it clear that achieving a (near) comprehensive draft of the cancer genome has been instrumental, leading to groundbreaking discoveries that are already shaping drug discovery efforts and changing cancer treatment. For example, more and more, various cancer types are now being classified and treated based specifically on their mutational landscapes, as described in the above AML and B-ALL sections of my introduction. Additionally, large scale sequencing studies have led directly to the discovery and subsequent targeting of previously unidentified driver mutations in specific cancer subtypes, such as *IDH1/2* in GBM and AML, and *BRAF* in melanoma (Mardis et al., 2009; Dang et al., 2009; Ward et al., 2010; Davies et al., 2002). Multiple inhibitors for specific mutations in these 3 genes (e.g. enasidenib, ivosidenib, and vemurafenib) were subsequently developed and have been approved by the FDA, and more than 80 such targeted therapies are now on the

market, due in large part to these types of studies (Sanchez et al., 2018; Golub et al., 2019; Prahallad et al., 2019). Lastly, these NGS sequencing efforts have paved the way for the creation of early, patient-specific therapeutic cancer vaccines that are starting to show clinical promise (Ott et al., 2017; Sahin et al., 2017; Ott & Wu, 2019). Clearly, the impact of this approach is undeniable, but serious limitations still exist.

A major challenge in cancer genomics is its limited ability to ascribe functional importance to specific mutations, especially if they occur in previously uncharacterized regions of the genome or outside of genes with well-established roles in cancer. Further, many of the genes that play essential functions in various aspects of cancer biology are rarely found to be altered in ways that would be predicted to affect their primary protein sequence (Luo et al., 2009). In AML, this is perhaps best exemplified by paucity of therapy resistance drivers that have been identified by NGS studies in matched diagnosis-relapse patient samples, as discussed in part I of my introduction. Instead, the emergence of resistance in this and other cancer types is likely to be multigenic, with alterations in multiple pathways conspiring together to promote relapse. With ongoing NGS studies in human tumor samples generating longer and longer lists of mutations with largely unknown functions or consequences, or that are not easily targetable (as in AML), new approaches are needed in order to comprehensively characterize the functional relevance of these alterations in this disease. Here, the completion of mammalian genome-scale, systematic phenotype-driven screens in physiologically relevant contexts will go a long way towards extending the impact that cancer genomics has already had, allowing researchers to unleash the full potential of both of these approaches in order to further advance cancer care and improve the lives of patients.

In this section, I will describe the various tools available for the completion of high-throughput forward genetic screens in mammalian systems while briefly reviewing relevant *in vivo* examples of their use in the cancer literature. While this discussion will include a brief overview of random mutagenesis techniques, I will be focusing most heavily on approaches that allow for targeted perturbations, namely RNAi and CRISPR. Additionally, I will put the studies described in this thesis into context by briefly reviewing results from other relevant screens aimed at examining resistance mechanisms in AML and in CAR-T therapy.

3. Available methodologies and relevant examples

Broadly speaking, functional genomics screening approaches can be subdivided into gain-of-function (GOF) or loss-of-function alterations. Together, these platforms are critical for a

full examination of cancer-associated genes, as both LOF and GOF alterations, including specific gene mutations, amplifications, deletions, and broad chromosomal changes have been shown to be critical for various aspects of tumor biology (Sack et al., 2018). Pioneering studies conducted in eukaryotic model organisms such as yeast (after the publication of its genome in 1996) provided an early proof of principle that this high-throughput, genome-wide approach was both practical and powerful in its ability to connect genes and proteins with the cellular functions they provide (Winzeler et al., 1999; Tong et al., 2001; Giaever et al., 2002). While the "awesome power of yeast genetics" and other genetically tractable eukaryotic model systems have provided critical contributions to our understanding of the biological properties of cells, human disease, and especially one as complicated as cancer, cannot be fully modeled in single-cell or even non-mammalian organisms. For this reason, modeling human tumors in the mouse has been the mainstay in cancer research over the last three decades, with a major goal of the field being to develop similar high-throughput screening platforms for more rapid discovery (Gargiulo, 2018). Although not without its own limitations, this approach has yielded some of the most profound discoveries to date (as described in earlier sections) and with the advent of precision screening tools for use in mammalian systems, the future of cancer therapy seems brighter than ever. As discussed above, cancer and the emergence of resistance phenotypes in this disease appear to be exquisitely dependent on the TME and it is now well established that a tumor's response to therapy *in vivo* will frequently fail to correlate with its response to the same agents while cultured in a dish (Gillet et al., 2013; Fiedler & Hemann, 2019). Hence, given our interest in understanding drug resistance in AML and CAR-T resistance in B-ALL, the following discussion will concentrate most heavily on *in vivo* screens completed in these cancer types and in the context of their respective therapies, when available. This discussion is by no means intended to be a comprehensive review of the cancer screening literature, as that is far beyond the scope of this introduction. Rather, the articles cited here are intended as illustrative examples of the application and power of functional genomics screens in mammalian systems.

3.1. Random mutagenesis—workhorse of the initial *in vivo* forward genetic screens in mice

Before the advent of targeted screening approaches like CRISPR and RNAi, random mutagenesis of human or mouse cells was accomplished via chemical means (eg. ethylnitrosourea [ENU], methylnitrosourea [MNU]), engineered transposons (e.g. Sleeping Beauty, PiggyBac), or retroviruses (e.g. MuLV [murine leukemia virus] and MMTV [mouse

mammary tumor virus]) and the application of these tools in cancer led to the discovery of various tumor suppressors and oncogenes (Copeland & Jenkins, 2010; Nguyen et al., 2010; Ranzani et al., 2013). Using these approaches, genes could be perturbed by point mutations (as with the alkylating agent ENU) or insertional mutagenesis with retroviruses and transposons. Importantly, retroviruses and transposons can alter genes either by directly inserting into protein coding regions of a gene to induce its loss/alteration, or by inserting near regulatory regions to enhance gene expression via the viral promoter or enhancer elements.

Chemical mutagenesis

An early landmark application of ENU mutagenesis in adult male mice led to the identification of the multiple intestinal neoplasia (Min) mouse model which was subsequently found to have causative point mutation in the *Adenomatous polyposis coli* (*Apc*) gene resembling the truncating *APC* alterations found in human familial adenomatous polyposis (FAP) (Moser et al., 1990). FAP predisposes affected individuals to develop intestinal cancers and the discovery of this first *Min* mouse allowed for subsequent investigations into the involvement of *Apc* in intestinal mutagenesis, greatly advancing the field (McCart et al., 2008). More recently, application of related carcinogen (MNU) in lung adenocarcinoma allowed for the comparison of the mutational landscapes of *Kras*-driven tumors that were induced via genetic engineering or random mutagenesis, showing that these approaches ultimately resulted in vastly different tumor genetic architectures and the selection of different oncogenic *Kras* alleles (Westcott et al., 2015).

Retroviral insertional mutagenesis (RIM)

The application of slow transforming retroviruses (RVs) like MuLV and MMTV in the mouse hematopoietic system and mammary glands (respectively) for insertional mutagenesis screens has also been instrumental in discovering transforming factors in cancers originating from these tissues (Ranzani et al., 2013). Unlike acute-transforming RVs that induce tumors with short latency (2-3 weeks) via the expression of virally encoded oncogenes, slow-transforming RVs drive the development of malignancies with long latency (3-12 months) by inserting into the host genome proximal to tumor suppressors or oncogenes. Historically, these screens were done by infecting newborn mice (before their immune systems had finished developing) with replication competent virions, leading to random proviral insertions across their genomes and a life-long viremia. When insertions inactivate a tumor suppressor gene or activate an oncogene, affected cells can gain a growth advantage, and after additional mutational events, fulminant

malignancies develop. Subsequent isolation of tumor cells and cloning of their viral integration sites then allows researchers to identify candidate transforming genes. Maloney murine leukemia virus (MMLV), the prototypical and most studied MLV, has specific tropism for the blood and thus leads to the formation of leukemias and lymphomas. Analysis of MMLV integration sites has led to the identification of various oncogenes in hematopoietic malignancies, such as *c-Myc*, *Pim1*, *Pim2*, *Evi1*, *Bim-1*, and *Pvtl* (Fan, 1997; Ranzani et al., 2013).

More recently, replication-defective RVs have been used in insertional mutagenesis screens investigating resistance to targeted therapies in AML and CML. By examining viral integration sites in AMLs induced by MLV on an *Nf1*-null background that predisposes mice to leukemia, Lauchle and colleagues identified Rasgrp1/4 overexpression and Mapk14 inactivation as mechanisms of resistance to MEK inhibitors (Lauchle et al., 2009). In another report, CML was induced in mice by infecting them with Bcr-Abl expressing retroviruses and subsequently, secondary recipients were treated with imatinib (Miething et al., 2007). When imatinib response was correlated with genomic locations of retroviral insertion sites, *Runx1/3* were identified and subsequently shown to induce resistance to this Bcr-Abl inhibitor when either gene is overexpressed. Although clearly powerful, this approach had been limited by the restricted tropism of RVs for specific tissues, the inability to perform negative selection screens for factors that hamper tumorigenesis or that potentiate the effects therapy (cells that would drop out of the population), and by the preferential emergence of oncogene GOF mutations seen in positive selection screens (this being due to the difficulty of inactivating genes in a diploid organism). In a landmark study, Brummelkamp and colleagues provided a solution to the latter issues when they established insertional mutagenesis screens in KBM7, a near-haploid human CML cell line, using a replication-defective gene trap viral vector (Carette et al., 2009). This system has now been use to define (for the first time in history) mammalian essential genes, to identify regulators of PD-L1 surface expression, and to examine resistance against cancer therapy agents like doxorubicin, carboplatin, antimetabolites, and imatinib (Carette et al., 2009; Wijdeven et al., 2015; Planells-Cases et al., 2015; Blomen et al., 2015; Shen et al., 2016; Mezzadra et al., 2017). In the study examining doxorubicin resistance mechanisms, researchers found that loss of Keap1 of the SWI/SNF pathway reduces DNA double strand break (DSB) formation by decreasing the expression of TopoIIα or preventing this protein from being loaded onto DNA (Wijdeven et al., 2015). Additionally, loss of another protein C9orf82 was also found to contribute to doxorubicin resistance by augmenting DSB repair, although the exact mechanism was not explored further.

Transposon mutagenesis

Another critical approach for genetic manipulation of the mammalian genome is the use of DNA transposons (Tn), mobile genetic elements that have been used extensively in cancer research, both *in vivo* and (more recently) *in vitro*. Transposons are DNA sequences that can move from one location in the genome to another by a simple "cut and paste" mechanism (Ranzani et al, 2013). Here, the recognition of specific sequences on either end of the Tn by a transposase enzyme provided in *trans* leads to the excision, and subsequent re-integration of the Tn at a different genomic region with a TA dinucleotide. As DNA Tns were found to be actively mobile in only plants and invertebrates, synthetic transposon systems for mammalian use had to be generated by reverse engineering of the Tcl/mariner Tn in teleost fish where the evolutionarily youngest Tns had accumulated inactivating mutations. Reactivation of this mobile element led to the establishment of the first active Tn system for use in mammals, named Sleeping Beauty (SB) and subsequently, the PiggyBac (PB) Tn system from moths was also reactivated (Ivics et al., 1997; Ding et al., 2005).

Traditionally, Tn screens were performed in progeny arising from a cross between mice expressing an active *SB* transposase (either constitutive, inducible, or later, in a tissue restricted manner using floxed transposase alleles and tissue specific Cre recombinases) and mice genetically engineered to express mutagenic (gene-trap) Tn concatemers. Here, Tns were engineered to contain specific features that allowed them to both disrupt the function of tumor suppressors (polyadenylation sites, splice acceptors) and induce the expression of proximal proto-oncogenes (viral LTRs with promoter/enhancer abilities, splice donors). Upon the induction of tumors, Tn junctions can be isolated via PCR and sequenced to identify affected candidate genes. The first *in vivo* screens completed with this approach generated mostly sarcomas (although these only emerged on a sensitized *Arf*-null background) or T-cell lymphomas (Dupuy et al., 2005; Collier et al., 2005). Further alterations to the mutagenic Tn, along with the use of conditional transposase expression via tissue specific Cre recombinases and floxed *SB* or *PB* alleles allowed for this technology to be used in *in vivo* screens in a variety of other tissue types (Dupy et al., 2009; Starr et al., 2009; Rad et al., 2010; Vassiliou et al., 2011). Using these approaches, novel genes critical for tumorigenesis in intestinal neoplasia, B-ALL, hepatic tumors, PDAC, medulloblastoma, breast cancer, and other cancer types have been discovered (reviewed in Ranzani et al., 2013 and in O'Donnell, 2018). Additionally, Tn systems have been used to identify cooperating mutations in both *NPM1* mutated AML, where mice develop leukemia with a protracted latency and the spectrum of cooperating lesions had not

been fully elucidated, and in *ETV6-RUNX1* mutated B-ALL, where suitable mouse models that recapitulated the human disease had not previously been established (Vassiliou et al., 2011; van der Weyden et al., 2011).

Tn screens have been used to investigate resistance mechanisms to various targeted and cytotoxic cancer therapeutics. *In vitro* screens examining resistance to agents such as 6-thioguanine, PARP inhibitors, antifolates, fludarabine, and others have been performed using either murine haploid embryonic stem (ES) cell lines or patient derived CLL cell lines (Pettitt et al., 2013; Pandzic et al., 2016; Pettitt et al., 2017). These efforts, particularly those pursued in murine ES cells, have yielded limited results thus far, but have managed to prove the specificity of PARP inhibitors for their molecular targets. In the CLL work, a Tn screen implicated increased BRAF/MAPK signaling as a potential mechanism of resistance to fludarabine. Additional resistance screens also have been completed *in vivo* using Tn technology. To date, resistance mechanisms to a BRAF inhibitor in melanoma, an FGFR inhibitor in breast cancer, radiotherapy in medulloblastoma, and to a p53-MDM2 interaction inhibitor in tumors arising in *Arf*-null Tn mutagenized mice have been examined (Perna et al., 2015; Morrissy et al., 2016; Chapeau et al., 2017; Kas et al., 2018). Here, authors were able to elucidate resistance mechanisms that correlated with clinical outcomes and patient data. For example, in a pioneering study, Perna and colleagues showed that *Eras* expression induced resistance to vemurafenib (BRAF inhibitor) by inducing Akt hyperphosphorylation, a result that was consistent with clinical trial data linking PI3K reactivation to BRAF and MEK inhibitor resistance in almost 20% of melanoma patients treated with these agents (Perna et al., 2015). Additionally, in a study that used diverse tumor types arising in *Arf*-null mice, overexpression of *Bcl-xL* was shown to be a novel mechanism of resistance to HDM201, an inhibitor of the TP53-MDM2 protein interaction, indicating that simultaneous inhibition of anti-apoptotic proteins and p53 activation are synthetic lethal (Chapeau et al., 2017). A similar mechanism was later identified in AML, leading to a phase II clinical trial that is currently ongoing (Pan et al., 2017).

As shown above, *in vivo* Tn screens are powerful in their ability to identify genes that are critical for various aspects of tumorigenesis. However, this approach has also been limited by the same issues encountered with RIM, namely that Tn screens are largely positive selection screens that are also most likely to identify GOF mutations in oncogenes when applied in diploid genomes. As in RIM, another problem arises in the form of the number of candidates identified. Because Tn screens also produce large amounts of background mutations, researchers must often rely on the set of oncogenes identified in their given screen as controls, or on other data

sets, such as the results of other screens, expression analysis data, of NGS studies in order to identify putative hits. This problem is amplified when trying to establish a causal role for a new gene that has not been previously implicated in cancer or is poorly annotated. As such, many of the novel genes identified *in vivo* with Tn screens remain unvalidated. Several of these problems are currently being addressed by various groups. Novel bioinformatics pipelines and algorithms have been recently developed to help with data analysis, and application of this technology in near-haploid mammalian cell lines is likely to provide a higher signal to noise ratio, as seen with RIM screens in KBM7 cells (reviewed in Gerhards & Rottenberg, 2018). Additionally, reducing the number of Tns embedded in the genome have also been shown to improve results (DeNicola et al., 2015). Finally, both *SB* and *PB* have been used in order to extend the applicability of both CRISPR and RNAi-based screening in autochthonous tumor models, increasing the ability to mutagenize cells directly *in vivo* as would occur in a patient (Rudalska et al., 2014; Weber et al., 2015; Xu et al., 2017). In one study, this approach was used to perform a genome-wide *in vivo* screen for genes that mediate tumorigenesis in the liver (Xu et al., 2017).

3.2. cDNA overexpression libraries for GOF screens

Gain of function screens have recently been made possible by the development of barcoded genome-scale complementary DNA (cDNA) libraries for use in human cells. Previously, this approach was used in yeast in order to systematically map protein-protein interactions (Rual et al., 2005). More recently, the Elledge lab applied this approach to human cancer cell lines of different tissue origins (Sack et al., 2018). Here, researchers showed that while some genes could be shown to induce similar phenotypes across cell lines, striking tissue-specific gene sets that are functionally relevant for tumor growth were identified and subsequently validated *in vivo*. In line with these data, genes that were identified to either promote or inhibit growth of a specific tumor type were found to be enriched in copy number alteration (CNA) regions frequently observed in patient samples from the corresponding tumor type. This indicates that the underlying genetic network that is established in a cell during its development is a major determinant of the drivers and aneuploidies that arise and are selected for in specific tumors derived from different tissues, with alterations that bolster this developmental network appearing to be critical in tumorigenesis. These findings may help explain why specific chromosomal alteration patterns are observed in certain cancer types, such as amplifications of chromosome 1 and 8 in breast cancer, chromosome 17 losses in ovarian cancer, and trisomy 8 or chromosomes 5 and 7 loss commonly detected in AML (Tavassoli et al., 1993; Kumar 2011; Goh

et al., 2017). It will be interesting to see how/if these tissue-specific underlying genetic architectures also dictate the resistance mechanisms that can be selected for across different cancers, especially in the context of combination therapy. Finally, this study also identified hundreds of novel genes that had not previously been linked to human cancer, however these were not validated in this study.

3.3. RNAi

Throughout history, advancements in biology have been extensively influenced by progress in the technology and tools available to researchers. Discovered in 1998 by Andrew Fire and Craig Mello, RNA interference (RNAi), a natural mechanism by which metazoan suppress the expression of cells, rapidly began to revolutionize the field of functional genetics (Fire et al., 1998). For the first time in mammals (after their genome sequences were published), each gene in the genome could be systematically knocked down and interrogated for its functional role within the cell, providing a powerful combination of both forward and reverse genetics (Berns et al., 2004). Initial iterations of this LOF technology came in the form of synthetic siRNA duplexes composed of 19 complementary base pairs and 2-nucleotide 3' overhangs. These 22mers can be delivered to cells either *in vitro* or *in vivo*, where once internalized, they are incorporated into the cell's RNA-induced silencing complex (RISC). Once loaded, the 22mer targets RISC to an mRNA of interest via complementary base-pairing, subsequently leading to the transcript's degradation, an effect that is transient when RNAi is applied in this fashion (Perrimon & Perkins, 2010). Vectors that direct stable expression of short-hairpin RNAs containing stem-loop structures from RNA polymerase III (Pol-III) promoters were subsequently established, leading to the creation of shRNA libraries intended for use in mouse and human cells (Brummelkamp et al., 2002; Sui et al., 2002; Yu et al., 2002). The development of more effective screening libraries, however, was greatly facilitated by the discovery and manipulation of naturally occurring RNAi triggers, such as the mir-30 microRNA (miRNA) scaffold discovered in HeLa cells (Lagos-Quintana et al., 2001). Here, researchers were able to show that designed shRNAs embedded within this endogenous miRNA context were fully processed intro mature stem-loop molecules ("shRNAmirs") by the cell's endogenous machinery (nuclear processing by the Drosha/DGCR8 microprocessor complex, followed by cytoplasmic processing by Dicer/TRBP), and that this approach greatly boosted the amount of mature shRNAs produced (Zeng et al., 2002; Silva et al., 2005). Additionally, by embedding shRNAs in endogenous RNAi triggers, their expression could be driven by Pol-II promoters, leading to the development of more sophisticated RNAi

tools, such as inducible systems, tissue-specific RNAi approaches, and reporter constructs with shRNAs embedded in the 3' UTR, all of which had decreased toxicity and less off-target effects than Pol-III driven constructs (Crotty & Pipkin, 2015). Critically, these new tools were shown to be able to effectively silence target genes upon the integration of only a single copy of the vector (Dickins et al., 2005; Stegmeier et al., 2005). As a result of this body of work, libraries of shRNAs embedded in endogenous miRNA contexts were developed and subsequently used for pooled screens in mice and in human cell lines. In chapter two of my thesis, we use a focused shRNA library based on the miR30 scaffold to complete an *in vivo* screen for chemoresistance in a mouse model of AML.

RNAi screens can be performed either in an arrayed or pool-based format, where either small populations of cells are infected with single constructs or large populations of cells are infected with a pooled shRNA library, respectively. In an arrayed screen, cells infected with many different single constructs are kept separate, seeded in multi-well plates and monitored for specific phenotypic changes, while pooled screens rely on the comparison between the proportion of cells carrying an shRNA in a control group versus a treated group. The enrichment or depletion of specific shRNAs is then used as a readout of the functional consequence of knocking down (KD) a gene on a specific cellular process, a method that has been greatly simplified by the advent of NGS. Until recently, most *in vivo* pooled screens had been completed using RNAi technology, and application of this methodology has allowed researchers to uncover novel regulators of tumor development, growth, and survival (most excitingly, tumor suppressors and genes that promote growth/survival of an already established tumor but are dispensable for transformation), as well as genes that suppress metastasis in various tumor types, including various hematopoietic malignancies, breast cancer, PDAC, epithelial cancers, glioblastoma, hepatocellular carcinoma, and others (Zender et al., 2008; Bric et al. 2009; Meacham et al., 2009; Iorns et al., 2012; Beronja et al., 2013; Gargiulo et al., 2013; Miller et al., 2013; Murugaesu et al., 2014; Schramek et al. 2014; Wolf et al., 2014; Meacham et al., 2015; Sa et al., 2015; Sasaki et al., 2017).

Some of the pioneering efforts in the *in vivo* screening space were led by our lab. One of these screens, completed both *in vitro* and *in vivo* using a mouse model of *Eμ-Myc* B-cell lymphoma, allowed Meacham and colleagues to represent nearly 1,000 unique shRNAs in a single mouse, identifying various genes with roles in cell motility, such as Rac2, Twf1, and CrkL, as novel, *in vivo*-specific growth dependencies in this cancer type (Meacham et al., 2009). Critically, this study also showed that inhibition of Rac2 specifically sensitized tumor cells to

therapy *in vivo* and had no effect when cells were cultured *in vitro*, highlighting the power of *in vivo* screens to uncover context-specific alterations and demonstrating, once again, that human cancer cannot be fully recapitulated in a dish. Another set of similar parallel screens, completed using the same mouse model of Ph^+ B-ALL employed in chapter three of my thesis, allowed our group to represent up to 30,000 unique shRNAs in a single mouse (Meacham et al., 2015). Here, Meacham and colleagues identified the gene Phf6 as an *in vivo*- and lineage-specific growth dependency in B-cell derived hematopoietic malignancies. Subsequently, our group showed that this gene is critical for B-cell identity via regulation of the chromatin landscape, a function that could only be gleaned when Phf6 was completely lost (using CRISPR) in B-ALL cells, resulting in the outgrowth of lymphomas that also expressed canonical T cell markers (Soto-Feliciano et al., 2017). Another relevant example came from the Ebert lab. Here, researchers developed the MLL-AF9 mouse model of AML used in chapter 2 in this thesis, and completed a focused RNAi screen for novel *in vivo* dependencies that could then be inhibited to better eradicate the disease (Miller et al., 2013). Using this approach, Miller and colleagues found that Integrin Beta 3 (*Itgb3*) was essential for AML growth in both the murine model and in human MLL-rearranged AML cells transplanted into immunocompromised animals. Mechanistically, loss of *Itgb3* prevent cells from homing to the endosteal niche and induced them to differentiate, due in part to attenuated Syk singling downstream of Itgb3. Interestingly, the possibility of a therapeutic window for targeting this protein was found when Itgb3 knockout mice were found to have normal hematopoietic function. Finally, another *in vivo* screen completed in this same MLL-AF9 mouse model of AML used a focused library curated to contain TF genes that are highly expressed in HSCs or LSCs, and that are co-expressed with *HoxA9* and *Meis1*, genes that are known stemness mediators in AML. Using this library, the Ebert lab screened for novel TF dependencies in LSCs, finding that inhibition of circadian rhythm TFs *Clock* and *Bmal1* led to impaired growth, blast differentiation, and depletion of LSCs both *in vitro* and *in vivo*. Importantly, this effect was not seen in normal HSCs acutely induced to lose *Bmal1* via the application an inducible Cre and floxed *Bmal1* allele, indicating that a therapeutic window might exist for the inhibition of these factors (Puram et al., 2016).

RNAi approaches have also recently been used to investigate resistance mechanisms *in vivo*. One of these pioneering studies used a focused shRNA library to target genes located in known amplified genomic regions of human hepatocellular carcinomas (HCC), looking specifically for genes that conferred resistance to the multikinase inhibitor sorafenib, recently approved for HCC (Rudalska et al., 2014). Here, the pooled library of shRNAs was carried on Tns

that also expressed $Nras^{G12V}$, allowing researchers to avoid *ex vivo* manipulation of cells when this library was delivered to the livers of *Arf*-null mice (a combination that induced aggressive, multifocal, sorafenib-resistant HCCs). This negative-selection screen found that Mapk14 KD significantly sensitized both human and murine HCC cells to this TKI, mechanistically showing that Mapk14 activates Mek-Erk and Atf2 to ultimately bypass signaling inhibition induced by sorafenib exposure. Critically, elevated Mapk14-Atf2 signaling was shown to portend poor response to sorafenib in patients, indicating that the identified mechanism was also clinically relevant. Indeed, clinical trials combining MAPK inhibitors with sorafenib have shown promising results in patients with advanced HCC and recent studies have shown that this too seems to be due to reduced levels of activated p-ERK (Hou et al., 2019). In another perhaps more relevant example (based on the agents used), Ashenden and colleagues recently used a focused shRNA library to uncover novel resistance mechanisms to combination chemotherapy (doxorubicin and cyclophosphamide) in a mouse model of breast cancer (BC) metastasis (Ashden et al., 2017). Using this approach, JNK signaling was identified a key determinant of chemotherapy response, as KD of this protein prevented tumor cells from cycling and blocked the activation of the pro-apoptotic protein Bax, thereby diminishing the effects of therapy. This study also showed that elevated JNK singling (as defined using a transcriptional signature from their experiments) predicted both enhanced response to therapy in a neoadjuvant setting and poor prognosis in untreated patients with triple negative breast cancer, indicating that this resistance mechanism may only be relevant in specific BC subtypes but may also be a marker of aggressiveness. One final example of pooled RNAi screens examining resistance to therapy could be identified in the preclinical literature. Here, parallel *in vivo* and *in vitro* pooled screens using a focused shRNA library targeting ~500 human kinases was completed in human melanoma xenografts, looking for genes that promoted *in vivo*-specific growth (Possik et al., 2014). These screens identified a more profound *in vivo* dependency on DNA damage response (DDR) pathways that were found to be activated by hypoxic environments via HIF signaling. Simultaneous pharmacological inhibition of DDRs (Chek1/2 inhibitor) and angiogenesis (via bevacizumab) were therefore shown to synergize *in vivo*, resulting in better tumor control.

As with all approaches, limitations with RNAi screens exist. These include an inability to induce the complete loss of a gene, although this can actually be an advantageous feature when screening for resistance mechanisms, as it is possible that this more closely recapitulates the effects that would be expected with pharmacologic inhibition. Other issues include high rates of off target effects that cannot always be easily predicted, the activation of innate immune

responses that are sequence independent (namely, the activation of the interferon and/or Toll-like receptor pathways), and inconsistent knockdown efficiencies between hairpins (Mohr & Perrimon, 2012; Schuster et al., 2019). Limitations notwithstanding, pooled RNAi screens have proved to be an intensely powerful approach towards examining various aspects of tumorigenesis. With the advent of CRISPR however, this technology is likely to be phased out and eventually replaced with newly developed CRISPR interference (CRISPRi) tools that are superior to RNAi in various ways, including a significantly reduced rate of off target effects (reviewed in Kampmann, 2017).

3.4. CRISPR

As the RNAi revolution ramped up, another technology that would come to transform the cancer genomics field in even more profound ways than RNAi, was sitting in bacterial genomes, largely flying under the radar (at least initially) of the broad biomedical research community. Discovered first in *E. coli* in 1987 and later in other bacteria, Clustered Regularly Interspersed Short Palindromic Repeats, or CRISPR, went nearly two decades without conclusive discoveries about its cellular function (Ishino et al., 1987; Kampmann et al., 2017). This changed rapidly beginning in 2005 when several groups reported that these sequences were strikingly similar to those of bacteriophage DNA, raising the possibility that CRISPR formed part of an adaptive defense system in bacteria (Bolotin et al., 2005; Pourcel et al., 2005; Mojica et al., 2005). Later, these studies were extended when CRISPR and its CRISPR-associated proteins (Cas) were indeed experimentally demonstrated to protect bacteria from bacteriophage infection by targeting foreign viral DNA and preventing re-infection via the integrating of small sequences (CRISPRs) complementary to the invading phage DNA into the bacterial genome (Barrangou et al., 2007). Here, two distinct RNAs, the CRISPR targeting (crTNA) and the trans-activating RNA (tracrRNA), were shown to activate and direct Cas proteins towards phage sequences, allowing them to bind and degrade the invading viral DNA (Deltcheva et al., 2011; Gasiunas et al., 2012; Jinek et al., 2012). These studies sparked a special interest in the type II CRISPR systems, as they required only a single Cas protein to target and cleave defined DNA sequences, a particularly attractive feature for a genome editing tool (Jinek et al., 2012). A further simplification of the system came when the crRNA and the tracrRNA were combined into a single guide RNA molecule (sgRNA) (Jinek et al., 2012). Finally, in 2013, researchers at Harvard and MIT showed, for the first time, that the type II Cas protein from *Streptococcus pyogenes* bacteria (SpCas9) could be programmed by these synthetic RNA guides to cleave specific DNA sequences in

mammalian cells, laying the foundation for using CRISPR-Cas9 as broadly applicable genome editing tool (Cong et al., 2013; Mali et al., 2013).

As a highly programmable genome editing tool, binding specificity of the CRISPR-Cas system is dictated by a 20-nucleotide sequence preceding a prototypical and Cas protein-dependent three nucleotide protospacer adjacent motif (PAM) (Deveau et al., 2008; Jinek et al., 2012; Sternberg et al., 2014). Once bound to unwound DNA via the PAM and sgRNA complementary sequence, two nuclease domains of the Cas9 protein introduce a DSB in the target sequence which can then be repaired by the cell via two main pathways: non-homologous end joining (NHEJ) or homology directed repair (HDR). If the break is repaired using the error prone NHEJ pathway, insertions or deletions (indels) can be introduced into a gene's reading frame, often leading to LOF mutations (e.g. frameshifts, premature stop codons). Instead, repair of DSBs via the HDR pathway uses homologous DNA sequences present in the cell (usually on a sister chromatid) as a template for reconstructing the cleaved site via recombination mechanisms. Here, exogenously provided donor templates with homology to the targeted region can allow researchers to rapidly introduce defined mutations into the genomes of mammalian cells. Additional modifications later improved this technology further. This included the engineering of an optimized sgRNA scaffold that allowed Cas9 to more efficiently bind its intended target DNA sequence, along with the discovery of alternate Cas proteins with different PAM motifs, different sizes, and different abilities in terms of the types of nucleic acid they can bind and cleave (Zhan et al., 2018). Lastly, further tool development in this space has led to the creation of a number of CRISPR variants, including a catalytically dead Cas9 (dCas9) protein that retains its sgRNA-directed DNA binding specificity but can no longer cut (Kampmann, 2018). Here, fusion of either transcriptionally repressive (e.g. the Krüpel-associated box [KRAB] domain) or activating (e.g. VP64, SunTag, SAM, and VPR approaches) domains to dCas9 enable one to control transcription in either direction at specific loci.

As the latest technology to be applied for mammalian genome editing purposes, the literature of CRISPR-based functional genomics screens is exceedingly new (although by no means small) and as a result, the majority of these pooled screens have been completed *in vitro* (reviewed in Gerhards & Rottenberg, 2018 and O'Loughlin & Gilbert, 2019). To date, this approach has allowed researchers to systematically explore mammalian gene function via both positive and negative selection (Wang et al. 2014; Shalem et al., 2014; Zhou et al., 2014; Wang et al., 2015; Tzelepis et al., 2016). Additionally, along with the aforementioned RIM screen in haploid human cells, CRISPR has powerfully been used to define, for the first time, the set of

mammalian genes that are essential for cell growth (Wang et al., 2015; Hart et al., 2015). Similarly, *in vitro* CRISPR screens have been used to define, potentially targetable cancer specific gene dependencies and synthetic lethality pairs, with hematopoietic cancer cell lines being widely used, and have convincingly shown (via validation studies) that many of the identified targets are likely relevant in human cancer *in vivo* (Wang et al., 2015; Shi et al., 2015; Toledo et al., 2015; Tzelepis et al., 2016; Steinhart et al., 2017; Wang et al., 2017; Lu et al., 2018; Yamauchi et al., 2018). In one relevant example, genome-wide *in vitro* screens completed in 5 human AML cell lines successfully identified known AML- and AML subtype-specific dependencies (e.g. *DOT1L*, *MEN1*, *BRD4, FLT3*, *NPM1*) while also identifying a number of new potentially actionable vulnerabilities, including STRADA (Tzelepis et al., 2016). Notably, this gene was also identified in our AML screen as a chemosensitizer. In another screen, regulators of the MAPK pathway were found to be synthetic lethal with oncogenic Ras in human AML lines (Wang et al., 2017). Related to therapy, *in vitro* genome-wide screens in human and murine cancer cell lines have been completed in order to identify genes whose LOF cause resistance towards drugs such as topo II inhibitors, antimetabolites, immunotherapy, targeted therapy (e.g. SYK, BRAF, and FLT3 inhibitors), Ara-C, and even CAR-T therapy (Koike-Yusa et al., 2014; Shalem et al., 2014; Wang et al., 2014; Kurata et al., 2016; Hou et al., 2017; Patel et al., 2017; Gallipoli et al., 2018; Cremer et al., 2020; Singh et al., 2020). Using this approach, researchers were able to identify known mediators of resistance (as defined by previous RNAi screens) to therapies, as well as novel candidate resistance drivers that had not been previously been implicated in cancer therapy resistance. As discussed below in the AML section however, some of these screens failed to identify any clinically relevant genes at all (Kurata et al., 2016). Screens that are relevant to our CAR-T work will also be discussed in a section below.

Pooled CRISPR screens *in vivo* have also been recently described in the literature, with the overwhelming majority of these being performed in order to examine various aspects of cancer biology (Chow & Chen, 2018). Some of the first *in vivo* applications in CRISPR demonstrated that this technology could be used to mutagenize cells residing in their native anatomical sites (lung, brain, liver), resulting in the rapid generation of clinically relevant cancer models with complicated mutational landscapes that were previously (before CRISPR) difficult to engineer (Sanchez-Rivera et al., 2014; Swiech et al., 2015; Xue et al., 2014; Chow et al., 2017). Similarly, the Ebert group used CRISPR/Cas9 to engineer better AML models that more closely recapitulate the mutational landscape of the human disease, where patients are found to have an average of 3-4 driver mutations, although this involved *ex vivo* manipulations to mutagenize

cells (Heckl et al., 2014). Soon thereafter, numerous large-scale screens were performed, screening for genes that are important for various aspects of tumorigenesis, including metastasis, relevant tumor suppressor and oncogenes, and synthetic lethality interactions (Weber et al., 2015; Katigbak et al., 2016; Kodama et al., 2017; Song et al., 2017; Yau et al., 2017). Additionally, some groups performed autochthonous CRISPR screens of variable scales, screening for guides that could induce tumorigenesis, and in some of these screens, the entire landscape of causal functional alterations could be described, even when adeno-associated viruses (AAV) that do not normally integrate were used to deliver guide molecules (Swiech et al., 2015; Weber et al., 2015; Rogers et al., 2017; Chow et al, 2017; Wang et al., 2018). Here, this was accomplished by the direct capture and sequencing of predicted sgRNA cutting sites (Chow et al, 2017; Wang et al., 2018).

Various groups have also performed *in vivo* screens to identify genes that when lost, sensitize tumors to various therapy modalities. One such study from our group established that CRISPRi and CRISPRa could be used *in vivo* to examine various cancer phenotypes, including response to several chemotherapy agents, representing the first *in vivo* transcriptional activation screen to be completed (Braun et al., 2016). Another interesting study recently performed a genome-wide *in vivo* CRISPR screen in CD8 T cells, looking for guides that could affect a CTL's ability to infiltrate tumors in a TNBC mouse model (Dong et al., 2019). Surprisingly, Dong and colleagues ended up with an exceedingly small number of hits, ultimately finding that that loss of Dhx37 significantly potentiated the antitumor effects of adoptively transferred CTLs. Studies like these that perform screens directly in T or other immune cells have the potential to improve upon CAR-based cell therapies and deepen our understanding of the immune system's functional contributions in cancer, and thus, are currently critically needed. Two other relevant studies have also examined *in vivo* responses to immunotherapy. In a landmark paper, Manguso and colleagues reported the results of a focused CRISPR screen completed in a syngeneic mouse model of melanoma, screening for guides that altered response to both anti-PD-1 antibodies or to a tumor vaccine (Manguso et al., 2019). This group convincingly showed that loss of genes in the INF**γ**/JAK/STAT pathway (*Ifrngr1*, *Ifngr2*, *Jak1*, *Jak2*, and *Stat1*) induced resistance to PD-1 blockade, while loss of *Ptpn2* significantly sensitized tumor cells to therapy by both activating TILs and by increasing antigen presentation via augmented INF**γ** signaling in tumor cells. Interestingly, the *in vitro* arm of our screen also consistently identified guides against *Ifrngr1*, *Ifngr2*, *Jak1*, *Jak2*, and *Stat1* as the top enriching hits, while guides against *Ptpn1* and *Ptpn2* were consistently among the top 10 depleting hits, indicating that similarities between

immunotherapies that aim to enhance T cell-based tumor killing are likely significant. A related study completed in a KRAS-driven mouse model of lung adenocarcinoma also identified an additional epigenetic gene (*Asf1a*, a histone chaperone) as a novel mediator of immunotherapy resistance, identifying Jak2 and Stat1 as resistance mediators in this mechanism (Li et al., 2020). Lastly, Szlachta and colleagues performed parallel *in vivo* and *in vitro* screens using a patient derived xenograft cell line of PDAC, looking for genes that altered the tumor's response to MEK inhibitors. This study found that inhibiting proper kinetochore function (via loss of *Cenpe*) sensitized cells to therapy (Szlachta et al., 2018). More interestingly however, this group also showed that screening results from their own work and that of other groups could be used to reliably predict drug response across various cell lines, an interesting concept whose utility will be interesting to investigate as more and more screens are performed.

With the growing number of methodologies, applications, and Cas proteins currently being discovered, it is clear that the cancer (and more broadly, the entire biomedical research) field is in the midst of a revolution. Further efforts to improve upon this new technology, including better CRISPRa tools, optimization to increase the rate of biallelic functional gene mutations that occur in an experiment, and the optimization of combinatorial screens in individual cells, should fuel this era of discovery for decades to come (Schuster et al., 2019). Future investigations are likely to yield a plethora of additional drug targets and cancer dependencies, allowing this approach, and specifically CRISPR-based screens, to complement those of large NGS efforts currently still underway. Here, the combination of cancer genomics with pooled genome-wide screens will significantly help the field achieve its overarching goal of defining functional roles for tumor mutations detected in patients. This is especially relevant for those alterations that occur at low frequencies and make up the "long tail" of oncogenic drivers observed in NGS studies, a group of mutations that in aggregate, represent a large population of patients with often limited prognostic information and treatment options.

4. Functional genomics approaches for investigating therapy resistance

4.1. Pooled screens to examine resistance in AML

The overwhelming majority of genetic screens completed in AML have been conducted using *in vitro* approaches and in these cases, investigators are generally seeking to identify novel, potentially targetable AML dependencies (Zuber et al., 2011; Cole et al., 2015; Shi et al., 2015; Tzelepis et al., 2016; Erb et al., 2017; Lu et al., 2018; Tarumoto et al., 2018; Yamauchi et al., 2018). Additionally, large scale CRISPR screens in AML cell lines have also been used to define

mammalian essential genes, an approach that has also been useful for identifying novel synthetic lethality pairs that could also be potentially targeted in specific AML subtypes (Wang et al., 2017). The same holds true with few screens that have been performed *in vivo* in this disease (Miller et al., 2013; Puram et al., 2016; Li et al., 2017). Here, validation in subsequent *in vivo* experiments using both human and murine models of AML proved that this approach is highly effective for identifying novel drug targets in this disease. However, these studies did little to advance the field's understanding of how AML becomes resistant to the frontline therapy agents used in the overwhelming majority of patients today.

In instances where AML screens *have* been conducted in the context of therapy, the agents employed have largely been targeted drugs, such as SYK, FLT3, or BET inhibitors (Rathert et al., 2015; Gallipoli et al., 2018; Cremer et al., 2020). This choice is perhaps best explained by the fact that *in vitro* screens conducted in the context of relevant AML chemotherapies fail to show any novel gene targets that are also clinically relevant. In one such report, a genome-wide CRISPR/Cas9 screen was conducted in the human AML cell lines U937 and MOLM13, in the context of cytarabine treatment given either at a low or high dose (Kurata et al., 2016). Strikingly, all of the resulting cells in both cell lines and in both conditions were shown to contain guides against DCK, the rate-limiting enzyme in the metabolic pathway that activated cytarabine, a result that mirrored that of a similar *in vitro* AML screen for Ara-C resistance by the same group (Rathe et al., 2014). When the screen was repeated in cell lines with non-sgRNA targetable DCK however, the only consistent hit reported was SLC29, a nucleoside transporter responsible for importing cytarabine into the cell - representing a resistance mechanism that had already been well described in the literature (Marin et al., 2016). Reports from groups attempting to identify mechanisms of resistance towards anthracyclines have also been reported, although these were not genetic screens but rather studies in cell lines that had been induced to become resistant via continuous culture with increasing levels of drug (Choi & Ling, 1997). Here, researchers identified the efflux pump PGP (encoded by the *MDR1* gene) as a mediator of resistance. This result has been shown in many studies, in multiple cancer types treated with different therapies *in vitro*. Yet, *in vivo* studies have failed to consistently demonstrate that better tumor control could be achieved by inhibiting efflux pumps (reviewed in Robey et al., 2018). Indeed, excitement over the development of inhibitors against ABC transporters like PGP has waned, as clinical trials for these agents have uniformly failed. Hence, *in vitro* approaches are clearly unable to identify clinically relevant resistance mechanisms to frontline cytotoxic chemo in AML, at least when they are applied as monotherapies. Additionally,

no examples of studies involving screening in the presence of anthracyclines and Ara-C *in vitro* simultaneously could be identified in the preclinical literature.

Together, the representative data summarized above make it clear that if we are to decipher how AML is becoming resistant to the combination chemo agents used today, new approaches are needed. Realistically, most AML patients who *can* currently be cured will likely continue to be cured by the application of high doses of anthracyclines and Ara-C (+/- allo-HSCT) for the next few decades, or at least until optimized schedules and combinations for novel targeting agents are established or new revolutionary drugs are introduce. These latter efforts have historically occurred over exceedingly long timelines, and while new agents *are* on the horizon in AML, their effective implementation into the clinic will not be immediate. Thus, it is currently imperative to investigate resistance mechanisms to combination chemotherapy agents in relevant *in vivo* settings if we are to potentiate the effects of these drugs and improve patient outcomes in this disease today. Fortunately, genetically tractable AML mouse models are well established. Additionally, mouse compatible version of the '7 + 3' schedule used in patients have been developed, opening the door for the completion of an *in vivo* pooled genetic screen for genes that, when lost, sensitize blast cells to combination chemo (Zuber et al., 2009). The result of such a screen are described in chapter two of this thesis and to our knowledge, this will be the first such screen to be reported in the literature (once it is published).

4.2. Pooled screens to examine CAR-T resistance in B-ALL

To date, only one screen directly examining CAR-T resistance mechanisms has been published. Here authors performed a genome-wide *in vitro* screen in NALM6, a human model of B-ALL exposed to either CD19-targeting CAR-T cells or a control (untransduced) T cell (Singh et al., 2020). A global examination of their data reveal an overall low dynamic range of fold changes across hits, indicating limited signal strength (low signal to noise ratio), possibly due to suboptimal experimental conditions. Issues notwithstanding, this study goes on to identify members of the extrinsic apoptosis pathway (BID, FADD, CASP8) as genes that confer significant resistance to CAR-T cells both *in vitro* and *in vivo*. A death receptor signature was then shown to stratify patients, but only if the authors only included patients with long-term responses and those who did not respond at all. Validation experiments in this study were not set up as competitions between cells lacking members of this pathway (FADD and BID) and unaltered cells (a more realistic scenario likely to occur in patients), but rather, used pure populations of *FADD*- or *BID*-null cells that were then challenged with CAR-T cells. CAR-T cells

are known to kill tumor cells partially through the extrinsic cell pathway, so loss of the factors that mediate this signal would be expected to render cells more resistant to CAR-T cell killing, something that is already known and well described in the T cell field (Martínez-Lostao et al., 2015). Additionally, chronic antigen exposure, as would be expected to occur in these experiments, is known to cause T cell exhaustion, a phenomenon that was also reported by the Singh study (Wherry et al., 2011). Given these considerations, it is unclear if the mechanism of resistance identified by this group will actually be relevant in patients, where intratumoral heterogeneity significantly contributes to relapse, a phenomenon that will undoubtedly affect CAR-T response as well (Pribluda et al., 2015; Ferrando & Otín, 2017).

Interestingly, two other relevant screens in melanoma cells have been completed, with authors looking for genes that alter a tumor's response to TCR-based killing (*in vitro*, contrived system) or PD-1 blockade (*in vivo*) (Manguso et al., 2017; Patel et al., 2017). Ultimately, PD-1 blockade functions to reactivate the effector functions of T cells (Lee et al., 2015). Hence, discussion of this *in vivo* screen is relevant. Here, both studies ultimately identified a role for the INFγ/Jak/Stat pathway as a determinant of therapeutic outcome. That an *in vivo* and an *in vitro* screen for related, but not identical T cell therapies would both identify this pathway is indicative of its critical importance for a tumor cell's response to T-cell mediated killing. Indeed, alterations in this pathway have already been described as contributors to resistance to PD-1 inhibitors (Herbst et al., 2014; Zaretsky et al., 2016). Still, significant differences between melanoma and leukemia are already evident by their vastly different clinical responses to CAR-T therapy (Simon & Uslu, 2018). Additionally, therapeutic outcomes in CAR-T treatment appear to be niche-specific in some cases, as discussed above in my CAR-T chapter, indicating that resistance mechanisms to CAR-T response are also likely to vary, at least to some degree, between tumor types residing at different anatomical niches. Lastly, also discussed previously, the full efficacy of a CAR-T cell's function cannot be assayed using only *in vitro* approaches. To address these issues and examine CAR-T resistance specifically in BM derived disease where relapse has now been shown to be a common and recurring challenge, we decided to complete parallel *in vivo* and *in vitro* screens for CAR-T resistance, described in chapter three of this thesis. As the microenvironmental milieu is constantly engaged in conversation with tumor cells, it will be interesting to see what B-ALL specific hits can be identified by our approach, once it is completed, and how those gene sets differ from those acquired in the aforementioned human B-ALL *in vitro* and melanoma screens.

References:

Abdel-Wahab, O. et al. Genetic analysis of transforming events that convert chronic myeloproliferative neoplasms to leukemias. *Cancer Res.* **70**, 447–452 (2010).

Akhavan, D. *et al.* CAR T cells for brain tumors: Lessons learned and road ahead. *Immunol. Rev.* **290**, 60–84 (2019).

Alfarouk, K. O. *et al.* Glycolysis, tumor metabolism, cancer growth and dissemination. A new pH-based etiopathogenic perspective and therapeutic approach to an old cancer question. *Oncoscience* **1**, 777–802 (2014).

Alfarouk, K. O. et al. The possible role of helicobacter pylori in gastric cancer and its management. *Front. Oncol.* **9**, (2019).

Alsaab, H. O. *et al.* PD-1 and PD-L1 checkpoint signaling inhibition for cancer immunotherapy: mechanism, combinations, and clinical outcome. *Front. Pharmacol.* **8**, 1–15 (2017).

Altenschmidt, U., Klundt, E. & Groner, B. Adoptive Transfer of in Vitro-Targeted, Activated T Lymphocytes Results in Total Tumor Regression. *J. Immunol.* **159**, 5509–5515 (1997).

Appelbaum, F. R. Acute Leukemias in Adults. *Abeloff's Clinical Oncology: Sixth Edition* (Elsevier Inc., 2020).

Anderson, K. et al. Genetic variegation of clonal architecture and propagating cells in leukaemia. *Nature* **469**, 356-361 (2011).

Andersson, A. K. et al. The landscape of somatic mutations in infant MLL-rearranged acute lymphoblastic leukemias. *Nat. Genet.* **47**, 330–337 (2015).

Arber, D. A. et al. The 2016 revision to the World Health Organization classification of myeloid neoplasms and acute leukemia. *Blood* **127**, 2391–2405 (2016).

Armstrong, S. A. et al. MLL translocations specify a distinct gene expression profile that distinguishes a unique leukemia. *Nat. Genet.* **30**, 41-47 (2002).

Ashenden, M. *et al.* An in vivo functional screen identifies JNK signaling as a modulator of chemotherapeutic response in breast cancer. *Mol. Cancer Ther.* **16**, 1967–1978 (2017).

Ashton, T. M., Gillies McKenna, W., Kunz-Schughart, L. A. & Higgins, G. S. Oxidative phosphorylation as an emerging target in cancer therapy. *Clin. Cancer Res.* **24**, 2482–2490 (2018).

Bagley, S. J. & O'Rourke, D. M. Clinical investigation of CAR T cells for solid tumors: Lessons learned and future directions. *Pharmacol. Ther.* **205**, (2020).

Barrangou, R. *et al.* CRISPR Provides Acquired Resistance Against Viruses in Prokaryotes. *Science* **315**, 1709–1712 (2007).

Behrmann, L., Wellbrock, J. & Fiedler, W. Acute myeloid leukemia and the bone marrow niche - Take a closer look. *Front. Oncol.* **8**, 1–13 (2018).

Beketic-Oreskovic, L., Durán, G. E., Chen, G., Dumontet, C. & Sikic, B. I. Decreased mutation rate for cellular resistance to doxorubicin and suppression of mdrl gene activation by the cyclosporin PSC 833. *J. Natl. Cancer Inst.* **87**, 1593–1602 (1995).

Bendall, L. J. & Bradstock, K. F. G-CSF: From granulopoietic stimulant to bone marrow stem cell mobilizing agent. *Cytokine Growth Factor Rev.* **25**, 355–367 (2014).

Benmebarek, M. R. et al. Killing mechanisms of chimeric antigen receptor (CAR) T cells. *Int. J. Mol. Sci.* **20**, (2019).

Berns, K. *et al.* A large-scale RNAi screen in human cells identifies new components of the p53 pathway. *Nature* **428**, 431–437 (2004).

Bernt, K. M. & Armstrong, S. A. Leukemia Stem Cells and Human Acute Lymphoblastic Leukemia. *Semin. Hematol.* **46**, 33–38 (2009).

Bernt, K. M. et al. MLL- rearranged leukemia is dependent on aberrant H3K79 methylation by DOT1L. *Cancer Cell* **20**, 66-78 (2011).

Bernt, K. M. & Hunger, S. P. Current concepts in pediatric Philadelphia chromosome-positive acute lymphoblastic leukemia. *Front. Oncol.* **4**, 1–21 (2014).

Beronja, S. *et al.* RNAi screens in mice identify physiological regulators of oncogenic growth. *Nature* **501**, 185–190 (2013).

Betti, C. J. et al. Cleavage of the MLL gene by activators of apoptosis is independent of topoisomerase II activity. *Leukemia* **19**, 2289–2295 (2005).
Bhowmick, N. A. et al. TGF-β Signaling in Fibroblasts Modulates the Oncogenic Potential of Adjacent Epithelia. *Science* **303**, 848–851 (2004).
Biswas, D. et al. Function of leukemogenic mixed lineage leukemia 1 (MLL) fusion proteins through distinct partner protein complexes. *Proc. Natl. Acad. Sci. U. S. A.* **108**, 15751-15756 (2011).
Blanco, J. G. et al. Molecular emergence of acute myeloid leukemia during treatment for acute lymphoblastic leukemia. *Proc. Natl. Acad. Sci. U. S. A.* **98**, 10338-10343 (2001).
Blomen, V. A. *et al.* Gene essentiality and synthetic lethality in haploid human cells. *Science* **350**, 1092–1096 (2015).
Bolotin, A., Quinquis, B., Sorokin, A. & Dusko Ehrlich, S. Clustered regularly interspaced short palindrome repeats (CRISPRs) have spacers of extrachromosomal origin. *Microbiology* **151**, 2551–2561 (2005).
Bonnet, D. & Dick, J. E. Human acute myeloid leukemia is organized as a hierarchy that originates from a primitive hematopoietic cell. *Nat. Med.* **3**, 730-737 (1997).
Borst, P. Cancer drug pan-resistance: Pumps, cancer stem cells, quiescence, epithelial to mesenchymal transition, blocked cell death pathways, persisters or what? *Open Biol.* **2**, 120066 (2012).
Borthakur, G. et al. BL-8040, a Peptidic CXCR4 Antagonist, Induces Leukemia Cell Death and Specific Leukemia Cell Mobilization in Relapsed/Refractory Acute Myeloid Leukemia Patients in an Ongoing Phase IIa Clinical Trial. *Blood* **124**, 950–950 (2014).
Bosc, C., Selak, M. A. & Sarry, J. E. Resistance Is Futile: Targeting Mitochondrial Energetics and Metabolism to Overcome Drug Resistance in Cancer Treatment. *Cell Metab.* **26**, 705–707 (2017).
Bouwman, P. & Jonkers, J. The effects of deregulated DNA damage signalling on cancer chemotherapy response and resistance. *Nat. Rev. Cancer* **12**, 587–598 (2012).
Boveri, T. Concerning the Origin of Malignant Tumours by Theodor Boveri. Translated and annotated by Henry Harris. *J. Cell Sci.* **121**, 1 LP – 84 (2008).
Bowman, R. L., Busque, L. & Levine, R. L. Clonal Hematopoiesis and Evolution to Hematopoietic Malignancies. *Cell Stem Cell* **22**, 157–170 (2018).
Bowman, R. L. & Levine, R. L. TET2 in Normal and Malignant Hematopoiesis. *Cold Spring Harb. Perspect. Med.* **7**, 1–12 (2017).
Braun, C. J. *et al.* Versatile in vivo regulation of tumor phenotypes by dCas9-mediated transcriptional perturbation. *Proc. Natl. Acad. Sci.* **113**, E3892–E3900 (2016).
Brentjens, R. J. *et al.* Safety and persistence of adoptively transferred autologous CD19-targeted T cells in patients with relapsed or chemotherapy refractory B-cell leukemias. *Blood* **118**, 4817–4828 (2011).
Bric, A. *et al.* Functional Identification of Tumor-Suppressor Genes through an In Vivo RNA Interference Screen in a Mouse Lymphoma Model. *Cancer Cell* **16**, 324–335 (2009).
Broeker, P. L. S. et al. Distribution of 11q23 breakpoints within the MLL breakpoint cluster region in de novo acute leukemia and in treatment-related acute myeloid leukemia: correlation with scaffold attachment regions and topoisomerase II consensus binding sites. *Blood* **87**, 1912–1922 (1996).
Broere, F. & van Eden, W. T Cell Subsets and T Cell-Mediated Immunity. in *Nijkamp and Parnham's Principles of Immunopharmacology* 23–35 (Springer International Publishing, 2019).
Brown, C. E. *et al.* Regression of glioblastoma after chimeric antigen receptor T-cell therapy. *N. Engl. J. Med.* **375**, 2561–2569 (2016).
Brummelkamp, T. R., Bernards, R. & Agami, R. A system for stable expression of short interfering RNAs in mammalian cells. *Science* **296**, 550–553 (2002).
Buelow, D. R. et al. Uncovering the Genomic Landscape in Newly Diagnosed and Relapsed Pediatric Cytogenetically Normal FLT3-ITD AML. *Clin. Transl. Sci.* **12**, 641–647 (2019).
Buick, R. N., Till, J. E. & Mcculloch, E. A. Colony assay for proliferative blast cells circulating in myeloblastic leukaemia. *Lancet* **1**, 862-863 (1977).
Burgess, D. J. et al. Topoisomerase levels determine chemotherapy response in vitro and in vivo. *Proc. Natl. Acad. Sci. U. S. A.* **105**, 9053–9058 (2008).
Campbell, P. J. *et al.* Pan-cancer analysis of whole genomes. *Nature* **578**, 82–93 (2020).
Campos-Sanchez, E. et al. Acute lymphoblastic leukemia and developmental biology. *Cell Cycle* **10**, 3473–3486 (2011).

Carette, J. E. *et al.* Haploid genetic screens in human cells identify host factors used by pathogens. *Science* **326**, 1231–1235 (2009).
Carpenito, C. et al. Control of large, established tumor xenografts with genetically retargeted human T cells containing CD28 and CD137 domains. *Proc. Natl. Acad. Sci. U. S. A.* **106**, 3360–3365 (2009).
Caslini, C. et al. Interaction of MLL amino terminal sequences with Menin is required for transformation. *Cancer Res* **67**, 7275–7283 (2007).
Cassier, P. A., Castets, M., Belhabri, A. & Vey, N. Targeting apoptosis in acute myeloid leukaemia. *Br. J. Cancer* **117**, 1089–1098 (2017).
Chan, A. K. N. & Chen, C. W. Rewiring the epigenetic networks in MLL-rearranged leukemias: Epigenetic dysregulation and pharmacological interventions. *Front. Cell Dev. Biol.* **7**, 1–15 (2019).
Chang, M. J. et al. Histone H3 lysine 79 methyltransferase Dot1 is required for immortalization by MLL oncogenes. *Cancer Res* **70**, 10234-10242 (2010).
Chapeau, E. A. *et al.* Resistance mechanisms to TP53-MDM2 inhibition identified by in vivo piggyBac transposon mutagenesis screen in an Arf-/-mouse model. *Proc. Natl. Acad. Sci. U. S. A.* **114**, 3151–3156 (2017).
Chapuis, N., Poulain, L., Birsen, R., Tamburini, J. & Bouscary, D. Rationale for targeting deregulated metabolic pathways as a therapeutic strategy in acute myeloid leukemia. *Front. Oncol.* **9**, 1–8 (2019).
Charles, N. J. & Boyer, D. F. Mixed-phenotype acute leukemia: Diagnostic criteria and pitfalls. *Arch. Pathol. Lab. Med.* **141**, 1462–1468 (2017).
Chavez, J. C., Bachmeier, C. & Kharfan-Dabaja, M. A. CAR T-cell therapy for B-cell lymphomas: clinical trial results of available products. *Ther. Adv. Hematol.* **10**, 1-10 (2019).
Chen, G. *et al.* Exosomal PD-L1 contributes to immunosuppression and is associated with anti-PD-1 response. *Nature* **560**, 382–386 (2018).
Chen, L. & Flies, D. B. Molecular mechanisms of T cell co-stimulation and co-inhibition. *Nat. Rev. Immunol.* **13**, 227–242 (2013).
Chen, S. *et al.* Genome-wide CRISPR screen in a mouse model of tumor growth and metastasis. *Cell* **160**, 1246–1260 (2015).
Chen, W. et al. Malignant transformation initiated by Mll-AF9: gene dosage and critical target cells. *Cancer Cell* **13**, 432–440 (2008).
Chen, Y. et al. CXCR4 downregulation of let-7a drives chemoresistance in acute myeloid leukemia. *J. Clin. Invest*. **123**, 2395–2407 (2013).
Chen, Y. X. et al. The tumor suppressor Menin regulates hematopoiesis and myeloid transformation by influencing Hox gene expression. *Proc. Natl. Acad. Sci. U. S. A.* **103**, 1018–1023 (2006).
Cheng, J. *et al.* Understanding the Mechanisms of Resistance to CAR T-Cell Therapy in Malignancies. *Front. Oncol.* **9**, 1–9 (2019).
Choi, C.-H. & Ling, V. Isolation and characterization of daunorubicin-resistant AML-2 sublines. *Mol. Cells* **7**, 170–177 (1997).
Chou, J. P. & Effros, R. B. T Cell Replicative Senescence in Human Aging. *Curr. Pharm. Des.* **19**, 1680–1698 (2013).
Chow, R. D. *et al.* AAV-mediated direct in vivo CRISPR screen identifies functional suppressors in glioblastoma. *Nat. Neurosci.* **20**, 1329–1341 (2017).
Chow, R. D. & Chen, S. Cancer CRISPR Screens In Vivo. *Trends in Cancer* **4**, 349–358 (2018).
Chowdhury, T. & Brady, H. J. M. Insights from clinical studies into the role of the MLL gene in infant and childhood leukemia. *Blood Cells Mol Dis* **40**, 192-199 (2008).
Chung, E. Y. *et al.* CD19 is a major B cell receptor–independent activator of MYC-driven B-lymphomagenesis. *J. Clin. Invest.* **122**, 2257–2266 (2012).
Churpek, J. E. & Bresnick, E. H. Transcription factor mutations as a cause of familial myeloid neoplasms. *J. Clin. Invest.* **129**, 476–488 (2019).
Clarkson, B., Ohkita, T., Ota, K. & Fried, J. Studies of cellular proliferation in human leukemia. I. Estimation of growth rates of leukemic and normal hematopoietic cells in two adults with acute leukemia given single injections of tritiated thymidine. *J. Clin. Invest.* **46**, 506-529 (1967).
Clarkson, B. D. Review of recent studies of cellular proliferation in acute leukemia. *Natl. Cancer Inst. Monogr.* **30**, 81-120 (1969).

Cole, A. et al. Inhibition of the Mitochondrial Protease ClpP as a Therapeutic Strategy for Human Acute Myeloid Leukemia. *Cancer Cell* **27**, 864–876 (2015).
Collins, C. T., and Hess, J. L. Deregulation of the HOXA9/MEIS1 axis in acute leukemia. *Curr. Opin. Hematol.* **23**, 354–361 (2016).
Cong, L. *et al.* Multiplex genome engineering using CRISPR/Cas systems. *Science* **339**, 819–823 (2013).
Copeland, N. G. & Jenkins, N. A. Harnessing transposons for cancer gene discovery. *Nat. Rev. Cancer* **10**, 696–706 (2010).
Corces-Zimmerman, M. R. et al. Preleukemic mutations in human acute myeloid leukemia affect epigenetic regulators and persist in remission. *Proc. Natl. Acad. Sci. U. S. A.* **111**, 2548–2553 (2014).
Cozzio, A. et al. Similar MLL-associated leukemias arising from self-renewing stem cells and short-lived myeloid progenitors. *Genes Dev.* **17**, 3029–3035 (2003).
Craddock, C. et al. Azacitidine fails to eradicate leukemic stem/ progenitor cell populations in patients with acute myeloid leukemia and myelodysplasia. *Leukemia* **27**, 1028-1036 (2013).
Cremer, A. *et al.* Resistance Mechanisms to SYK Inhibition in Acute Myeloid Leukemia. *Cancer Discov.* **10**, 214–231 (2020).
Crispino, J. D. & Horwitz, M. S. GATA factor mutations in hematologic disease. *Blood* **129**, 2103–2110 (2017).
Crotty, S. & Pipkin, M. E. In vivo RNAi screens: Concepts and applications. *Trends Immunol.* **36**, 315–322 (2015).
Daigle, S. R. et al. Potent inhibition of DOT1L as treatment of MLL-fusion leukemia. *Blood* **122**, 1017-1025 (2013).
Daley, G., Van Etten, R. & Baltimore, D. Induction of chronic myelogenous leukemia in mice by the $P210^{bcr/abl}$ gene of the Philadelphia chromosome. *Science* **247**, 824–830 (1990).
Dang, L. et al. Cancer-associated IDH1 mutations produce 2-hydroxyglutarate. *Nature* **462**, 739-744 (2009).
Daniyan, A. F. O. & Brentjens, R. J. At the Bench: Chimeric antigen receptor (CAR) T cell therapy for the treatment of B cell malignancies. *J. Leukoc. Biol.* **100**, 1255–1264 (2016).
Davies, H. *et al.* Mutations of the BRAF gene in human cancer. *Nature* **417**, 949–954 (2002).
De Kouchkovsky, I. & Abdul-Hay, M. Acute myeloid leukemia: A comprehensive review and 2016 update. *Blood Cancer J.* **6**, (2016).
De Rosa, V. et al. Reversal of warburg effect and reactivation of oxidative phosphorylation by differential inhibition of EGFR signaling pathways in non-small cell lung cancer. *Clin. Cancer Res.* **21**, 5110–5120 (2015).
de Thé, H., Pandolfi, P. P. & Chen, Z. Acute Promyelocytic Leukemia: A Paradigm for Oncoprotein-Targeted Cure. *Cancer Cell* **32**, 552–560 (2017).
Del Nagro, C. J. *et al.* CD19 Function in Central and Peripheral B-Cell Development. *Immunol. Res.* **31**, 119–132 (2005).
Delhommeau F, Dupont S, Della Valle V, James C, Trannoy S, Masse A et al. Mutation in TET2 in myeloid cancers. *N. Engl. J. Med.* **360**, 2289–2301 (2009).
Deltcheva, E. *et al.* CRISPR RNA maturation by trans-encoded small RNA and host factor RNase III. *Nature* **471**, 602–607 (2011).
DeNicola, G. M., Karreth, F. A., Adams, D. J. & Wong, C. C. The utility of transposon mutagenesis for cancer studies in the era of genome editing. *Genome Biol.* **16**, 1–15 (2015).
Depil, S., Duchateau, P., Grupp, S. A., Mufti, G. & Poirot, L. 'Off-the-shelf' allogeneic CAR T cells: development and challenges. *Nat. Rev. Drug Discov.* **19**, 185–199 (2020).
Deveau, H. *et al.* Phage response to CRISPR-encoded resistance in Streptococcus thermophilus. *J. Bacteriol.* **190**, 1390–1400 (2008).
DeVita, V. T. & Chu, E. A History of Cancer Chemotherapy. *Cancer Res.* **68**, 8643–8653 (2008).
Dhillon, S. Ivosidenib: first global approval. *Drugs* **78**, 1509-1516 (2018).
Dickins, R. A. *et al.* Probing tumor phenotypes using stable and regulated synthetic microRNA precursors. *Nat. Genet.* **37**, 1289–1295 (2005).
DiNardo, C. D. & Cortes, J. E. Mutations in AML: prognostic and therapeutic implications. *Hematol. Am. Soc. Hematol. Educ. Progr.* **2016**, 348–355 (2016).

DiNardo, C. D. et al. Safety and preliminary efficacy of venetoclax with decitabine or azacitidine in elderly patients with previously untreated acute myeloid leukaemia: a non-randomised, open-label, phase 1b study. *Lancet Oncol.* **19**, 216–228 (2018).
DiNardo, C. D. et al. Venetoclax combined with decitabine or azacitidine in treatment-naive, elderly patients with acute myeloid leukemia. *Blood* **133**, 7–17 (2019).
Ding, L., et al: Clonal evolution in relapsed acute myeloid leukaemia revealed by whole-genome sequencing. *Nature* **481**, 506-510 (2012).
Ding, L. et al. Perspective on Oncogenic Processes at the End of the Beginning of Cancer Genomics. *Cell* **173**, 305-320.e10 (2018).
Ding, S. *et al.* Efficient transposition of the piggyBac (PB) transposon in mammalian cells and mice. *Cell* **122**, 473–483 (2005).
DiNofia, A. M. & Maude, S. L. Chimeric Antigen Receptor T-Cell Therapy Clinical Results in Pediatric and Young Adult B-ALL. *HemaSphere* **3**, e279 (2019).
Djabali, M. et al. A trithorax-like gene is interrupted by chromosome 11q23 translocations in acute leukaemias. *Nat. Genet.* **2**, 113-118 (1992).
Dobosz, P. & Dzieciątkowski, T. The Intriguing History of Cancer Immunotherapy. *Front. Immunol.* **10**, (2019).
Dobson, C. L., Warren, A. J., Pannell, R., Forster, A., Rabbitts, T. H. Tumorigenesis in mice with a fusion of the leukaemia oncogene Mll and the bacterial lacZ gene. *EMBO J.* **19**, 843-851 (2000).
Döhner, H., Weisdorf, D. J. & Bloomfield, C. D. Acute myeloid leukemia. *N. Engl. J. Med.* **373**, 1136–1152 (2015).
Döhner, H. et al. Global Acute Myeloid Leukemia Epidemiology and Patient Flow Analysis 2016. *Blood* **129**, 424–448 (2017).
Dolberg, D. S. & Bissell, M. J. Inability of Rous sarcoma virus to cause sarcomas in the avian embryo. *Nature* **309**, 552–556 (1984).
Dong, M. B. *et al.* Systematic Immunotherapy Target Discovery Using Genome-Scale In Vivo CRISPR Screens in CD8 T Cells. *Cell* **178**, 1189-1204.e23 (2019).
Druker, B. J. et al. Effects of a selective inhibitor of the Abl tyrosine kinase on the growth of Bcr–Abl positive cells. *Nat. Med.* **2**, 561–566 (1996).
Druker, B. J. et al. Efficacy and Safety of a Specific Inhibitor of the BCR-ABL Tyrosine Kinase in Chronic Myeloid Leukemia. *N. Engl. J. Med.* **344**, 1031–1037 (2001a).
Druker, B. J. et al. Activity of a Specific Inhibitor of the BCR-ABL Tyrosine Kinase in the Blast Crisis of Chronic Myeloid Leukemia and Acute Lymphoblastic Leukemia with the Philadelphia Chromosome. *N. Engl. J. Med.* **344**, 1038–1042 (2001b).
Drynan, L. F. et al. Mll fusions generated by Cre-loxP-mediated de novo translocations can induce lineage reassignment in tumorigenesis. *EMBO J.* **24**, 3136–3146 (2005).
Duan, C. W. et al. Leukemia propagating cells rebuild an evolving niche in response to therapy. *Cancer Cell* **25**, 778–793 (2014).
Dupuy, A. J., Akagi, K., Largaespada, D. A., Copeland, N. G. & Jenkins, N. A. Mammalian mutagenesis using a highly mobile somatic Sleeping Beauty transposon system. *Nature* **436**, 221–226 (2005).
Dupuy, A. J. *et al.* A modified sleeping beauty transposon system that can be used to model a wide variety of human cancers in mice. *Cancer Res.* **69**, 8150–8156 (2009).
Ebinger, S. et al. Characterization of Rare, Dormant, and Therapy-Resistant Cells in Acute Lymphoblastic Leukemia. *Cancer Cell* **30**, 849–862 (2016).
Eppert, K. et al. Stem cell gene expression programs influence clinical outcome in human leukemia. *Nat. Med.* **17**, 1086–1093 (2011).
Erb, M. A. *et al.* Transcription control by the ENL YEATS domain in acute leukaemia. *Nature* **543**, 270–274 (2017).
Eyquem, J. *et al.* Targeting a CAR to the TRAC locus with CRISPR/Cas9 enhances tumour rejection. *Nature* **543**, 113–117 (2017).
Falini, B. et al. Cytoplasmic nucleophosmin in acute myelogenous leukemia with a normal karyotype. *N Engl J Med.***352**, 254-266 (2005).

Fan, H. Leukemogenesis by Moloney murine leukemia virus: A multistep process. *Trends Microbiol.* **5**, 74–82 (1997).
Farge, T. et al. Chemotherapy-Resistant Human Acute Myeloid Leukemia Cells Are Not Enriched for Leukemic Stem Cells but Require Oxidative Metabolism. *Cancer Discov* **7**, 716–735 (2017).
Farrar, J. E. et al. Genomic profiling of pediatric acute myeloid leukemia reveals a changing mutational landscape from disease diagnosis to relapse. *Cancer Res.* **76**, 2197–2205 (2016).
Fernandez, H. F. *et al.* Anthracycline Dose Intensification in Acute Myeloid Leukemia. *N. Engl. J. Med.* **361**, 1249–1259 (2009).
Ferrando, A. A. & López-Otín, C. Clonal evolution in leukemia. *Nat. Med.* **23**, 1135–1145 (2017).
Ferrara, J. L., Levine, J. E., Reddy, P. & Holler, E. Graft-versus-host disease. *Lancet* **373**, 1550–1561 (2009).
Feucht, J. *et al.* Calibration of CAR activation potential directs alternative T cell fates and therapeutic potency. *Nat. Med.* **25**, 82–88 (2019).
Fiedler, E. C. & Hemann, M. T. Aiding and Abetting: How the Tumor Microenvironment Protects Cancer from Chemotherapy. *Annu. Rev. Cancer Biol.* **3**, 409–428 (2019).
Figueroa, M. E. et al. DNA methylation signatures identify biologically distinct subtypes in acute myeloid leukemia. *Cancer Cell* **17**, 13-27 (2010a).
Figueroa, M. E. et al. Leukemic IDH1 and IDH2 mutations result in a hypermethylation phenotype, disrupt TET2 function, and impair hematopoietic differentiation. *Cancer Cell* **18**, 553–567 (2010b).
Fire, A. *et al.* Potent and specific genetic interference by double-stranded RNA in Caenorhabditis elegans. *Nature* **391**, 806–811 (1998).
Fischer, K. *et al.* Inhibitory effect of tumor cell-derived lactic acid on human T cells. *Blood* **109**, 3812–3819 (2007).
Fraietta, J. A. *et al.* Determinants of response and resistance to CD19 chimeric antigen receptor (CAR) T cell therapy of chronic lymphocytic leukemia. *Nat. Med.* **24**, 563–571 (2018).
Frigault, M. J. & Maus, M. V. State of the art in CAR T cell therapy for CD19+ B cell malignancies. *J. Clin. Invest.* **130**, 1586–1594 (2020).
Fry, T. J. *et al.* CD22-targeted CAR T cells induce remission in B-ALL that is naive or resistant to CD19-targeted CAR immunotherapy. *Nat. Med.* **24**, 20–28 (2018).
Gagné, L. M., Boulay, K., Topisirovic, I., Huot, M. É. & Mallette, F. A. Oncogenic Activities of IDH1/2 Mutations: From Epigenetics to Cellular Signaling. *Trends Cell Biol.* **27**, 738–752 (2017).
Gallipoli, P. *et al.* Glutaminolysis is a metabolic dependency in FLT3ITDacute myeloid leukemia unmasked by FLT3 tyrosine kinase inhibition. *Blood* **131**, 1639–1653 (2018).
Gardner, R. *et al.* Acquisition of a CD19-negative myeloid phenotype allows immune escape of MLL-rearranged B-ALL from CD19 CAR-T-cell therapy. *Blood* **127**, 2406–2410 (2016).
Gardner, R. A. *et al.* Intent-to-treat leukemia remission by CD19 CAR T cells of defined formulation and dose in children and young adults. *Blood* **129**, 3322–3331 (2017).
Garg, M. et al. Profiling of somatic mutations in acute myeloid leukemia with FLT3-ITD at diagnosis and relapse. *Blood* **126**, 2491–2501 (2015).
Gargiulo, G. *et al.* In Vivo RNAi Screen for BMI1 Targets Identifies TGF-β/BMP-ER Stress Pathways as Key Regulators of Neural- and Malignant Glioma-Stem Cell Homeostasis. *Cancer Cell* **23**, 660–676 (2013).
Gargiulo, G. Next-generation in vivo modeling of human cancers. *Front. Oncol.* **8**, (2018).
Gasiunas, G., Barrangou, R., Horvath, P. & Siksnys, V. Cas9-crRNA ribonucleoprotein complex mediates specific DNA cleavage for adaptive immunity in bacteria. *Proc. Natl. Acad. Sci.* **109**, E2579–E2586 (2012).
Genovese G, Kähler AK, Rose SA et al. Clonal hematopoiesis and blood-cancer risk inferred from blood DNA sequence. *N Engl J Med.* **371**, 2477-2487 (2014).
Gentles, A. J., Plevritis, S. K., Majeti, R., Alizadeh, A. A. Association of a leukemic stem cell gene expression signature with clinical outcomes in acute myeloid leukemia. *JAMA* **304**, 2706–2715 (2010).
Gerhards, N. M. & Rottenberg, S. New tools for old drugs: Functional genetic screens to optimize current chemotherapy. *Drug Resist. Updat.* **36**, 30–46 (2018).

Geyer, M. B. et al. Overall survival among older US adults with ALL remains low despite modest improvement since 1980: SEER analysis. *Blood* **129**, 1878–1881 (2017).
Ghassemi, S. *et al.* Reducing ex vivo culture improves the antileukemic activity of chimeric antigen receptor (CAR) T cells. *Cancer Immunol. Res.* **6**, 1100–1109 (2018).
Giaever, G. *et al.* Functional profiling of the Saccharomyces cerevisiae genome. *Nature* **418**, 387–391 (2002).
Gillet, J.-P., Varma, S. & Gottesman, M. M. The Clinical Relevance of Cancer Cell Lines. *JNCI J. Natl. Cancer Inst.* **105**, 452–458 (2013).
Goardon, N. et al. Coexistence of LMPP-like and GMP-like leukemia stem cells in acute myeloid leukemia. *Cancer Cell* **19**, 138–152 (2011).
Golub, D. *et al.* Mutant Isocitrate Dehydrogenase Inhibitors as Targeted Cancer Therapeutics. *Front. Oncol.* **9**, (2019).
Gross, G., Waks, T. & Eshhar, Z. Expression of immunoglobulin-T-cell receptor chimeric molecules as functional receptors with antibody-type specificity. *Proc. Natl. Acad. Sci. U. S. A.* **86**, 10024–10028 (1989).
Gu, Y. et al. The t(4;11) chromosome translocation of human acute leukemias fuses the ALL-1 gene, related to Drosophila trithorax, to the AF-4 gene. *Cell* **71**, 701-708 (1992).
Hamieh, M. *et al.* CAR T cell trogocytosis and cooperative killing regulate tumour antigen escape. *Nature* **568**, 112–116 (2019).
Hanahan, D. & Weinberg, R. A. Hallmarks of cancer: The next generation. *Cell* **144**, 646–674 (2011).
Hartwell, L. H., Culotti, J., Pringle, J. R. & Reid, B. J. Genetic Control of the Cell Division Cycle in Yeast: A model to account for the order of cell cycle events is deduced from the phenotypes of yeast mutants. *Science,* **183**, 46–51 (1974).
He, N. et al. Human polymerase-associated factor complex (PAFc) connects the super elongation complex (SEC) to RNA polymerase II on chromatin. *Proc. Natl. Acad. Sci. U. S. A.* **108**, E636-645 (2011).
Heckl, D. *et al.* Generation of mouse models of myeloid malignancy with combinatorial genetic lesions using CRISPR-Cas9 genome editing. *Nat. Biotechnol.* **32**, 941–946 (2014).
Hegde, M. *et al.* Expansion of HER2-CAR T cells after lymphodepletion and clinical responses in patients with advanced sarcoma. *J. Clin. Oncol.* **35**, 10508 (2017).
Heisterkamp, N. et al. Acute leukaemia in bcr/abl transgenic mice. *Nature* **344**, 251–253 (1990).
Herbst, R. S. *et al.* Predictive correlates of response to the anti-PD-L1 antibody MPDL3280A in cancer patients. *Nature* **515**, 563–567 (2014).
Heuser, M. et al. Cell of origin in AML: susceptibility to MN1-induced transformation is regulated by the MEIS1/AbdB-like HOX protein complex. Cancer Cell **20**, 39–52 (2011).
Hirsch, P. et al. Genetic hierarchy and temporal variegation in the clonal history of acute myeloid leukaemia. *Nat. Commun.* **7**, (2016).
Ho, T.C. et al. Evolution of acute myelogenous leukemia stem cell properties after treatment and progression. *Blood* **128**, 1671-1678 (2016).
Holohan, C., Van Schaeybroeck, S., Longley, D. B. & Johnston, P. G. Cancer drug resistance: an evolving paradigm. *Nat. Rev. Cancer* **13**, 714–726 (2013).
Horowitz, M. M. et al. Graft-versus-leukemia reactions after bone marrow transplantation. *Blood* **75**, 555–562 (1990).
Horton, T. M., Steuber, C. P. & Aster, J. C. Overview of the presentation and diagnosis of acute lymphoblastic leukemia in children. *UpToDate*, accessed March 10, 2020, from: https://www.uptodate.com/contents/overview-of-the-clinical-presentation-and-diagnosis-of-acute-lymphoblastic-leukemia-lymphoma-in-children (2019).
Hou, P. *et al.* A Genome-Wide CRISPR Screen Identifies Genes Critical for Resistance to FLT3 Inhibitor AC220. *Cancer Res.* **77**, 4402–4413 (2017).
Hou, W. *et al.* The MEK inhibitors enhance the efficacy of sorafenib against hepatocellular carcinoma cells through reducing p-ERK rebound. *Transl. Cancer Res.* **8**, 1224–1232 (2019).
Hunger, S. P. & Mullighan, C. G. Acute Lymphoblastic Leukemia in Children. *N. Engl. J. Med.* **373**, 1541–1552 (2015).

Huntly, B. J. et al. MOZ-TIF2, but not BCR-ABL, confers properties of leukemic stem cells to committed murine hematopoietic progenitors. *Cancer Cell* **6**, 587–596 (2004).
Iacobucci, I. & Mullighan, C. G. Genetic basis of acute lymphoblastic leukemia. *J. Clin. Oncol.* **35**, 975–983 (2017).
Inaba, H., Greaves, M. & Mullighan, C.G. Acute lymphoblastic leukemia. *Lancet* **381**, 1943-1955 (2013).
Ippolito, L. et al. Metabolic shift toward oxidative phosphorylation in docetaxel resistant prostate cancer cells. *Oncotarget* **7**, 61890–61904 (2016).
Ishikawa, F. et al. Chemotherapy-resistant human AML stem cells home to and engraft within the bone-marrow endosteal region. *Nat. Biotechnol.* **25**, 1315–1321 (2007).
Ishino, Y., Shinagawa, H., Makino, K., Amemura, M. & Nakatura, A. Nucleotide sequence of the iap gene, responsible for alkaline phosphatase isoenzyme conversion in Escherichia coli, and identification of the gene product. *J. Bacteriol.* **169**, 5429–5433 (1987).
Ivics, Z., Hackett, P. B., Plasterk, R. H. & Izsvák, Z. Molecular Reconstruction of Sleeping Beauty, a Tc1-like Transposon from Fish, and Its Transposition in Human Cells. *Cell* **91**, 501–510 (1997).
Jacoby, E. *et al.* CD19 CAR immune pressure induces B-precursor acute lymphoblastic leukaemia lineage switch exposing inherent leukaemic plasticity. *Nat. Commun.* **7**, 12320 (2016).
Jain, N., et al. Ph-like acute lymphoblastic leukemia: a high-risk subtype in adults. *Blood* **129**, 572-581 (2017).
Jaiswal, S., et al. Age-related clonal hematopoiesis associated with adverse outcomes. *N. Engl. J. Med.* **371**, 2488-2498 (2014).
Jamieson, C. H. et al. Granulocyte-macrophage progenitors as candidate leukemic stem cells in blast-crisis CML. N*. Engl. J. Med.* **351**, 657–667 (2004).
Jan, M. et al. Clonal evolution of preleukemic hematopoietic stem cells precedes human acute myeloid leukemia. *Sci. Transl. Med.* **4**, 149ra118 (2012).
Jinek, M. *et al.* A programmable dual-RNA-guided DNA endonuclease in adaptive bacterial immunity. *Science* **337**, 816–821 (2012).
Jones, C. L. et al. Inhibition of Amino Acid Metabolism Selectively Targets Human Leukemia Stem Cells. *Cancer Cell* **34**, 724-740.e4 (2018).
Jones, W. D. et al. De novo mutations in MLL cause Wiedemann-Steiner syndrome. *Am. J. Hum. Genet.* **91**, 358-364 (2012).
Jongen-Lavrencic, M. et al. Molecular minimal residual disease in acute myeloid leukemia. *N. Engl. J. Med.* **378**, 1189–1199 (2018).
Joyce, J. A. & Fearon, D. T. T cell exclusion, immune privilege, and the tumor microenvironment. *Science* **348**, 74–80 (2015).
June, C. H., O'Connor, R. S., Kawalekar, O. U., Ghassemi, S. & Milone, M. C. CAR T cell immunotherapy for human cancer. *Science* **359**, 1361–1365 (2018).
Jung, N., Dai, B., Gentles, A. J., Majeti, R. & Feinberg, A. P. An LSC epigenetic signature is largely mutation independent and implicates the HOXA cluster in AML pathogenesis. *Nat. Commun*. **6**, 8489 (2015).
Kampmann, M. CRISPRi and CRISPRa Screens in Mammalian Cells for Precision Biology and Medicine. *ACS Chem. Biol.* **13**, 406–416 (2018).
Kas, S. M. *et al.* Transcriptomics and transposon mutagenesis identify multiple mechanisms of resistance to the FGFR inhibitor AZD4547. *Cancer Res.* **78**, 5668–5679 (2018).
Katigbak, A. *et al.* A CRISPR/Cas9 Functional Screen Identifies Rare Tumor Suppressors. *Sci. Rep.* **6**, 1–8 (2016).
Kawalekar, O. U. *et al.* Distinct Signaling of Coreceptors Regulates Specific Metabolism Pathways and Impacts Memory Development in CAR T Cells. *Immunity* **44**, 380–390 (2016).
Kershaw, M. H. et al. A phase I study on adoptive immunotherapy using gene-modified T cells for ovarian cancer. *Clin. Cancer Res.* **12**, 6106–6115 (2006).
Kim, E. S. Enasidenib: first global approval. *Drugs* **77**, 1705–1711 (2017).
Kim, T. et al. Clonal dynamics in a single AML case tracked for 9 years reveals the complexity of leukemia progression. *Leukemia* **30**, 295–302 (2016).
Kim, W. Y. & Sharpless, N. E. The Regulation of INK4/ARF in Cancer and Aging. *Cell* **127**, 265–275 (2006).

Klemm, F. & Joyce, J. A. Microenvironmental regulation of therapeutic response in cancer. *Trends Cell Biol.* **25**, 198–213 (2015).
Klichinsky, M. et al. Human chimeric antigen receptor macrophages for cancer immunotherapy. *Nat. Biotechnol.* (2020). doi:10.1038/s41587-020-0462-y [Epub ahead of print]
Kochenderfer, J. N. et al. Construction and preclinical evaluation of an anti-CD19 chimeric antigen receptor. *J. Immunother.* **32**, 689–702 (2009).
Kochenderfer, J. N. *et al.* Eradication of B-lineage cells and regression of lymphoma in a patient treated with autologous T cells genetically engineered to recognize CD19. *Blood* **116**, 4099–4102 (2010).
Kochenderfer, J. N. *et al.* Lymphoma Remissions Caused by Anti-CD19 Chimeric Antigen Receptor T Cells Are Associated With High Serum Interleukin-15 Levels. *J. Clin. Oncol.* **35**, 1803–1813 (2017).
Kodama, M. *et al.* In vivo loss-of-function screens identify KPNB1 as a new druggable oncogene in epithelial ovarian cancer. *Proc. Natl. Acad. Sci. U. S. A.* **114**, E7301–E7310 (2017).
Kode, A. et al. Leukaemogenesis induced by an activating β-catenin mutation in osteoblasts. *Nature* **506**, 240–244 (2014).
Kode, A. et al. FoxO1-dependent induction of acute myeloid leukemia by osteoblasts in mice. *Leukemia* **30**, 1–13 (2016).
Koike-Yusa, H., Li, Y., Tan, E. P., Velasco-Herrera, M. D. C. & Yusa, K. Genome-wide recessive genetic screening in mammalian cells with a lentiviral CRISPR-guide RNA library. *Nat. Biotechnol.* **32**, 267–273 (2014).
Kong, Y. et al. CD34+CD38+CD19+ as well as CD34+CD38−CD19+ cells are leukemia-initiating cells with self-renewal capacity in human B-precursor ALL. *Leukemia* **22**, 1207–1213 (2008).
Konoplev, S. et al. Overexpression of CXCR4 predicts adverse overall and event-free survival in patients with unmutated FLT3 acute myeloid leukemia with normal karyotype. *Cancer* **109**, 1152–1156 (2007).
Konopleva, M. et al. Efficacy and biological correlates of response in a phase II study of venetoclax monotherapy in patients with acute Myelogenous Leukemia. *Cancer Discov.* **6**, 1106–1117 (2016).
Kreitz, J. et al. Metabolic Plasticity of Acute Myeloid Leukemia. *Cells* **8**, 805 (2019).
Kreso, A. & Dick, J. E. Evolution of the cancer stem cell model. *Cell Stem Cell* **14**, 275–291 (2014).
Krivtsov, A. V. et al. Transformation from committed progenitor to leukaemia stem cell initiated by MLL–AF9. *Nature* **442**, 818–822 (2006).
Krivtsov, A. V. & Armstrong, S. A. MLL translocations, histone modifications and leukaemia stem-cell development. *Nat. Rev. Cancer* **7**, 823–833 (2007).
Krivtsov, A. V. et al. H3K79 methylation profiles define murine and human MLL-AF4 leukemias. *Cancer Cell* **14**, 355-368 (2008).
Krivtsov, A. V. et al. Cell of origin determines clinically relevant subtypes of MLL-rearranged AML. *Leukemia* **27**, 852–860 (2013).
Krönke, J. et al. Clonal evolution in relapsed NPM1-mutated acute myeloid leukemia. *Blood* **122**, 100-108 (2013).
Kumar, C. C. Genetic abnormalities and challenges in the treatment of acute myeloid Leukemia. *Genes and Cancer* **2**, 95–107 (2011).
Kuntz, E. M. et al. Targeting mitochondrial oxidative phosphorylation eradicates therapy-resistant chronic myeloid leukemia stem cells. *Nat. Med.* **23**, 1234–1240 (2017).
Kurata, M. *et al.* Using genome-wide CRISPR library screening with library resistant DCK to find new sources of Ara-C drug resistance in AML. *Sci. Rep.* **6**, 4–13 (2016).
Lagadinou, E. D. et al. BCL-2 inhibition targets oxidative phosphorylation and selectively eradicates quiescent human leukemia stem cells. *Cell Stem Cell* **12**, 329–341 (2013).
Lagos-Quintana, M., Rauhut, R., Lendeckel, W. & Tuschl, T. Identification of novel genes coding for small expressed RNAs. *Science* **294**, 853–858 (2001).
Lai, C., Doucette, K. & Norsworthy, K. Recent drug approvals for acute myeloid leukemia. *J. Hematol. Oncol.* **12**, 1–20 (2019).
Lamers, C. H. J. *et al.* Immune responses to transgene and retroviral vector in patients treated with ex vivo-engineered T cells. *Blood* **117**, 72–82 (2011).
Lapidot, T. et al. A cell initiating human acute myeloid leukaemia after transplantation into SCID mice. *Nature* **367**, 645-648 (1994).

Lauchle, J. O. *et al.* Response and resistance to MEK inhibition in leukaemias initiated by hyperactive Ras. *Nature* **461**, 411–414 (2009).
Lawrence, H. J. et al. Mice bearing a targeted interruption of the homeobox gene HOXA9 have defects in myeloid, erythroid, and lymphoid hematopoiesis. *Blood* **89**, 1922-1930 (1997).
Lawrence, M. S. et al. Mutational heterogeneity in cancer and the search for new cancer-associated genes. *Nature* **499**, 214-218 (2013).
Lawrence, M. S. et al. Discovery and saturation analysis of cancer genes across 21 tumour types. *Nature* **505**, 495-501 (2014).
le Viseur, C. et al. In Childhood Acute Lymphoblastic Leukemia, Blasts at Different Stages of Immunophenotypic Maturation Have Stem Cell Properties. *Cancer Cell* **14**, 47–58 (2008).
Lee, D. W. *et al.* T cells expressing CD19 chimeric antigen receptors for acute lymphoblastic leukaemia in children and young adults: A phase 1 dose-escalation trial. *Lancet* **385**, 517–528 (2015).
Lee, D. W. et al. Long-term outcomes following CD19 CAR T cell therapy for B-ALL are superior in patients receiving a fludarabine/cyclophosphamide preparative regimen and post-CAR hematopoietic stem cell transplantation. *Blood* **128**, 218 (2016).
Lee, J., Ahn, E., Kissick, H. T. & Ahmed, R. Reinvigorating exhausted T cells by blockade of the PD-1 pathway. *For. Immunopathol. Dis. Therap.* **6**, 7–18 (2015).
Lee, K. et al. MYC and MCL1 Cooperatively Promote Chemotherapy-Resistant Breast Cancer Stem Cells via Regulation of Mitochondrial Oxidative Phosphorylation. *Cell Metab.* **26**, 633-647.e7 (2017).
Ley, T. J. et al. DNA sequencing of a cytogenetically normal acute myeloid leukaemia genome. *Nature* **456**, 66-72 (2008).
Ley, T. J. et al. DNMT3A mutations in acute myeloid leukemia. *N. Engl. J. Med.* **363**, 2424–2433 (2010).
Li, F. *et al.* In vivo epigenetic crispr screen identifies asf1a as an immunotherapeutic target in kras-mutant lung adenocarcinoma. *Cancer Discov.* **10**, 270–287 (2020).
Li, H. *et al.* The EMT regulator ZEB2 is a novel dependency of human and murine acute myeloid leukemia. *Blood* **129**, 497–508 (2017).
Li, Y. et al. AF9 YEATS domain links histone acetylation to DOT1L-mediated H3K79 methylation. *Cell* **159**, 558-571 (2014).
Li, Z. et al. Consistent deregulation of gene expression between human and murine MLL rearrangement leukemias. *Cancer Res.* **69**, 1109-1116 (2009).
Liu, Y.-F. et al. Genomic Profiling of Adult and Pediatric B-cell Acute Lymphoblastic Leukemia. *EBioMedicine* **8**, 173–183 (2016).
Locke, F. L. *et al.* Phase 1 Results of ZUMA-1: A Multicenter Study of KTE-C19 Anti-CD19 CAR T Cell Therapy in Refractory Aggressive Lymphoma. *Mol. Ther.* **25**, 285–295 (2017).
Locke, F. L. *et al.* Long-term safety and activity of axicabtagene ciloleucel in refractory large B-cell lymphoma (ZUMA-1): a single-arm, multicentre, phase 1–2 trial. *Lancet Oncol.* **20**, 31–42 (2019).
Long, A. H. *et al.* 4-1BB costimulation ameliorates T cell exhaustion induced by tonic signaling of chimeric antigen receptors. *Nat. Med.* **21**, 581–590 (2015).
Lorns, E. *et al.* Whole genome in vivo RNAi screening identifies the leukemia inhibitory factor receptor as a novel breast tumor suppressor. *Breast Cancer Res. Treat.* **135**, 79–91 (2012).
Louis, C. U. *et al.* Antitumor activity and long-term fate of chimeric antigen receptor-positive T cells in patients with neuroblastoma. *Blood* **118**, 6050–6056 (2011).
Löwenberg, B. *et al.* Cytarabine Dose for Acute Myeloid Leukemia. *N. Engl. J. Med.* **364**, 1027–1036 (2011).
Lu, B. *et al.* A Transcription Factor Addiction in Leukemia Imposed by the MLL Promoter Sequence. *Cancer Cell* **34**, 970-981.e8 (2018).
Lucero, O. M. *et al.* Phenotype switch in acute lymphoblastic leukaemia associated with 3 years of persistent CAR T cell directed-CD19 selective pressure. *Br. J. Haematol.* **186**, 333–336 (2019).
Lugo, T., Pendergast, A., Muller, A. & Witte, O. Tyrosine kinase activity and transformation potency of bcr-abl oncogene products. *Science* **247**, 1079–1082 (1990).
Luo, J., Solimini, N. L. & Elledge, S. J. Principles of Cancer Therapy: Oncogene and Non-oncogene Addiction. *Cell* **136**, 823–837 (2009).

Luo, Z., Lin, C. & Shilatifard, A. The super elongation complex (SEC) family in transcriptional control. *Nat. Rev. Mol. Cell Biol.* **13**, 543–547 (2012).
Ma, X. et al. Rise and fall of subclones from diagnosis to relapse in pediatric B-acute lymphoblastic leukaemia. *Nat. Commun.* **6**, (2015).
Madan, V. et al. Comprehensive mutational analysis of primary and relapse acute promyelocytic leukemia. *Leukemia* **30**, 1672–1681 (2016).
Maher, J., Brentjens, R. J., Gunset, G., Rivière, I. & Sadelain, M. Human T-lymphocyte cytotoxicity and proliferation directed by a single chimeric TCRζ /CD28 receptor. *Nat. Biotechnol.* **20**, 70–75 (2002).
Majzner, R. G. & Mackall, C. L. Tumor antigen escape from car t-cell therapy. *Cancer Discov.* **8**, 1219–26 (2018).
Majzner, R. G. & Mackall, C. L. Clinical lessons learned from the first leg of the CAR T cell journey. *Nat. Med.* **25**, 1341–1355 (2019).
Mali, P. *et al.* RNA-guided human genome engineering via Cas9. *Science* **339**, 823–826 (2013).
Manguso, R. T. *et al.* In vivo CRISPR screening identifies Ptpn2 as a cancer immunotherapy target. *Nature* **547**, 413–418 (2017).
Mann, R., Mulligan, R. C., & Baltimore, D. Construction of a retrovirus packaging mutant and its use to produce helper-free defective retrovirus. *Cell* **33**, 153–159 (1983).
Mardis, E. R. et al. Recurring mutations found by sequencing an acute myeloid leukemia genome. *N. Engl. J. Med.* **361**, 1058-1066 (2009).
Marin, J. J. G., Briz, O., Rodríguez-Macias, G., Díez-Martín, J. L. & Macias, R. I. R. Role of drug transport and metabolism in the chemoresistance of acute myeloid leukemia. *Blood Rev.* **30**, 55–64 (2016).
Martin, M. E. et al. Dimerization of MLL fusion proteins immortalizes hematopoietic cells. *Cancer Cell* **4**, 197–207 (2003).
Martínez-Lostao, L., Anel, A. & Pardo, J. How Do Cytotoxic Lymphocytes Kill Cancer Cells? *Clin. Cancer Res.* **21**, 5047–5056 (2015).
Masetti, R. et al. Genomic complexity and dynamics of clonal evolution in childhood acute myeloid leukemia studied with whole-exome sequencing. *Oncotarget* **7**, 56746–56757 (2016).
Matsunaga, T. et al. Interaction between leukemic-cell VLA-4 and stromal fibronectin is a decisive factor for minimal residual disease of acute myelogenous leukemia. *Nat. Med.* **9**, 1158–1165 (2003).
Maude, S. L. *et al.* Chimeric Antigen Receptor T Cells for Sustained Remissions in Leukemia. *N. Engl. J. Med.* **371**, 1507–1517 (2014).
Maude, S. L., Teachey, D. T., Porter, D. L. & Grupp, S. A. CD19-targeted chimeric antigen receptor T-cell therapy for acute lymphoblastic leukemia. *Blood* **125**, 4017–4023 (2015).
Maude, S. L. et al. Sustained remissions with CD19-specific chimeric antigen receptor (CAR)-modified T cells in children with relapsed/refractory ALL. *J. Clin. Oncol.* **34**, 3011 (2016).
Maude, S. L. *et al.* Tisagenlecleucel in children and young adults with B-cell lymphoblastic leukemia. *N. Engl. J. Med.* **378**, 439–448 (2018).
Maus, M. V. *et al.* T cells expressing chimeric antigen receptors can cause anaphylaxis in humans. *Cancer Immunol. Res.* **1**, 26–31 (2013).
McCart, A. E., Vickaryous, N. K. & Silver, A. Apc mice: Models, modifiers and mutants. *Pathol. Res. Pract.* **204**, 479–490 (2008).
McClellan, J. S. & Majeti, R. The cancer stem cell model: B cell acute lymphoblastic leukaemia breaks the mould. *EMBO Mol. Med.* **5**, 7–9 (2013).
McCulloch, E. A. Stem cells in normal and leukemic hemopoiesis (Henry Stratton lecture, 1982). *Blood* **62**, 1-13 (1983).
Meacham, C. E., Ho, E. E., Dubrovsky, E., Gertler, F. B. & Hemann, M. T. In vivo RNAi screening identifies regulators of actin dynamics as key determinants of lymphoma progression. *Nat. Genet.* **41**, 1133–1137 (2009).
Meacham, C. E. *et al.* A genome-scale in vivo loss-of-function screen identifies phf6 as a lineage-specific regulator of leukemia cell growth. *Genes Dev.* **29**, 483–488 (2015).
Metcalf, D., Moore, M. A. & Warner, N. L. Colony formation in vitro by myelomonocytic leukemic cells. *J. Natl. Cancer Inst.* **43**, 983-1001 (1969).

Meyer, J. A. et al. Relapse-specific mutations in NT5C2 in childhood acute lymphoblastic leukemia. *Nat. Genet.* **45**, 290–294 (2013).
Mezzadra, R. *et al.* Identification of CMTM6 and CMTM4 as PD-L1 protein regulators. *Nature* **549**, 106–110 (2017).
Miething, C. *et al.* Retroviral insertional mutagenesis identifies RUNX genes involved in chronic myeloid leukemia disease persistence under imatinib treatment. *Proc. Natl. Acad. Sci. U. S. A.* **104**, 4594–4599 (2007).
Miller, A. D. Retrovirus packaging cells. *Hum. Gene. Ther.* **1**, 5–14 (1990).
Miller, J. F. Immunological function of the thymus. *Lancet* **2**, 748–749 (1961)
Miller, P. G. *et al.* In Vivo RNAi Screening Identifies a Leukemia-Specific Dependence on Integrin Beta 3 Signaling. *Cancer Cell* **24**, 45–58 (2013).
Milone, M. C. et al. Chimeric receptors containing CD137 signal transduction domains mediate enhanced survival of T cells and increased antileukemic efficacy in vivo. *Mol. Ther.* **17**, 1453–1464 (2009).
Mintz, B. & Illmensee, K. Normal genetically mosaic mice produced from malignant teratocarcinoma cells. *Proc. Natl. Acad. Sci. U. S. A.* **72**, 3585–3589 (1975).
Mitchison, N. A. Studies on the immunological response to foreign tumor transplants in the mouse. I. The role of lymph node cells in conferring immunity by adoptive transfer. *J. Exp. Med.* **102**, 157–177 (1955).
Möhle, R. et al. The chemokine receptor CXCR-4 is expressed on CD34+ hematopoietic progenitors and leukemic cells and mediates transendothelial migration induced by stromal cell-derived factor-1. *Blood* **91**, 4523–4530 (1998).
Mohr, S. E. & Perrimon, N. RNAi screening: New approaches, understandings, and organisms. *Wiley Interdiscip. Rev. RNA* **3**, 145–158 (2012).
Mohseni, M., Uludag, H. & Brandwein, J. M. Advances in biology of acute lymphoblastic leukemia. *Am. J. Blood Res.* **8**, 29–56 (2018).
Mojica, F. J. M., Díez-Villaseñor, C., García-Martínez, J. & Soria, E. Intervening Sequences of Regularly Spaced Prokaryotic Repeats Derive from Foreign Genetic Elements. *J. Mol. Evol.* **60**, 174–182 (2005).
Molina, J. R. et al. An inhibitor of oxidative phosphorylation exploits cancer vulnerability. *Nat. Med.* **24**, 1036–1046 (2018).
Moore, M. A., Williams, N. & Metcalf, D. In vitro colony formation by normal and leukemic human hematopoietic cells: Characterization of the colony-forming cells. *J. Natl. Cancer Inst.* **50**, 603-623 (1973).
Morgan, R. A. *et al.* Case report of a serious adverse event following the administration of t cells transduced with a chimeric antigen receptor recognizing ERBB2. *Mol. Ther.* **18**, 843–851 (2010).
Moritz, D., Wels, W., Mattern, J. & Groner, B. Cytotoxic T lymphocytes with a grafted recognition specificity for ERBB2- expressing tumor cells. *Proc. Natl. Acad. Sci. U. S. A.* **91**, 4318–4322 (1994).
Morrissy, A. S. *et al.* Divergent clonal selection dominates medulloblastoma at recurrence. *Nature* **529**, 351–357 (2016).
Moser, A., Pitot, H. & Dove, W. A dominant mutation that predisposes to multiple intestinal neoplasia in the mouse. *Science* **247**, 322–324 (1990).
Mueller, K. T. *et al.* Clinical Pharmacology of Tisagenlecleucel in B-cell Acute Lymphoblastic Leukemia. *Clin. Cancer Res.* **24**, 6175–6184 (2018).
Mullighan, C. G. et al. Genome-wide analysis of genetic alterations in acute lymphoblastic leukaemia. *Nature* **446**, 758–764 (2007).
Murugaesu, N. *et al.* An in vivo functional screen identifies ST6GalNAc2 sialyltransferase as a breast cancer metastasis suppressor. *Cancer Discov.* **4**, 304–317 (2014).
Neelapu, S. S. *et al.* Axicabtagene ciloleucel CAR T-cell therapy in refractory large B-Cell lymphoma. *N. Engl. J. Med.* **377**, 2531–2544 (2017).
Nervi, B. et al. Chemosensitization of acute myeloid leukemia (AML) following mobilization by the CXCR4 antagonist AMD3100. *Blood* **113**, 6206–6214 (2009).
Nguyen, A. T., Taranova, O., He, J., & Zhang, Y. Dot1l, the H3K79 methyltransferase, is required for MLL-AF9-mediated leukemogenesis. *Blood* **117**, 6912-6922 (2011).
Nguyen, N. *et al.* Random mutagenesis of the mouse genome: A strategy for discovering gene function and the molecular basis of disease. *Am. J. Physiol. - Gastrointest. Liver Physiol.* **300**, (2011).

Nitiss, J. L. Targeting DNA topoisomerase II in cancer chemotherapy. *Nat. Rev. Cancer* **9**, 338–350 (2009).
Nowell, P. C. & Hungerford, D. A. Chromosome Studies on Normal and Leukemic Human Leukocytes. *JNCI J. Natl. Cancer Inst.* **25**, 85–109 (1960).
Nurse, P. Genetic control of cell size at cell division in yeast. *Nature* **256**, 547–551 (1975).
Nutt, S. L. & Kee, B. L. The Transcriptional Regulation of B Cell Lineage Commitment. *Immunity* **26**, 715–725 (2007).
O'Brien, S. G. et al. Imatinib Compared with Interferon and Low-Dose Cytarabine for Newly Diagnosed Chronic-Phase Chronic Myeloid Leukemia. *N. Engl. J. Med.* **348**, 994–1004 (2003).
O'Donnell, K. A. Advances in functional genetic screening with transposons and CRISPR/Cas9 to illuminate cancer biology. *Curr. Opin. Genet. Dev.* **49**, 85–94 (2018).
Oiseth, S. J. & Aziz, M. S. Cancer immunotherapy: a brief review of the history, possibilities, and challenges ahead. *J. Cancer Metastasis Treat.* **3**, 250 (2017).
O'Loughlin, T. A. & Gilbert, L. A. Functional Genomics for Cancer Research: Applications In Vivo and In Vitro. *Annu. Rev. Cancer Biol.* **3**, 345–363 (2019).
Orkin, S. H. & Zon, L. I. Hematopoiesis: An Evolving Paradigm for Stem Cell Biology. *Cell* **132**, 631–644 (2008).
O'Rourke, D. M. *et al.* A single dose of peripherally infused EGFRvIII-directed CAR T cells mediates antigen loss and induces adaptive resistance in patients with recurrent glioblastoma. *Sci. Transl. Med.* **9**, (2017).
Othus, M. *et al.* Declining rates of treatment-related mortality in patients with newly diagnosed AML given 'intense' induction regimens: a report from SWOG and MD Anderson. *Leukemia* **28**, 289–292 (2014).
Ott, P. A. *et al.* An immunogenic personal neoantigen vaccine for patients with melanoma. *Nature* **547**, 217–221 (2017).
Ott, P. A. & Wu, C. J. Cancer Vaccines: Steering T Cells Down the Right Path to Eradicate Tumors. *Cancer Discov.* **9**, 476–481 (2019).
Pandzic, T. *et al.* Transposon mutagenesis reveals fludarabine resistance mechanisms in chronic lymphocytic leukemia. *Clin. Cancer Res.* **22**, 6217–6227 (2016).
Papaemmanuil, E. et al. Genomic classification and prognosis in acute myeloid leukemia. *N. Engl. J. Med.* **374**, 2209-2221 (2016).
Pardee, T. S. et al. A phase i study of cpi-613 in combination with high-dose cytarabine and mitoxantrone for relapsed or refractory acute myeloid leukemia. *Clin. Cancer Res.* **24**, 2060–2073 (2018).
Park, J. H. *et al.* Long-Term Follow-up of CD19 CAR Therapy in Acute Lymphoblastic Leukemia. *N. Engl. J. Med.* **378**, 449–459 (2018).
Patel, S. J. *et al.* Identification of essential genes for cancer immunotherapy. *Nature* **548**, 537–542 (2017).
Paul, S., Kantarjian, H. & Jabbour, E. J. Adult Acute Lymphoblastic Leukemia. *Mayo Clin. Proc.* **91**, 1645–1666 (2016).
Pearce, D. J. et al. AML engraftment in the NOD/SCID assay reflects the outcome of AML: implications for our understanding of the heterogeneity of AML. *Blood* **107**,1166-1173 (2006).
Perea, G. et al. Adverse prognostic impact of CD36 and CD2 expression in adult de novo acute myeloid leukemia patients. *Leuk. Res.* **29**, 1109–1116 (2005).
Perl, A. E. The role of targeted therapy in the management of patients with AML. *Blood Adv.* **1**, 2281–2294 (2017).
Perna, D. *et al.* BRAF inhibitor resistance mediated by the AKT pathway in an oncogenic BRAF mouse melanoma model. *Proc. Natl. Acad. Sci. U. S. A.* **112**, E536–E545 (2015).
Perrimon, N., Ni, J. Q. & Perkins, L. In vivo RNAi: today and tomorrow. *Cold Spring Harb. Perspect. Biol.* **2**, (2010).
Pettitt, S. J. *et al.* A Genetic Screen Using the PiggyBac Transposon in Haploid Cells Identifies Parp1 as a Mediator of Olaparib Toxicity. *PLoS One* **8**, 1–10 (2013).
Pettitt, S. J. *et al.* Genome-wide barcoded transposon screen for cancer drug sensitivity in haploid mouse embryonic stem cells. *Sci. Data* **4**, 1–8 (2017).

Pina, C., May, G., Soneji, S., Hong, D., & Enver, T. MLLT3 regulates early human erythroid and megakaryocytic cell fate. *Cell Stem Cell* **2**, 264–273 (2008).
Planells-Cases, R. *et al.* Subunit composition of VRAC channels determines substrate specificity and cellular resistance to P t-based anti-cancer drugs. *EMBO J.* **34**, 2993–3008 (2015).
Pollyea, D. A. et al. Venetoclax with azacitidine disrupts energy metabolism and targets leukemia stem cells in patients with acute myeloid leukemia. *Nat. Med.* **24**, 1859–1866 (2018).
Pommier, Y., Leo, E., Zhang, H. & Marchand, C. DNA Topoisomerases and Their Poisoning by Anticancer and Antibacterial Drugs. *Chem. Biol.* **17**, 421–433 (2010).
Porter, D. L., Levine, B. L., Kalos, M., Bagg, A. & June, C. H. Chimeric antigen receptor-modified T cells in chronic lymphoid leukemia. *N. Engl. J. Med.* **365**, 725–733 (2011).
Porter, D. L. *et al.* Chimeric antigen receptor T cells persist and induce sustained remissions in relapsed refractory chronic lymphocytic leukemia. *Sci. Transl. Med.* **7**, 1–13 (2015).
Possik, P. A. *et al.* Parallel In Vivo and In Vitro Melanoma RNAi Dropout Screens Reveal Synthetic Lethality between Hypoxia and DNA Damage Response Inhibition. *Cell Rep.* **9**, 1375–1386 (2014).
Poulos, M. G. et al. Activation of the vascular niche supports leukemic progression and resistance to chemotherapy. *Exp. Hematol.* **42**, 976-986.e3 (2014).
Pourcel, C., Salvignol, G. & Vergnaud, G. CRISPR elements in Yersinia pestis acquire new repeats by preferential uptake of bacteriophage DNA, and provide additional tools for evolutionary studies. *Microbiology* **151**, 653–663 (2005).
Prahallad, A., Jensen, M. R. & Chapeau, E. A. Deciphering mechanisms of response and resistance in large-scale mouse cancer screens. *Curr. Opin. Genet. Dev.* **54**, 48–54 (2019).
Pribluda, A., De La Cruz, C. C. & Jackson, E. L. Intratumoral heterogeneity: From diversity comes resistance. *Clin. Cancer Res.* **21**, 2916–2923 (2015).
Pule, M. A. et al. Virus-specific T cells engineered to coexpress tumor-specific receptors: Persistence and antitumor activity in individuals with neuroblastoma. *Nat. Med.* **14**, 1264–1270 (2008).
Puram, R. V. *et al.* Core Circadian Clock Genes Regulate Leukemia Stem Cells in AML. *Cell* **165**, 303–316 (2016).
Qadir, M. et al. Cyclosporin A is a broad-spectrum multidrug resistance modulator. *Clin. Cancer Res.* **11**, 2320–2326 (2005).
Quek, L. et al. Genetically distinct leukemic stem cells in human CD34- acute myeloid leukemia are arrested at a hemopoietic precursor-like stage. *J Exp Med.* **213**, 1513-1535 (2016).
Rad, R. *et al.* PiggyBac Transposon Mutagenesis: A Tool for Cancer Gene Discovery in Mice. *Science* **330**, 1104–1107 (2010).
Raffel, S. et al. BCAT1 restricts αkG levels in AML stem cells leading to IDHmut-like DNA hypermethylation. *Nature* **551**, 384–388 (2017).
Raje, N. *et al.* Anti-BCMA CAR T-cell therapy bb2121 in relapsed or refractory multiple myeloma. *N. Engl. J. Med.* **380**, 1726–1737 (2019).
Ran, D. et al. Aldehyde dehydrogenase activity among primary leukemia cells is associated with stem cell features and correlates with adverse clinical outcomes. *Exp. Hematol.* **37,** 1423-1434 (2009).
Ranzani, M., Annunziato, S., Adams, D. J. & Montini, E. Cancer gene discovery: Exploiting insertional mutagenesis. *Mol. Cancer Res.* **11**, 1141–1158 (2013).
Rathe, S. K. *et al.* Using RNA-seq and targeted nucleases to identify mechanisms of drug resistance in acute myeloid leukemia. *Sci. Rep.* **4**, 1–9 (2014).
Rathert, P. *et al.* Transcriptional plasticity promotes primary and acquired resistance to BET inhibition. *Nature* **525**, 543–547 (2015).
Rehe, K. et al. Acute B lymphoblastic leukaemia-propagating cells are present at high frequency in diverse lymphoblast populations. *EMBO Mol. Med.* **5**, 38–51 (2013).
Roberts, K. G. et al. High Frequency and Poor Outcome of Philadelphia Chromosome-Like Acute Lymphoblastic Leukemia in Adults. *J. Clin. Oncol.* **35**, 394–401 (2017).
Robey, R. W. *et al.* Revisiting the role of ABC transporters in multidrug-resistant cancer. *Nat. Rev. Cancer* **18**, 452–464 (2018).
Rogers, Z. N. *et al.* A quantitative and multiplexed approach to uncover the fitness landscape of tumor suppression in vivo. *Nat. Methods* **14**, 737–742 (2017).

Ronson, A., Tvito, A. & Rowe, J. M. Treatment of Relapsed/Refractory Acute Lymphoblastic Leukemia in Adults. *Curr. Oncol. Rep.* **18**, (2016).
Roschewski, M., Staudt, L. M. & Wilson, W. H. Diffuse large B-cell lymphoma - Treatment approaches in the molecular era. *Nat. Rev. Clin. Oncol.* **11**, 12–23 (2014).
Rosenbauer, F. & Tenen, D. G. Transcription factors in myeloid development: Balancing differentiation with transformation. *Nat. Rev. Immunol.* **7**, 105–117 (2007).
Rosenberg, S. A. & Terry, W. D. Passive Immunotherapy of Cancer in Animals and Man. in *Advances in Cancer Research* **25**, 323–388 (1977).
Rosenberg, S. A., Spiess, P. & Lafreniere, R. A new approach to the adoptive immunotherapy of cancer with tumor-infiltrating lymphocytes. *Science* **233**, 1318–1321 (1986).
Rosenberg, S. A. et al. Use of Tumor-Infiltrating Lymphocytes and Interleukin-2 in the Immunotherapy of Patients with Metastatic Melanoma. *N. Engl. J. Med.* **319**, 1676–1680 (1988).
Rosenberg, S. A. & Restifo, N. P. Adoptive cell transfer as personalized immunotherapy for human cancer. *Science* **348**, 62–68 (2015).
Rual, J. F. *et al.* Towards a proteome-scale map of the human protein-protein interaction network. *Nature* **437**, 1173–1178 (2005).
Rudalska, R. *et al.* In vivo RNAi screening identifies a mechanism of sorafenib resistance in liver cancer. *Nat. Med.* **20**, 1138–1146 (2014).
Ruella, M. *et al.* Induction of resistance to chimeric antigen receptor T cell therapy by transduction of a single leukemic B cell. *Nat. Med.* **24**, 1499–1503 (2018).
Sa, J. K. *et al.* In vivo RNAi screen identifies NLK as a negative regulator of mesenchymal activity in glioblastoma. *Oncotarget* **6**, 20145–20159 (2015).
Sack, L. M. *et al.* Profound Tissue Specificity in Proliferation Control Underlies Cancer Drivers and Aneuploidy Patterns. *Cell* **173**, 499-514.e23 (2018).
Sadelain, M. & Mulligan, R. C. in 8th International Congress of Immunology (ed. International Congress of Immunology) (Springer-Verlag, Budapest; Hungary, 1992).
Sadelain, M. CAR therapy: the CD19 paradigm. *J. Clin. Invest.* **125**, 3392–3400 (2015).
Sahin, U. *et al.* Personalized RNA mutanome vaccines mobilize poly-specific therapeutic immunity against cancer. *Nature* **547**, 222–226 (2017).
Saito, Y. et al. Induction of cell cycle entry eliminates human leukemia stem cells in a mouse model of AML. *Nat. Biotechnol.* **28**, 275–280 (2010).
Samudio, I. et al. Pharmacologic inhibition of fatty acid oxidation sensitizes human leukemia cells to apoptosis induction. *J. Clin. Invest.* **120**, 142–156 (2010).
Sanchez, J. N., Wang, T. & Cohen, M. S. BRAF and MEK Inhibitors: Use and Resistance in BRAF-Mutated Cancers. *Drugs* **78**, 549–566 (2018).
Sanchez-Rivera, F. J. *et al.* Rapid modelling of cooperating genetic events in cancer through somatic genome editing. *Nature* **516**, 428–431 (2014).
Sarry, J.E. et al. Human acute myelogenous leukemia stem cells are rare and heterogeneous when assayed in NOD/SCID/IL2Rγc-deficient mice. *J. Clin. Invest.* **121**, 384–395 (2011).
Sasaki, K. *et al.* Genome-wide in vivo RNAi screen identifies ITIH5 as a metastasis suppressor in pancreatic cancer. *Clin. Exp. Metastasis* **34**, 229–239 (2017).
Sattler, M. & Griffin, J. D. Molecular mechanisms of transformation by the BCR-ABL oncogene. *Semin. Hematol.* **40**, 4–10 (2003).
Savoldo, B. et al. CD28 costimulation improves expansion and persistence of chimeric antigen receptor–modified T cells in lymphoma patients. *J. Clin. Invest.* **121**, 1822–1826 (2011).
Schramek, D. *et al.* Direct in Vivo RNAi Screen Unveils Myosin IIa as a Tumor Suppressor of Squamous Cell Carcinomas. *Science* **343**, 309–313 (2014).
Schiffer, C. A. & Gurbuxani, S. Clinical manifestations, pathologic features, and diagnosis of acute myeloid leukemia. *UpToDate*, accessed March 10, 2020, from: https://www.uptodate.com/contents/clinical-manifestations-pathologic-features-and-diagnosis-of-acute-myeloid-leukemia (2019).
Schuster, A. *et al.* RNAi/CRISPR Screens: from a Pool to a Valid Hit. *Trends Biotechnol.* **37**, 38–55 (2019).

Schuster, S. J. *et al.* Tisagenlecleucel in adult relapsed or refractory diffuse large B-cell lymphoma. *N. Engl. J. Med.* **380**, 45–56 (2019).
Schuurhuis, G. J. et al. Minimal/measurable residual disease in AML: a consensus document from the European LeukemiaNet MRD Working Party. *Blood* **131**, 1275–1291 (2018).
Schwab, C. & Harrison, C. J. Advances in B-cell Precursor Acute Lymphoblastic Leukemia Genomics. *HemaSphere* **2**, 1–9 (2018).
Sciacovelli, M. & Frezza, C. Oncometabolites: Unconventional triggers of oncogenic signalling cascades. *Free Radic. Biol. Med.* **100**, 175–181 (2016).
SEER. Cancer stat facts: leukemia — acute myeloid leukemia (AML). National Cancer Institute https://seer.cancer.gov/statfacts/html/amyl.html (2020a).
SEER. Cancer stat facts: leukemia — acute lymphoblastic leukemia (ALL). National Cancer Institute https://seer.cancer.gov/statfacts/html/alyl.html (2020b).
Shafat, M. S. et al. Leukemic blasts program bone marrow adipocytes to generate a pro-tumoral microenvironment. *Blood* **129**, 1320–1332 (2017).
Shaffer, B. C. et al. Drug resistance: Still a daunting challenge to the successful treatment of AML. *Drug Resist. Updat.* **15**, 62–69 (2012).
Shah, N. N. & Fry, T. J. Mechanisms of resistance to CAR T cell therapy. *Nat. Rev. Clin. Oncol.* **16**, 372–385 (2019).
Shalem, O. *et al.* Genome-Scale CRISPR-Cas9 Knockout Screening in Human Cells. *Science* **343**, 84–87 (2014).
Shalem, O., Sanjana, N. E. & Zhang, F. High-throughput functional genomics using CRISPR-Cas9. *Nat. Rev. Genet.* **16**, 299–311 (2015).
Shen, H. *et al.* Identification of genes that modulate susceptibility to formaldehyde and imatinib by functional genomic screening in human haploid KBM7 cells. *Toxicol. Sci.* **151**, 10–22 (2016).
Shi, J. *et al.* Discovery of cancer drug targets by CRISPR-Cas9 screening of protein domains. *Nat. Biotechnol.* **33**, 661–667 (2015).
Shiba, N. et al. Whole-exome sequencing reveals the spectrum of gene mutations and the clonal evolution patterns in paediatric acute myeloid leukaemia. *Br. J. Haematol.* **175**, 476–489 (2016).
Shih, A. H., Abdel-Wahab, O., Patel, J. P., Levine, R. L. The role of mutations in epigenetic regulators in myeloid malignancies. *Nat. Rev. Cancer* **12**, 599–612 (2012).
Shilatifard, A. The COMPASS family of histone H3K4 methylases: mechanisms of regulation in development and disease pathogenesis. *Annu. Rev. Biochem.,* **81**, 65-95 (2012).
Shimasaki, N., Jain, A. & Campana, D. NK cells for cancer immunotherapy. *Nat. Rev. Drug Discov.* **19**, 200–218 (2020).
Shivarov, V. & Bullinger, L. Expression profiling of leukemia patients: Key lessons and future directions. *Exp. Hematol.* **42**, 651-660 (2014).
Shlush, L. I. et al. Identification of pre-leukaemic haematopoietic stem cells in acute leukaemia. *Nature* **506**, 328-333 (2014).
Shlush, L. I. *et al.* Tracing the origins of relapse in acute myeloid leukaemia to stem cells. *Nature* **547**, 104–108 (2017).
Short, N. J., Jabbour, E. & Chiaretti, S. Should treatment of philadelphia chromosome-positive acute lymphoblastic leukemia be intensive? *Clin. Adv. Hematol. Oncol.* **14**, 892–896 (2016).
Siegel, R. L., Miller, K. D. & Jemal, A. Cancer statistics, 2020. *CA. Cancer J. Clin.* **70**, 7–30 (2020).
Sieweke, M. H., Thompson, N. L., Sporn, M. B. & Bissell, M. J. Mediation of wound-related rous sarcoma virus tumorigenesis by TGF-β. *Science* **248**, 1656–1660 (1990).
Silva, J. M. *et al.* Second-generation shRNA libraries covering the mouse and human genomes. *Nat. Genet.* **37**, 1281–1288 (2005).
Simon, B. & Uslu, U. CAR-T cell therapy in melanoma: A future success story? *Exp. Dermatol.* **27**, 1315–1321 (2018).
Singh, A. K. & McGuirk, J. P. CAR T cells: continuation in a revolution of immunotherapy. *Lancet Oncol.* **21**, e168–e178 (2020).
Singh, N. *et al.* Impaired Death Receptor Signaling in Leukemia Causes Antigen-Independent Resistance by Inducing CAR T-cell Dysfunction. *Cancer Discov.* **10**, 552–567 (2020).

Škrtić, M. et al. Inhibition of Mitochondrial Translation as a Therapeutic Strategy for Human Acute Myeloid Leukemia. *Cancer Cell* **20**, 674–688 (2011).
So, C. W., Karsunky, H., Wong, P., Weissman, I. L., Cleary, M. L. Leukemic trans- formation of hematopoietic progenitors by MLL-GAS7 in the absence of Hoxa7 or Hoxa9. *Blood* **103**, 3192-3199 (2004).
Somasundaram, R., Prasad, M. A. J., Ungerbäck, J. & Sigvardsson, M. Transcription factor networks in B-cell differentiation link development to acute lymphoid leukemia. *Blood* **126**, 144–152 (2015).
Song, C. Q. *et al.* Genome-Wide CRISPR Screen Identifies Regulators of Mitogen-Activated Protein Kinase as Suppressors of Liver Tumors in Mice. *Gastroenterology* **152**, 1161-1173.e1 (2017).
Sood, R. et al. Somatic mutational landscape of AML with inv(16) or t(8;21) identifies patterns of clonal evolution in relapse leukemia. *Leukemia* **30**, 501–520 (2016).
Sood, R., Kamikubo, Y. & Liu, P. Role of RUNX1 in hematological malignancies. *Blood* **129**, 2070–2082 (2017).
Soto-Feliciano, Y. M. *et al.* PHF6 regulates phenotypic plasticity through chromatin organization within lineage-specific genes. *Genes Dev.* **31**, 973–989 (2017).
Sriskanthadevan, S. et al. AML cells have low spare reserve capacity in their respiratory chain that renders them susceptible to oxidative metabolic stress. *Blood* **125**, 2120–2130 (2015).
Stadtmauer, E. A. *et al.* CRISPR-engineered T cells in patients with refractory cancer. *Science* **367**, (2020).
Starr, T. K. *et al.* A Transposon-Based Genetic Screen in Mice Identifies Genes Altered in Colorectal Cancer. *Science* **323**, 1747–1750 (2009).
Stegmeier, F., Hu, G., Rickles, R. J., Hannon, G. J. & Elledge, S. J. A lentiviral microRNA-based system for single-copy polymerase II-regulated RNA interference in mammalian cells. *Proc. Natl. Acad. Sci. U. S. A.* **102**, 13212–13217 (2005).
Stehelin, D., Varmus, H. E., Bishop, J.M., & Vogt, P.K. DNA related to the transforming gene(s) of avian sarcoma viruses is present in normal avian DNA. *Nature* **260**, 170–173 (1976).
Stein, E. M. et al. The DOT1L inhibitor pinometostat reduces H3K79 methylation and has modest clinical activity in adult acute leukemia. *Blood* **131**, 2662–2669 (2018).
Steinhart, Z. *et al.* Genome-wide CRISPR screens reveal a Wnt–FZD5 signaling circuit as a druggable vulnerability of RNF43-mutant pancreatic tumors. *Nat. Med.* **23**, 60–68 (2017).
Sternberg, S. H., Redding, S., Jinek, M., Greene, E. C. & Doudna, J. A. DNA interrogation by the CRISPR RNA-guided endonuclease Cas9. *Nature* **507**, 62–67 (2014).
Storz, U. Rituximab: How approval history is reflected by a corresponding patent filing strategy. *MAbs* **6**, 820–837 (2014).
Straathof, K. *et al.* Abstract CT145: A Cancer Research UK phase I trial of anti-GD2 chimeric antigen receptor (CAR) transduced T-cells (1RG-CART) in patients with relapsed or refractory neuroblastoma. *Cancer Res.* **78**, CT145 (2018).
Sui, G. *et al.* A DNA vector-based RNAi technology to suppress gene expression in mammalian cells. *Proc. Natl. Acad. Sci. U. S. A.* **99**, 5515–5520 (2002).
Sun, Y. et al. HOXA9 Reprograms the Enhancer Landscape to Promote Leukemogenesis. *Cancer Cell* **34**, 643-658.e5 (2018).
Swiech, L. *et al.* In vivo interrogation of gene function in the mam malian brain using CRISPR-Cas9. *Nat. Biotechnol.* **33**, 102–106 (2015).
Szlachta, K. *et al.* CRISPR knockout screening identifies combinatorial drug targets in pancreatic cancer and models cellular drug response. *Nat. Commun.* **9**, 4275 (2018).
Tabe, Y. et al. Survival of acute monocytic leukemia cells is driven by fatty acid oxidation-mediated activation of AMPK in bone marrow adipocytes. *Cancer Res* **77**, 1453–1464 (2017).
Tabin, C. J., Bradley, S. M., Bargmann, C. I., Weinberg, R. A., Papageorge, A. G., Scolnick, E. M., Dhar, R., Lowy, D. R., and Chang, E. H. Mechanism of activation of a human oncogene. *Nature* **300**, 143–149 (1982).
Tarumoto, Y. *et al.* LKB1, Salt-Inducible Kinases, and MEF2C Are Linked Dependencies in Acute Myeloid Leukemia. *Mol. Cell* **69**, 1017-1027.e6 (2018).

Taussig, D. C. et al. Leukemia-initiating cells from some acute myeloid leukemia patients with mutated nucleophosmin reside in the CD34(-) fraction. *Blood* **115**, 1976-1984 (2010).
Tavassoli, M. et al. Whole chromosome 17 loss in ovarian cancer. *Genes Chromosom. Cancer* **8**, 195-198 (1993).
Tawana, K. et al. Disease evolution and outcomes in familial AML with germline CEBPA mutations. *Blood* **126**, 1214–1223 (2015).
Tawana, K., Rio-Machin, A., Preudhomme, C. & Fitzgibbon, J. Familial CEBPA-mutated acute myeloid leukemia. *Semin. Hematol.* **54**, 87–93 (2017).
Terwilliger, T. & Abdul-Hay, M. Acute lymphoblastic leukemia: a comprehensive review and 2017 update. *Blood Cancer J.* **7**, e577 (2017).
Thanarajasingam, G. et al. Beyond maximum grade: modernising the assessment and reporting of adverse events in haematological malignancies. *Lancet Haematol.* **5**, e563–e598 (2018).
The Cancer Genome Atlas Research Network. Genomic and Epigenomic Landscapes of Adult De Novo Acute Myeloid Leukemia. *N. Engl. J. Med*. **368**, 2059-2074 (2013).
Thomas, D. & Majeti, R. Biology and relevance of human acute myeloid leukemia stem cells. *Blood* **129**, 1577–1585 (2017).
Thoms, J. A. I., Beck, D. & Pimanda, J. E. Transcriptional networks in acute myeloid leukemia. *Genes Chromosom. Cancer* **58**, 859–874 (2019).
Till, B. G. et al. Adoptive immunotherapy for indolent non-hodgkin lymphoma and mantle cell lymphoma using genetically modified autologous CD20-specific T cells. *Blood* **112**, 2261–2271 (2008).
Tkachuk, D. C., Kohler, S., Cleary, M. L. Involvement of a homolog of Drosophila trithorax by 11q23 chromosomal translocations in acute leukemias. *Cell* **71**, 691-700 (1992).
Tokarew, N., Ogonek, J., Endres, S., von Bergwelt-Baildon, M. & Kobold, S. Teaching an old dog new tricks: next-generation CAR T cells. *Br. J. Cancer* **120**, 26–37 (2019).
Toledo, C. M. *et al.* Genome-wide CRISPR-Cas9 Screens Reveal Loss of Redundancy between PKMYT1 and WEE1 in Glioblastoma Stem-like Cells. *Cell Rep.* **13**, 2425–2439 (2015).
Tong, A. H. Y. Systematic Genetic Analysis with Ordered Arrays of Yeast Deletion Mutants. *Science* **294**, 2364–2368 (2001).
Torres, J., Mehandru, S., Colombel, J. F. & Peyrin-Biroulet, L. Crohn's disease. *Lancet* **389**, 1741–1755 (2017).
Torres-Collado, A. & Jazirehi, A. Overcoming Resistance of Human Non-Hodgkin's Lymphoma to CD19-CAR CTL Therapy by Celecoxib and Histone Deacetylase Inhibitors. *Cancers (Basel).* **10**, 200 (2018).
Turtle, C. J. *et al.* CD19 CAR–T cells of defined CD4+:CD8+ composition in adult B cell ALL patients. *J. Clin. Invest.* **126**, 2123–2138 (2016).
Turtle, C. J. *et al.* Durable molecular remissions in chronic lymphocytic leukemia treated with CD19-Specific chimeric antigen Receptor-modified T cells after failure of ibrutinib. *J. Clin. Oncol.* **35**, 3010–3020 (2017).
Tyner, J. W. et al. Functional genomic landscape of acute myeloid leukaemia. *Nature* **562**, 526–531 (2018).
Tzoneva, G. et al. Activating mutations in the NT5C2 nucleotidase gene drive chemotherapy resistance in relapsed ALL. *Nat. Med.* **19**, 368–371 (2013).
Ungaro, R., Mehandru, S., Allen, P. B., Peyrin-Biroulet, L. & Colombel, J. F. Ulcerative colitis. *Lancet* **389**, 1756–1770 (2017).
Tzelepis, K. *et al.* A CRISPR Dropout Screen Identifies Genetic Vulnerabilities and Therapeutic Targets in Acute Myeloid Leukemia. *Cell Rep.* **17**, 1193–1205 (2016).
Van Der Weyden, L. *et al.* Modeling the evolution of ETV6-RUNX1-induced B-cell precursor acute lymphoblastic leukemia in mice. *Blood* **118**, 1041–1051 (2011).
Van Deursen, J. M. The role of senescent cells in ageing. *Nature* **509**, 439–446 (2014).
van Rhenen, A. et al. High stem cell freqency in acute myeloid leukemia at diagnosis predicts high minimal residual disease and poor survival. *Clin. Cancer Res*. **11**, 6520-6527 (2005).
Valk, P. J. et al. Prognostically useful gene-expression profiles in acute myeloid leukemia. *N. Engl. J. Med.* **350**, 1617–1628 (2004).

Vassiliou, G. S. *et al.* Mutant nucleophosmin and cooperating pathways drive leukemia initiation and progression in mice. *Nat. Genet.* **43**, 470–476 (2011).
Vazquez, F. et al. PGC1α Expression Defines a Subset of Human Melanoma Tumors with Increased Mitochondrial Capacity and Resistance to Oxidative Stress. *Cancer Cell* **23**, 287–301 (2013).
Vinay, D. S. et al. Immune evasion in cancer: Mechanistic basis and therapeutic strategies. *Semin. Cancer Biol.* **35**, S185–S198 (2015).
Visvader, J. E. Cells of origin in cancer. *Nature* **469**, 314–322 (2011).
Vo, T. T. et al. Relative mitochondrial priming of myeloblasts and normal HSCs determines chemotherapeutic success in AML. *Cell* **151**, 344–355 (2012).
Wacholder, S. Precursors in cancer epidemiology: aligning definition and function. *Cancer Epidemiol. Biomarkers Prev.* **22**, 521-527 (2013).
Walenkamp, A. M. E., Lapa, C., Herrmann, K. & Wester, H. J. CXCR4 ligands: The next big hit? *J. Nucl. Med.* **58**, 77S-82S (2017).
Wang, G. *et al.* Mapping a functional cancer genome atlas of tumor suppressors in mouse liver using AAV-CRISPR-mediated direct in vivo screening. *Sci. Adv.* **4**, (2018).
Wang, T., Wei, J. J., Sabatini, D. M. & Lander, E. S. Genetic Screens in Human Cells Using the CRISPR-Cas9 System. *Science* **343**, 80–84 (2014).
Wang, T. *et al.* Identification and characterization of essential genes in the human genome. *Science* **350**, 1096–1101 (2015).
Wang, T. *et al.* Gene Essentiality Profiling Reveals Gene Networks and Synthetic Lethal Interactions with Oncogenic Ras. *Cell* **168**, 890-903.e15 (2017).
Ward, P. S. et al. The common feature of leukemia-associated IDH1 and IDH2 mutations is a neomorphic enzyme activity converting α-ketoglutarate to 2-hydroxyglutarate. *Cancer Cell* **17**, 225-234 (2010).
Weber, J. *et al.* CRISPR/Cas9 somatic multiplex-mutagenesis for high-Throughput functional cancer genomics in mice. *Proc. Natl. Acad. Sci. U. S. A.* **112**, 13982–13987 (2015).
Westcott, P. M. K. *et al.* The mutational landscapes of genetic and chemical models of Kras-driven lung cancer. *Nature* **517**, 489–492 (2015).
Wherry, E. J. T cell exhaustion. *Nat. Immunol.* **12**, 492–499 (2011).
Wijdeven, R. H. *et al.* Genome-wide identification and characterization of novel factors conferring resistance to topoisomerase II poisons in cancer. *Cancer Res.* **75**, 4176–4187 (2015).
Williams, R. T., Roussel, M. F. & Sherr, C. J. Arf gene loss enhances oncogenicity and limits imatinib response in mouse models of Bcr-Abl-induced acute lymphoblastic leukemia. *Proc. Natl. Acad. Sci. U. S. A.* **103**, 6688–6693 (2006).
Williams, R. T., Besten, W. Den & Sherr, C. J. Cytokine-dependent imatinib resistance in mouse. *Genes Dev.* **21**, 2283–2287 (2007).
Winters, A. C. & Bernt, K. M. MLL-rearranged leukemias- An update on science and clinical approaches. *Front. Pediatr.* **5**, 1–21 (2017).
Winzeler, E. A. *et al.* Functional characterization of the S. cerevisiae genome by gene deletion and parallel analysis. *Science* **285**, 901–906 (1999).
Wong, P., Iwasaki, M., Somervaille, T. C., So, C. W., Cleary, M. L. Meis1 is an essential and rate-limiting regulator of MLL leukemia stem cell potential. *Genes Dev.* **21**, 2762–2774 (2007).
Wolf, J. *et al.* An in vivo RNAi screen identifies SALL1 as a tumor suppressor in human breast cancer with a role in CDH1 regulation. *Oncogene* **33**, 4273–4278 (2014).
Wu, G. et al. Overcoming treatment resistance in cancer: Current understanding and tactics. *Cancer Lett.* **387**, 69–76 (2017).
Xiao, X., Ho, M., Zhu, Z., Pastan, I. & Dimitrov, D. S. Identification and characterization of fully human anti-CD22 monoclonal antibodies. *MAbs* **1**, 297–303 (2009).
Xie M, Lu C, Wang J et al. Age-related mutations associated with clonal hematopoietic expansion and malignancies. *Nat. Med.***20**,1472-1478 (2014).
Xu, C. *et al.* piggyBac mediates efficient in vivo CRISPR library screening for tumorigenesis in mice. *Proc. Natl. Acad. Sci. U. S. A.* **114**, 722–727 (2017).
Xue, W. *et al.* CRISPR-mediated direct mutation of cancer genes in the mouse liver. *Nature* **514**, 380–384 (2014).

Yagi, H. et al. Growth disturbance in fetal liver hematopoiesis of Mll-mutant mice. *Blood* **92**, 108-117 (1998).
Yamauchi, T. *et al.* Genome-wide CRISPR-Cas9 Screen Identifies Leukemia-Specific Dependence on a Pre-mRNA Metabolic Pathway Regulated by DCPS. *Cancer Cell* **33**, 386-400.e5 (2018).
Yan, H. et al. Association of a cytarabine chemosensitivity related gene expression signature with survival in cytogenetically normal acute myeloid leukemia. *Oncotarget* **8**, 1529–1540 (2017).
Yang, Y. *et al.* TCR engagement negatively affects CD8 but not CD4 CAR T cell expansion and leukemic clearance. *Sci. Transl. Med.* **9**, 1–13 (2017).
Yau, E. H. *et al.* Genome-wide CRISPR screen for essential cell growth mediators in mutant KRAS colorectal cancers. *Cancer Res.* **77**, 6330–6339 (2017).
Ye, H. et al. Leukemic Stem Cells Evade Chemotherapy by Metabolic Adaptation to an Adipose Tissue Niche. *Cell Stem Cell* **19**, 23–37 (2016).
Yokoyama, A. et al. The Menin tumor suppressor protein is an essential oncogenic cofactor for MLL-associated leukemogenesis. *Cell* **123**, 207–18 (2005).
Yokoyama, A., Cleary, M. L. Menin critically links MLL proteins with LEDGF on cancer-associated target genes. *Cancer Cell* **14**, 36-46 (2008).
Yokoyama, A., Lin, M., Naresh, A., Kitabayashi, I., Cleary, M. L. A higher-order complex containing AF4 and ENL family proteins with P-TEFb facilitates oncogenic and physiologic MLL-dependent transcription. *Cancer Cell* **17**, 198-212 (2010).
Yokoyama, A. et al. Proteolytically cleaved MLL subunits are susceptible to distinct degradation pathways. *J. Cell Sci.,* **124**, 2208-2219 (2011).
Yu, B. D., Hess, J. L., Horning, S. E., Brown, G. A. J., Korsmeyer, S. J. Altered Hox expression and segmental identity in Mll-mutant mice. *Nature* **378**, 505-508 (1995).
Yu, J. Y., DeRuiter, S. L. & Turner, D. L. RNA interference by expression of short-interfering RNAs and hairpin RNAs in mammalian cells. *Proc. Natl. Acad. Sci. U. S. A.* **99**, 6047–6052 (2002).
Yuan, T. et al. Dual FLT3 inhibitors: Against the drug resistance of acute myeloid leukemia in recent decade. *Eur. J. Med. Chem.* **178**, 468–483 (2019).
Yucel, B. & Sonmez, M. Repression of oxidative phosphorylation sensitizes leukemia cell lines to cytarabine. *Hematology* **23**, 330–336 (2018).
Zaretsky, J. M. *et al.* Mutations associated with acquired resistance to PD-1 blockade in melanoma. *N. Engl. J. Med.* **375**, 819–829 (2016).
Zender, L. *et al.* An Oncogenomics-Based In Vivo RNAi Screen Identifies Tumor Suppressors in Liver Cancer. *Cell* **135**, 852-864 (2008).
Zeng, Y., Wagner, E. J. & Cullen, B. R. Both natural and designed micro RNAs can inhibit the expression of cognate mRNAs when expressed in human cells. *Mol. Cell* **9**, 1327–1333 (2002).
Zeng, Z. et al. Targeting the leukemia microenvironment by CXCR4 inhibition overcomes resistance to kinase inhibitors and chemotherapy in AML. *Blood* **113**, 6215–6224 (2009).
Zhan, T., Rindtorff, N., Betge, J., Ebert, M. P. & Boutros, M. CRISPR/Cas9 for cancer research and therapy. *Semin. Cancer Biol.* **55**, 106–119 (2019).
Zhang, X., Rastogi, P., Shah, B. & Zhang, L. B lymphoblastic leukemia/lymphoma: New insights into genetics, molecular aberrations, subclassification and targeted therapy. *Oncotarget* **8**, 66728–66741 (2017).
Zhang, Y. & Rowley, J. D. Chromatin structural elements and chromosomal translocations in leukemia. *DNA Repair (Amst).* **5**, 1282–1297 (2006).
Zhou, Y. *et al.* High-throughput screening of a CRISPR/Cas9 library for functional genomics in human cells. *Nature* **509**, 487–491 (2014).
Zhu, L. et al. ASH1L links histone H2 lysine 36 dimethylation to MLL leukemia. *Cancer Discov.* **7**, 770-783 (2016).
Zuber, J. *et al.* Mouse models of human AML accurately predict chemotherapy response. *Genes Dev.* **23**, 877–889 (2009).
Zuber, J. *et al.* RNAi screen identifies Brd4 as a therapeutic target in acute myeloid leukaemia. *Nature* **478**, 524–528 (2011).

CHAPTER 2

A targeted *in vivo* RNAi screen identifies *Suclg2* as a novel mediator of resistance in acute myeloid leukemia

Azucena Ramos, Riley Hellinger, Yunpeng Liu, Luis Ruben Millan-Barea, Catherine Koch, Zhaoqi Li, Daniel Schmidt, Iva M. T. Gramatikov, Nina Fenouille, Gabriela Alexe, Jessica Spinelli, David M. Sabatini, Matthew G. Vander Heiden, Kimberly Stegmaier, Alexandre Puissant, Michael T. Hemann

AR, AP, KS, and MTH designed the study. AR, RH, LRMB, CK, NF, and AP conducted experiments. RH provided support with the Suclg2 cDNA rescue, dosing human AML cells in physiologic medium *in vitro*, and the *in vivo* knock down of Suclg1 and Sucla2. CK provided support with *in vitro* dosing experiments. YL performed RNAseq analysis and generated the chemoresistance signature. LRMB provided support with the initial *in vivo* competition assays. MVH and ZL provided reagents and support with the GC/MS experiments. DS and IMTG provided reagents and support with the physiologic medium experiments. GA completed the screen analysis and the analysis exploring the association of SUCLG2 expression and AML genetic subtypes. DMS and JS provided reagents and support with the seahorse experiments. MTH gave vital conceptual advice and AR wrote the manuscript.

Abstract

Treatment options that effectively cure patients diagnosed with acute myeloid leukemia (AML) continue to represent an area of unmet need in oncology clinical care. Relapse driven by therapy resistant cells that persist in the body after treatment is the principal source of fatality in AML patients. Therefore, understanding how and where these leukemic cells survive treatment *in vivo* may help advance the rational development of highly synergistic combination therapies. Using *in vivo* RNAi screening approaches and a new mouse model of AML chemoresistance ($Chemo^R$) generated in our lab, we have identified several putative mediators of therapy resistance. Transcriptional profiling of the $Chemo^R$ model allowed us to generate a chemoresistance gene signature that we overlapped with the results of our shRNA screen to identify high-confidence genes of interest. The top genes from a ranked list of the most highly overexpressed genes in $Chemo^R$ cells and the top depleted genes from the shRNA screen in the context of therapy treatment and relapse were selected as high interest hits. One of the most highly rated genes on that list encodes Succinate-CoA Ligase GDP-Forming Beta Subunit, or Suclg2 (also known as SCS-G). Validation studies demonstrated that SUCLG2 depletion/loss significantly sensitized both murine and human AML cells to frontline therapy *in vivo* but not *in vitro*. Suclg2 depletion also significantly extended life in chemo treated animals, a phenotype that could be rescued by exogenous expression of an shRNA-resistant Suclg2 cDNA. Mechanistically, I show that loss of Suclg2 does not lead to changes in intracellular TCA intermediates and results in cells with less mitochondrial mass that also exhibits enhanced oxidative capacity. Consistent with this finding, transcriptional analysis of acutely treated Suclg2 knockdown cells harvested from the bone marrow revealed an upregulation of gene sets important for oxidative phosphorylation (OXPHOS). A chemosensitization gene expression signature derived from downregulated genes in these acutely treated Suclg2 KD cells predicted better outcomes in patients whose tumors expressed a more stem cell-derived transcriptional program, in therapy refractory patients, in patients whose expression data was generated from AML cells harvested directly from the marrow, and in patients whose AMLs expressed low levels of SUCLG2 as compared to the alternate SCS-β subunit, SUCLA2. Lastly, KD of the other SCS complex members *in vivo* revealed that these proteins are important for AML cell proliferation and also sensitize cells to therapy. Together, these data suggest that proper function of the SCS complex is critical for AML blasts, and specifically for AML LSCs, to survive therapy. Here, depletion of SCS members, including Suclg2 may lead to altered tumor energetic features that ultimately sensitize AML cells to combination chemotherapy.

Introduction

AML, the most common type of leukemia in adults, is a hematologic cancer characterized by the rapid clonal outgrowth of somatically transformed myeloid progenitors. Recent advances in –omics based technologies, particularly in next-generation sequencing (NGS) have provided us with a wealth of information regarding the molecular genetics and pathophysiology of this aggressive disease (TCGA, 2013; Döhner et al., 2015). While these intensive research efforts have led to the development of a small number of therapies targeted to mutational events commonly found in AML, the current standard of care has remained largely unchanged over the last 40 years (Lai et al., 2019). In the 1970's, cytarabine (Ara-C) and anthracyclines were found to be effective and were later combined into what is now the '7 + 3' backbone of AML therapy. Under this paradigm, patients are treated with Ara-C over 7 days, with an anthracycline concomitantly given at high doses during the first three days. Cycles of treatment with this combination of chemotherapeutics results in high initial response rates that have been reported to be as high as 80% (Saultz & Garzon, 2016). However, the majority of patients, even those in remission, harbor residual AML that leads to relapse within 3-5 years of diagnosis. Worse still, AMLs that recur after treatment failure(s) become increasingly resistant to therapy, leading to dismal cure rates of 35-40% in patients under 60, and of 5-15% in patients over 60 years of age (Döhner et al., 2015).

The population of leukemic cells that survive therapy represent minimal residual disease (MRD). MRD-derived relapse is the foremost source of fatality in AML patients receiving frontline treatment (Schuurhuis et al., 2018; Jongen-Lavrencic, et al., 2018). Chemotherapy can fail to kill MRD cells for numerous reasons. Impaired drug effectiveness can, for instance, be due to reduced levels of active chemo agents in target cells as a consequence of decreased uptake, increased efflux, or decreased delivery of drug to target tissues (Shaffer et al., 2012; Marin et al., 2016). Other cell intrinsic processes, such as deregulation of apoptosis (Vo et al., 2012; Cassier et al., 2017), amplification or modification of drug targets (Tyner et al., 2018; Yuan et al., 2019), altered cancer cell metabolism (Stuani et al., 2019), increased capacity for DNA damage repair (Bouwman & Jonkers, 2012), and activation of prosurvival signaling (Holohan et al., 2013) can similarly render tumors insensitive to therapy. Recently, leukemia stem cells (LSCs) have also been shown to be intrinsically more resistant to frontline agents that effectively eliminates bulk tumor cells (reviewed in Pollyea & Jordan, 2017). Importantly, this is clinically relevant, as AML patients whose tumors transcriptionally resemble a less differentiated, LSC-like state have been shown to have a significantly worse prognosis than patients whose AMLs transcriptionally

resemble more differentiated cells (Valk et al., 2004; Gentles et al., 2010; Eppert et al., 2011). Thus, in light of these and other recent data, LSCs are currently thought to serve as a reservoir for relapse in AML patients. Selectively eliminating these resistant LSC populations would likely lead to better outcomes and possibly even curative therapeutic options for AML patients. Indeed, this idea has already begun to accumulate clinical support. Venetroclax, an anti-BCL-2 agent, was previously shown to specifically target LSCs in preclinical models by directly inhibiting oxidative phosphorylation (OXPHOS) metabolism that LSCs specifically and inflexibly depend on for survival (Lagadinou et al., 2013). Follow up studies were conducted in elderly patients who were treated with a combination of venetoclax and azacitidine, a nucleoside analog and hypomethylating agent (Pollyea et al., 2018). Here, direct characterization of blast cells throughout treatment showed the same LSC-targeting effects, ultimately leading to long-lasting remissions that are superior to conventional treatment options in this patient population.

As the first proven LSC-targeting agent on the market, venetoclax's clinical success has sparked interest in the development of other such drugs. Here, identifying strategies by which MRD/LSCs can be specifically eradicated while in the context of frontline treatment could ultimately have the effect of extending this approach to a more broad population of patients. However, this would require a more thorough examination of the mechanisms by which MRD/LSCs survive conventional high-dose chemotherapy. Today, outside of OXPHOS based mechanisms, the other putative resistance pathways outlined above have not been examined in clinically relevant therapeutic settings. Thus, it is presently unclear whether MRD/LSCs can also survive therapy through alternate (non-OXPHOS) cell autonomous mechanisms, through stochastic chance (Ding et al., 2012), or through mechanisms governed by the tumor microenvironment (TME) (Fiedler & Hemann, 2019).

In order to systematically investigate relapse phenotypes in AML, we conducted an *in vivo* RNAi screen in a transplantable and aggressive mouse model of this disease (Miller et al., 2013; Puram et al., 2016). To identify genes that alter therapeutic response, we optimized and treated animals with a mouse-compatible version of 7 + 3 combination schedule and looked for genes that when lost, sensitized blast cells to therapy (Zuber et al., 2009). Here, we focused on genes with known roles in maintaining stemness properties, mediating interactions with the TME, and promoting chemoresistance in other cancers. We also screened genes that play critical roles in cell metabolism. Recent studies beyond those completed with BCL-2/venetoclax/OXPHOS have confirmed that LSCs can be defined, and possibly targeted via their metabolic properties. These include low levels of reactive oxygen species (ROS), increased levels of glutathione

(Lagadinou et al., 2013), increased dependence on amino acid metabolism (Raffel et al., 2017; Hattori et al., 2017; Jones et al., 2018), increased reliance on mitochondrial translation and the respiratory chain (Skrtic et al., 2011; Chan et al., 2015; Cole et al., 2015), elevated levels of fatty acid oxidation (FAO) (Ye et al., 2016), and a reliance on AMP-activated protein kinase (AMPK) signaling in order to survive metabolic stress (Saito et al., 2015; Pei et al., 2018). Further, other work has also uncovered a role for specific metabolites in cancer. Here, the abnormal accumulation of "oncometabolites," such as succinate, 2-hydroxyglutarate (R-2HG), and fumarate has been shown to lead to both metabolic and non-metabolic dysregulation in cells, alterations that ultimately promote tumorigenesis (Sciacovelli & Frezza, 2016). As more and more metabolic dependencies are being described in the literature, it is thus currently imperative to explore the mechanisms by which these unique properties contribute to treatment failure. As shown with venetoclax, these studies could also lead to the development of improved therapeutic options in AML.

In addition to our RNAi screen, we decided to approach the problem of resistance by modeling the repeated cycles of therapy that patients normally receive in the clinic. Here, we performed serially repeated cycles of transplantation followed by exposure to combination therapy in chemo-naïve AML cells. Seven consecutive cycles of treatment and reinjection were sufficient to generate chemoresistant cells. Transcriptional profiling of the Chemo^{R} model allowed us to identify a chemoresistance gene signature that we overlapped with the results of the shRNA screen to identify high-confidence genes of interest. The top genes from a ranked list of the most highly overexpressed genes in Chemo^{R} cells and the top depleted genes from the shRNA screen were selected as high interest hits. Using this approach, we identified the tricarboxylic acid cycle (TCA) gene Succinate-CoA Ligase GDP-Forming Beta Subunit, or *Suclg2*, suggesting that it may represent an uncharacterized therapeutic target that promotes resistance in AML.

Suclg2 encodes the GTP-specific beta subunit of the mitochondrial protein complex Succinyl-CoA synthetase (SCS), or SCS-G. Here, SCS-G or SCS-A (the ATP-specific beta subunit encoded by *Sucla2*) forms a heterodimer with SUCLG1. Together, this complex is responsible for catalyzing the reversible reaction of succinyl-CoA to succinate and CoA, accompanied by the phosphorylation of either ADP or GDP to form ATP or GTP, depending on the β subunit used (Johnson et al., 1998; Li et al., 2013). Interestingly, tissue specific difference in the expression of SCS-G and SCS-A have been described, indicating non-redundant roles for these proteins in human metabolism (Johnson et al., 1998; Fraser et al., 2000; Lambeth et al.,

2004; Philips et al., 2009). SCS-A is strongly expressed in catabolic and highly oxidative tissues, such as the brain, skeletal muscle, and heart. Conversely, SCS-G is scarcely detectable in brain and muscle where its expression is limited to the vasculature. Instead, SCS-G is robustly expressed in anabolic tissues that serve biosynthetic roles, such as the liver and kidney. Recently, heterozygous mutations in the SCS complex have been linked to human diseases (Wong et al., 2013). Alterations in SUCLG1 and SUCLA2 have been shown to lead to lethal infantile Leigh or Leigh-like syndromes that are characterized by severe neurological disorder, hypotonia, and deafness, along with a depletion of mtDNA and elevations of methylmalonic acid (MMA) (Elpeleg et al., 2005; Ostergaard et al., 2008; Donti et al., 2014; Carrozzo et al., 2016; Zhao et al., 2017). Mutations in SUCLG2 have never been observed in humans, and LOF mutations in any of the SCS members are embryonic lethal in mice (Kacso et al., 2016). However, a recent study has shown that knocking down SUCLG2 in human primary fibroblasts leads to severe mtDNA depletion that is more severe than that observed in fibroblasts from patients with SUCLA2 mutations or when SUCLA2 is knocked down in control fibroblasts (Miller et al., 2011). Lastly, a direct association between the SCS complex and mitochondrial nucleoside-diphosphate kinase mtNDPK has been reported to be indispensable for the stability of mtNDPK protein (Lacombe et al., 2018). As proper mtNDPK function is crucial for maintaining mt nucleotide pools, mtDNA depletion phenotypes associated with SCS mutations are thought to occur via destabilization of this protein (Zhao et al., 2017).

The most extensive literature on the function of SCS-GTP is in pancreatic islet cells. Here, mitochondrial GTP (mtGTP) has been shown to promote the release of insulin via a non-canonical mechanism that is OXPHOS independent (Kibbey et al., 2007). As no mitochondrial GTP transporter exists in mammalian cells, mtGTP generated in the TCA cycle by the SCS/SCS-G complex is trapped in the mitochondrial matrix (Vozza et al., 2004; Stark et al., 2014). Additionally, mtGTP is only metabolically generated in the mitochondria by turns of the TCA cycle that involve the participation of SCS-G (Kibbey et al., 2007; Jesinkey et al., 2019). These features significantly distinguish mitochondrial GTP from ATP, as the latter is predominantly generated via the respiratory chain and rapidly exported to the cytoplasm via its ATP/ADP transporter. Together, mtGTP's slow cytoplasmic exchange and roughly stoichiometric production from every molecule of glucose oxidized (assuming equal flux through both β subunits) make it especially well-suited to reflect the rate of glucose oxidation through the TCA cycle in these cells. This provides islet cells with a mtGTP-dependent mechanism by which to sense glucose in and around it (Jesinkey et al., 2019). The rate of mtGTP production would then be set by relative

levels and activities of the SCS-G and alternate SCS-A β-subunits which would then compete for the same substrates (except GDP). Here, research has shown that mtGTP hydrolysis by mitochondrial phosphoenolpyruvate carboxykinase (PEPCK-M encoded by *PCK2*) is coupled to the conversion of oxaloacetate (OAA) to phosphoenolpyruvate (PEP). Mitochondrial PEP can then shuttled into the cytoplasm where it is converted to pyruvate and ATP, thereby biochemically transmitting the nutrient sensing signal (Stark et al., 2009; Jesinkey et al., 2019). The generation of PEP driven by mtGTP also accomplishes the removal of oxaloacetate (OAA) from the TCA cycle. Hence, mtGTP has also been shown to be a major regulator of cataplerosis and gluconeogenesis (Wang & Dong, 2019).

To date, the SCS complex and SCS-GTP specifically, is poorly annotated in cancer. Recent reports have shown that SUCLG2 is upregulated in breast cancer mammospheres (Lamb et al., 2014) and in follicular carcinoma where it was shown to be a biomarker for this disease (Lai et al., 2017). Another study also showed that knocking down SUCLG1 in osteocarcinoma and renal carcinoma cells significantly reduced intracellular succinate levels, but had no effects on the metabolic properties or growth kinetics of the cells studied (Mullen et al., 2014). Lastly, SUCLG2 knockdown and depletion of mtGTP in non-small cell lung cancer (NSCLC) prevented cells engaging gluconeogenesis pathways (Vincent et al., 2015). However, the inability of NSCLC cells to use this anabolic pathway only reduced growth rates when cells were grown in media that was completely devoid of glucose. Hence, the relevance of this phenotype for *in vivo* cancer growth is unclear, as anatomical glucose levels *are* 2-3 fold lower than those in culture medium, but certainly, never completely absent (supplemental table 2.1; Cantor et al., 2017; Voorde et al., 2019).

In the present study, we establish a direct role for SUCLG2, and potentially, for the SCS complex as a whole, in promoting AML chemoresistance. Through genetic methods, we show that loss of SUCLG2 leads to the *in vivo*-specific chemosensitization of AML cells in both murine and human models of the disease. Ultimately, our data suggest that targeting SUCLG2 in the context of therapy might represent a novel mechanism by which MRD/LSC-based relapse and resistance can be overcome to efficiently eradicate tumor cells.

Results

In order to uncover novel mediators of resistance to frontline therapy (anthracyclines and cytarabine) in AML, we completed a focused *in vivo* RNAi screen (Figure 2.1a) using a transplantable Actin-DsRed+ MLL-AF9 mouse model of AML developed in the Ebert lab (Miller

et al., 2013; Puram et al., 2016). In order to avoid screening for genes that are critical for engraftment, we utilized a doxycycline inducible miR30 backbone shown in Figure 2.1b, developed in the Lowe lab (Zuber et al., 2011). In the absence of doxycycline, cells infected with this vector constitutively express a fluorescent Venus cassette and a reverse tetracycline transactivator (rtTA3) from a phosphoglycerate kinase (PGK) promoter, and can thus be detected via green fluorescence on flow cytometric (FC) analysis. Once doxycycline is provided, the rtTA3 molecule can bind the tet-responsive reporter (TRE) in the vector, promoting the expression of a far-red fluorescent marker, E2-Crimson, and a designed hairpin embedded in an endogenous miR-30 RNAi context. Two focused custom libraries targeting 429 murine cell energetic genes (2115 hairpins) or 94 genes (304 hairpins) known to be important for stemness features and chemoresistance in other hematologic malignancies were synthesized and subsequently screened. Treatment naïve DsRed+ MLL-AF9 cells were infected *ex vivo* with these libraries such that each cell contained, on average, less than one integrant. Green cells were sorted and injected into twenty sublethally irradiated secondary recipients that were randomized into 4 groups (GP) and treated as indicated in Figure 2.1a. Leukemia cells were harvested at various timepoints, also as indicated in Figure 2.1a. Using this approach, upwards of 70% and 80% of our high-quality libraries could be represented *in vivo*, with the vast majority of input shRNAs identified upon sequencing (Figure 2.2). A comparison of hairpin representation between groups GP2 and GP3, GP2 and GP4, or GP3 and GP4 identified 62 depleted and 69 enriched genes in the context of therapy (figure 2.3a-b). At this point, we also took an orthogonal approach based on clinical practice, where patients are treated with repeated cycles of combination chemotherapy (Döhner et al., 2015). To model this process in mice, we transplanted chemo naïve cells into animals and treated them with combination chemotherapy. Upon relapse, leukemic cells were sorted from animals and reinjected into new recipient mice that were then treated identically. After seven cycles of serial treatments and transplantations, Chemo^{R} cells were shown to be completely therapy-refractory (Figure 2.3c). In order to prioritize chemosensitizing (depleted) genes for follow-up studies, we overlapped the transcriptional profile of the Chemo^{R} model with hits from our screen, a comparison that assumes that expression changes of a gene could mean that it is important in a cell's response to therapy. Still, the top genes that were both highly expressed in Chemo^{R} cells and also scored as chemosensitizers in our *in vivo* screen were tagged for follow-up experiments (Figure 2.3b-d). Data for 7 of these genes is shown in figure 2.3d (*Gabarap*, *Prkag1*, *Sod1*, *Strada*, *Ctsa*, *Aldoc*, and *Suclg2*).

In order to approach validation studies via orthogonal methods, we initially attempted to generate Cas9 and dCas9 expressing MLL-AF9 cells using the pLenti-Cas9-Blast vector from Feng Zhang's lab and a published retroviral vector from our lab (Sanjana et al., 2014; Braun et al., 2016). However, expression of Cas9 using retroviral vectors was toxic to MLL-AF9 cells *in vitro*. Any cells that could ultimately be single cell-cloned did not propagate disease in any mouse model tested (including NSG mice; data not shown), an expected phenotype given that this model is known to differentiate and lose its AML propagating properties when cultured for more than 1-2 weeks. Ultimately, no CRISPR/Cas9 model could be established in these cells, and efforts to generate Cas9+ mouse models of AML by directly infecting GMPs from Cas9+ mice with retroviral vectors that induce MLL-AF9 expression are currently underway. Interestingly, it appears as though our experience with this approach is not unique, as the Scadden lab recently reported using the same approach (using Cas9+ mice rather than the established MLL-AF9 mouse cells) to generate such a model that was subsequently used to perform a screen (Mercier et al., 2017). Additionally, we attempted to use the improved miR-E system to enhance the efficacy of our hairpins and further validate our results (Fellmann et al., 2013). While the vectors for inducible miR-30 and inducible miR-E expression are highly similar, robust expression of mir-E embedded hairpins and their E2-crimson reporter cassette could never be achieved in this AML model. Notably, the miR-E system works well in human AML cell lines and in some of our other mouse models. Lastly, I also began developing tool compounds with the Koehler lab that specifically target SUCLG2 so that I may also approach these studies pharmacologically. Here, we completed a screen for small molecule binders of this protein and plan on following up on these data.

Validation studies for *Suclg2*, *Strada*, *Ctsa*, and *Gabarap* were subsequently completed *in vivo*, with only *Suclg2* (Figure 2.4a-f) and *Strada* (data not shown) consistently demonstrating chemosensitization phenotypes when new hairpins against these genes (generated to begin to rule out off-target effects) were tested in competition assays (Figure 2.4a). We chose to focus on *Suclg2*, as the sensitization phenotype of this knockdown appeared more robust and consistent across various *in vivo* assays (only 1 of 3 new hairpins against *Strada* extended life in chemo treated animals in subsequent experiments. Data not shown. For Suclg2, both hairpins tested extended life). As shown in figure 2.4c-f, chemotherapy treatment selectively eliminated cells bearing *Suclg2*-targeting hairpins more efficiently than cells bearing a control hairpin (shLuc) in all anatomic locations assayed. *Suclg2* knockdown efficiency was assayed using qPCR (Figure 2.4b). Further experiments using two new hairpins showed that the degree of life extension

following chemotherapy correlated with the extent of Suclg2 knockdown in leukemia cells (Figure 2.5a-d). Because our screen identified *Suclg2* as a gene that is critically important for relapse, and not for acute response to therapy, tumor burden was assayed for *Suclg2* levels once treated mice had become moribund. Cells sorted from moribund animals treated with either a vehicle control (Figure 2.5c) or combination chemotherapy (Figure 2.5d) showed that, at relapse, cells that could no longer repress SCS-G levels had been selected out during therapy. This result further suggests that SCS-G loss is detrimental to cells in the context of combination chemotherapy. To rule out RNAi off-target effects, we generated an shRNA non-targetable *Suclg2* cDNA cassette and cloned it into a mammalian expression vector (Figure 2.6a). This vector successfully restored Suclg2 protein levels (figure 2.7), and the expression of a PGK driven E2-Crimson cassette could be successfully used to sort out cDNA-expressing cells (figure 2.6b). As shown in figure 2.7a-b, the chemosensitization phenotype imparted by *Suclg2* KD could be rescued by the expression of shRNA-resistant *Suclg2* cDNA and the reinstatement of SCS-G protein levels (figure 2.7c-d). Hence, *Suclg2* is a novel AML dependency, specifically in the context of chemotherapy.

We next sought to more directly examine the relevance of *SUCLG2* in human AML. First, we confirmed that *SUCLG2* was present in AML using expression data from the cancer cell line encyclopedia (CCLE) generated at the Broad institute (Figure 2.8, black arrow indicating AML) and from the Human Protein Atlas (data not shown). Next, we examined SCS-G expression in various AML genetic subtypes gathered from two independent patient cohorts. Here, we found that high expression of this gene is significantly associated with *NPM1* mutations, *CEBPA* wildtype, and *NPM1* and *FLT3-ITD* mutated AMLs, along with M4 and M5 French-American-British (FAB) subtypes (figure 2.9a-b). To perform *in vitro* validation experiments in human cells, we chose to focus our efforts on MLL-rearranged cell lines, with or without FLT3-ITD mutations, including MV4-11, MOLM-14, THP-1, and NOMO1. We also used U937 cells which are FLT3-ITD negative and non-MLL-rearranged, as CCLE data indicated that *SUCLG2* was highly expressed in these cells. Initial studies to determine if SUCLG2 loss altered cell growth *in vitro* showed no differences in KD vs. control cells (figure 2.10a). Additionally, neither depletion nor complete loss of SUCLG2 sensitized any cell lines tested to frontline chemotherapy *in vitro*, given either in combination doses (representative data shown in figure 2.10b) or as single agents (representative data shown in figure 2.10d-i), although *SUCLG2* knockouts could not be generated in U937 or THP-1 cells (data not shown). That SCS-G depletion does not sensitize cells to therapy *in vitro* is not unexpected, as depletion of SCS-G in murine cells also did not

recapitulate the chemosensitization phenotype when dosed *in vitro* (figure 2.10f-g)—even when cells were grown (figure 2.10h) and dosed (figure 2.10i) in physiologic (nutrient-depleted) medium generated from protein depleted mouse plasma. Additionally, SUCLG2 did not score in large scale *in vitro* RNAi and CRISPR screening data from the Cancer Dependency Map (DepMap) project (figure 2.11a), despite being highly expressed in the AML cell lines used in these screens (figure 2.11b).

To determine if *SUCLG2* loss specifically sensitized human AML lines to therapy *in vivo*, xenograft experiments using MOLM-14 knockout cells (KO, generated using CRISPR-Cas9 technology) in NSG mice were completed. Here, GFP+ tdTomato– Cas9+ cells that are either wildtype (parental line) or genetically null (GFP+ tdTomato+) for *SUCLG2* were mixed in a 1:1 ratio and injected into NSG mice. Upon the emergence of peripheral disease (~2-5% blood burden, as assayed by peripheral bleeds), mice were dosed with an optimized NSG compatible version of the 7 + 3 schedule used clinically (Wunderlich et al., 2013). Loss of *SUCLG2* specifically sensitized MOLM-14 cells to therapy in the bone marrow, as compared to vehicle treated control animals (figure 2.12a-b). Additionally, we observed decreased levels of other proteins making up the SCS complex in SUCLG2 KO MOLM-14 (figure 2.12c) and MV4-11 cells (figure 2.10d). Previously, both Suclg2$^{-/+}$ and Sucla2$^{-/+}$ mice had been shown to have a decrease in Suclg1 protein levels, however no decreases in Sucla2 expression were reported in Suclg2$^{-/+}$ mice (Kacso et al., 2016). As no sequence similarity exists among the coding or regulatory regions of these three proteins (as assessed using NCBI BLAST tool and reported in Johnson et al., 1998), it is exceedingly unlikely that off target-effects could account for these effects. Instead, it is likely that the expression of these interacting protein members is tightly linked to ensure proper function of the complex.

To begin to explore the mechanisms by which SUCLG2 depletion may sensitize hAML cells to therapy, we quantified TCA intermediates in control and Suclg2 KD/KO cells, harvested both *in vitro* (figures 2.13 and 2.14) and *in vivo* (figures 2.15 and 2.16). As succinate has recently been identified as an oncometabolite (Sciacovelli & Frezza, 2016), it is possible that treating AML cells with combination therapy increases either the expression of SUCLG2 or flux through SCS, ultimately resulting in increased cellular concentrations of succinate. These increased levels of succinate could then promote resistance to frontline chemotherapy through the tumorigenic properties of this metabolite. However, no consistent, significant changes in intracellular metabolite pools between control and SUCLG2 KO or KD cells (murine or human) treated *in vitro* with combination chemotherapy could be detected (figures 2.13 and 2.14). Additionally, cells

harvested from the leukemia laden (>90% leukemic burden) BM and spleens of mice also failed to show any significant differences between control cells and cells bearing Suclg2-targeting shRNAs, although some differences in metabolite pools between cells residing in different organs could be detected (figures 2.15 and 2.16). Lastly, in all cases examined, no consistent, significant differences could be found in the intracellular pool sizes of amino acids, including most notably, glutamine, glutamate, asparagine, aspartate, histidine, proline, valine, isoleucine, methionine, tyrosine, or phenylalanine (representative data shown in figures 2.13-16, panels g-h).

Next, to examine the mechanism of Suclg2-mediated chemoreistance in a more unbiased manner, I treated animals bearing Suclg2 hairpins with frontline chemo and, 48 hours later, sorted leukemia cells from the BM or spleen and isolated RNA for transcriptional profiling experiments (figure 2.17a). Differential gene expression analysis between treated Suclg2 KD and treated control cells was used to define a "chemotherapy response signature," representing a chemosensitized state in cells with low Suclg2 expression (BM signature shown in figure 2.17b). We reasoned that since *Suclg2* appears to be important specifically at relapse and AML LSCs have been shown to be a reservoir for disease recurrence (Thomas & Majeti, 2017), that our BM chemosensitization signature might be able to stratify patients whose tumors are more LSC-like. Indeed, the downregulated gene signature in Suclg2 KD BM cells was able to predict outcomes in the large BeatAML patient cohort (Tyner et al., 2018) examined (figure 2.17c-e). Here, patients whose tumors were enriched for our chemotherapy response signature (indicating that they might respond better to therapy) had a significantly better outcome than patients whose tumors were depleted of this signature. A similar trend was obtained using data from the smaller set of patients assayed in TCGA studies, although this comparison did not reach statistical significance (figure 2.17f-g). Next, we reasoned that since Suclg2 was identified using a treatment-naïve mouse model with an inherent amount of preexisting therapy resistance, that our chemosensitization signature might have the greatest relevance in treatment refractory patients (although, as shown in figure 2.17e, the LSC-high cohort from the BeatAML dataset *is* enriched for treatment refractory patients). Notably, these subsequent analyses are only possible with the BeatAML cohort, as this database is extensively annotated with clinical information, better than any other data set of which we are aware. Indeed, when we performed the same analysis in treatment refractory cases, our signature could again stratify patients, showing that, as before, an enrichment of our "chemosensitization" signature predicted longer survival (figure 2.18a-b). Together, these patient stratification results suggested that loss of Suclg2 (and an inability to

upregulate partner genes) might be especially detrimental to LSCs resident in the BM, and dispensable for bulk tumor cells. As the BeatAML cohort also contains information about the anatomical location from which blast cells were harvested and transcriptionally profiled, this was a question we could further investigate. Strikingly, the same analysis done again in the BeatAML patient cohort showed that our "chemosensitization" signature could again stratify patients whose expression data had been generated from cells harvested via a bone marrow aspirate and not from peripheral blasts (figure 2.18c-d). As before, patients whose tumors were enriched for our chemosensitization signature were significantly more likely to survive longer. Notably, our spleen chemosensitization signature was never able to stratify any of the patient cohorts analyzed.

We had one final thought about where our BM chemosensitization signature might stratify patients, outside of LSCs and microenvironmental niches. The WB analyses completed throughout our experiments are completed using bulk tumor tissue that is sorted based on the background label(s) it is given, and not fractionated in any other way. However, SUCLG2 and SUCLA2 have been shown to have non-redundant roles and tissue specific differences in gene expression. Here, catabolic tissues express more SUCLA2 and anabolic tissues express more SUCLG2, suggesting that these proteins might regulate or demarcate different metabolic and/or cellular states. To this point, pancreatic islet cells express both SUCLG2 and SUCLA2, and altering the ratio of these two proteins relative to one another can significantly alter a cell's properties, including its metabolism, differentiation state, and overall ability to deal with metabolic stress (Jesinkey et al., 2019). Our WB results in bulk AML cells might then be a result of an admixture of cells expressing different levels of either of these proteins. Hence, we wondered if the ratio of SUCLA2 to SUCLG2 might be a relevant way to further stratify patients. Here, the inability of a cell to engage SUCLG2 and its partner genes could have a more dramatic effect in cells that already express a low amount of SUCLG2 relative to SUCLA2, given that these proteins appear to be largely non-redundant, at least in some tissues. This idea leads to the hypothesis that our signature would best stratify patients with a high SUCLA2:SUCLG2 (A2:G2) ratio (defined as patients with A2:G2 ratios above 1). Indeed, this is what we found, with enrichment of our signature again predicting significantly better outcomes in patients with a low A2:G2 ratio (figure 2.18e-f). Interestingly, it also appears as though a high A2:G2 ratio also pulls out most of the long term survivors in this data set. Overall, these data suggest that an inability to engage SUCLG2-driven programs may be especially detrimental for LSCs in the context of therapy. Additionally, a high A2:G2 ratio may be a marker of cells that would be especially unable

to engage SUCLG2-mediated cellular programs. The lack of flexibility in switching to these programs appears to be especially detrimental *in vivo* when leukemic cells are challenged with combination chemotherapy.

Next, we further interrogated our treatment response RNAseq data. Gene set enrichment analysis (GSEA) of the most differentially expressed genes between Suclg2 KD cells and cells bearing a control hairpin (shLuc) showed a significant upregulation of OXPHOS pathway genes in KD cells (figure 2.19a). Interestingly, Chemo^R cells also show a significant enrichment in OXPHOS genes (figure 2.19b), and upregulated OXPHOS metabolism has already been shown to promote chemoresistance in AML and other cancers (Vazquez et al., 2013; De Rosa et al., 2015; Ippolito et al., 2016; Kuntz et al., 2017; Bosc et al., 2017; Lee et al., 2017; Farge et al., 2017; Ashton et al., 2018). Thus, our results could indicate that upregulation of OXPHOS might be promoting survival to therapy in Chemo^R cells. Depletion of Suclg2 could then possibly lead to altered OXPHOS or mitochondria, which might then lead to compensatory changes in other OXPHOS pathways members. To further investigate this idea, we stained murine AML cells with MitoTracker deep red, a dye that passively diffuses across the plasma membrane and accumulates in mitochondria regardless of mitochondrial membrane potential. Here, we observed significantly less signal in KD versus control cells, but only when this was assayed directly from leukemic animals, and not if cells had been cultured overnight first (figure 2.19c-d). Additionally, increased dye signal was noted in Chemo^R cells, further suggesting that mitochondrial mass might be affected in KD cells, resulting in a chemosensitization phenotype. This notion is supported by findings from other groups indicating that both LSCs and residual Ara-C-resistant AML cells are inflexibly dependent on OXPHOS for survival (Lagadinou et al., 2013; Farge et al., 2017; Jones et al., 2018; Pollyea et al., 2018).

To follow up on these results, we completed mitochondrial stress tests in control and Suclg2 KD/KO cells to examine mitochondrial function. As shown in Figure 2.20a-b, this assay is based on the measurement of oxygen consumption rates after the administration of inhibitors known to affect specific members of the electron transport chain, allowing researchers to examine the health and functionality of mitochondria. Given our staining data, we expected KD and likely, KO cells to show less functional or more damaged mitochondria, including an increased proton leak, decreased spare reserve capacity, and less ATP-linked respiration, if mitochondria are indeed damaged or depleted. Surprisingly, we observed the opposite effects in both KD and KO cells, which appear to have increased oxidative capacities, including an increased maximal respiration rate, increased basal respiration rate, increased spare reserve

capacity, decreased or unchanged proton leak, and increased ATP production (figure 2.21 and 2.22). Overall, this assay showed that in response to stress, cellular energy phenotypes appear to be enhanced for aerobic capacities upon SCS-G KO or KD (figure 2.23a-b). Together, our mitochondrial assays thus far show that Suclg2 KD/KO cells appear to have less mitochondria that are also more active and able to engage OXPHOS metabolism than control cells. Unlike in normal LSCs and Ara-C resistant MRD however, increased OXPHOS alone is not enough to protect cells from chemotherapy-induced killing in the context of SCS-G depletion (Lagadinou et al., 2013; Farge et al., 2017; Jones et al., 2018; Pollyea et al., 2018). Thus, alternate mechanisms are likely responsible for the chemosensitization phenotype imparted by Suclg2 loss.

Lastly, we examined the effects of knocking down other members of the SCS complex, both in the context of treatment and in saline control animals. Here, we anticipated that Suclg1 KD would sensitize cells to therapy, as it is the common alpha subunit of the SCS complex in which SCS-G functions and thus, should phenocopy SCS-G depletion. We also suspected that Sucla2 KD would show no effect, as it did not score as a hit in any condition in our screen. With this experiment, we ultimately hoped to narrow down the chemosensitization phenotype to either the common reaction catalyzed by this complex or to difference between the two reactions—the nucleotide triphosphate generated by each subunit: mitochondrial GTP (mtGTP) by SCS-G or ATP by SCS-A. Here, KD of Sucla2 that leads to the same phenotype as Suclg2 depletion (chemosensitization) would point towards mechanisms downstream of the common metabolites, succinyl-CoA and succinate, interconverted by this complex. A result where Sucla2 depletion is not chemosensitizing or shows and different phenotype could then indicate that the production of mtGTP would be important. Surprisingly, loss of Suclg1 or Sucla2 appeared to both sensitize cells to chemotherapy and extend life in animals treated with a vehicle control (figure 24a-g, corresponding P-values adjusted for multiple hypothesis testing are shown in panel 2.24g). Critically, this was not due to timing issues with dosing, as blood taken from 4 animals from each hairpin group before treatment (2/5 from each of the chemo-treated or saline treated groups, per hairpin) showed that all animals had reached a peripheral blood burden of ~15% (the level at which we begin treatment in this model). Additionally, depletion of Suclg1 and Sucla2 protein levels were confirmed via western blot (figure 2.24d-e). Together, these data suggest that beyond Suclg2, the proper function of this entire complex is possibly important in AML, both as a general dependency (as in the case of Sucla2) and in the context of therapy. Here, it may be that balanced flux through both SCS-β isoforms, and the ability to switch between the two is critical

for blast survival *in vivo*, both for general growth and in the context of chemotherapy insult. This idea is supported by the aforementioned observation that the expression of SCS members appears to be tightly linked. Here, loss or knockdown of one SCS-β isoform can lead to changes in the other complex members, as observed in our hAML SUCLG2 KO data (figure 2.10e and 2.12b-c), in mice heterozygous for either or both SCS-β isoforms, or in pancreatic islet cells depleted of either the SCS-A or SCS-G using siRNAs (Kibbey et al., 2007; Kacso et al., 2016). This idea is further supported by our RNAseq data from control murine AML cells harvested from the BM 48hrs after vehicle control, 48hrs after being acutely treated with combination chemo, or harvested at relapse, after chemotherapy exposure (figure 2.25). Here, cells express nearly twice as much SUCLA2 at baseline and engage SUCLG2 pathways upon treatment, lowering the A2:G2 ratio. At relapse, upon becoming increasingly chemoresistant, bulk blast cells express even higher levels of SUCLA2, the SCS-β subunit associated with highly oxidative tissues. As the MLL-AF9 mouse model used here has been shown to have a substantially high proportion of LSCs, it is likely that these data also reflect alternating A2:G2 ratios in the LSC pool.

Discussion

In this study, we perform the first *in vivo* AML screen completed in the context of frontline chemotherapy and establish a new mouse model of resistance. We utilized both of these orthogonal approaches to uncover mediators of resistance, ultimately identifying and validating SUCLG2 as a novel, *in vivo*-specific AML dependency in the context of a clinically relevant course of combination therapy. Here, Suclg2 appears to be most important in relapse after therapy, where it scores as a chemosensitizer in the top 5% of all depleted genes, and in resistance, where it is overexpressed in our Chemo^{R} model. As an aggressive, and mostly lethal disease with increasing, but few treatment options, the identification of such targets in AML is sorely needed. Suclg2 is a poorly annotated gene in the cancer literature and as such, it has not previously been implicated as being important in AML, in any context. To our knowledge, this is the first and only study in which this protein or the SCS complex as a whole has ever been shown to be important for therapeutic response in any cancer type. This is despite significant efforts in the field to screen for functionally relevant genes that modulate therapeutic outcome in various cancer types *in vitro*. Here, this speaks to the power of the functional genomics approach we have taken in our study *and* the efforts we have made to apply these techniques in clinically relevant *in vivo* settings. As such, our successful identification of SUCLG2 here suggests that future studies aimed at identifying relevant and novel drug targets would also substantially

benefit from this approach. Further investigation of Suclg2's role in promoting resistance, along with studies investigating the effects of its inhibition in normal cells (specifically in the context of chemotherapy) could allow for the development of novel AML therapeutics. To this end, we have also begun screening for small molecules that bind and inhibit SCS-GTP. From our data, SUCLG2 and potentially, SCS inhibitors would be expected to potentiate the effects of the frontline agents used in the majority of patients today. Thus, this study provides the first crucial stepping stone for efforts that could ultimately result in both a better understanding of the major determinants of therapeutic outcome in AML, and in new and more efficacious treatment options for patients.

Other than the critical identification of a previously unknown *in vivo*-specific resistance gene in a devastating disease, perhaps the most intriguing data from our study is that obtained from the stratification of large patient cohorts. Here, the downregulated genes from our acute response signature are significantly associated with better outcomes in specific patient populations. Notably, these patient backgrounds were predicted by the context in which the depletion of Suclg2 was discovered to sensitize cells to frontline therapy. Since *Suclg2* scored in the relapse-specific arm of a screen completed in a treatment-naïve mouse model with inherent chemoresistance, we reasoned that our signature would be relevant in patients who are treatment refractory and who harbor tumors driven by more LSC-like cells known to fuel relapse. Strikingly, this is precisely what we observe. On these backgrounds, enrichment of our 'down' response signature significantly correlates with longer survival, indicating that the LSCs might represent the sensitized background on which Suclg2 loss/depletion is relevant and has a substantial effect. This model then directly posits that our signature might be best suited to stratify patients whose AMLs are profiled using blasts resident in the marrow, where the largest proportion of LSCs are known reside. Again, this is precisely what we observe, with our chemosensitzation signature again predicting significantly better outcomes in these patients. Lastly, we reasoned that since SCS-β isoforms appear to be largely non-redundant in mammalian cells, that an inability to engage SUCLG2 and its partner genes might be most detrimental in cells with already low SUCLG2 levels (Johnson et al., 1998; Fraser et al., 2000; Lambeth et al., 2004; Kibbey et al., 2007; Philips et al., 2009). Indeed, our chemosensitization signature was again able to stratify patients with high SUCLA2:SUCLG2 ratios in the expected pattern, with enrichment of our signature predicting significantly better outcomes in patients.

Together with the compelling results from patient cohorts, our data suggest a particularly intriguing mechanism for how SUCLG2 depletion could be potentiating the effects of

chemotherapy. In this model, the depletion of SUCLG2 could be selectively sensitizing precise cell populations enriched in MRD that fuel relapse: LSCs or LSC-like (MRD) cells. Previous studies have shown that increased OXPHOS desensitizes AML LSCs and cells from other cancer subtypes to a variety of frontline and targeted chemotherapeutics (Vazquez et al., 2013; De Rosa et al., 2015; Ippolito et al., 2016; Kuntz et al., 2017; Bosc et al., 2017; Lee et al., 2017; Farge et al., 2017; Henkenius et al., 2017; Ashton et al., 2018; Jones et al., 2018). As Suclg2 KD and KO cells appear to have less mitochondrial mass that is also more active and enhanced for its oxidative capacities, upregulation of OXPHOS alone does not appear to be enough to allow cells to overcome chemotherapy-induced killing in this context. Intriguingly, recent studies from the Jordan lab have shown that LSCs have reduced mitochondrial mass and are exquisitely reliant of OXPHOS for their survival (Lagadinou et al., 2013). To fuel this high rate of respiratory metabolism, LSCs were shown to rely heavily on amino acid uptake (Jones et al., 2018). Upon depletion of this fuel source, LSCs specifically were unable to switch to alternate sources (namely, glycolysis/glucose or fatty acid oxidation [FAO]) to maintain their energy production. Thus, LSCs are metabolically inflexible in terms of the processes they require for survival (OXPHOS) and the fuel they use to maintain those processes.

In light of our data, it is possible that KD or KO of either SCS-β subunit might be metabolically rewiring LSCs to be even more inflexible in the pathways that they can engage to process various fuel sources, produce specific biomass precursors, and survive *in vivo*—either at baseline or during chemotherapy exposure. It is important to note here that altering A2:G2 ratios in either direction has already been shown to metabolically rewire islet cells, impacting their differentiation, synthetic metabolic profile, ability to sense glucose/release insulin, and overall ability to withstand metabolic stress (Kibbey et al., 2007; Stark et al., 2009; Jesinkey et al., 2019). Thus, it is possible that our manipulations of SCS-G and SCS-A accomplish similar outcomes in AML cells. In Suclg2 KD/KO for instance, LSCs would be forced to express much more of the SCS-A subunit that is linked to catabolic tissues with high levels of OXPHOS. Here, the inability to engage in the synthetic metabolism pathways (namely, cataplerosis and gluconeogenesis) promoted by SCS-G and mtGTP may be specifically detrimental in the context of therapy (Wang & Dong, 2019). Similarly, inhibiting SCS-A could be having the effect of forcing cells to engage more synthetic metabolism pathways at the expense of OXPHOS and the need to maintain cellular energy levels via this process. This would have the effect of specifically inhibiting both the baseline *in vivo* survival of LSCs and their survival in response to therapy, as previously described (Lagadinou et al., 2013; Farge et al., 2017; Kuntz et al., 2017; Pollyea et al.,

2018; Jones et al., 2018). Thus, in the absence of direct evidence, we speculate that some amount of metabolic flexibility, namely the ability to switch synthetic metabolism on and off at specific times, is critical for a cell's survival in response to chemotherapy (Figure 2.25 and 2.26). This possibility is particularly interesting in light of data from the hematopoietic stem cell (HSC) field where it has been shown that metabolic switches can directly determine HSC fate decisions (Takubo et al., 2013; Yu et al., 2013).

Importantly, other hits from our screen also support the aforementioned model. Of the three key enzymes that are exclusive to gluoconeogenesis (not shared with glycolysis) and are known to regulate it in mammalian cells (phosphoenolpyruvate-carboxy kinase [PEPCK], fructose-1,6-bisphosphatase [FBPase], and glucose-6-phosphatase [G6Pase]), two scored in our screen (Wang & Dong, 2019). The gene encoding mitochondrial PEPCK (*Pck2*), which requires mtGTP for its function, scores as a general growth dependency (gene 30 of 31, P-value=0.09, with significance set at P-value≤0.1, as indicated in the methods). Thus, *Pck2* would be unlikely to score as a chemosensitizer in our screen at any timepoint, as it would have already depleted with the induction of hairpin expression. Conversely, the cytosolic PEPCK isoform (*Pck1*) is not a hit in any of our conditions. That only *Pck2* scores in our screen is not surprising, as *Pck1* is not expressed in our murine AML model, in any of the CCLE AML cell lines, or in any of the human AML patient samples in the BeatAML data set (Tyner et al., 2018; data analyzed using accompanying online tool at vizome.org). Moreover, it has already been shown that increased levels of PEPCK1 and PEPCK2 are mutually exclusive in different cancers, as appears to be the case in AML (Balsa-Martinez & Puigserver, 2015; Wang & Dong, 2019). The gene that encodes FBPase (*Fbp1*) also scores as a top chemosensitizer in both relapse (gene 2 of 62, P-value=0) and in acute response (gene 1 of 62, P-value =0), but not as a general dependency. Lastly, G6Pase is encoded by three genes (*G6PC*, *G6PC2*, and *G6PC3*), of which only *G6pc* was targeted in our screen. This gene did not score in any condition assayed, but as with *Pck1*, *G6pc* is not expressed in our murine AML cells, in human AML cell lines, or in the AML patient samples in the BeatAML cohort. This indicates that the glycolytic intermediates being regenerated by AML blasts through gluconeogenesis are not secreted as glucose. Rather, these intermediates must be fully utilized within the cell to fuel growth. This exact finding was also found in other cancers that rewired their anabolic metabolism using a truncated form of gluconeogenesis mediated by *Pck1*/2 to maintain tumorigenic growth in nutrient-poor settings (Montal et al., 2015; Vincent et al., 2015; Balsa-Martinez & Puigserver, 2015). Hence, various genes regulating the

synthetic metabolism pathways involving Suclg2 also score as either general dependencies or chemosensitizers in our screen.

As limiting various nutrient sources using physiologic medium does not seem to be able to recapitulate our phenotype *in vitro*, it is possible that either the metabolic milieu of the BM is so different from the plasma that it cannot be recapitulated in our experiments, or that other factors, orthogonal to nutrient availability also conspire to rewire LSCs in this context. In the latter case, we suspect that direct signaling from the TME could be playing a role. This could then explain why culturing cells before staining them with mitochondrial stains repeatedly yields no differences in mitochondrial mass among any cells assayed (including shLuc, Suclg2 KD, and Chemo^{R}) while cells taken directly from animals consistently differ in this respect. Additionally, the fact that SUCLG2 overexpression is consistently associated with specific AML subtypes also supports this idea, as the mutational landscape of an AML cell has already been shown to alter various cellular properties. These properties include a blast cell's metabolism and signaling profile (Wouters et al., 2009; Pollyea & Jordan et al., 2017; Fenouille et al., 2017; Tyner et al., 2018). Future experiments will formally examine the idea that LSCs are specifically sensitized by SUCLG2 depletion. Here, I will mix Suclg2 KD or KO cells with their corresponding control cells (Suclg2 WT), inject them into animals, and sacrifice chemo or vehicle dosed animals at various time points, staining for canonical LSC markers such as CD34+CD38−. Here we hypothesize that Suclg2 KD/KO LSCs will be more sensitized to therapy over time (i.e. they die out more in response to chemo) as compared to both bulk Suclg2 KD/KO cells and control LSCs. Further characterization of LSCs compared to bulk tumor in the context of SUCLG2 KD/KO would then be warranted, such as untargeted metabolomics profiling and tracing experiments. Similarly, it will also be critical to better characterize the exact underlying metabolic, (epi)genetic, signaling, or other properties that define this sensitized background (other than stemness). Here, our analysis of patients using the ratio of SUCLA2 to SUCLG2 might provide some hints, as a high A2:G2 ratio appears to identify long-term survivors while a low A2:G2 ratio (SUCLG2 overexpression, compared to SUCLA2) appears to be associated with poorer outcomes. This suggests that in AML, the A2:G2 ratios might be a major determinant of therapeutic response. Moreover, how A2:G2 ratios relate to stemness is also an open question that will require additional investigation. One intriguing possibility is that A2:G2 ratios could further functionally fractionate LSC populations, both by their ability to survive therapy and their underlying metabolic properties. As LSCs have already been shown to be a heterogeneous population of

cells in AML, this result might be particularly helpful in the field's efforts to better understand and target this challenging cell type (Pollyea & Jordan et al., 2017).

SUCLG2 is a protein that functions within the mitochondrial matrix to catalyze the conversion of succinyl-CoA and GDP to CoASH, succinate, and GTP. As such, SUCLG2 sits at the intersection of several critical metabolic pathways, such as heme synthesis, fatty acid metabolism, branched chain amino acid metabolism, and many others that have already been shown to be important in AML (Fukuda et al., 2017; Jones et al., 2018; Lin et al., 2019; Kreitz et al., 2019; Tabe et al., 2020). In recent years, efforts to more fully characterize the metabolic profiles of different cellular populations (namely, LSCs) in various AML subtypes have found specific and targetable dependencies (Pollyea & Jordan, 2017; Stuani et al., 2019). Many of these identified pathways actually involve the SUCLG2/SCS and its metabolites, at least peripherally. Yet, as mentioned before, no direct evidence linking this protein to physiologically relevant tumor growth or chemoresistance has ever been reported. Additionally, oncometabolites have garnered tremendous attention, especially In AML and glioblastoma (GBM) where these TCA metabolites have been shown to directly inhibit α-KG-dependent dioxygenases (AKGDDs) such as the Jumonji C domain–containing histone lysine demethylases (KDMs) and the ten eleven translocation (TET) family of 5-methylcytosine (5mC) hydroxylases (Sciacovelli & Frezza, 2016). Inhibition of these AKGDDs results in epigenetic changes that alter the expression of cell differentiation and proliferation genes, leading to the acquisition of malignant features (Bowman & Levine, 2017). Our initial efforts to examine these and other potential downstream mechanisms by which this protein promotes resistance in our models have already consistently shown that intracellular metabolite pools do not appear to be altered. Thus, perhaps one reason why SUCLG2/SCS has not been identified in cancer might be that the flux through this metabolic node and the ability to toggle between SUCLG2 and SUCLA2 mediated pathways is what is critical for a cell's survival in specific contexts. Here, it is likely that flux is not always reflected by the individual expression levels of either isoform or by static metabolite pools. Indeed, previous studies have shown that only small changes in expression can lead to striking differences in the activity of either β-subunit in any given tissue (Johnson et al., 1998). Furthermore, studies have shown that the ratio of the expression of β-subunits is a better indicator of the rate of synthetic metabolism (regulated by SCS-G) that can be engaged by islet cells (Jesinkey et al., 2019). Here, cells with a lower A2:G2 ratio have a higher amount of mtGTP, are better able to engage the synthetic metabolisms pathways involving SCS-G, and are more resilient to metabolic stress. In terms of our work in AML, tracing experiments, more extensive

metabolic profiling, and the direct measurement of mtGTP levels would be extremely helpful towards examining the effect of losing SUCLG2.

Ultimately, we provide evidence that SUCLG2, and likely, the entire SCS complex as a whole, plays a critical role in allowing AML cells to survive therapeutic insults *in vivo*. This likely occurs by sensitizing LSCs to therapy in an OXPHOS independent manner. With agents like venetoclax already showing success in the clinic, it is crucial to further explore and expand the range of LSC-targeting treatments to develop highly efficacious drug regimens for AML. Thus, future work aimed at targeting SCS-G could yield significant progress towards better therapeutic options that lead to increased patient survival in this devastating disease. Additionally, we provide a novel paradigm by which future studies can continue to examine the key genes and pathways that ultimately determine chemotherapeutic outcome in AML. As this area of research is still in its infancy, we provide a critically important framework by which this problem can continue to be addressed.

Methods

In vivo pooled shRNA screening and statistical analysis

Two custom libraries were used. One library of 2,115 hairpins directed against 429 murine genes involved in cellular stress response with a minimum of 4 hairpins per gene was synthesized as an Oligomix from LC Sciences. Another library of 304 hairpins directed against 94 murine genes involved in chemoresistance, stemness, and interactions with the microenvironment with a minimum of 3 hairpins per gene was synthesized as a custom set from Transomic Technologies. Both of these libraries were cloned into a retroviral TRMPVI-Crimson vector. To preserve library complexity, a minimum of 500-fold coverage of the shRNA library was maintained at each step of the screen. 6-week-old C57BL/6 male donor mice (The Jackson Laboratory) were injected with 200,000 MLL-AF9-DsRed-L-GMP cells into the tail vein. Bone marrow was harvested from femur, tibia and humerus, and red blood cells were lysed (Sigma). DsRed sorted cells were resuspended in transplant medium made with 20 ng/ml IL-3 (Peprotech, 213-13), 20 ng/ml IL-6 (Peprotech, 216-16), 100 ng/ml FLT3-ligand (Peprotech, 250-31L) and 100 ng/ml SCF (Peprotech, 250-03) and then transduced with TRMPVI-Crimson-library vector by one round of spin-infection. 10×10^6 cells in 3 mL transplant medium containing 5 μg/mL polybrene (Sigma) and 7.5 mM HEPES buffer (Sigma) were centrifuged in the presence of virus for 4 hours at 1800g to promote cell transduction. After 24 hours, cells were sorted based on expression of the GFP fluorescent protein and then reinjected into 20 secondary recipient mice. These mice were

randomized into 4 groups with 5 mice each: i) one group no doxycycline, sacrificed at day 15 (GP1); ii) one group treated with doxycycline, sacrificed at day 15 (GP2); iii) one group treated with doxycycline, cytarabine (100 mg/kg), and doxorubicin (1 mg/kg), sacrificed at day 15 (GP3); iv) one group treated with doxycycline, cytarabine (100 mg/kg), and doxorubicin (1 mg/kg) and sacrificed at relapse (GP4). Doxycycline induction was started 7 days post-injection by supplementation of the drinking water with 1 mg/ml doxycycline and 5% sucrose. MLL-AF9 cells were harvested and sorted based on the expression of the crimson fluorescent dye. The antisense strand of shRNA was amplified from genomic DNA using primers that include 1-basepair mutation to barcode individual samples. Hairpins were amplified in multiple 50 µl reactions using HotStar Taq (Qiagen). After PCR amplification, samples were pooled and prepared for sequencing with Illumina's genomic adaptor kit. At least 41 bases of the PCR product were sequenced with an Illumina HiSeq 2000 machine and then aligned with bowtie2 to the mouse mm9 genome at the Swanson Biotechnology Center, Koch Institute, Massachusetts Institute of Technology. shRNAs with less than 100 reads in the input sample were excluded from further analysis, and read numbers for each shRNA were normalized to the total read numbers per sample to allow for cross-comparison between samples.

The genes whose depletion altered therapy response significantly between the groups of mice (GP2 vs. GP3, GP2 vs. GP4, GP3 vs. GP4; n=5 per group) were determined based on the EdgeR (Dai et al., 2014; Robinson et al., 2010) method followed by the RIGER method (Luo et al., 2008) (https://software.broadinstitute.org/GENE-E/extensions/RIGER.jar). EdgeR was used to perform the differential analysis on the shRNA count data between the groups of mouse samples (i vs. ii, ii vs. iii, ii vs. iv, iii vs. iv). RIGER ranked all the shRNAs according to their differential score between the classes of samples, then identified the genes targeted by the shRNAs at the top of the list, by computing a Kolmogorov-Smirnov statistic for gene enrichment in the top hairpins. The significance of the enrichment score was estimated through a permutation P-value (n=109 repetitions) adjusted for false discovery based on the Benjamini-Hochberg method with a significance cut-off ≤ 0.10. The significance cut-off was estimated as 0.10 instead of 0.05 due to the small size of the hairpin library. In this way, the EdgeR/RIGER methods identified 62 significantly depleted genes and 69 significantly enriched genes.

Mouse maintenance and studies

All mouse experiments were conducted under IUCAC-approved animal protocols at the Massachusetts Institute of Technology. The mouse strains used in this study included C57BL/6 (Jackson) and NOD-SCID/IL2Rg$^{-/-}$ (NSG; Jackson Laboratory). Immunocompetent recipient mice were sublethally irradiated (1 x 5 Gy [500 rads] prior to tail vein transplantation, as noted in the text. Transplanted cells were resuspended in 200 µl Hank's balanced salt solution (Lonza) and loaded in 27.5 gauge syringes (Becton Dickinson). Chemotherapy was administered when mice reached a peripheral leukemic blood burden of ~10-15% in immunocompetent animals, and when NSG animals showed a peripheral blood burden of 2-5%, as assayed by cheek bleeds. These peripheral blood burdens represent approximately equal BM burdens of about 50%. Combination chemotherapy doses were as follows in the specific mouse lines used: C57BL/6—cytarabine given via intraperitoneal (i. p.) injection at 100 mg/kg over 5 days and doxorubicin given i. p. at the same time, but for 3 days at 1 mg/kg. NSG—cytarabine (50 mg/kg) and doxorubicin (0.5 mg/kg) given together via tail vein injection for 3 days (necessary to avoid doxorubicin-induced liver necrosis in NSG mice, as indicated in Wunderlich et al., 2013), followed by i. p. administration of cytarabine (50 mg/kg) for two additional days.

Physiologic mouse plasma

Physiologic mouse plasma medium was prepared and generously provided by the Vander Heiden lab. This protocol is not yet published. Briefly, venous blood is collected from euthanized animals via venipuncture and is transferred to a prechilled heparinized tube. All subsequent centrifugation steps are performed at 4C. Plasma is collected after centrifugation. The resulting plasma is then filtered through a polyethersulfone (PES) column with a molecular weight cutoff of 3kDa (Pierce, 88514) overnight. The filtered product constitutes the physiologic mouse plasma medium which is supplemented with 10% dialyzed FBS for culturing experiments.

Plasmids, cloning, shRNAs, and sgRNAs

A modified version of the TRMPVIR vector (Addgene, 27994) generated in the Lowe lab was used for inducible-RNAi expression. Here, the DsRed cassette was replaced with an E2-Crimson cassette using the BamHi and NotI cut sites. Resulting vector was then sequence verified. For constitutive expression, pMLS-Sv40-EGFP (Addgene, 46919) was used. Hairpins were designed, cloned and expressed in the miR30 context as described in Fiedler et al., 2018 and Gilbert et al., 2013. The 97-mers used in this study are:

Murine Suclg2:

sh#7 (5'-
TGCTGTTGACAGTGAGCGCACGAAACAAACTCCAAAAGAATAGTGAAGCCACAGATG
TATTCTTTTGGAGTTTGTTTCGTTTGCCTACTGCCTCGGA)

sh#8 (5'-
TGCTGTTGACAGTGAGCGAAAGAGGAAAAGGTGTCTTCAATAGTGAAGCCACAGATGT
ATTGAAGACACCTTTTCCTCTTCTGCCTACTGCCTCGGA)

sh#1660 (5'-
TGCTGTTGACAGTGAGCGACAGATCTAGGTTCATTCACAATAGTGAAGCCACAGATGT
ATTGTGAATGAACCTAGATCTGGTGCCTACTGCCTCGGA)

sh#1444 (5'-
TGCTGTTGACAGTGAGCGCCACAAGGATCATCATGTGAAATAGTGAAGCCACAGATGT
ATTTCACATGATGATCCTTGTGTTGCCTACTGCCTCGGA)

Human SUCLG2:

shSUCLG2#6 (5'-
TGCTGTTGACAGTGAGCGCTGGGTACAATCTAGCGACAAATAGTGAAGCCACAGATG
TATTTGTCGCTAGATTGTACCCAATGCCTACTGCCTCGGA)

shSUCLG2#7 (5'-
TGCTGTTGACAGTGAGCGCAAGAGACTAAATGCAAAAGAATAGTGAAGCCACAGATGT
ATTCTTTTGCATTTAGTCTCTTATGCCTACTGCCTCGGA)

shSUCLG2#8 (5'-
TGCTGTTGACAGTGAGCGACAGGAATACCAGAGCAAGAAATAGTGAAGCCACAGATG
TATTTCTTGCTCTGGTATTCCTGCTGCCTACTGCCTCGGA)

Murine Suclg1

shSuclg1 #1 (5'-
TGCTGTTGACAGTGAGCGCCAGAGACAGATAATAAATCTATAGTGAAGCCACAGATGT
ATAGATTTATTATCTGTCTCTGTTGCCTACTGCCTCGGA)

shSucgl1 #2 (5'-
TGCTGTTGACAGTGAGCGCACTGTGTAACAGAGACAGATATAGTGAAGCCACAGATGT
ATATCTGTCTCTGTTACACAGTATGCCTACTGCCTCGGA)

Murine Sucla2

shSucla2 #1 (5'-
TGCTGTTGACAGTGAGCGCCACACGCAGATTGATAAGAAATAGTGAAGCCACAGATG
TATTTCTTATCAATCTGCGTGTGTTGCCTACTGCCTCGGA)

Renilla Luciferase (Referred to as Ren.713 in Fellmann et al., 2013)

shLuc (5'-
TGCTGTTGACAGTGAGCGCAGGAATTATAATGCTTATCTATAGTGAAGCCACAGATGT
ATAGATAAGCATTATAATTCCTATGCCTACTGCCTCGGA

To generate Cas9+ human cell lines, lentiCas9-Blast (Addgene, 52962) was used and cells were selected with Blasticidin (Gibco, A1113903) at 20 µg/mL for 7 days and then single cell cloned and assayed for Cas9 expression via WB. Guide RNAs for human SUCLG2 were designed using the Broad Institute sgRNA Designer (Doench et al., 2014) and cloned into our retroviral sgTomato vector as described in Braun et al., 2016. Here, guide bearing cells could be identified via the expression of a tdTomato cassette. Guide RNAs used are below (Forward/Reverse):

Human *SUCLG2*

sgRNA#62 (5'- TTGGGCCCCACGCTCACCTGGGACCGTTTAAGAGC)/(5'-
TTAGCTCTTAAACGGTCCCAGGTGAGCGTGGGGCCCAACAAG)
sgRNA#58 (5'- TTGGGCACTGCAAATGAAGCTCTCGGTTTAAGAGC)/(5'-
TTAGCTCTTAAACCGAGAGCTTCATTTGCAGTGCCCAACAAG)

Cell culture

MLL-AF9: Sorted cells were cultured in RPMI with L-glutamine (Corning, 10-040-CM), medium supplemented with 10%FBS, 20 ng/ml IL-3 (Peprotech, 213-13), 20 ng/ml IL-6 (Peprotech, 216-16), 100 ng/ml FLT3-ligand (Peprotech, 250-31L) and 100 ng/ml SCF (Peprotech, 250-03). Cell line was mycoplasma negative.

Human cell lines: All AML cell lines (U973, MV4-11, MOLM-14, NOMO-1, THP-1) were all mycoplasma negative and were cultures in RPMI with L-glutamine (Corning, 10-040-CM) supplemented with 10% FBS. THP-1 medium was also supplemented with 2-mercaptoethanol to a final concentration of 0.05mM (Gibco, 21985023).

Drug dosing

To dose cells, 10,000 cells/well were plated in 96-well plates and media containing doxorubicin (Sigma-Aldrich, D1515), cytarabine (Selleckchem, S1648), or both were added to achieve the indicated final concentrations. In combination dosing, cells were dosed to LD_{80-90} at doses that ensured roughly identical killing. Cell viability was assessed 72 hours post-treatment by DAPI (BioLegend, 422801) exclusion and flow cytometry. Drug dilutions were made in cell medium immediately before use.

RNAseq

Smart-seq2

Whole RNA was isolated and sequencing libraries were prepped from $0.5x10^6$ cells sorted from acutely treated animals using the Smart-seq2 protocol (Picelli et al., 2013). Mapped read counts for each transcript were normalized using the Bioconductor package DESeq2 in R (Love et al., 2014). Differential expression analysis was also performed using DESeq2. No additional variance stabilization transformation was performed on top of RLE. We mapped all 3pDGE data against the mm9 genome assembly and quantitated murine genes based on refseq annotation using the ESAT package (Derr et al., 2016) (http://garberlab.umassmed.edu/software/esat/ and http://genome.cshlp.org/content/early/2016/09/15/gr.207902.116), with parameters -task score3p -alignments $sample_list -wLen 50 -wExt 5000 -wOlap 0 -sigTest 0.01 -multimap ignore. For GSEA genes were ranked with the test statistic from DESeq2. To obtain the chemosensitization signature, we compared BM samples with and without Suclg2 knockdown 48h after combination chemotherapy and used genes whose expression was down regulated (FDR < 0.05) in the Suclg2 knockdown samples compared to those bearing a control hairpin. We then computed the negative average expression of these down regulated genes in human patient cohorts as the chemosensitization signature.

3'DGE

Whole RNA was isolated from 10^6 cells sorted from relapsed animals using the NucleoSpin RNA plus kit (Takara Bio Inc., 740984.50) and were submitted to the Swanson Biotechnology Center, Koch Institute, Massachusetts Institute of Technology for 3' tag digital gene expression profiling. 3' DGE FASTQ sequencing reads were collapsed to one representative read per unique molecular identifier using a custom python script. Gene expression was quantified using salmon (version 1.2.1, Patro et al., 2017) using a transcriptome prepared from the mouse mm10 primary genome assembly using the ensembl version 100 annotation. The resulting counts were

summarized to the gene level using R (version 4) running tximport (version 1.16.0, Soneson et al., 2015) and counts per million (cpm) were calculated using utilities implement in edgeR (version 3.30.0, Chen et al., 2014). The cpm values with a +1 offset were transformed to log2 space for visualization. Differential expression for treatments within cell lines and between untreated cell lines was done using DESeq2 (version 1.28.1, Love et al., 2014) and apeglm log fold change shrinkage. Data assembly and visualization was done using Tibco Spotfire Analyst (version 7.11.1). Pre-ranked Gene Set Enrichment Analysis (version 4.0.3, Subramanian et al., 2005) was run using DESeq2 Wald statistic as a ranking metric and gene set collections from msigDB (version 7.0, Liberazon et al., 2015).

Metabolite measurements

Gas-chromatography coupled to mass spectrometry (GC/MS) analysis was done as described previously (Lewis et al., 2014). Dried metabolite samples were derivatized with 20 µL of methoxamine (MOX) reagent (ThermoFisher, TS-45950) and 25 µL of N-tert-butyldimethylsilyl-N-methyltrifluoroacetamide with 1% tert-butyldimethylchlorosilane (Sigma, 375934). Following derivatization, samples were analyzed using a DB-35MS column (30m × 0.25mm i.d. × 0.25 µm, Agilent J&W Scientific) in an Agilent 7890 gas chromatograph (GC) coupled to an Agilent 5975C mass spectrometer (MS). Data were corrected for natural isotope abundance using in-house algorithms as in (Lewis et al., 2014).

Western Blotting

Cells were lysed with RIPA buffer (Boston BioProducts, BP-115) supplemented with 1X protease inhibitor mix (cOmplete EDTA-free, 11873580001, Roche). Protein concentration of cell lysates was determined using Pierce BCA Protein Assay (ThermoFisher Scientific, 23225). Total protein (40-60µg) was separated on 4-12% Bis-Tris gradient SDS-PAGE gels (Life Technologies) and then transferred to PVDF membranes (IPVH00010, EMD Millipore) for blotting.

Antibodies

Western blotting: anti-Vinculin (Sigma, V4505), anti-SUCLG2 (ThermoFisher, PA5-21810), anti-SUCLG1 (ThermoFisher, PA5-22006), anti-SUCLA2 (Abcam, ab202582), Cas9 (ActiveMotif, 61577).

Flow cytometry: anti-murine CD36 APC(Biolegend, 102611), Armenian hamster IgG isotype control APC (Biolegend, 400911).

Quantitative PCR (qPCR)

RNA was isolated using RNeasy Kit (Qiagen). Synthesis of cDNA was performed using M-MLV Reverse Transcriptase (28025, Life Technologies) with oligo$(dT)_{20}$ primer. qPCR was done in Applied Biosystems StepOnePlus machine with TaqMan Fast Universal PCR Master Mix (4352042, Life Technologies). Data were analyzed with the comparative $2^{(-\Delta\Delta CT)}$ method, and were normalized to the levels of *Actin*. Primer sequences (Forward/Reverse):

Suclg2 (5'-CCCCGAAGATGGCTGAACC)/(5'-ACCTCCTTTCAAACCGCTATTG)

ActB (5'-GGCTGTATTCCCCTCCATCG)/(5'-CCAGTTGGTAACAATGCCATGT)

Mitochondrial stress test

Mitochondrial stress tests were performed as described in Ron-Harel et al., 2016. Briefly, oxygen consumption rates (OCR) were measured from cells in non-buffered RPMI containing 5mM glucose, 2mM L-glutamine, and 1mM sodium pyruvate, under basal conditions and in response to mitochondrial respiratory chain inhibitors: oligomycin (6μM), FCCP (6μM), rotenone (0.5μM), and antimycin A (0.5μM) (all from Sigma) on the XF-96 Extracellular Flux Analyzer (Agilent Technologies).

MitoTracker DeepRed stains

Cells were harvested from moribund animals, red blood cells lysed (Sigma), and resulting cells counted three times. The count was adjusted for the exact percentage of MLL-AF9 cells present in the sample. In all cases, BM and spleen leukemic burden exceeded 90% as assayed by flow cytometry. For each mouse, $2x10^6$ cells were isolated in triplicate and stained in Dulbecco's phosphate buffered saline (Corning, 21-031-CV) with MitoTracker Deep Red (ThermoFisher, M22426) at a final concentration of 100 nM (for *in vivo* samples) or at 25 nM, 50 nM, 100 nM, or 250 nM (for *in vitro* experiments) for 30 minutes at 37°C, as indicated by the manufacturer. Cells were then washed twice and analyzed via flow cytometry. The average of the three replicates was then graphed as a single dot per mouse.

Statistical analysis

Statistical analyses were performed using GraphPad Prism 7 (GraphPad Software Inc). The specific statistical tests performed are specified in figure legends. Differences are considered significant for P-values ≤ 0.05, or as indicated when adjustments for multiple hypothesis testing was required.

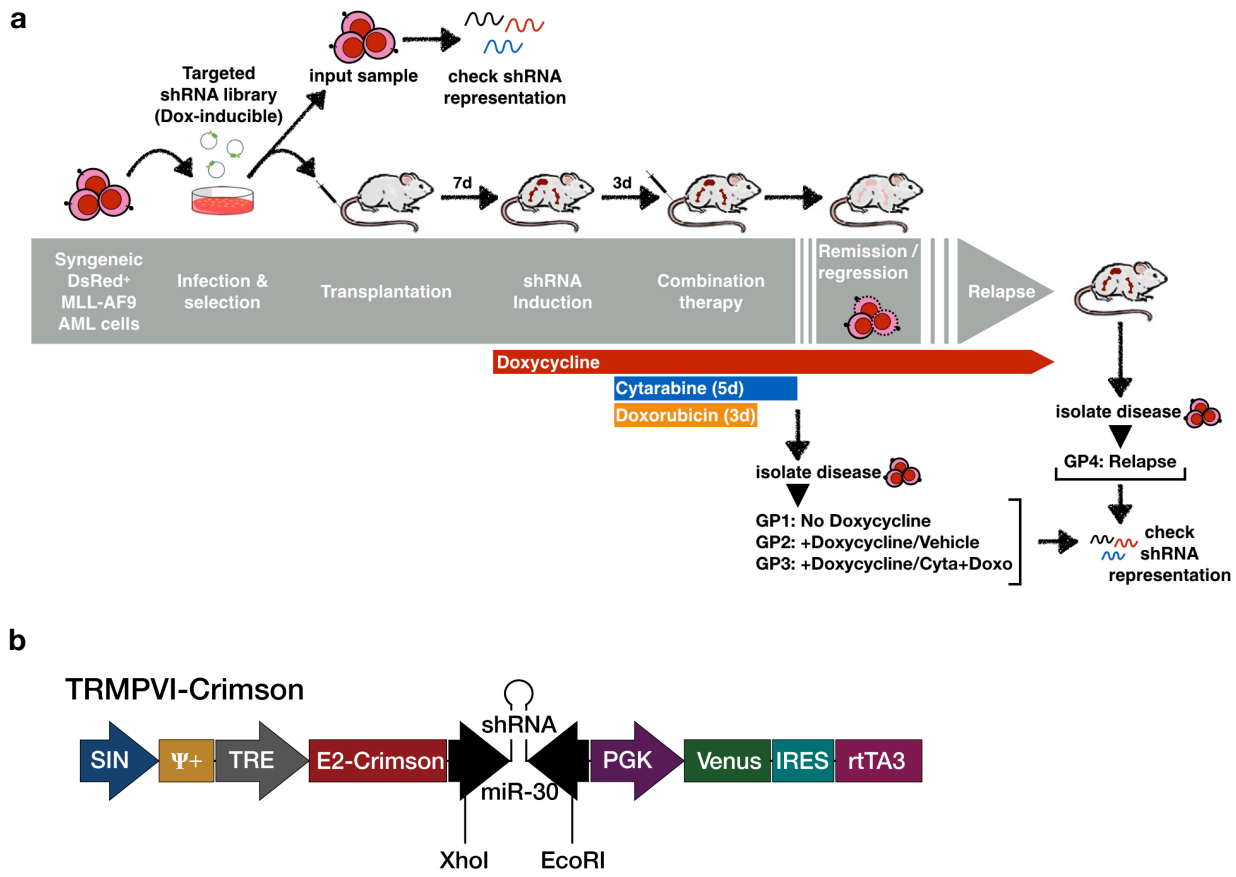

Figure 2.1. Layout of the targeted *in vivo* RNAi screen for chemosensitizing genes. (a) Schematic representation of the layout of a focused *in vivo* RNAi screen in the established Actin-DsRed+ mouse model of MLL-AF9 AML (Miller et al., 2013; Puram et al., 2016). Two libraries targeting either cell energetic genes ('Auto' or 'Cell energy' library) or genes known to be important for stemness and chemoresistance ('Chemo' or 'Chemoresistance' library) were cloned into the doxycycline-inducible vector TRMPVI-Crimson (b) and screened separately. Briefly, murine AML cells infected with RNAi libraries were injected into 20 recipient mice which were then randomized into four groups (n=5 each, GP1-4) that were treated as indicated after a 7 day engraftment period. On day 15, mice from groups GP1-3 were sacrificed and AML cells collected. Upon relapse, GP4 mice were sacrificed and their cells collected. Genomic DNA was isolated and processed for sequencing.

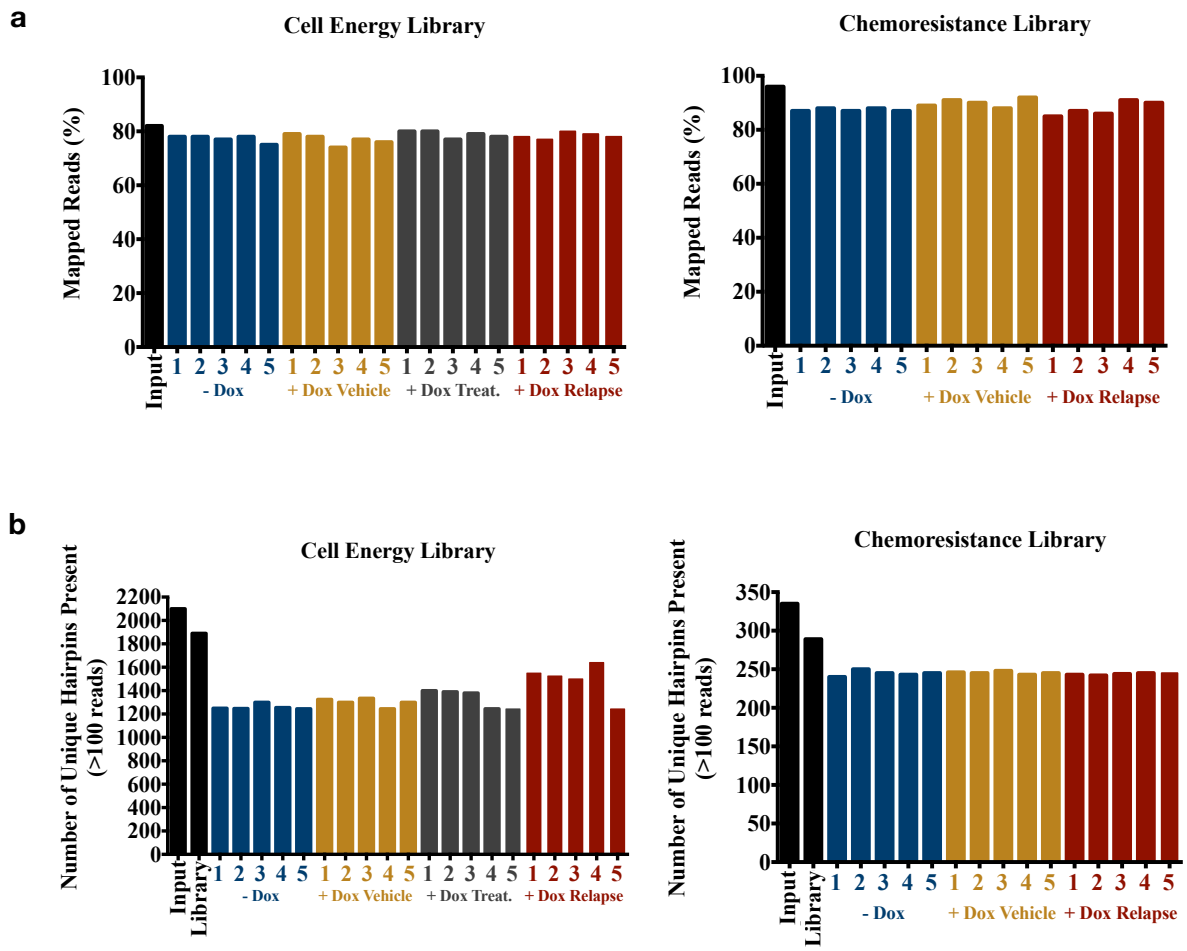

Figure 2.2. High quality RNAi libraries can successfully maintain representation *in vivo*. (a) We are successfully able to recover the vast majority of shRNA hairpin species upon sequencing of amplicons from *in vivo* treated cells. (b) At a 500x representation, upwards of 70% (cell energy library) and 80% (chemoresistance library) of our high quality libraries can be represented and maintained *in vivo*, both before and after doxycycline/therapy treatment.

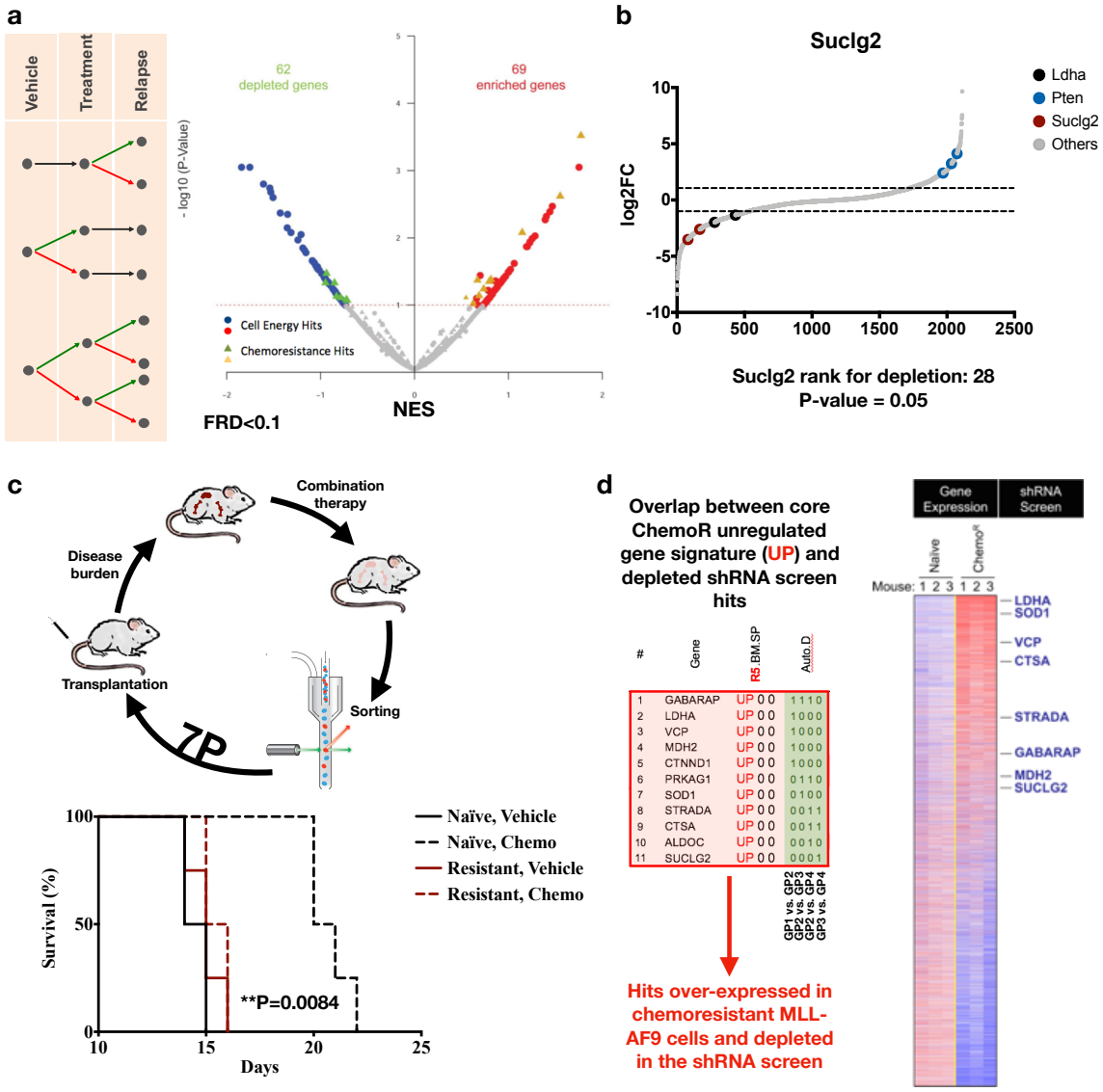

Figure 2.3. Suclg2 depletion sensitizes AML cells to combination chemotherapy and is overexpressed in a chemoresistant mouse model of AML . (a) Volcano plot showing the top enriched and depleted genes from pairwise edgeR and RIGER analyses of vehicle versus all treatment and relapsed conditions. The comparisons in hairpin representation between groups GP2 (+doxycycline & vehicle) and GP3 (+doxycycline & combination chemo), groups GP2 and GP4 (+doxycycline & combination chemo, collected at relapsed), and groups GP3 and GP4 are shown in the volcano plot and are represented by the schematic to the left of the plot. (b) Hockey plot showing the global distribution of hairpins and the location of enrichment controls (Pten), depletion controls (Ldha), and Suclg2. Suclg2 was ranked as gene 28 in relapsed samples with an adjusted p-value of 0.05. (c) Top: schematic of the serial transplantation and treatment approach used to generate Chemo^R cells. Bottom: Survival analysis of mice transplanted with Chemo^S (treatment Naïve) and Chemo^R (Resistant) cells. Treatment with combination chemo significantly extends life in naïve Chemo^S cells but not in Chemo^R cells after 7 cycles of serial treatment *in vivo*. A log rank test comparing chemo-treated naïve vs. resistant cells was used to determine significance (d) Left: A partial list of the hits prioritized by overlapping the top overexpressed genes in Chemo^R cells and the top depleting genes in the screen. Suclg2 scores as a gene that is important in relapse and not in acute response. Right: Whole genome expression profile of treatment naïve versus Chemo^R MLL-AF9 AML cells from three mice per group with some of the high confidence genes of interest shown.

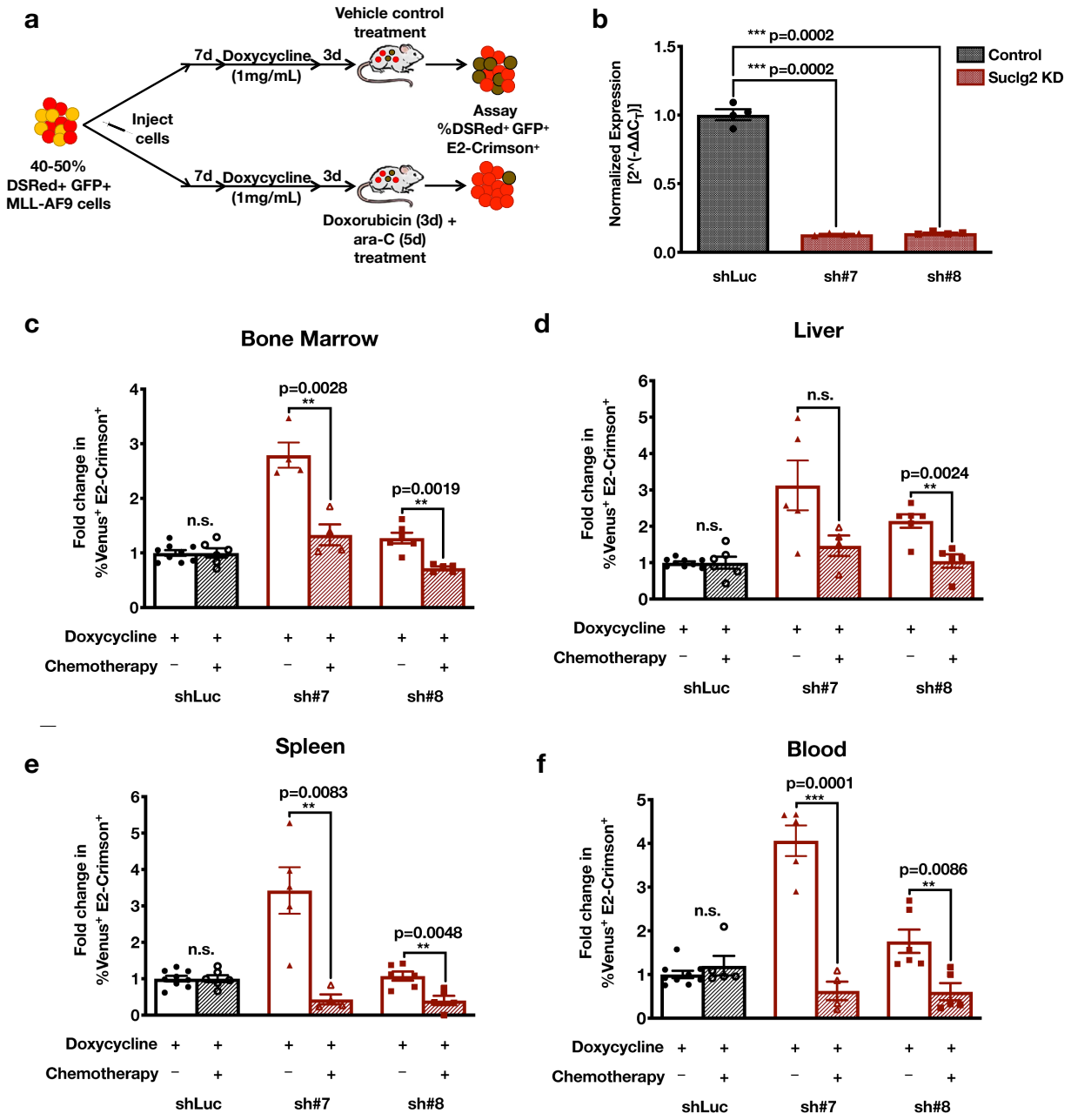

Figure 2.4. Suclg2 validates as an AML chemosensitizer. (a) General layout of an *in vivo* competition assay used to validate hits. Briefly, cells are infected with shRNAs against either Suclg2 or Renilla Luciferase (shLuc, a neutral control hairpin; Fellmann et al., 2013) in TRMPVI-Crimson to 15-30% (MOI<1) and then sorted to produce a population that is roughly equal parts GFP- (non-hairpin bearing) and GFP+ (hairpin-bearing). Mixed cell populations are then injected into animals and allowed to engraft. After 7 days, shRNA expression is induced with doxycycline and 3 days later, mice are dosed with combination chemo or saline over 5 days. Upon relapse, the proportion of hairpin bearing cells was assayed in various organ sites and the knockdown efficiency quantified via qPCR (b). Using this approach, Suclg2 depletion sensitized cells to therapy in the BM (c), liver (d), spleen (e), and blood (f). Data are means ± SEM and significance is determined via a two-tailed unpaired student's t-test and n=4-9 animals in all groups.

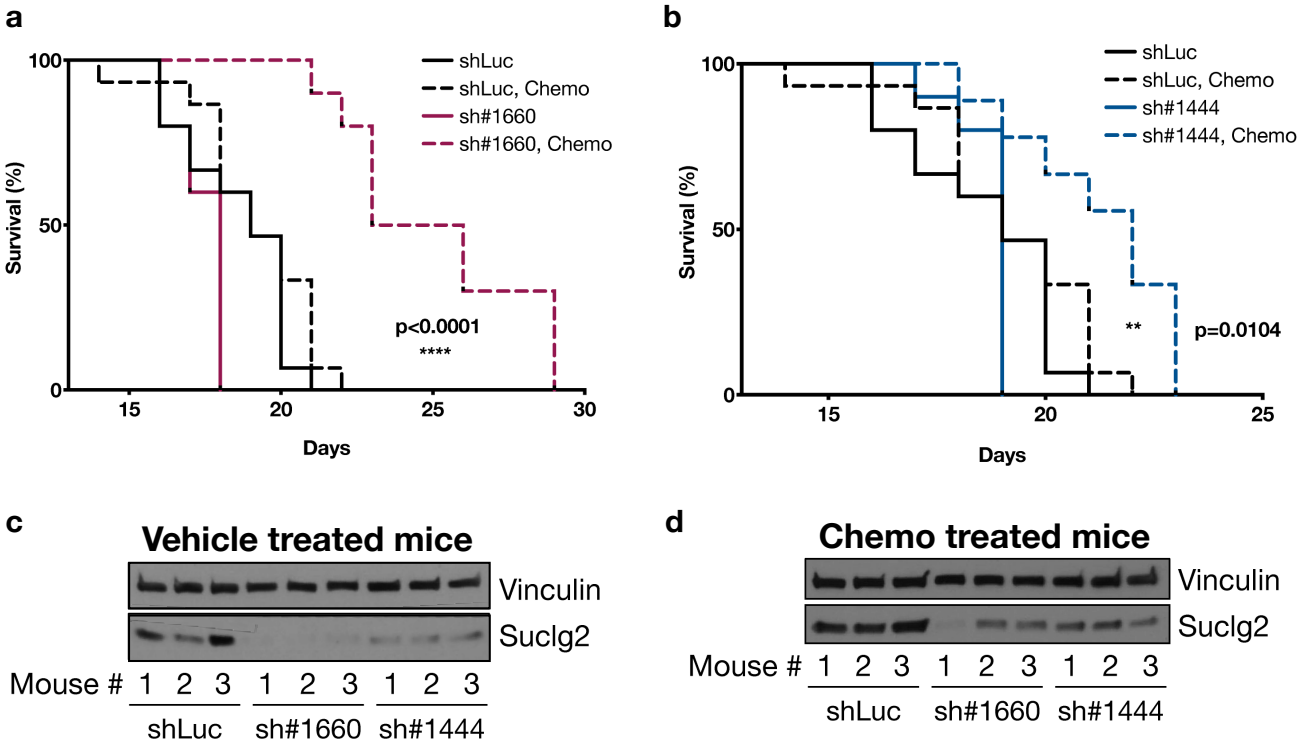

Figure 2.5. Suclg2 depletion significantly extends life in animals treated with combination chemotherapy. (a-b) Using a constitutively expressing miR30 vector, two new hairpins were used to infect murine MLL-AF9 cells (MOI<1). Pure populations of cells were sorted and injected into recipient mice that were dosed with combination chemotherapy or saline control as before. Here, Suclg2 depletion extends life in a dose dependent manner, as assayed via (c) western blot (WB) analysis of cells collected from relapsed animals treated with a vehicle control. (d) In chemo-treated animals, therapy appears to have selected for cells that were less able to suppress Suclg2 expression. Log rank tests to compare chemo-treated shLuc and chemo-treated sh#1660 or chemo-treated sh#1444 were completed and the P-values are shown. For each shLuc group: n=15, each sh#1660 group: n=10, each sh#1444 group: n=10 (control) or 9 (chemo).

a

b

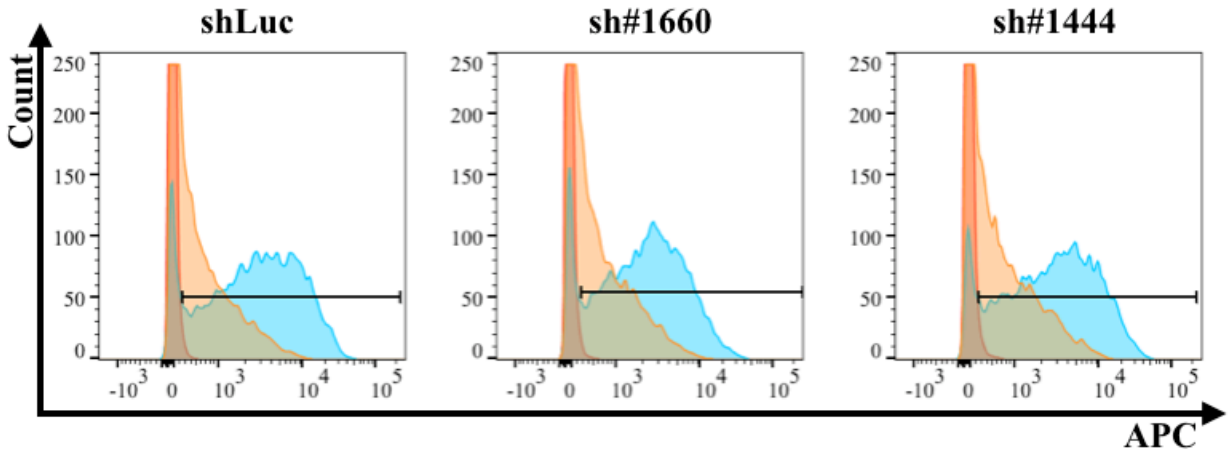

Luciferase population	Chart color	%Crimson positive
Uninfected		0.70
Empty vector		87.1
cDNA expressing		52.2

sh#1660 population	Chart color	%Crimson positive
Uninfected		0.56
Empty vector		87.1
cDNA expressing		60.6

sh#1444 population	Chart color	%Crimson positive
Uninfected		0.50
Empty vector		89.2
cDNA expressing		57.1

Figure 2.6. Using mammalian expression vectors to set up a cDNA rescue. (a) A mammalian expression vector was used to set up a cDNA rescue experiment. (b) cDNA expressing cells were isolated using E2-Crimson signal expressed from the same vector. In the actual experiment, hairpin-bearing cells were infected to 30-40% E2-Crimson+ and the top 50-60% brightest E2-Crimson+ cells were sorted and used in the actual cDNA rescue experiment.

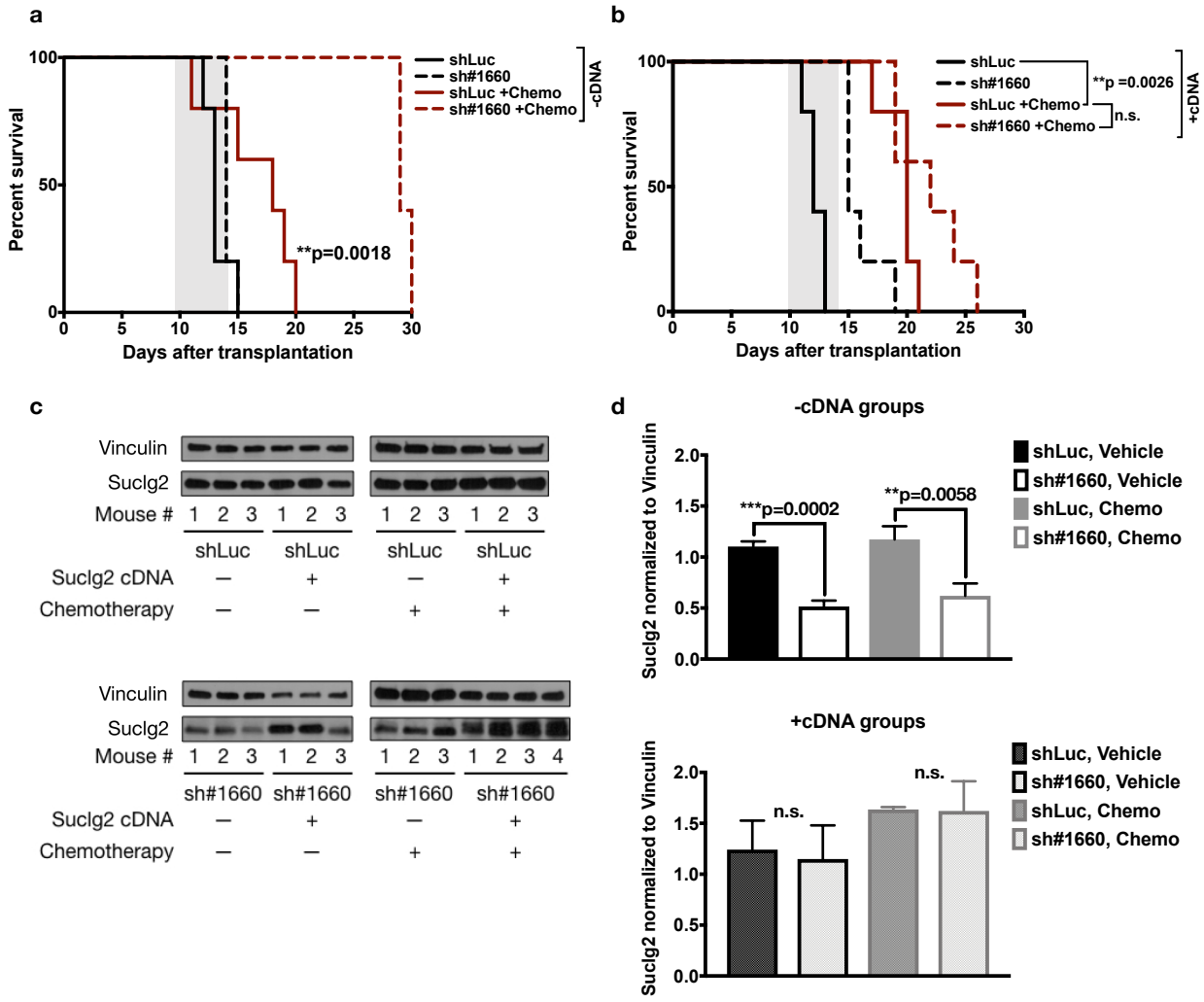

Figure 2.7. The chemosensitization phenotype imparted by Suclg2 depletion is not an off target-effect, as shown by a cDNA rescue (a) Hairpin (sh#1660) bearing cells were infected with an empty vector control or (b) a vector containing an shRNA non-targetable *Suclg2* cDNA and dosed as indicated (n=5 in each group). Empty vector infected cells with Suclg2 KD were still sensitive to therapy, but this phenotype was abrogated when Suclg2 levels were restored with the expression of a non-targetable *Suclg2* cDNA, as determined with a log-rank test. Representative WBs are shown in (c). WBs from all animals assayed (n=4-5 per group) are quantified in (d) where data are means ± SEM and student's unpaired two-tailed t-test.

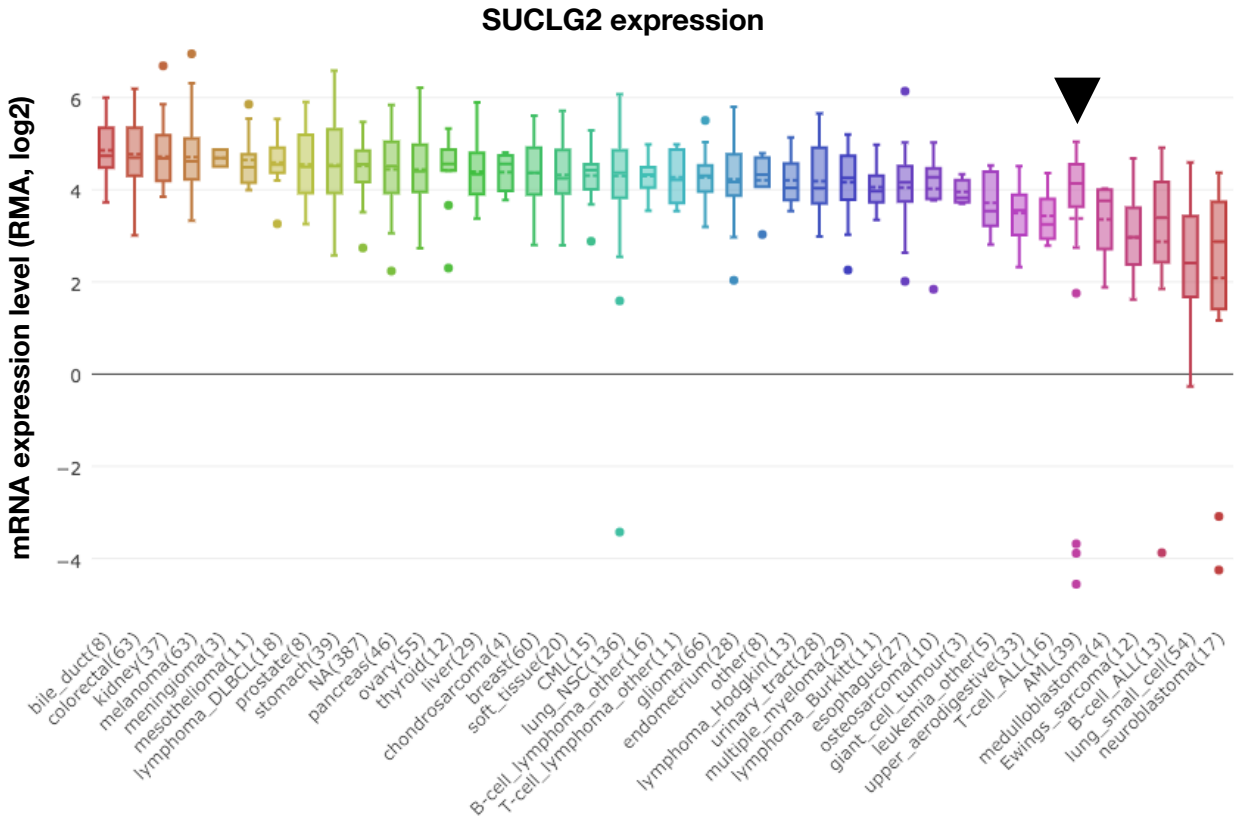

Figure 2.8. SUCLG2 is highly expressed in human AML cell lines. (a) Data from the MIT and Harvard Broad Institute's Cancer Cell Line Encyclopedia (CCLE) showing that SUCLG2 is highly expressed in AML (black arrow).

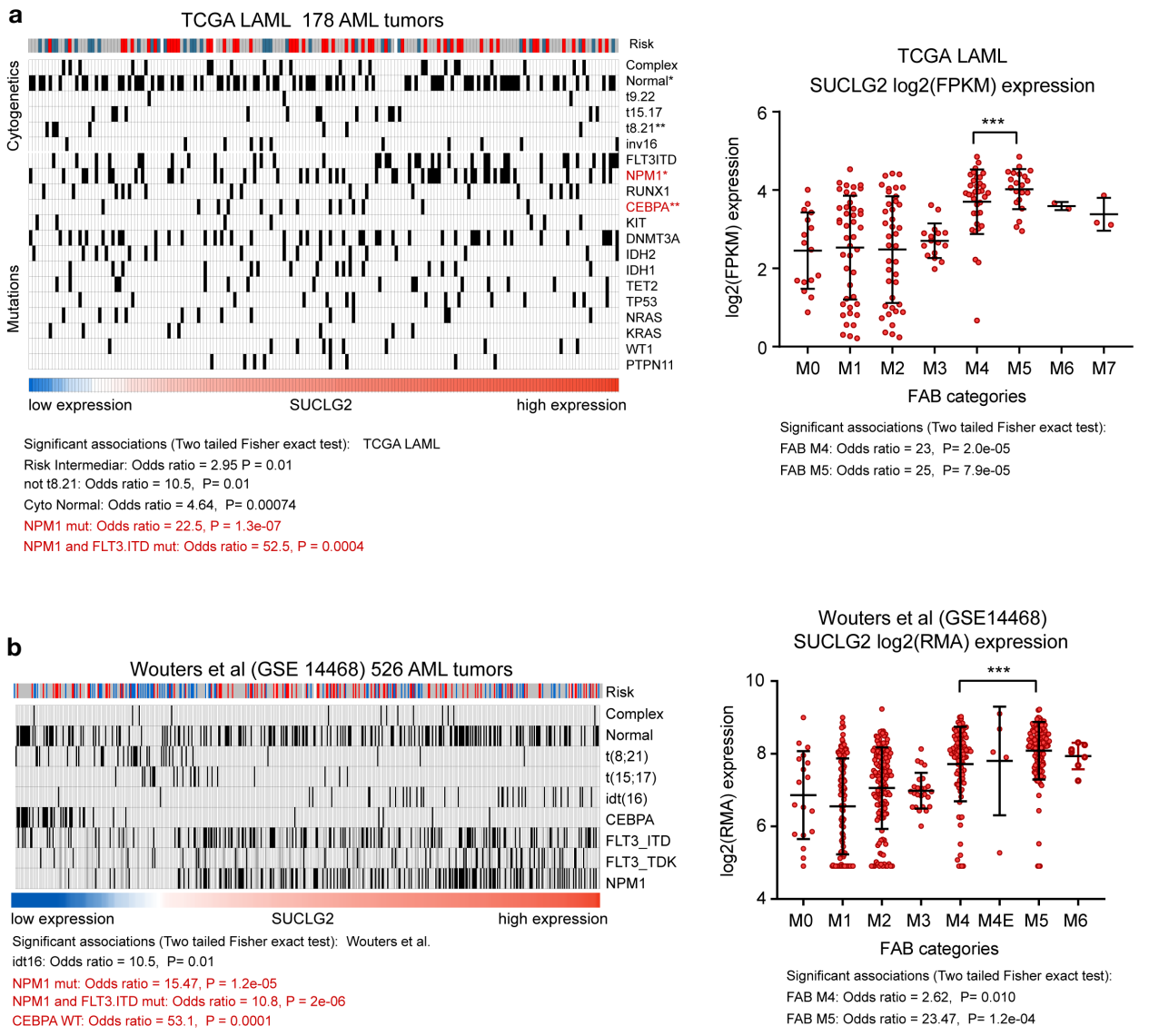

Figure 2.9. SUCLG2 expression is associated with FAB M4, FAB M5, FLT3-ITD and NPM1 mutated, NPM1 mutated, and CEBPA wild type human AML, as assessed in two independent patient cohorts. SUCLG2 expression was correlated with AML genetic and French-American-British subtypes in (a) 178 AML tumors profiled by TCGA and (b) 526 AML tumors profiled by Wouters et al. 2009. Suclg2 expression is associated with FAB M4 and M5 subtypes, and with FLT3-ITD and NPM1 mutated, CEBPA WT, and NPM1 mutated subtypes. Determined using two-tailed Fisher's exact test.

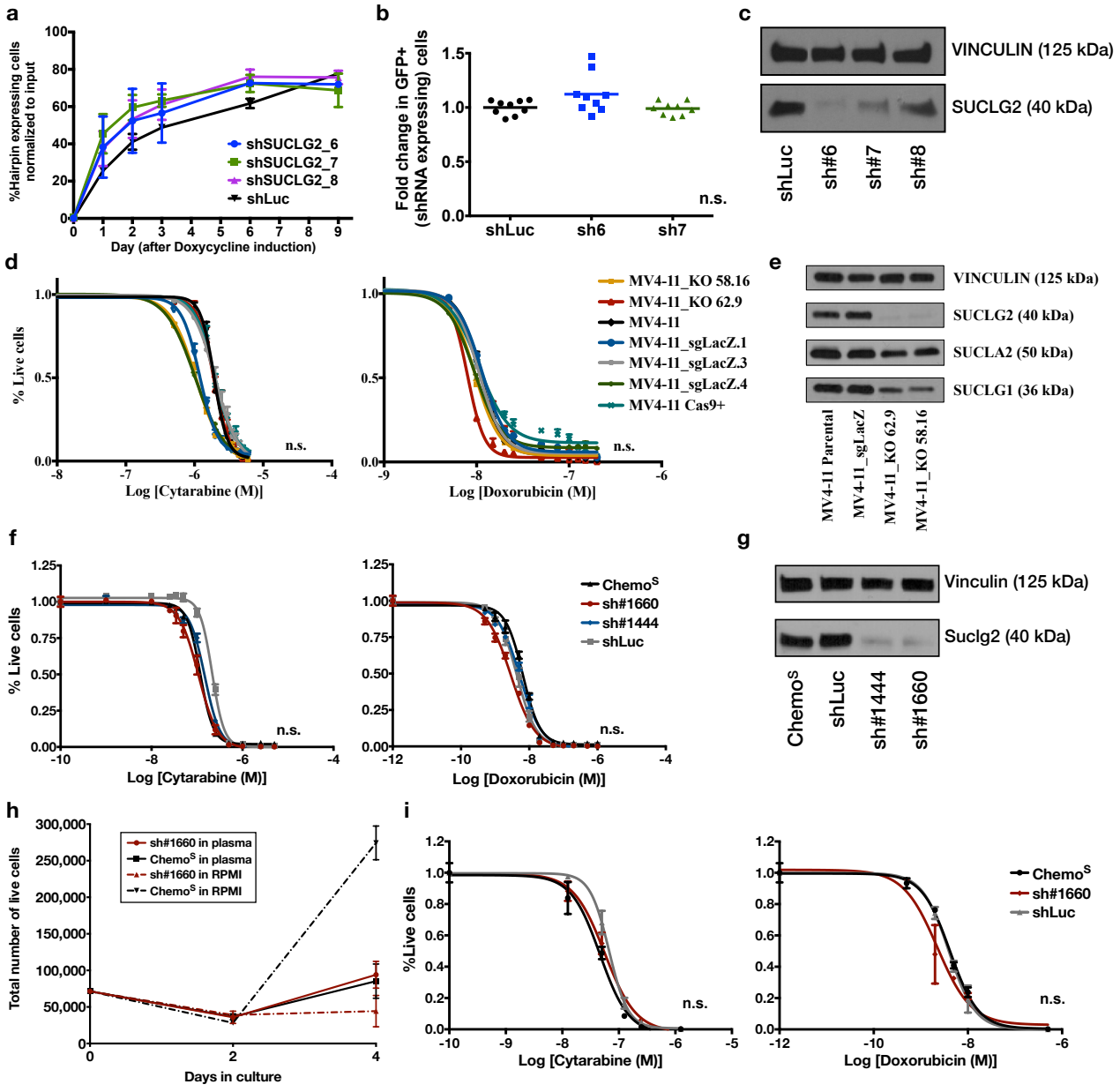

Figure 2.10. Suclg2 is an *in vivo* specific chemosensitizer and this phenotype cannot be recapitulated in physiologic medium. (a) Representative data from MV4-11 cells infected with doxycycline-inducible SUCLG2-targeting hairpins and monitored for growth abnormalities, although none could be detected. (b) Human cell lines were partially transduced (MOI<1) and sorted to a 50:50 mix of hairpin to non-hairpin expressing cells. Mixtures were then dosed with both Ara-C and doxorubicin at an LD80-90 in order to complete *in vitro* competition assays in the context of chemotherapy. All doses assayed, including those where killing was roughly equal from both drugs or mainly contributed by one drug showed no specific depletion of SUCLG2 KD cells from the mixture. Representative data from three independent experiments in MOLM-14 cells are shown. Identical experiments with U937, MV4-11, NOMO-1, and THP-1 human cell lines yielded the same result. Significance is determined by one-way ANOVA with Turkey's post-hoc test adjusted for multiple comparisons. (c) WB analysis shows that SUCLG2 levels are successfully knocked down using hairpins sh#6-8 in MV4-11 cells. Repeated experiments in this and all other cell lines showed the same result. (d) *SUCLG2* KO cells were generated in various hAML cell lines using CRISPR-Cas9 and dosed *in vitro* with doxorubicin or cytarabine as shown. The proportion of live cells was measured 72 hours

later by quantifying DAPI⁻ cells on flow cytometric analysis. Data from MV4-11 cells is shown. Repeated experiments in this and other cell lines showed the same result. Knocking out *SUCLG2* also resulted in decreases in the two other pathway members of the SCS complex, as shown in (e), a result that is likely not due to off target effects as no sequence homology among these SCS complex members exists. (f) Murine Suclg2 KD cells were dosed *in vitro* and showed no significant differences in their response to either doxorubicin or cytarabine. (g) Suclg2 KD was confirmed via WB analysis. (h) Murine Suclg2 KD cells were grown in triplicate in physiologic mouse plasma medium and counted over 4 days, showing that at least sh#1660 cells grow equally well in this medium over the time required for a dosing assay, while Chemo^{S} cells appear to grow more slowly. (i) Suclg2 KD cells were dosed in physiologic medium in triplicate with either doxorubicin or cytarabine. No significant differences in drug response were seen. In all cases except the physiologic media experiments, cells were also dosed with combinations of cytarabine and doxorubicin and in those cases, no significant difference in treatment response could detected at any of the doses used, in either KD or KO cells (representative data shown in b). Significance is determined using one-way ANOVA with Bonferroni post-tests in all cases.

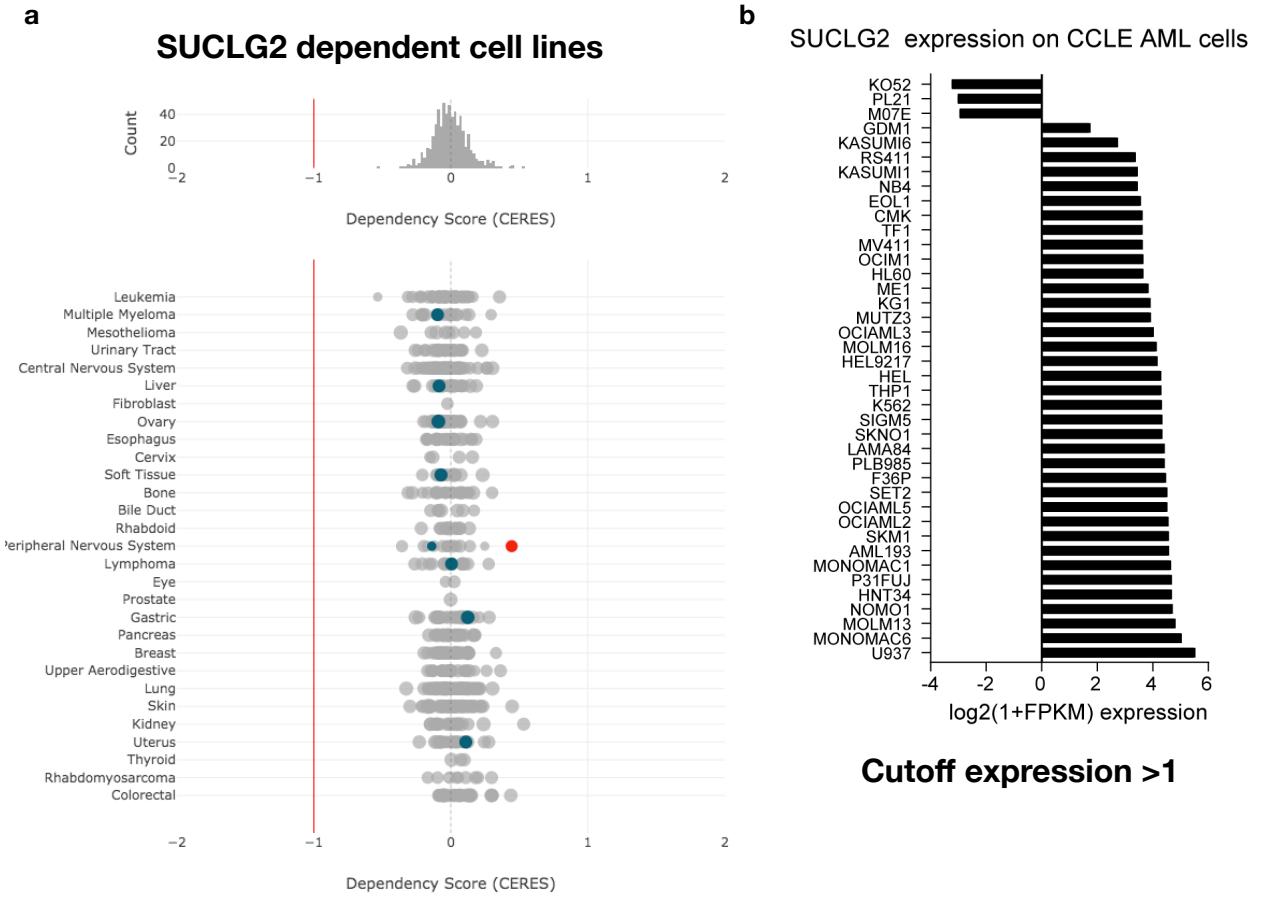

Figure 2.11. SUCLG2 does not score as an AML dependency in large scale *in vitro* screens, despite being highly expressed in most human AML cell lines. (a) SUCLG2 does not score in any of the genome-scale *in vitro* RNAi and CRISPR-Cas9 screens completed through the Broad's Dependency Map (DepMap) project. (b) Here, AML cell lines screened show significant expression of SUCLG2, as assayed by RNAseq and as reported by the CCLE.

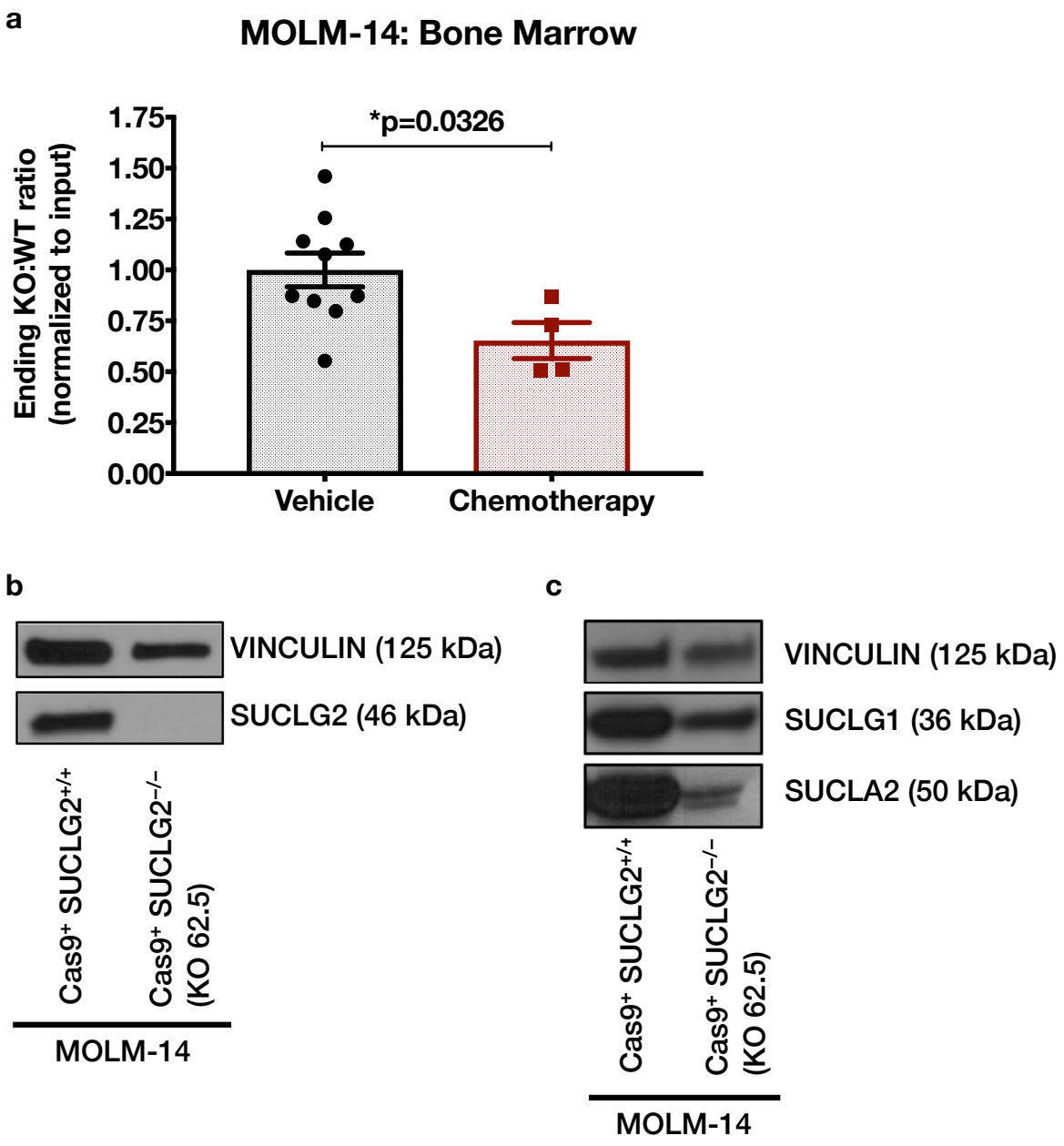

Figure 2.12. SUCLG2 loss sensitizes MLL-AF9 and FLT3-ITD mutated human AML cells to combination chemotherapy *in vivo*. (a) Loss of *SUCLG2* significantly sensitizes MOLM14 cells to therapy *in vivo*, in NSG xenograft experiments. Here, GFP+ tdTomato− Cas9+ SUCLG2+ MOLM14 cells (parental WT) are mixed with GFP+ tdTomato+ Cas9+ SUCLG2− cells (KO) in approximately a 1:1 ratio and injected into NSG mice. Upon 2-5% peripheral blood burden, mice are dosed with an NSG compatible version of combination chemotherapy. Upon relapse, moribund mice are sacrificed and the ratio of live KO:WT cells is assessed in the marrow via flow cytometry. Data shown are means ± SEM (individual mice shown with their own symbol) from two experiments and statistical significance is determined by an unpaired two-tailed student's t-test. (b) WB analysis showed a complete loss of SUCLG2 in 62.5 KO cells. (c) SUCLG2 KO cells also show a reduction in the protein levels of SUCLG1 and SUCLA2, the α and alternate β subunits of the SCS heterodimer.

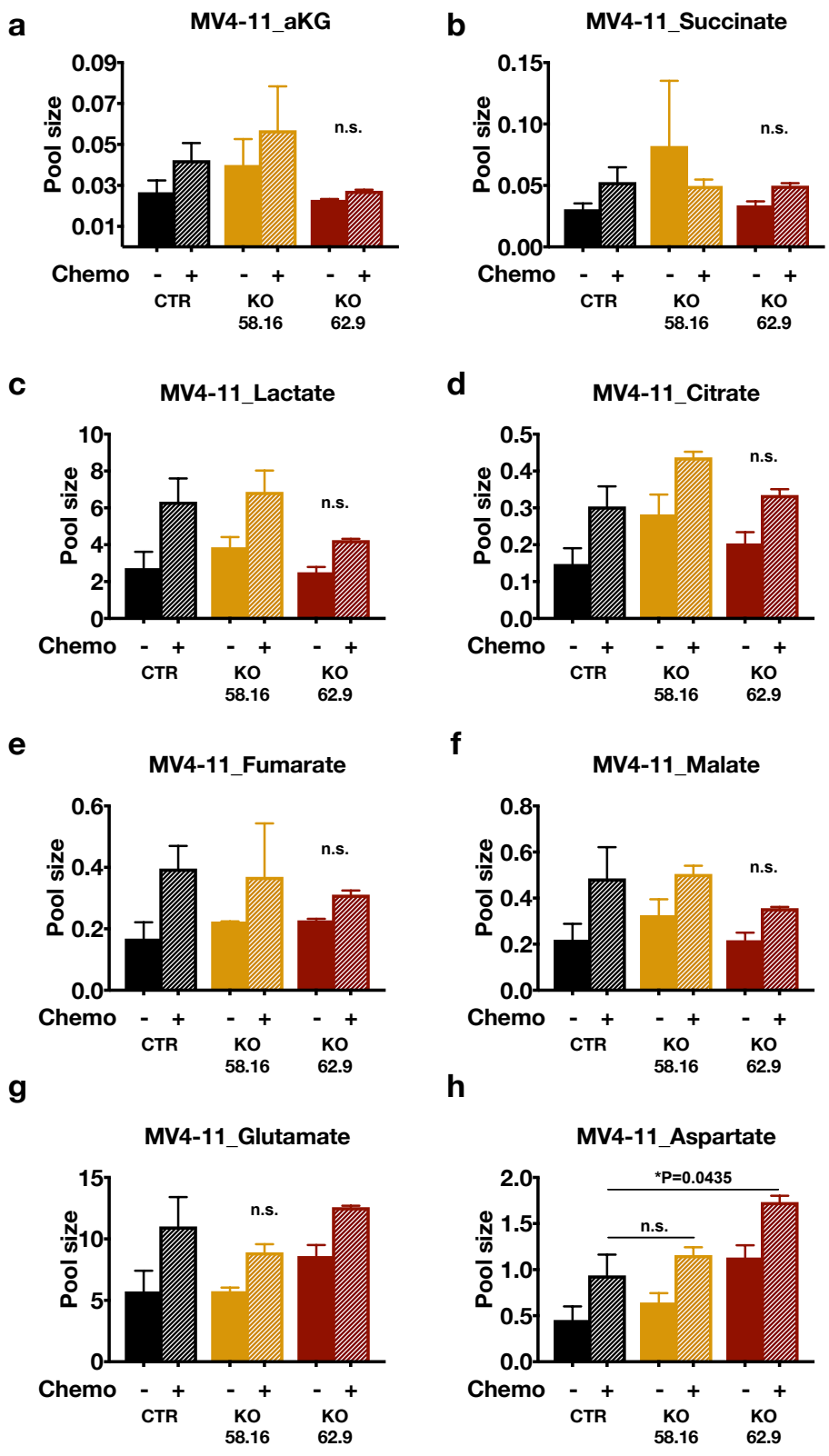

Figure 2.13. SUCLG2 loss does not consistently alter intracellular metabolite pools in human MLL-r and FLT3-ITD mutated human AML cells treated with combination chemotherapy *in vitro*. (a-g) Gas chromatography-mass spectrometry (GC/MS) was used to measure intracellular TCA cycle metabolite and amino acid pools in SUCLG2 KO cells. Cells were either dosed with combination chemotherapy (doxorubicin and Ara-C) at an LD80-90 (with roughly equal contribution from both drugs) or cultured with a vehicle control. No significant differences in pool sizes could be appreciated. Representative data from TCA cycle intermediates and two amino acids are shown (h) Aspartate was significantly increased in KO 62.9 cells in response to chemo. However, this feature was not consistently seen in KO 58.16 cells. Data shown are means ± SEM from three experiments, with each condition completed in triplicate each time. Similar experiments where cells were dosed with individual drugs also showed no significant differences in intracellular metabolite pools between KO and parental cells. Significance is determined by two-way ANOVA with Turkey's post-hoc test adjusted for multiple comparisons.

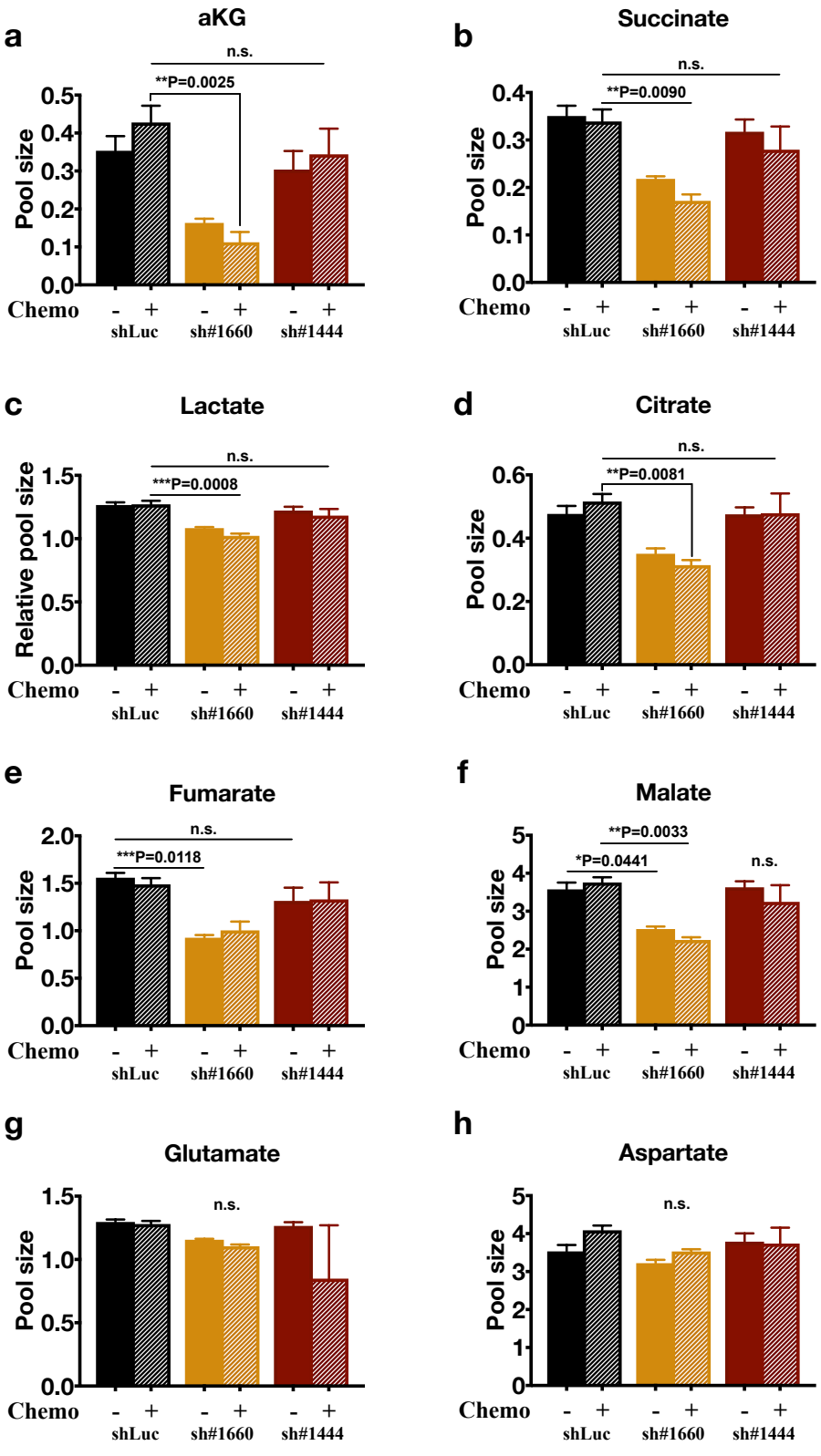

Figure 2.14. Suclg2 depletion does not consistently alter intracellular metabolite pools in murine MLL-AF9 AML cells treated with combination chemotherapy *in vitro*. GC/MS was used to measure TCA cycle metabolite and amino acid pools in murine Suclg2 KD cells. Cells were either dosed with combination chemotherapy as before or cultured with a vehicle control. (a-d) Drug induced difference in α-ketoglutarate, succinate, lactate and citrate could be appreciated. However, these results were not consistent between both hairpins. (e-f) Similarly, statistically significant differences in fumarate and malate pools between untreated control and KD cells were seen. However, this was not consistent between hairpins. (g-h) No significant differences in amino acid intracellular pools could be found between KD and control cells Data shown are means ± SEM from three experiments, with each condition completed in triplicate each time. Similar experiments where cells were dosed with individual drugs also showed no significant differences in intracellular metabolite pools between KD and control cells. Significance is determined by two-way ANOVA with Turkey's post-hoc test adjusted for multiple comparisons.

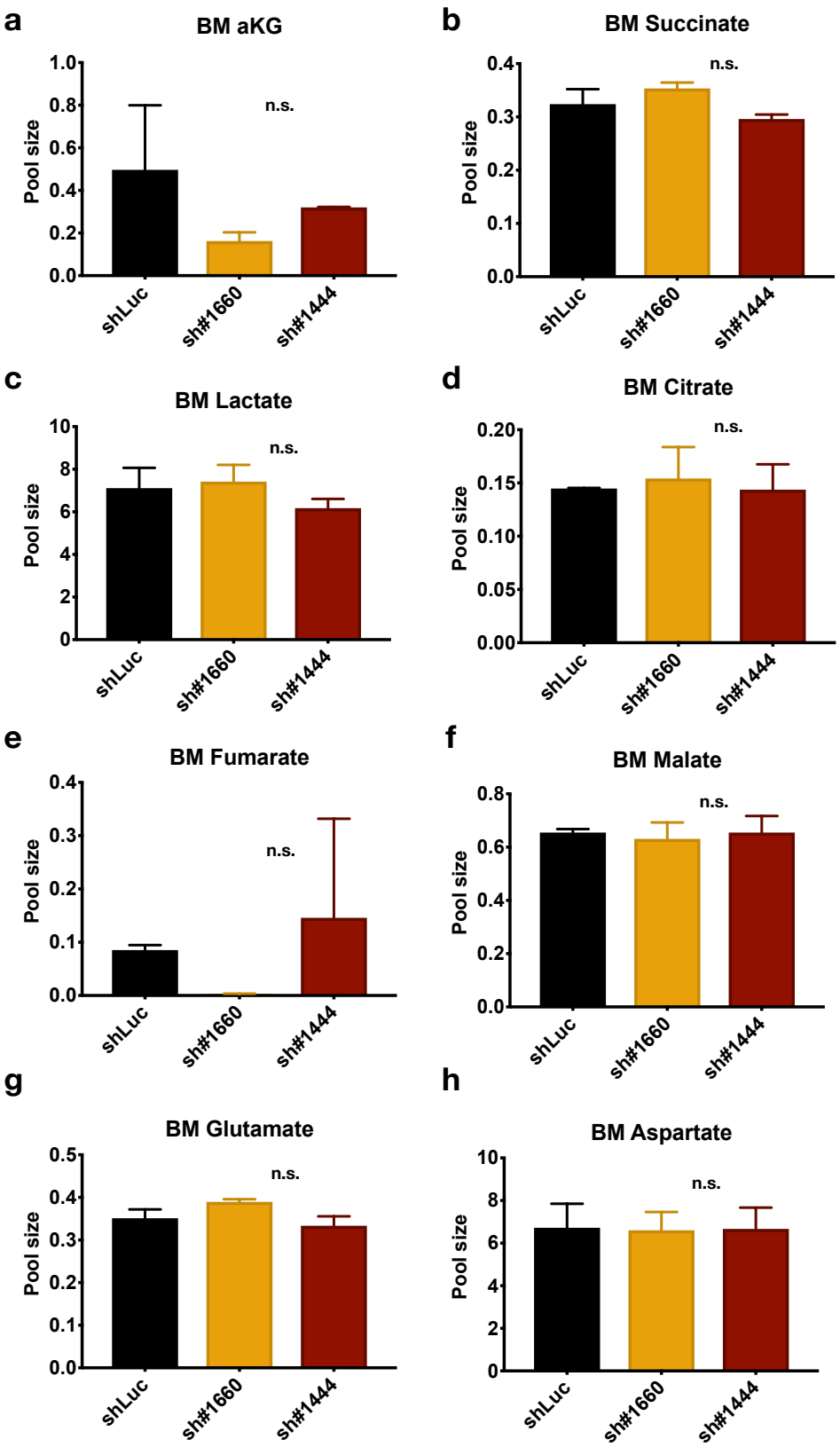

Figure 2.15. Suclg2 depletion does not consistently alter intracellular metabolite pools in murine MLL-AF9 AML cells collected from the leukemia-laden bone marrow of moribund animals. (a-h) GC/MS was used to measure intracellular metabolite pools in cells isolated directly from the marrows of moribund animals. Samples were normalized by weight and in every case, the organ examined was composed of more than 85% AML cells (as assayed by flow cytometry). No significant differences in any metabolite measured could be observed. Data shown are means ± SEM and n=6 for each hairpin group. Significance is determined by one-way ANOVA with Turkey's post-hoc test adjusted for multiple comparisons.

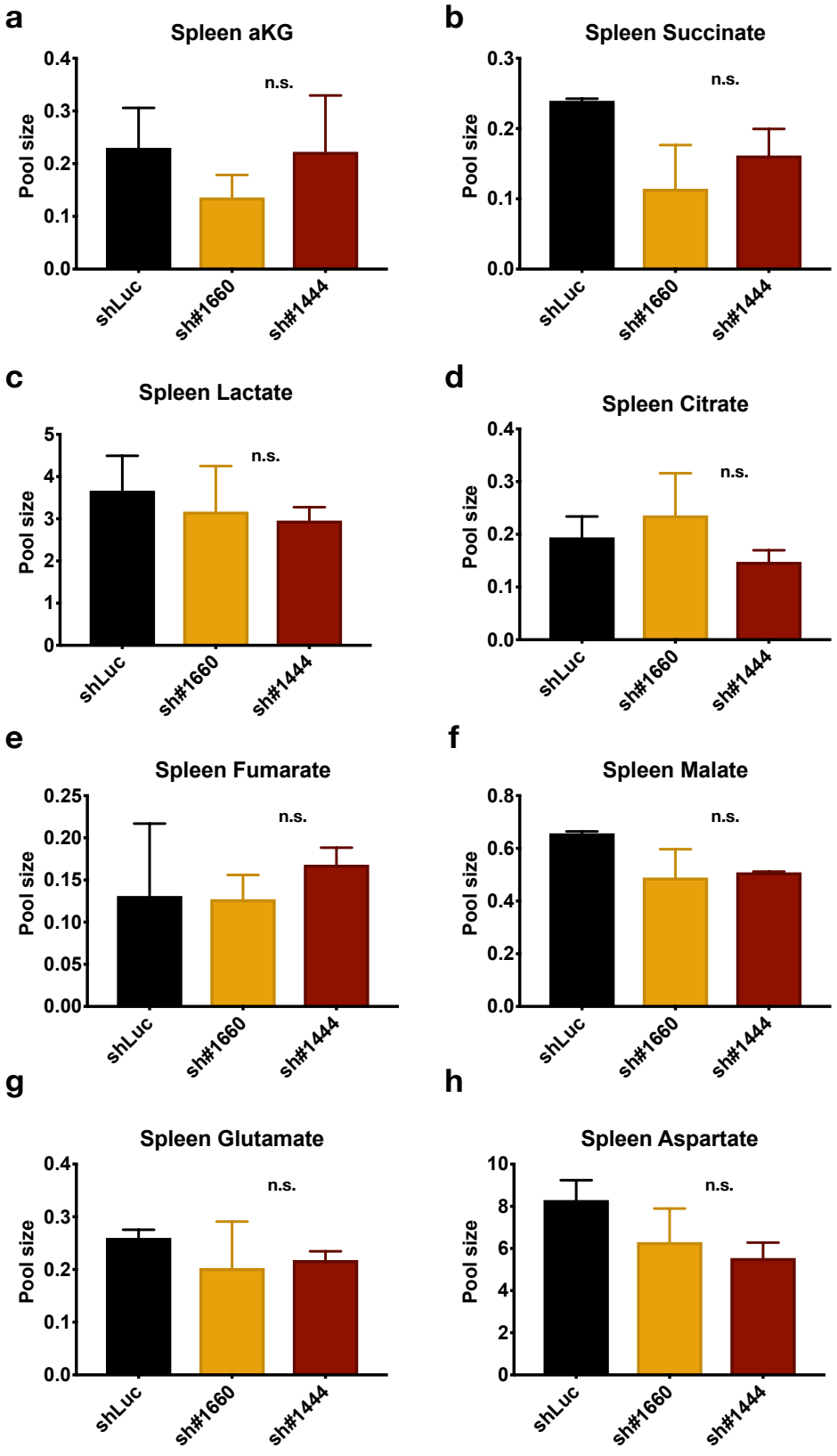

Figure 2.16. Suclg2 depletion does not consistently alter intracellular metabolite pools in murine MLL-AF9 AML cells collected from the leukemia-laden spleens of moribund animals. (a-h) GC/MS was used to measure intracellular metabolite pools in cells isolated directly from the spleens of moribund animals. Samples were normalized by weight and in every case, the organ examined was composed of more than 75% AML cells (as assayed by flow cytometry). No significant differences in any metabolite measured could be observed. Data shown are means ± SEM with each hairpin group having n=6 mice each. Significance is determined by one-way ANOVA with Turkey's post-hoc test adjusted for multiple comparisons

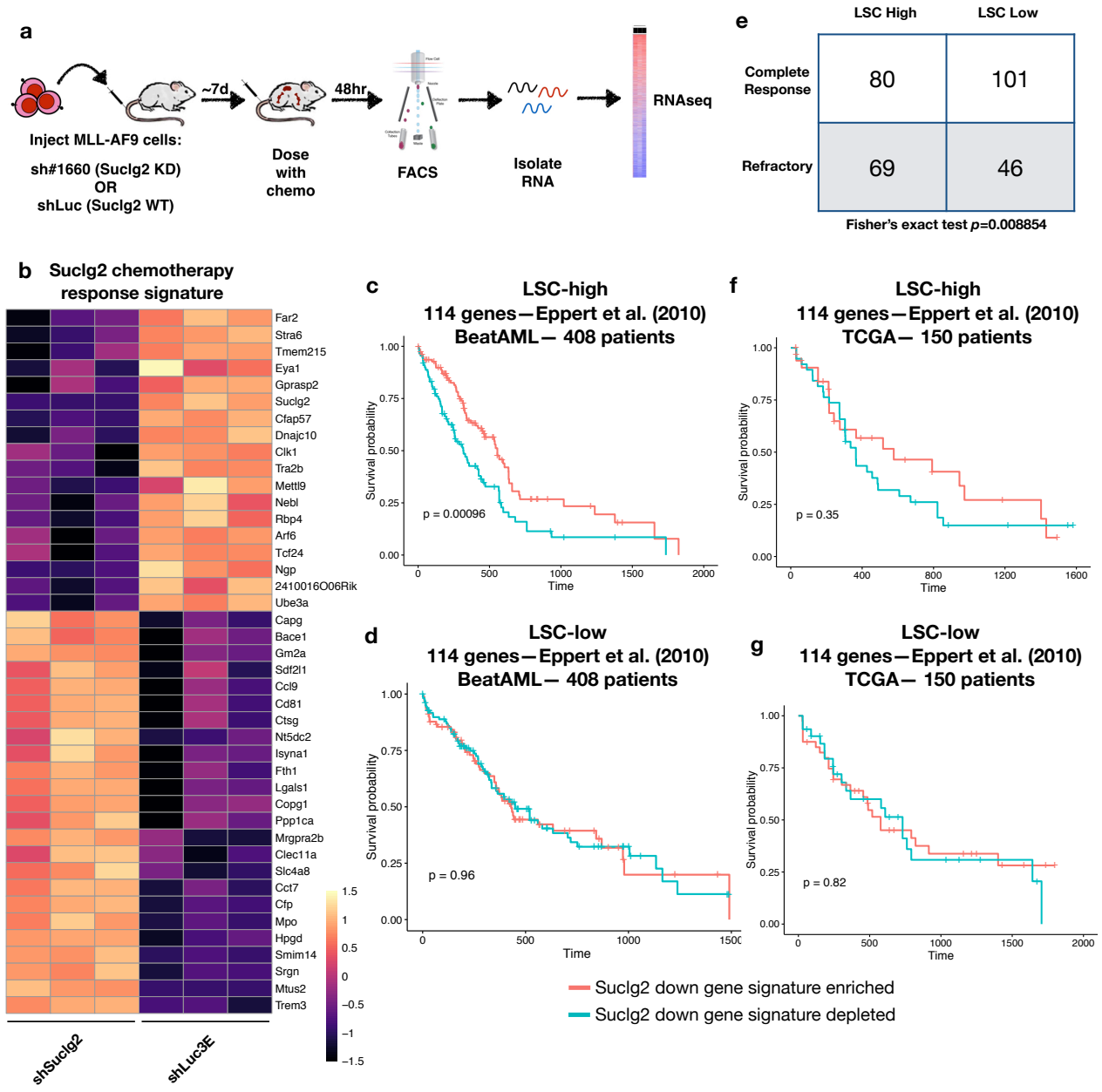

Figure 2.17. A Suclg2 depletion chemosensitization signature stratifies patients whose leukemias are more stem cell-like. (a) Suclg2 KD or control cells were injected into 12 recipient mice each that were randomized into four groups (n=3 each) per hairpin (8 groups of 3 mice total). For each hairpin, half of the mice were treated with a vehicle control and the other half with combination chemo as indicated by the schematic. Mice were sacrificed 24 or 48 hours later, live cells from the spleen and marrow were sorted, and RNA was extracted for transcriptional profiling. (b) A chemosensitization signature was derived from the most differentially expressed genes between treated KD and control cells taken from the marrow at 48hours. (c-d) The down-regulated genes from our signature could stratify patients whose tumors were more stem-like and enrichment of our sensitization signature was associated with significantly better outcomes in a large patient data set (Tyner et al., 2018). Significance is determined by a log-rank test. (e) In the BeatAML data set, the LSC high cohort was enriched for treatment-refractory patients. Notably, this clinical information was not available for all samples. Data shown are for the samples where this information was reported. Significance is determined by a Fisher's exact test. (f-g) The same analysis in TCGA patients were not statistically significant. However, a similar trend was observed. Upregulated genes from our BM

signature were never able to stratify the patient cohorts examined. Similarly, our splenic signature was also never able to stratify any of the patient cohorts examined.

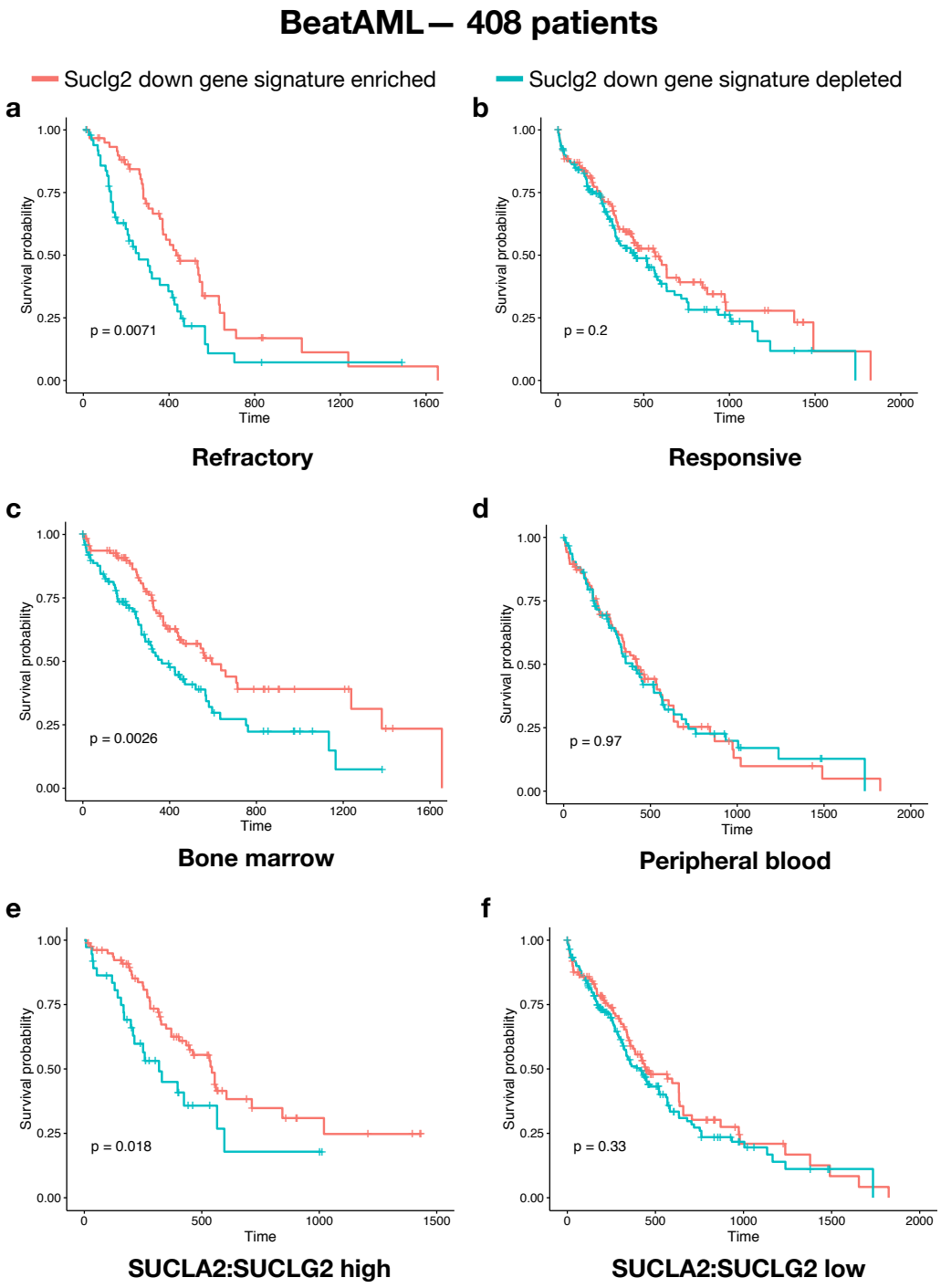

Figure 2.18. A Suclg2 depletion chemosensitization signature predicts better outcomes in therapy-refractory disease, in patient samples harvested from the marrow, and in patients with a high SUCLA2 to SUCLG2 ratio. The highly clinically annotated BeatAML data set was further examined using the downregulated genes from our sensitization signature. Here, enrichment of our chemosensitization signature was also associated with significantly better outcomes in treatment refractory patients (a-b), in patients whose tumors were transcriptionally profiled using AML cells from a bone marrow aspirate (c-d), and in patients whose tumors displayed a high SUCLA2 to SUCLG2 ratio (e-f). Significance is determined using a log-rank test.

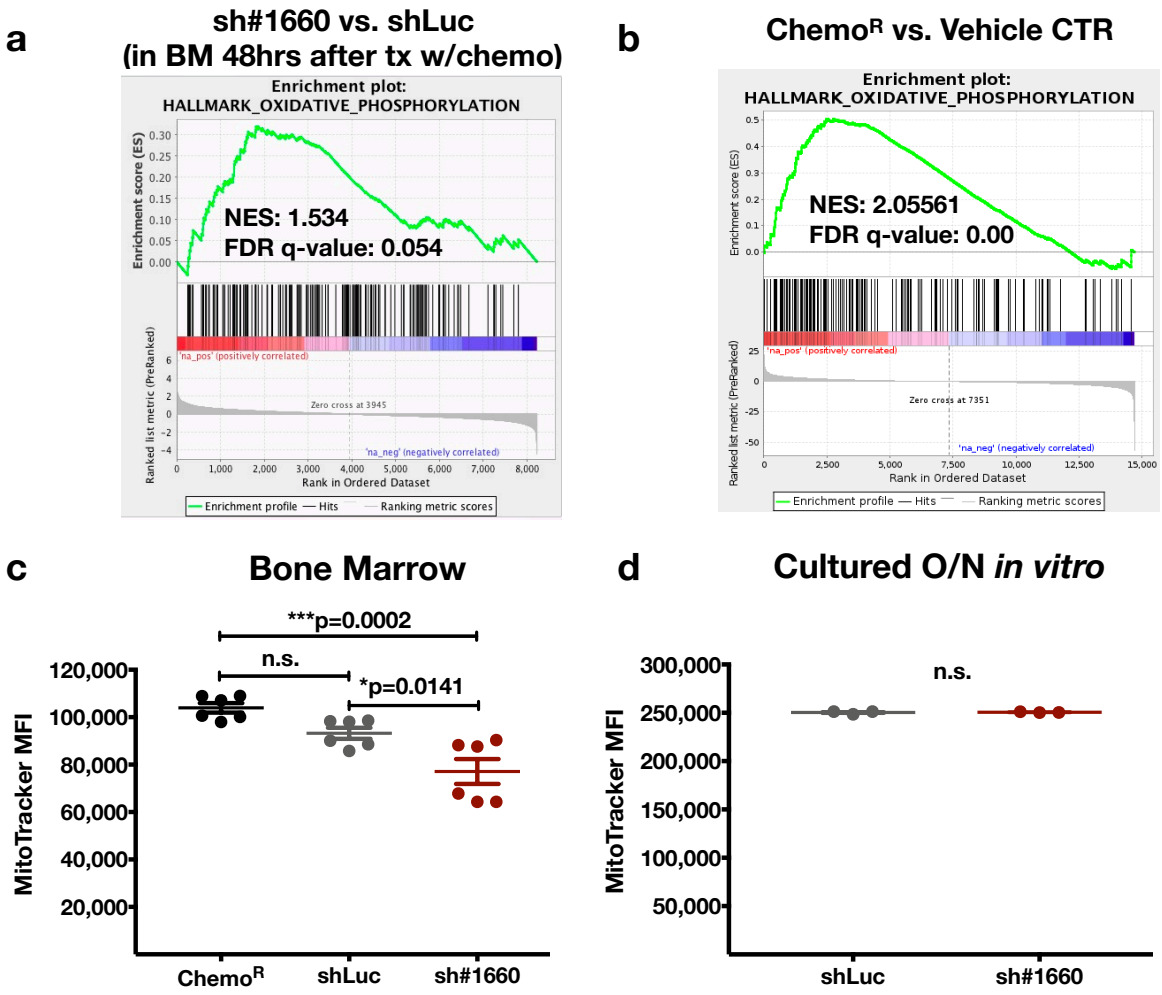

Figure 2.19. Murine MLL-AF9 AML cells resident in the bone marrow upregulate oxidative phosphorylation gene sets in response to acute treatment with combination chemotherapy and display less mitochondrial mass. Gene set enrichment analysis (GSEA) showed an upregulation of genes involved in oxidative metabolism in both acutely treated BM KD cells (a) and in BM Chemo^R cells (b), as compared to their corresponding control cells. Enrichment statistics are calculated as described in Subramanian et al., 2005. (c) MitroTracker stains to examine mitochondrial mass in cells harvested directly from animals showed that chemosensitized KD cells had the lowest signal, followed by shLuc control cells and finally, Chemo^R cells (highest signal). In all instances, AML cells made up >90% of all live cells assayed, as assessed by flow cytometry. In all groups, data from n=6 mice are shown. (d) This effect could not be observed if cells were cultured overnight before the assay was completed. Representative data from one experiment is shown, however this result was observed in four independent experiments testing various dye concentrations, and thus results could not be combined into one graph. Data shown are means ± SEM for (c-d) and significance is determined by either one-way ANOVA with Turkey's post-hoc test adjusted for multiple comparisons in (c), or with unpaired two-tailed student's t test in (d).

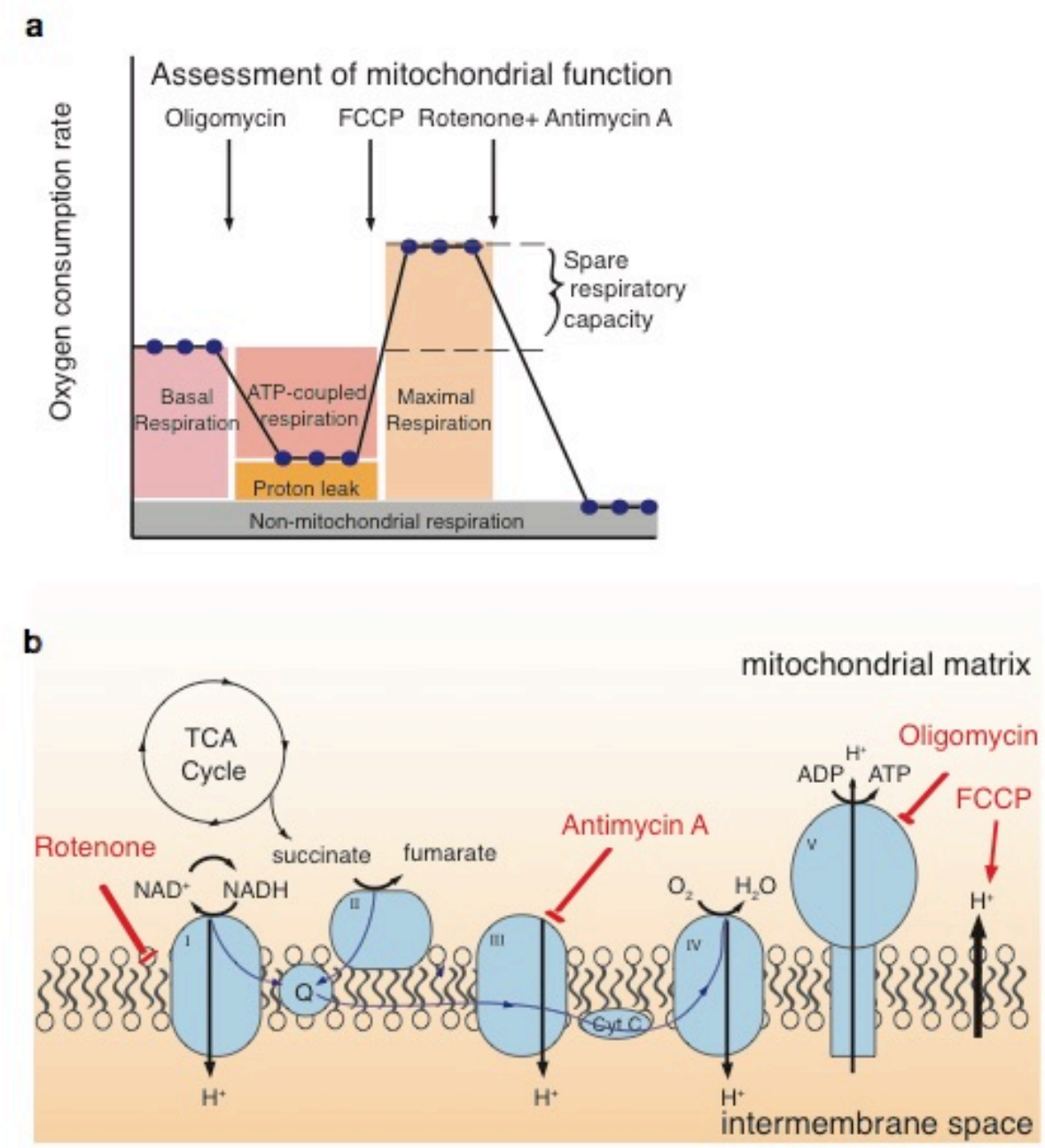

Figure 2.20. Overview of the mitochondrial stress test as a functional assay for mitochondrial function and OXPHOS energetic features. (a) A schematic overview of a mitochondrial stress test. Here, oxygen consumption is measured before, during, and after inhibitors for specific members of the respiration chain (b) are administered to cells.

Reprinted from Cell Metabolism, 24, Ron-Harel, N. et al. Mitochondrial Biogenesis and Proteome Remodeling Promote One-Carbon Metabolism for T Cell Activation, 104–117, 2016, with permission from Elsevier.

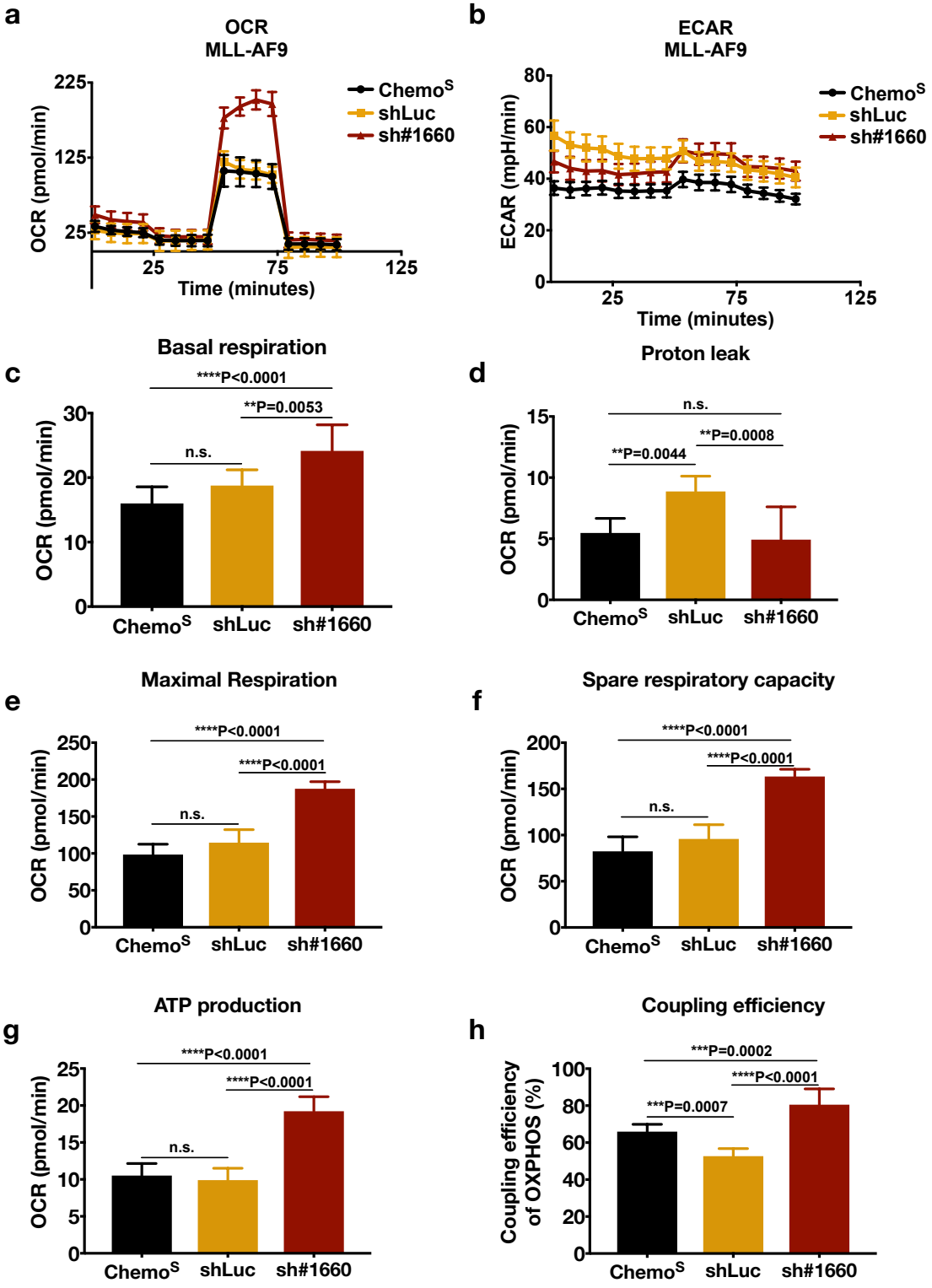

Figure 2.21. Murine MLL-AF9 AML cells depleted of Suclg2 have a higher basal respiration rate, a lower proton leak, greater spare reserve capacity, and better coupling efficiency than control cells. (a) Oxygen consumption rates (OCR), a measure of oxidative metabolism and (b) extracellular acidification rate (ECAR), a measure of glycolytic metabolism) were measured in sorted Suclg2 KD (sh#1660) and control cells (Chemo^S and shLuc) during a mitochondrial stress test. KD cells showed increased oxidative

metabolism phenotypes, including increased basal respiration (c), decreased or unchanged proton leak (d), increased maximal respiration rates (e), increased spare reserve capacity (f), increased ATP production (g), and an increased coupling of substrate oxidation to the phosphorylation of ADP to ATP (h). Suclg2 KD cells appear to have become more glycolytic in response to the uncoupling agent FCCP, however this would have to be confirmed via glycolytic stress tests and the direct measurement of lactate excretion and glucose consumption. Data shown are means ± SEM and n=9-10 for each group. Significance is determined by one-way ANOVA with Turkey's post-hoc test adjusted for multiple comparisons.

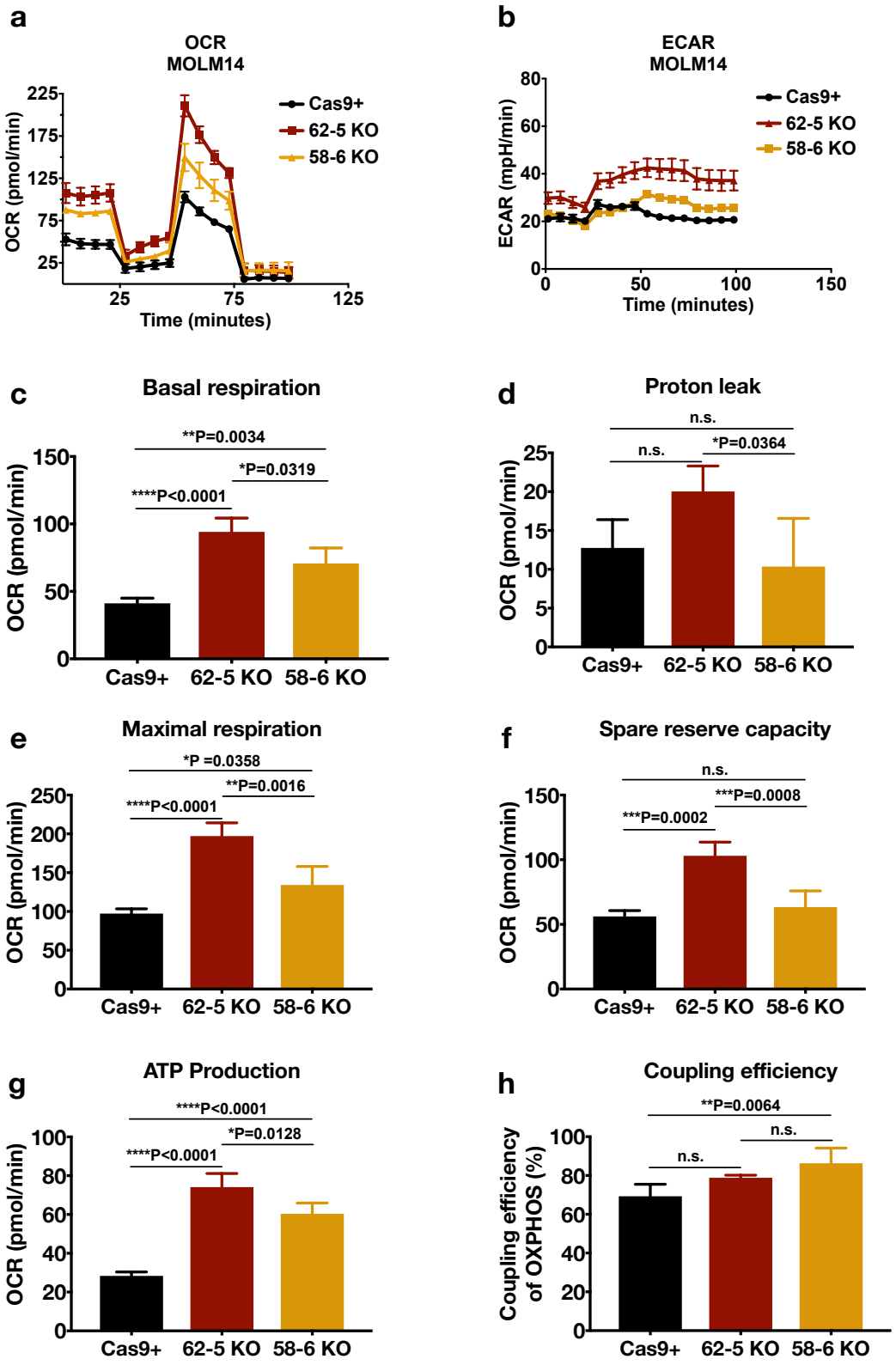

Figure 2.22. *SUCLG2*-null human MLL-AF9 and FLT3-ITD mutated AML cells have a higher basal respiration rate, a lower (or unchanged) proton leak, and greater (or unchanged) spare reserve capacity than control cells. (a) OCR and (b) ECAR were measured in SUCLG2 KO cells (62.5 and

58.6) and in their parental Cas9+ SUCLG2 WT cell line (Cas9+) during a mitochondrial stress test. KO cells consistently showed enhanced oxidative capacities, including increased basal respiration (c), unchanged proton leak (d), increased maximum respiration (e), increased or unchanged spare reserve capacity (f), Increase ATP production (g), and an unchanged or increased coupling of substrate oxidation to the phosphorylation of ADP to ATP (h). Here, 62.5 KO cells appear to become more glycolytic in response to oligomycin and 58.6 KO cells appear to become more glycolytic upon the addition of FCCP, but these phenotypes would have to be confirmed via glycolytic stress tests and the direct measurement of lactate excretion and glucose consumption. Data shown are means ± SEM and n=8-10 per group. Significance is determined by one-way ANOVA with Turkey's post-hoc test adjusted for multiple comparisons.

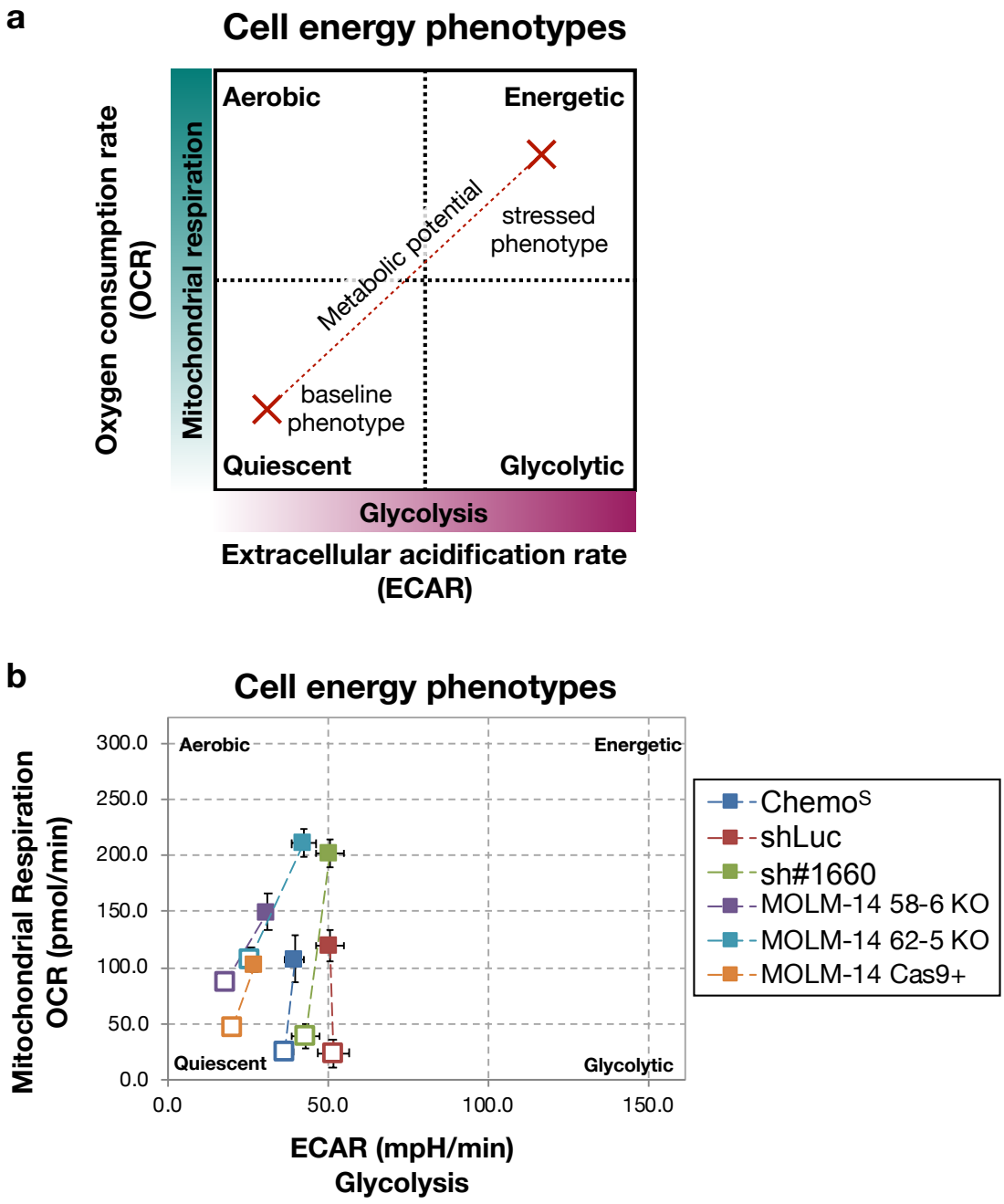

Figure 2.23. SUCLG2 loss or depletion alters the energy phenotypes of AML cells towards enhanced oxidative capacity. (a) The energy phenotypes of cells can be described using OCR and ECAR measurements. (b) When stressed, all cells became more aerobic, with less engagement of glycolysis. SUCLG2 KO/KD cells demonstrated an enhanced ability to engage oxidative metabolism in stressed scenarios.

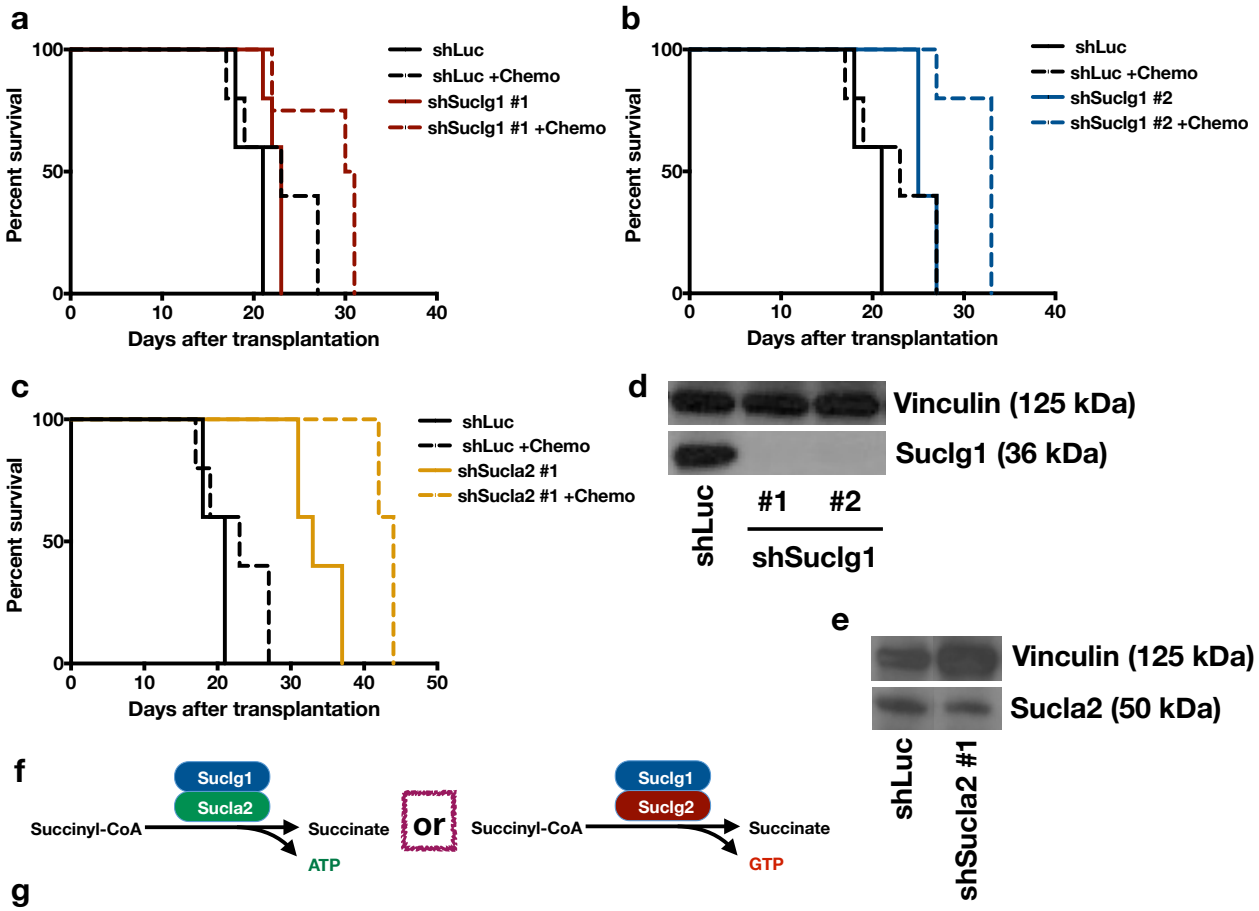

g

Curve 1	Curve 2	P-value	Rank	Benjamini-Hochberg critical value (10% FDR)
shSucla2_Vehicle	shSucla2_Chemo	0.0042	1	0.01
shLuc_Vehicle	shSuclg1-2_Vehicle	0.0043	2	0.02
shLuc_Vehicle	shSucla2_Vehicle	0.0043	3	0.03
shLuc_Chemo	shSucla2_Chemo	0.0043	4	0.04
shSuclg1-2_Vehicle	shSuclg1-2_Chemo	0.0094	5	0.05
shLuc_Chemo	shSuclg1-2_Chemo	0.0101	6	0.06
shLuc_Vehicle	shSuclg1-1_Vehicle	0.0132	7	0.07
shLuc_Chemo	shSuclg1-1_Chemo	0.0848	8	0.08
shSuclg1-1_Vehicle	shSuclg1-1_Chemo	0.1032	9	0.09
shLuc_Vehicle	shLuc_Chemo	0.3379	10	0.1

Figure 2.24. Depletion of other members of the succinyl-CoA synthetase complex affects both proliferation and response to therapy *in vivo*. (a-g) New constitutively expressed hairpins designed against Suclg1 and Sucla2 of the SCS complex (f) were generated and tested for their ability to sensitize AML cells to therapy. Surprisingly, Sucla2 KD (c) and to some extent, Suclg1 KD (a-b) extended life in vehicle treated control animals (f). Additionally, KD of both of these proteins also appeared to sensitize cells to therapy *in vivo*. Here, only one hairpin against Suclg1 (shSuclg1-2) reached statistical significance, while shSuclg1-1 showed a trend towards life extension in chemo treated animals, but did not reach statistical significance (adjusted p-value highlighted in yellow in panel g). The level of KD was validated via WB (d-e). In all groups in a-c, n=5 mice each, except shSuclg1#1+chemo where n=4. (f) Significance is determined using log rank tests and P-values were adjusted for multiple hypothesis testing using Benjamini-Hochberg critical value (g).

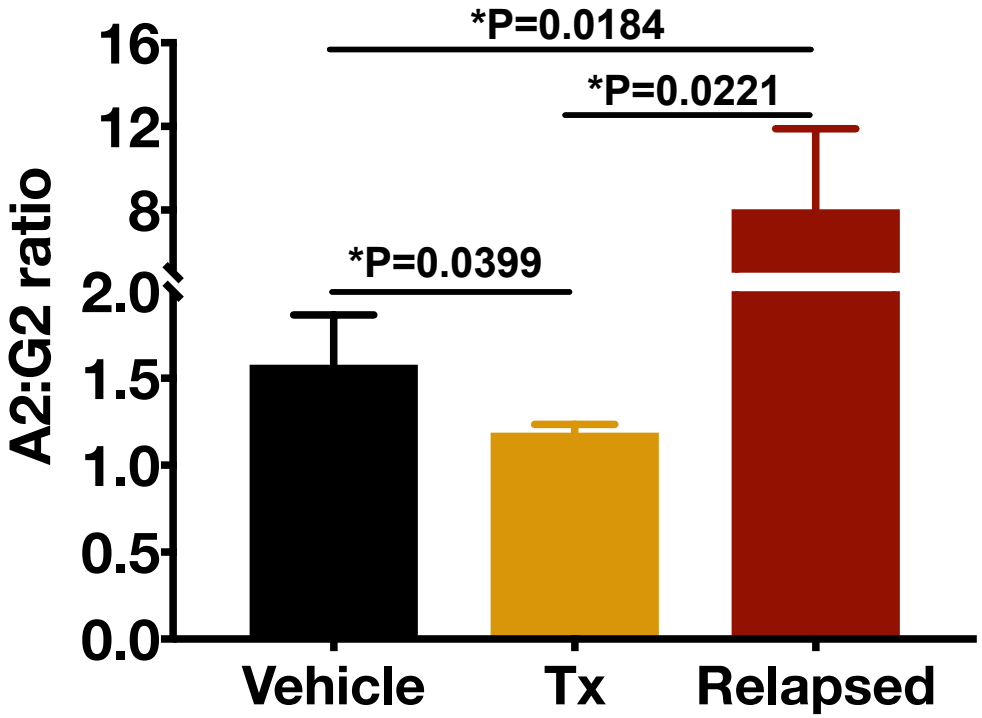

Figure 2.25. The ratio of Sucla2:Suclg2 fluctuates throughout AML disease course *in vivo*, in control murine MLL-AF9 cells. Sucla2 to Suclg2 (A2:G2) ratios were determined using previously completed RNAseq experiments in murine MLL-AF9 cells transduced with a neutral control hairpin (shLuc). Transcriptional data from shLuc cells harvested from the BM of mice 48 hours after they were treated with a vehicle control (Vehicle), 48 hours after they were treated with combination chemotherapy (Tx), or after mice had relapsed following combination chemotherapy (Relapsed) were analyzed. Initially, bulk AML cells express almost twice as much SCS-A as SCS-G. Upon acute chemo treatment, the ratio of A2:G2 begins to drop as cells begin to engage SCS-G mediated pathways. Finally, when mice relapse after chemo treatment, cells express significantly upregulate SCS-A (as compared to SCS-G), the SCS-β subunit associated with high levels of OXPHOS metabolism. In each group, n=3 mice. Significance is determined by one-way ANOVA with Turkey's post-hoc test adjusted for multiple comparisons.

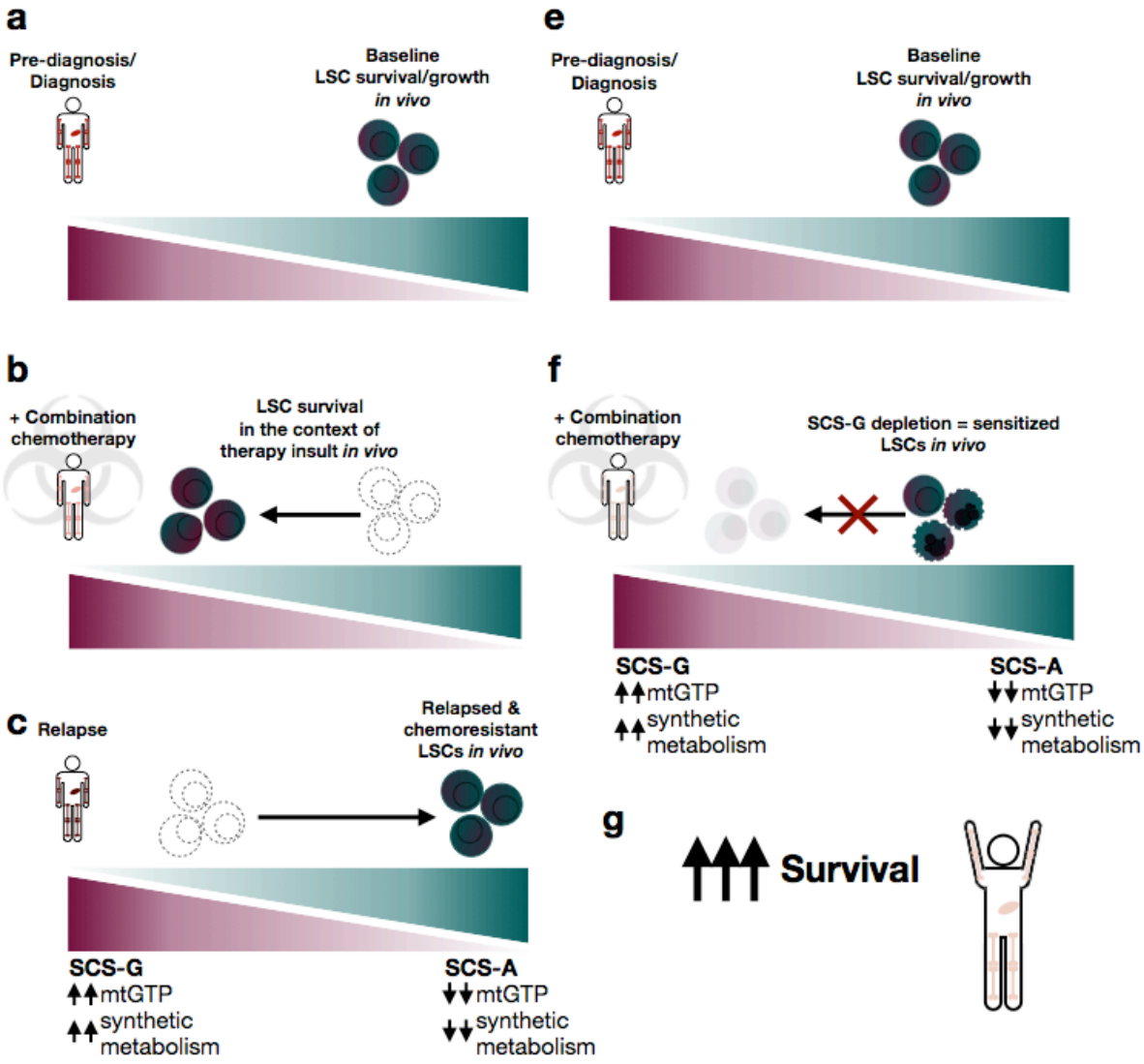

Figure 2.26. Switching synthetic metabolism on and off at specific time points via the modulation of SCS-G and SCS-A subunits could be important for AML LSC survival *in vivo*, both at baseline and in the context of therapeutic insult. (a) To establish leukemia *in vivo*, LSCs have been shown to rely heavily on OXPHOS metabolism, associated with SCS-A. (b) Upon treatment with combination chemotherapy, AML LSCs appear to engage SCS-G and the pathways associated with that SCS-β subunit, namely cataplerosis and gluconeogenesis, both involved in synthetic metabolism. (c) As cells become increasingly resistant and relapse after therapy, OXPHOS metabolism is again upregulated, as reported in the literature. (e) In the context of SCS-G depletion, baseline growth is unaffected, likely because cells are not dependent on SCS-G and its associated pathways in this context. (f) Once chemotherapy is given however, the need for synthetic metabolism appears to increase and cells unable to engage these pathways are sensitized, leading to longer survival (g).

Supplemental Table 2.1. Comparison of the nutrient makeup of RPMI versus physiologic mouse plasma medium used in this thesis. Formulation for RPMI medium is as reported by Corning. Physiologic mouse plasma medium measurements are courtesy of Keene Abbot and Ahmed Ali and were quantified using liquid chromatography-mass spectrometry, as in Sullivan et al., 2019.

Nutrient/Metabolite	Concentration in RPMI (Corning# 10-040) [uM]	Concentration in mouse plasma medium (MPM) [uM]	Fold difference (RPMI/MPM)
Inorganic salts			
$Ca(NO_3)_2 \cdot 4H_2O$	423.46	423.73	1.00
KCl	5365.53	5333.33	1.01
$MgSO_4$	405.42	407.00	1.00
NaCl	102669.40	103448.27	0.99
Na_2HPO_4	5640.32	5633.80	1.00
$NaHCO_3$	23806.69	23809.53	1.00
Amino acids			
L-Arginine	1148.11	114.87	9.99
L-Asparagine	378.47	50.78	7.45
L-Aspartic acid	150.26	52.03	2.89
L-Cystine	208.17	14.53	14.33
L-Glutamic acid	135.93	102.95	1.32
L-Glutamine	2052.83	793.92	2.59
Glycine	133.21	321.25	0.41
L-Histidine	96.68	129.38	0.75
L-Isoleucine	381.18	136.12	2.80
L-Leucine	381.18	197.68	1.93
L-Lysine • HCl	219.00	300.05	0.73
L-Methionine	100.53	81.38	1.24
L-Phenylalanine	90.80	123.36	0.74
L-Proline	152.52	148.23	1.03
L-Serine	285.47	93.69	3.05
L-Threonine	167.90	235.70	0.71
L-Tryptophan	24.48	83.77	0.29
L-Tyrosine	110.38	90.89	1.21
L-Valine	170.72	328.48	0.52
Vitamins			
Biotin	0.82	0.09	9.5
D-Calcium pantothenate	1.05	1.53	0.7
Choline chloride	21.49	24.53	0.9
Folic acid	2.27	0.01	429.8
i-Inositol	194.27	227.32	0.9
Nicotinamide	8.19	4.20	1.9
Para-Aminobenzoic acid	7.29	4.00	1.8
Pyridoxcine • HCl	4.91	1.95	2.5
Riboflavin	0.53	0.03	15.5
Thiamine • HCl	2.96	3.00	1.0
Vitamin B_{12}	0.004	0.005	0.7
Other			
D-Glucose	11101.24	8280.76	1.34

Glutathione (reduced)	3.25	7.48	0.44
Phenol red	14.11	13.28	1.06

References

Anders, S. & Huber, W. Differential expression analysis for sequence count data. *Genome Biol.* **11**, R106 (2010).

Ashton, T. M., Gillies McKenna, W., Kunz-Schughart, L. A. & Higgins, G. S. Oxidative phosphorylation as an emerging target in cancer therapy. *Clin. Cancer Res.* **24**, 2482–2490 (2018).

Balsa-Martinez, E. & Puigserver, P. Cancer Cells Hijack Gluconeogenic Enzymes to Fuel Cell Growth. *Mol. Cell* **60**, 509–511 (2015).

Bosc, C., Selak, M. A. & Sarry, J. E. Resistance Is Futile: Targeting Mitochondrial Energetics and Metabolism to Overcome Drug Resistance in Cancer Treatment. *Cell Metab.* **26**, 705–707 (2017).

Bouwman, P. & Jonkers, J. The effects of deregulated DNA damage signalling on cancer chemotherapy response and resistance. *Nat. Rev. Cancer* **12**, 587–598 (2012).

Bowman, R. L. & Levine, R. L. TET2 in Normal and Malignant Hematopoiesis. *Cold Spring Harb. Perspect. Med.* **7**, 1–12 (2017).

Braun, C. J. *et al.* Versatile in vivo regulation of tumor phenotypes by dCas9-mediated transcriptional perturbation. *Proc. Natl. Acad. Sci.* **113**, E3892–E3900 (2016).

Cantor, J. R. *et al.* Physiologic Medium Rewires Cellular Metabolism and Reveals Uric Acid as an Endogenous Inhibitor of UMP Synthase. *Cell* **169**, 258-272.e17 (2017).

Carrozzo, R. *et al.* Succinate-CoA ligase deficiency due to mutations in SUCLA2 and SUCLG1: phenotype and genotype correlations in 71 patients. *J. Inherit. Metab. Dis.* **39**, 243–252 (2016).

Cassier, P. A., Castets, M., Belhabri, A. & Vey, N. Targeting apoptosis in acute myeloid leukaemia. *Br. J. Cancer* **117**, 1089–1098 (2017).

Chan, S. M. *et al.* Isocitrate dehydrogenase 1 and 2 mutations induce BCL-2 dependence in acute myeloid leukemia. *Nat. Med.* **21**, 178–184 (2015).

Chen, Y., Lun, A. T. L. & Smyth, G. K. From reads to genes to pathways: Differential expression analysis of RNA-Seq experiments using Rsubread and the edgeR quasi-likelihood pipeline [version 2; referees: 5 approved]. *F1000Research* **5**, 1–49 (2016).

Cole, A. *et al.* Inhibition of the Mitochondrial Protease ClpP as a Therapeutic Strategy for Human Acute Myeloid Leukemia. *Cancer Cell* **27**, 864–876 (2015).

Dai, Z. *et al.* edgeR: a versatile tool for the analysis of shRNA-seq and CRISPR-Cas9 genetic screens. *F1000Research* **3**, 95 (2014).

De Rosa, V. *et al.* Reversal of Warburg effect and reactivation of oxidative phosphorylation by differential inhibition of EGFR signaling pathways in non-small cell lung cancer. *Clin. Cancer Res.* **21**, 5110–5120 (2015).

Derr, A. *et al.* End Sequence Analysis Toolkit (ESAT) expands the extractable information from single-cell RNA-seq data. *Genome Res.* **26**, 1397–1410 (2016).

Ding, L. *et al.* Clonal evolution in relapsed acute myeloid leukaemia revealed by whole-genome sequencing. *Nature* **481**, 506–510 (2012).

Doench, J. G. *et al.* Rational design of highly active sgRNAs for CRISPR-Cas9-mediated gene inactivation. *Nat. Biotechnol.* **32**, 1262–1267 (2014).

Döhner, H., Weisdorf, D. J. & Bloomfield, C. D. Acute myeloid leukemia. *N. Engl. J. Med.* **373**, 1136–1152 (2015).

Donti, T. R. *et al.* Screen for abnormal mitochondrial phenotypes in mouse embryonic stem cells identifies a model for succinyl-CoA ligase deficiency and mtDNA depletion. *DMM Dis. Model. Mech.* **7**, 271–280 (2014).

Elpeleg, O. *et al.* Deficiency of the ADP-forming succinyl-CoA synthase activity is associated with encephalomyopathy and mitochondrial DNA depletion. *Am. J. Hum. Genet.* **76**, 1081–1086 (2005).

Eppert, K. *et al.* Stem cell gene expression programs influence clinical outcome in human leukemia. *Nat. Med.* **17**, 1086–1093 (2011).

Farge, T. *et al.* Chemotherapy-resistant human acute myeloid leukemia cells are not enriched for leukemic stem cells but require oxidative metabolism. *Cancer Discov.* **7**, 716–735 (2017).

Fellmann, C. *et al.* An optimized microRNA backbone for effective single-copy RNAi. *Cell Rep.* **5**, 1704–1713 (2013).

Fenouille, N. *et al.* The creatine kinase pathway is a metabolic vulnerability in EVI1-positive acute myeloid leukemia. *Nat. Med.* **23**, 301–313 (2017).
Fiedler, E. C. & Hemann, M. T. Aiding and Abetting: How the Tumor Microenvironment Protects Cancer from Chemotherapy. *Annu. Rev. Cancer Biol.* **3**, 409–428 (2019).
Fiedler, E. R. C., Bhutkar, A., Lawler, E., Besada, R. & Hemann, M. T. In vivo RNAi screening identifies Pafah1b3 as a target for combination therapy with TKIs in BCR-ABL11 BCP-ALL. *Blood Adv.* **2**, 1229–1242 (2018).
Fraser, M. E., James, M. N. G., Bridger, W. A. & Wolodko, W. T. Phosphorylated and dephosphorylated structures of pig heart, GTP-specific succinyl-CoA synthetase. *J. Mol. Biol.* **299**, 1325–1339 (2000).
Fukuda, Y. *et al.* Upregulated heme biosynthesis, an exploitable vulnerability in MYCN-driven leukemogenesis. *JCI insight* **2**, 1–12 (2017).
Gentles, A. J., Plevritis, S. K., Majeti, R. & Alizadeh, A. A. Association of a leukemic stem cell gene expression signature with clinical outcomes in acute myeloid leukemia. *JAMA - J. Am. Med. Assoc.* **304**, 2706–2715 (2010).
Gilbert, L. A. *et al.* CRISPR-Mediated Modular RNA-Guided Regulation of Transcription in Eukaryotes. *Cell* **154**, 442–451 (2013).
Hattori, A. *et al.* Cancer progression by reprogrammed BCAA metabolism in myeloid leukaemia. *Nature* **545**, 500–504 (2017).
Holohan, C., Van Schaeybroeck, S., Longley, D. B. & Johnston, P. G. Cancer drug resistance: an evolving paradigm. *Nat. Rev. Cancer* **13**, 714–726 (2013).
Ippolito, L. *et al.* Metabolic shift toward oxidative phosphorylation in docetaxel resistant prostate cancer cells. *Oncotarget* **7**, 61890–61904 (2016).
Jesinkey, S. R. *et al.* Mitochondrial GTP Links Nutrient Sensing to β Cell Health, Mitochondrial Morphology, and Insulin Secretion Independent of OxPhos. *Cell Rep.* **28**, 759-772.e10 (2019).
Johnson, J. D., Mehus, J. G., Tews, K., Milavetz, B. I. & Lambeth, D. O. Genetic evidence for the expression of ATP- and GTP-specific succinyl- CoA synthetases in multicellular eucaryotes. *J. Biol. Chem.* **273**, 27580–27586 (1998).
Jones, C. L. *et al.* Inhibition of Amino Acid Metabolism Selectively Targets Human Leukemia Stem Cells. *Cancer Cell* **34**, 724-740.e4 (2018).
Jongen-Lavrencic, M. *et al.* Molecular minimal residual disease in acute myeloid leukemia. *N. Engl. J. Med.* **378**, 1189–1199 (2018).
Kacso, G. *et al.* Two transgenic mouse models for beta subunit components of succinate-CoA ligase yielding pleiotropic metabolic alterations. *Biochem. J.* **473**, 3463–3485 (2016).
Kibbey, R. G. *et al.* Mitochondrial GTP Regulates Glucose-Stimulated Insulin Secretion. *Cell Metab.* **5**, 253–264 (2007).
Kreitz, J. *et al.* Metabolic Plasticity of Acute Myeloid Leukemia. *Cells* **8**, 805 (2019).
Kuntz, E. M. *et al.* Targeting mitochondrial oxidative phosphorylation eradicates therapy-resistant chronic myeloid leukemia stem cells. *Nat. Med.* **23**, 1234–1240 (2017).
Lacombe, M. L., Tokarska-Schlattner, M., Boissan, M. & Schlattner, U. The mitochondrial nucleoside diphosphate kinase (NDPK-D/NME4), a moonlighting protein for cell homeostasis. *Lab. Investig.* **98**, 582–588 (2018).
Lagadinou, E. D. *et al.* BCL-2 inhibition targets oxidative phosphorylation and selectively eradicates quiescent human leukemia stem cells. *Cell Stem Cell* **12**, 329–341 (2013).
Lai, C., Doucette, K. & Norsworthy, K. Recent drug approvals for acute myeloid leukemia. *J. Hematol. Oncol.* **12**, 1–20 (2019).
Lai, X. *et al.* Identification of novel biomarker and therapeutic target candidates for diagnosis and treatment of follicular carcinoma. *J. Proteomics* **166**, 59–67 (2017).
Lamb, R. *et al.* Mitochondria as new therapeutic targets for eradicating cancer stem cells: Quantitative proteomics and functional validation via MCT1/2 inhibition. *Oncotarget* **5**, 11029–11037 (2014).
Lambeth, D. O., Tews, K. N., Adkins, S., Frohlich, D. & Milavetz, B. I. Expression of two succinyl-CoA synthetases with different nucleotide specificities in mammalian tissues. *J. Biol. Chem.* **279**, 36621–36624 (2004).

Lee, K. min *et al.* MYC and MCL1 Cooperatively Promote Chemotherapy-Resistant Breast Cancer Stem Cells via Regulation of Mitochondrial Oxidative Phosphorylation. *Cell Metab.* **26**, 633-647.e7 (2017).
Lewis, C. A. *et al.* Tracing Compartmentalized NADPH Metabolism in the Cytosol and Mitochondria of Mammalian Cells. *Mol. Cell* **55**, 253–263 (2014).
Li, H. *et al.* The Sequence Alignment/Map format and SAMtools. *Bioinformatics* **25**, 2078–2079 (2009).
Li, X., Wu, F. & Beard, D. A. Identification of the kinetic mechanism of succinyl-CoA synthetase. *Biosci. Rep.* **33**, 145–163 (2013).
Liberzon, A. *et al.* The Molecular Signatures Database Hallmark Gene Set Collection. *Cell Syst.* **1**, 417–425 (2015).
Lin, K. H. *et al.* Systematic Dissection of the Metabolic-Apoptotic Interface in AML Reveals Heme Biosynthesis to Be a Regulator of Drug Sensitivity. *Cell Metab.* **29**, 1217-1231.e7 (2019).
Love, M. I., Huber, W. & Anders, S. Moderated estimation of fold change and dispersion for RNA-seq data with DESeq2. *Genome Biol.* **15**, 1–21 (2014).
Luo, B. *et al.* Highly parallel identification of essential genes in cancer cells. *Proc. Natl. Acad. Sci. U. S. A.* **105**, 20380–20385 (2008).
Marin, J. J. G., Briz, O., Rodríguez-Macias, G., Díez-Martín, J. L. & Macias, R. I. R. Role of drug transport and metabolism in the chemoresistance of acute myeloid leukemia. *Blood Rev.* **30**, 55–64 (2016).
Mercier, F. *et al.* A genome-wide, in vivo, dropout crispr screen in acute myeloid leukemia identifies an essential role for beta-galactosylation in leukemic cell homing. *Blood* **130**, 2493 (2017).
Miller, C., Wang, L., Ostergaard, E., Dan, P. & Saada, A. The interplay between SUCLA2, SUCLG2, and mitochondrial DNA depletion. *Biochim. Biophys. Acta - Mol. Basis Dis.* **1812**, 625–629 (2011).
Miller, P. G. *et al.* In Vivo RNAi Screening Identifies a Leukemia-Specific Dependence on Integrin Beta 3 Signaling. *Cancer Cell* **24**, 45–58 (2013).
Montal, E. D. *et al.* PEPCK Coordinates the Regulation of Central Carbon Metabolism to Promote Cancer Cell Growth. *Mol. Cell* **60**, 571–583 (2015).
Mullen, A. R. *et al.* Oxidation of alpha-ketoglutarate is required for reductive carboxylation in cancer cells with mitochondrial defects. *Cell Rep.* **7**, 1679–1690 (2014).
Ostergaard, E. Disorders caused by deficiency of succinate-CoA ligase. *J. Inherit. Metab. Dis.* **31**, 226–229 (2008).
Patro, R., Duggal, G., Love, M. I., Irizarry, R. A. & Kingsford, C. Salmon provides fast and bias-aware quantification of transcript expression. *Nat. Methods* **14**, 417–419 (2017).
Pei, S. *et al.* AMPK/FIS1-Mediated Mitophagy Is Required for Self-Renewal of Human AML Stem Cells. *Cell Stem Cell* **23**, 86-100.e6 (2018).
Phillips, D., Aponte, A. M., French, S. A., Chess, D. J. & Balaban, R. S. Succinyl-CoA Synthetase Is a Phosphate Target for the Activation of Mitochondrial Metabolism. *Biochemistry* **48**, 7140–7149 (2009).
Picelli, S. *et al.* Smart-seq2 for sensitive full-length transcriptome profiling in single cells. *Nat. Methods* **10**, 1096–1100 (2013).
Pollyea, D. A. & Jordan, C. T. Therapeutic targeting of acute myeloid leukemia stem cells. *Blood* **129**, 1627–1635 (2017).
Pollyea, D. A. *et al.* Venetoclax with azacitidine disrupts energy metabolism and targets leukemia stem cells in patients with acute myeloid leukemia. *Nat. Med.* **24**, 1859–1866 (2018).
Puram, R. V. *et al.* Core Circadian Clock Genes Regulate Leukemia Stem Cells in AML. *Cell* **165**, 303–316 (2016).
Raffel, S. *et al.* BCAT1 restricts αkG levels in AML stem cells leading to IDHmut-like DNA hypermethylation. *Nature* **551**, 384–388 (2017).
Robinson, M. D., McCarthy, D. J. & Smyth, G. K. edgeR: a Bioconductor package for differential expression analysis of digital gene expression data. *Bioinformatics* **26**, 139–140 (2010).
Ron-Harel, N. *et al.* Mitochondrial Biogenesis and Proteome Remodeling Promote One-Carbon Metabolism for T Cell Activation. *Cell Metab.* **24**, 104–117 (2016).
Saito, Y., Chapple, R. H., Lin, A., Kitano, A. & Nakada, D. AMPK Protects Leukemia-Initiating Cells in Myeloid Leukemias from Metabolic Stress in the Bone Marrow. *Cell Stem Cell* **17**, 585–596 (2015).

Sanjana, N. E., Shalem, O. & Zhang, F. Improved vectors and genome-wide libraries for CRISPR screening. *Nat. Methods* **11**, 783–784 (2014).
Saultz, J. & Garzon, R. Acute Myeloid Leukemia: A Concise Review. *J. Clin. Med.* **5**, 33 (2016).
Schuurhuis, G. J. *et al.* Minimal/measurable residual disease in AML: a consensus document from the European LeukemiaNet MRD Working Party. *Blood* **131**, 1275–1291 (2018).
Sciacovelli, M. & Frezza, C. Oncometabolites: Unconventional triggers of oncogenic signalling cascades. *Free Radic. Biol. Med.* **100**, 175–181 (2016).
Shaffer, B. C. *et al.* Drug resistance: Still a daunting challenge to the successful treatment of AML. *Drug Resist. Updat.* **15**, 62–69 (2012).
Škrtić, M. *et al.* Inhibition of Mitochondrial Translation as a Therapeutic Strategy for Human Acute Myeloid Leukemia. *Cancer Cell* **20**, 674–688 (2011).
Soneson, C., Love, M. I. & Robinson, M. D. Differential analyses for RNA-seq: Transcript-level estimates improve gene-level inferences [version 2; referees: 2 approved]. *F1000Research* **4**, 1–22 (2016).
Stark, R. & Kibbey, R. G. The mitochondrial isoform of phosphoenolpyruvate carboxykinase (PEPCK-M) and glucose homeostasis: Has it been overlooked? *Biochim. Biophys. Acta - Gen. Subj.* **1840**, 1313–1330 (2014).
Stark, R. *et al.* Phosphoenolpyruvate cycling via mitochondrial phosphoenolpyruvate carboxykinase links anaplerosis and mitochondrial GTP with insulin secretion. *J. Biol. Chem.* **284**, 26578–26590 (2009).
Stuani, L., Sabatier, M. & Sarry, J. E. Exploiting metabolic vulnerabilities for personalized therapy in acute myeloid leukemia. *BMC Biol.* **17**, 57 (2019).
Subramanian, A. *et al.* Gene set enrichment analysis: A knowledge-based approach for interpreting genome-wide expression profiles. *Proc. Natl. Acad. Sci. U. S. A.* **102**, 15545–15550 (2005).
Sullivan, M. R. *et al.* Quantification of microenvironmental metabolites in murine cancers reveals determinants of tumor nutrient availability. *Elife* **8**, 1–27 (2019).
Tabe, Y., Konopleva, M. & Andreeff, M. Fatty Acid Metabolism, Bone Marrow Adipocytes, and AML. *Front. Oncol.* **10**, 1–7 (2020).
Takubo, K. *et al.* Regulation of glycolysis by Pdk functions as a metabolic checkpoint for cell cycle quiescence in hematopoietic stem cells. *Cell Stem Cell* **12**, 49–61 (2013).
The Cancer Genome Atlas Research Network. Genomic and Epigenomic Landscapes of Adult De Novo Acute Myeloid Leukemia. *N. Engl. J. Med.* **368**, 2059–2074 (2013).
Tyner, J. W. *et al.* Functional genomic landscape of acute myeloid leukaemia. *Nature* **562**, 526–531 (2018).
Valk, P. J. M. *et al.* Prognostically Useful Gene-Expression Profiles in Acute Myeloid Leukemia. *N. Engl. J. Med.* **350**, 1617–1628 (2004).
Vazquez, F. *et al.* PGC1α Expression Defines a Subset of Human Melanoma Tumors with Increased Mitochondrial Capacity and Resistance to Oxidative Stress. *Cancer Cell* **23**, 287–301 (2013).
Vincent, E. E. *et al.* Mitochondrial Phosphoenolpyruvate Carboxykinase Regulates Metabolic Adaptation and Enables Glucose-Independent Tumor Growth. *Mol. Cell* **60**, 195–207 (2015).
Vo, T. T. *et al.* Relative mitochondrial priming of myeloblasts and normal HSCs determines chemotherapeutic success in AML. *Cell* **151**, 344–355 (2012).
Voorde, J. Vande *et al.* Improving the metabolic fidelity of cancer models with a physiological cell culture medium. *Sci. Adv.* **5**, (2019).
Vozza, A., Blanco, E., Palmieri, L. & Palmieri, F. Identification of the mitochondrial GTP/GDP transporter in Saccharomyces cerevisiae. *J. Biol. Chem.* **279**, 20850–20857 (2004).
Wang, Z. & Dong, C. Gluconeogenesis in Cancer: Function and Regulation of PEPCK, FBPase, and G6Pase. *Trends in Cancer* **5**, 30–45 (2019).
Wong, L. J. C. *Mitochondrial Disorders Caused by Nuclear Genes*. *Mitochondrial Disorders Caused by Nuclear Genes* **9781461437**, (Springer New York, 2013).
Wouters, B. J. *et al.* Double CEBPA mutations, but not single CEBPA mutations, define a subgroup of acute myeloid leukemia with a distinctive gene expression profile that is uniquely associated with a favorable outcome. *Blood* **113**, 3088–3091 (2009).
Wunderlich, M. *et al.* AML cells are differentially sensitive to chemotherapy treatment in a human xenograft model. *Blood* **121**, e90–e97 (2013).

Ye, H. *et al.* Leukemic Stem Cells Evade Chemotherapy by Metabolic Adaptation to an Adipose Tissue Niche. *Cell Stem Cell* **19**, 23–37 (2016).
Yu, W. M. *et al.* Metabolic regulation by the mitochondrial phosphatase PTPMT1 is required for hematopoietic stem cell differentiation. *Cell Stem Cell* **12**, 62–74 (2013).
Yuan, T. *et al.* Dual FLT3 inhibitors: Against the drug resistance of acute myeloid leukemia in recent decade. *Eur. J. Med. Chem.* **178**, 468–483 (2019).
Zhao, Y. *et al.* Loss of succinyl-CoA synthase ADP-forming β subunit disrupts mtDNA stability and mitochondrial dynamics in neurons. *Sci. Rep.* **7**, 1–10 (2017).
Zuber, J. *et al.* Toolkit for evaluating genes required for proliferation and survival using tetracycline-regulated RNAi. *Nat. Biotechnol.* **29**, 79–85 (2011).
Zuber, J. *et al.* Mouse models of human AML accurately predict chemotherapy response. *Genes Dev.* **23**, 877–889 (2009).

CHAPTER 3

Investigating *in vivo* mechanisms of resistance to chimeric antigen receptor T (CAR-T) cells using genome-wide CRISPR-Cas9 genetic screens

Azucena Ramos*, Catherine Koch*, Yunpeng Liu*, Riley Hellinger, Taeyoon Kyung, Aviv Regev, John G. Doench, Marcela Maus, Michael E. Birnbaum, Michael T. Hemann

*These authors contributed equally to this work. AR, CK, YL, and MTH designed the study. AR, CK, YL, and RH conducted experiments. RH provided support with the characterization of clone 20.12 and the entirety of both screens. TK provided critical support in designing and cloning the CAR constructs. AV, JGD, MM, and MEB gave vital conceptual advice and provided reagents. AR wrote the manuscript.

Abstract

The recent clinical success of immunotherapy, borne from leveraging decades of investigation in oncoimmunology to better eliminate malignant cells from the body, has revolutionized anticancer therapy. Of these approaches, adoptive transfer of T cells engineered to express chimeric antigen receptors (CARs) that target specific proteins expressed on tumor cells have garnered exceptional attention. Clinical trials using CD19-targeting CAR-T cells have demonstrated the profound power of this approach to induce long-term remissions and in some cases, even cures in patients with terminal, multiply relapsed and therapy refractory hematological malignancies. Based on unprecedented successes in early phase trials where response rates as high as 80-90% were frequently reported, two CAR-T products were rapidly approved by the FDA in 2017. However, as time elapses and outcome data from CAR-T treated patients is collected over longer periods of follow up, it is now clear that resistance will be a frequent and ongoing problem. As an exceedingly new therapy, little is known about the underlying factors that drive resistance or response to CAR-T cells. Thus, until focused studies aimed at addressing this question are completed in physiologically relevant contexts, including an intact immune system, the full promise of this new "living therapy" cannot be fully realized. In order to investigate CAR-T resistance phenotypes that result from tumor cell alterations in a massively parallel and unbiased manner, we have performed genome-wide CRISPR-Cas9 loss of function (LOF) screens both *in vitro* and *in vivo*. This approach was made possible by the use of an experimentally tractable mouse model of BCR-ABL^{+} B-ALL and the optimization a highly efficient and cost-effective protocol for CAR-T cell production. In this chapter, I describe our efforts to set up this screen and briefly report on the results of both a small pilot screen completed *in vivo*, and the entirety of the *in vitro* arm of our final genome-wide screen. Our goal is to overlay the results from both our *in vitro* and *in vivo* approaches in order to nominate, and subsequently, validate candidate genes that specifically alter a cancer cell's response to CAR-T therapy *in vivo*. Ultimately, the completion of these screens will provide the field with a critically necessary data set that can then potentially guide efforts to uncover highly synergistic agents that potentiate the effects of this promising, but expensive treatment modality.

Introduction

The importance of immunotherapy is now well established and, collectively, these novel therapeutic agents are now considered the "fifth pillar" of cancer treatment, along with surgery, chemotherapy, targeted therapy, and radiation. Today, one of the most promising immunotherapy agents in oncology clinical care is the adoptive cell transfer (ACT) of autologous T lymphocytes engineered to express chimeric antigen receptors (CARs). CAR-T cells represent a direct product of a broader and more profound understanding of oncoimmunology, and a landmark advancement borne from significant interdisciplinary efforts over various scientific and clinical subfields (Sadelain et al., 2017). Functionally, CARs redirect the cytotoxicity of immune cells towards a patient's tumor. Groundbreaking trials in multiply relapsed B cell malignancies that were likely incurable demonstrated that this strategy was extraordinarily effective, even in clinically difficult patient cohorts (Locke et al., 2017; Maude et al., 2018; Schuster et al., 2019). Early response rates were staggering, with upwards of 50 to 90% of previously terminal patients experiencing complete responses, half of which were maintained after a year of follow-up. Subsequently, these early stellar results led to the rapid approval of CAR-T cell therapy by the FDA in 2017, representing the first approved gene therapies in the U.S.

A complete appreciation of the true efficacy of any cancer treatment requires the existence and collection of long term follow up data. As a young therapy, such data for CAR-T cells have only recently begun to emerge but suggest that the problem of relapse is likely to be significant. Recent studies have shown that upwards of 60% of patients will eventually experience disease recurrence after CAR-T therapy and, for most, this will occur within the first year following treatment (Shah & Fry, 2019; Cheng et al., 2019). Here, the median overall survival (OS) has been found to be 12 months in non-Hodgkin lymphoma (NHL) cases and anywhere from 12.9 to 20.1 months in B cell acute lymphoblastic leukemia (B-ALL) patients. While these figures still represent a significant clinical benefit, especially given the overrepresentation of historically intractable cases in CAR-T treated patient cohorts thus far, high failure rates call into question the ultimate utility of this expensive therapy in most patients.

To date, investigations aimed at understanding resistance to CAR-T therapy have largely focused on the treatment modality itself. These reports have demonstrated that as with endogenous and unmodified T lymphocytes, CAR-T cell dysfunction can significantly contribute to treatment failure (Shah & Fry, 2019). However, mutations in tumor cells have also been shown to induce resistance to immunotherapies. For example, loss of function mutations in the interferon gamma receptor signaling molecules Janus kinases 1/2 (*JAK1/2*) or the HLA class I

molecule β-2-microglobulin (B2M) have been shown to render tumors refractory to checkpoint inhibitors (Restifo et al., 1996; Zaretsky et al., 2016). Outside of target antigen loss and mutations in the extrinsic apoptosis pathway genes *BID* and *FADD*, no additional CAR-T resistance mechanisms driven by mutations in cancer cells have been described in the literature (Singh et al., 2020). Thus, the identity and functionality of the genes that underlie CAR-T cell response and failure are, as of yet, unknown. To systematically investigate this question in an unbiased manner, we performed parallel *in vitro* and *in vivo* screens in a transplantable and immunocompetent mouse model of BCR-ABL^{+} B-ALL. In this chapter, I describe our efforts to establish this screen, including the extensive optimization of a highly efficient murine CAR-T production protocol. I also briefly describe preliminary results from a small pilot study and data from the entire *in vitro* arm of our final genome-wide screen.

Results

Cas9 is not additionally immunogenic in a BCR-ABL+ mouse model of B cell acute lymphoblastic leukemia, enabling in vivo screens in immunocompetent mice.

To determine if *in vivo* CAR-T screens using immunocompetent mice would be tractable on a genome-wide scale, we asked if Cas9 protein was immunogenic in our lab's preferred mouse model of B-ALL. This transplantable C57BL/6 mouse model of Ph+ Arf$^{-/-}$ B-ALL was developed by the Sherr lab and has been extensively utilized by our lab to complete hairpin screens (Williams et al., 2006; Williams et al., 2007; Meacham et al., 2015; Fiedler et al., 2018). Limiting dilution experiments performed in non-irradiated hosts showed that as few as 20 cells can induce fulminant B-ALL with a latency of 3 weeks, indicating an exceedingly high LSC frequency that was estimated to be one in every two cells (Williams et al., 2007). As this model is generated by transducing male murine BM cells with human p190 BCR-ABL, we hypothesized that expressing Cas9 would not induce any appreciable immunogenicity in mice—even in non-irradiated and fully immunocompetent C57BL/6 males. We reasoned that if Cas9 expression induced any xenographic barriers, this would likely manifest as delayed *in vivo* growth kinetics over time. Cas9 expressing clones generated to be roughly growth matched to their parental lines *in vitro* were transplanted into non-irradiated immunocompetent male mice. No significant growth delays in Cas9 cells could be detected *in vivo*, in any hematopoietic organ assayed (Figure 3.1a). In fact, Cas9 expressing cells grew significantly faster at later time points (days 8 and 10) than even their parental line, results that are in line with clone 20.8's slightly faster *in vitro* growth kinetics compared Cas9- Tomato+ parental cells (data not shown).

To further explore this question, parallel experiments in non-irradiated male C57BL/6 mice and non-irradiated immunocompromised NOD-SCID/IL2Rg$^{-/-}$ (NSG) mice were completed. We reasoned that if Cas9 was in fact immunogenic, NSG mice transplanted with 20.8 cells would succumb faster to disease than C57BL/6 mice, but no differences in disease latency were found in repeated experiments (Figure 3.1b). To further characterize 20.8 cells, we performed a Cas9 cut assay based on diminishing EGFP fluorescence after transfection of a vector expressing a fast-degrading version of EGFP and a validated sgRNA against this marker (Doench et al., 2014). After 11 days, more than 75% of all 20.8 cells were negative for GFP, indicating a highly efficient cutting rate and a "screenable" clone that expresses high levels of Cas9 protein (Figure 3.1c-d). To ensure that 20.8 cells could functionally be knocked out for other genes, we generated multiple guides against murine CD19 and other non-essential genes (data not shown). Single live 20.8 cells expressing our sgRNAs were sorted into individual wells of a 96-well dish without knowledge of surface CD19 expression and 2.5 weeks later, murine CD19 expression was assessed in 30 clones per guide RNA. All 30 clones from both guides were found to be knocked out (KO) for mCD19 (representative data shown in figure 3.1e). Given that previous work from our lab has shown that up to 30,000 unique shRNAs can be represented *in vivo* in this model, an *in vivo* genome-wide CRISPR-Cas9 screen in immunocompetent mice is experimentally tractable (Meacham et al., 2015).

An optimized protocol efficiently produces high rates of murine CAR-T cells

Traditional CAR-T production protocols using bead-based activation and retronectin-based transduction protocols of retroviral (RV) vectors were cost prohibitive for a screen of this size (Kochenderfer et al., 2010; Jacoby et al. 2016; Kurachi et al., 2017). Thus, we attempted another infection protocol that touted high infection rates (30-50%) but used plate bound antibodies for activation (Zhong et al., 2010). When we followed this exact protocol multiple times and over multiple researchers, no more than 15% of T cells (overall viability rates were 20-40%) could ever be infected in our hands (Figure 3.2a-b, untransduced control in a, representative data in b). We then figured that low infection rates might still be overcome by the enrichment of live and functional CAR-T cells. As sorted T cells showed significant reductions in viability, we adopted a Percoll based density centrifugation step shown to be able to boost T cell infection rates by isolating activated cells that are highly RV-susceptible (Kurachi et al., 2017). Using both plate based activation and this density centrifugation step, we could boost T cell infections to upwards of 45-55% while keeping viability extremely high (60-70%, data not shown). However,

significant cell loss at the Percoll step resulted in a donor to recipient ratio of 3.9 to 1 (at a dose of $7x10^6$ CAR-T cells per treated recipient mouse), which was again cost prohibitive. We attempted to boost the number of T cells collected from animals but this resulted in only a minor increase in yield that also significantly increased dissection times.

To continue to try to solve this problem, we compared the efficiency of T cell activation using beads versus plate bound antibodies at the doses used by Zhong and colleagues (1μg/mL of anti-CD3e and 2μg/mL of anti-CD28) (Zhong et al., 2010). Hoechst stains demonstrated that significantly more T cells activated using beads, as compared to plate-bound antibodies, were induced to cycle and were thus highly RV susceptible (data not shown). Thus, we hypothesized that more robust activation, as seen with beads, would boost infection rates. Extensive experimental optimization testing a wide range of plate bound activating antibody concentrations (at varying ratios) were completed. In the end, the best combination that yielded the highest infection and viability rates while balancing the expression of exhaustion markers on T cells was 5μg/mL of each activating antibody. Using this approach, consistent T cell infection and viability rates of upwards of 70-90% and 85-95% can be achieved without Percoll centrifugation. Notably, our CAR-T cells do express higher levels of PD-1, CTLA-4, and CD25 than bead-activated cells, but as this metric is not predictive of CAR-T success in clinical trials and, as every other approach was cost-prohibitive for our screen, we decided to proceed testing CAR-T cells from our optimized protocol (Shah & Fry, 2019).

CAR-T cells produced with our newly optimized transduction protocol are functional in vitro and induce a dramatic antigen loss phenotype in target cells

To begin to test the functionality of our CAR-T cells, we performed *in vitro* cytotoxicity assays followed by the measurement of interferon gamma (a cytokine released by T cells in proinflammatory conditions) in the resulting tissue culture supernatant. Several experiments testing CAR-T cells produced using different protocols were completed at different times and consistently showed that our CAR-T cells performed just as well as cells generated using all other protocols described (representative data shown in figure 3.3a-c). Surprisingly, all experiments showed that murine B-ALL cells could not be eliminated in *in vitro* experiments, even at very high effector to target (E:T) ratios (Figure 3.3a). Instead, CAR-T cells induced rapid and dramatic loss of the CD19 target epitope on the surface of B-ALL cells (Figure 3.3b). Importantly, this still resulted in activated CAR-T cells that released significant IFN-gamma after being co-cultured with cells expressing their target antigen for 16-24 hours (Figure 3.3c). To

determine if this was a feature unique to this disease model or this target epitope, we tested our anti-murine CD19 CAR-T cells against a CD19+ mouse model of Burkitt's lymphoma (Eμ-Myc), our anti-human CD19 CAR-T cells against a CD19+ human Burkitt's lymphoma cell line (Raji) and a CD19+ human B-ALL cell line (NALM6), and our anti-hEGFRvIII CAR-T cells against GL261 mouse GBM cells induced to express hEGFRvIII via retroviral expression (data not shown). In all cases except NALM6 cells, massive epitope loss was seen, indicating that this phenotype is target antigen-independent and not a unique feature of our murine B-ALL model. In NALM6 cells, disease was successfully suppressed and no antigen loss could be appreciated. In hEGFRvIII+ GBM cells, both significant disease suppression and significant antigen loss was observed, indicating that the kinetics of target epitope loss are considerably accelerated in B cell malignancies.

Murine CAR-T cells targeting mCD19 significantly suppress disease, induce target antigen epitope loss, and extend life in treated mice

We next wondered if our CAR-T cells would be able to suppress disease *in vivo*, given that this goal was never effectively achieved in *in vitro* studies. As previous work by other groups has extensively shown that the *in vivo* efficacy of CAR-T cells cannot be fully recapitulated *in vitro*, we hypothesized that at high enough doses, we would be able to suppress disease (Eyquem et al., 2017; Shah & Fry, 2019; Feucht et al., 2019). To begin, we compared cyclophosphamide (200-300 mg/kg, single i.p. dose) and irradiation-based (5 Gy) lymphodepletion over time. As reported previously, no significant differences in the immune suppression between techniques was noted (Kochenderfer et al., 2010; Davila et al., 2013; Paszkiewicz et al., 2016). To streamline our experimental pipeline, we opted to use an irradiation-based (5 Gy) lymphodepletion protocol. Next, to decide on CAR doses, we examined the preclinical literature and found a large range of CAR-T cells doses ($5x10^4$ to $10x10^6$ CAR-T cells/mouse) could be used *in vivo* (Kochenderfer et al., 2010; Davila et al., 2013; Jacoby et al., 2016; Paszkiewicz et al., 2016; Eyquem et al., 2017). In experiments utilizing CD28-based 2nd generation murine CARs specifically, reported doses were most frequently in the millions of cells ($5x10^6$ to $10x10^6$) per animal (Kochenderfer et al., 2010; Davila et al.). Hence, we completed our *in vivo* experiments within this range of CAR-T cells per mouse. At a dose of $7x10^6$ CAR-T cells per animal, administered two days after the transplantation of $6x10^5$ B-ALL cells, significant disease suppression and life extension can be achieved (representative data shown in Figure 3.4). At relapse, no significant disease suppression in the BM could be detected over multiple

experiments (figure 3.4a). On the other hand, B-ALL disease remained suppressed in both the spleen (figure 3.4b) and peripheral blood (PB, figure 3.4c), speaking to the well-known, but poorly understood observation that CAR-T efficacy varies dramatically based on microenvironment. Target antigen loss was also seen across all anatomical locations assayed (figure 3.4d-f), but was again significantly different in the marrow of treated animals in this experiment (figure 3.4d). Other similar experiments, however, did show significant antigen loss in the marrow, but overall, the emergence of this phenotype is heterogeneous, even within experiments. We also examined CAR-T cell persistence and found that these cells could still be detected in relapsing mice, even after 23 days from the time of ACT (figure 3.4g-i). To simultaneously monitor disease suppression in real time, we took advantage of the fact that this cell line is background-labeled to express *Renilla* firefly luciferase (Fiedler et al., 2018). Bioluminescence imaging completed on days three (figure 3.4j-l), four (figure 3.4m-o), seven (figure 3.4p-r), and ten (figure 3.4s-u) after ACT demonstrated that anti-mCD19 CAR-T cells could significantly suppress disease over time, leading to a life extension in animals treated with this CAR versus control CAR-T cells (figure 3.4v). Later experiments also showed that mice transplanted with 20.8 cells and treated with anti-hCD19 control CARs succumb to disease at the same time (data not shown).

Given the *in vivo* functionality of our CAR-T cells that was on par with previously reported data, we completed dose finding experiments for use in the screen. To keep guide RNA coverage above 150x while limiting the number of *in vivo* experiments to be completed, we decided to use a similar cell dose used by our lab to perform other screens in this model (Meacham et al., 2015; Fiedler et al., 2018). Using $3x10^6$ Cas9+ B-ALL cells would allow us to screen up to 20,000 at a minimum of 150-fold representation, parameters that are in line with our previous work. To determine the appropriate CAR-T cell dose, we irradiated immunocompetent mice, transplanted them with 20.8 cells, ACTed varying amounts of CAR-T cells two days later, monitored mice daily using bioluminescence experiments, and sacrificed animals at peak disease suppression which ultimately ended up occurring on day 3-5, depending on CAR-T dose administered. Here, we aimed for approximately an 80-90% disease suppression rate in any given organ. For the marrow, this was accomplished using $7x10^6$ CAR-T cells, while splenic disease was suppressed to this level at a CAR dose of $3.5x10^6$ CAR-T cells (representative data shown in figure 3.5a-b).

Completion of a small pilot screen

After extensive optimization efforts, we settled on the screening layout shown in figure 3.6a. To facilitate this and other future *in vivo* screens, we collaborated with the Broad Institute's

Genomic Perturbation Platform (GPP) to generate a custom sgRNA library cloned into an optimized pRDA-Crimson_170 lentiviral backbone (figure 3.6b-c). The SKY library is composed of 48 sub pools targeting the protein coding regions of approximately 430 unique murine genes with 4 guides each. Importantly, each sub pool can be used as a stand-alone screening library, as each contains all of the requisite controls for a screen (figure 3.6c). Given the unique and powerful screening platform that our murine B-ALL model represents, we were able to further pool our 48 sub pools into groups of eight (as described above), limiting our entire genome-wide *in vivo* screen to six total experiments which were then completed in two large-scale efforts. The *in vivo* arms of our screen followed the layout of our previously described and optimized *in vivo* dose finding experiments (figure 3.5). In our pilot screen, at least $10x10^6$ cells were sorted and re-plated without CAR-T cells after 24hours of co-culture to mimic our *in vitro* killing assay. Tissue culture supernatant was also collected at the 24hr mark of co-culture for future IFN-gamma measurements that can help corroborate proper and robust CAR-T cell function.

Using this approach, we were successfully able to recover the vast majority of sgRNA species upon sequencing of amplicons from *in vivo* and *in vitro* treated cells. At about 200-fold representation, upwards of 80-90% of our high quality pilot library can be represented and maintained *in vivo* after CAR-T treatment, in all but one condition (figure 3.7a). Across 4 mice, only an average of about 50% (range: 29.9-95%) of our library could be represented in the spleens of mice treated with $3.5x10^6$ anti-mCD19 CAR-T cells. This result could indicate that the CAR-T dose used might have been too high (although this is unlikely given our previous dose finding experiments) or that a significant amount of genes that sensitize splenic B-ALL cells to CAR-T therapy are represented in the first eight sub pools of our libraries. Representation is more uniformly maintained *in vitro*, with upwards of 90-95% of our library being conserved after treatment (data not shown).

Unfortunately, examination of the overall fold changes in our pilot screen between control and anti-mCD19 CAR treated animals demonstrated a very low signal-to-noise ratio (Figure 3.8a-b). To inspect the health of our screen, we inspected the behavior of guides against murine *Cd19*. We also examined the behavior of guides against *Bid* and *Fadd*, genes that were previously show to promote CAR-T resistance after they were found to weakly enrich in an *in vitro* screen in human B-ALL cells (NALM6) (Singh et al., 2020). In our *in vitro* studies, CD19 guides enrich in a dose dependent manner, showing about a 1.1 fold difference in samples treated with anti-mCD19 CAR-T cells (over input) as compared to control CARs both administered at an E:T ratio

of 1:2 (figure 3.8a). At an increased E:T ratio of 5:1, this fold difference rises to 1.6, but inconsistent behavior in one of three replicates dropped the p-value or this event below significance. In the stage of analysis shown in figures 3.8 through 3.23, data were completely unfiltered to remove guides or biological/technical replicated with inconsistent behavior. When the data were further filtered to identify genes with robust guide behavior (1. For each gene, inspect guides with the top 2 absolute fold changes over pre-screen input and discard the gene if the directionality of fold change for these two guides are opposite of each other; and 2. For each gene retained from step 1, calculate the coefficient of variation (CV) for the log fold changes of the top 2 guides. Rank genes by the corresponding CV values and retain those among the lowest 30%), signals were significantly increased. Here, CD19 guides enriched 1.5 fold at an E:T of 1:2 and 2.4 fold at an E:T of 1:5 in conditions where cells were treated with anti-mCD19 CAR-T cells as compared to control CARs *in vitro*. However, this approach also severely reduced the number of scoring genes in all arms of our screen. In our *in vivo* arms, CD19 guides again enrich in a dose dependent manner, enriching more robustly in the marrow when $7x10^6$ anti-mCD19 CAR-T cells are administered, as compared to mice treated with $3.5x10^6$ anti-mCD19 CAR-T cells (figure 3.8b). Extreme enrichment of these guides can also be seen in the spleen of mice treated with $3.5x10^6$ CAR-T cells, albeit with a low p-value in completely unfiltered data. The appropriate analysis of this entire data set (*in vivo* and *in vitro* arms) is still being determined.

As a further quality control measure, we inspected the behavior of cell essential genes (defined as the common essential genes from the Broad Institute's DepMap project). Here, we expected to see an enrichment towards depletion phenotypes (as compared to input) for guides against these genes. Consistently, in all arms of the screen, this is what we see (figures 3.9 to 3.14). However, cell essential genes should, in fact, represent some of the strongest signals in a screen, even in the context of inefficient cutting.

Next, we aimed to determine if the weak signals achieved in this screen were due to inefficient cutting or to issues with our CAR-T cells. To begin to answer this question, we examined the behavior of the four individual guides against murine *Cd19* in unfiltered data from all of our pilot screens (Figures 3.15 to 3.23). Here, if CAR-T cells are functional, then CD19 guides should be randomly distributed when cells are treated with control CAR-T cells. These guides should then consistently enrich, in a dose dependent manner, when anti-mCD19 CAR-T cells are administered. Both *in vitro* (Figures 3.15 to 3.16) and *in vivo* (figures 3.17 to 3.23) this is precisely what we observe. To further examine CAR-T cell functionality, we inspected results

from our flow cytometric analysis completed using small aliquots of cells taken from each screening condition on the date the screens were completed (all completed on the same day). As before, CAR-T cells against mCD19, administered at any dose, did not significantly suppress disease in the BM of moribund animals (figure 3.24a). In the spleen however, B-ALL disease remained suppressed, even at relapse (figure 3.24b). Significant target antigen loss was also found in both the marrow and spleen of mice treated with anti-mCD19 CAR-T cells (figure 3.24c-d). We also examined CAR-T persistence in both of these anatomical locations (figure 3.24e-f). As expected, we found that we could still detect anti-mCD19 CAR-T cells in the marrow at both doses, but at much lower rates than we had previously noted in non-screening experiments (figures 3.24e). However, this is likely not due to diminished CAR-T efficacy, as CAR-T persistence in the spleen matched the results from our previous experiments (figure 3.24f). Rather, these data suggest that this difference is more likely a result of changes in the BM microenvironment induced by the introduction of our sgRNA library. Additionally, bioluminescence imaging completed four days after ACT demonstrated that both CAR-T doses could significantly suppress disease in mice, and while not statistically significant, this appears to be CAR-T dose dependent (figure 3.24g). In our *in vitro* arms, dramatic antigen loss was again evident in cells treated with either dose of anti-mCD19 CAR-T cells (figure 3.24h). Lastly, no difference in viability or CAR-T production rate could be noted between the batch of CAR-T cells used in the screen and the batch used in every other preliminary experiment completed (data not shown). Together with the observation that *Cd19*-targeting guides enrich in a dose-dependent manner in response to anti-CD19 CAR-T cells, these results indicate that the CAR-T cells used in our pilot screen were highly functional and thus, unlikely to be the culprit behind the suboptimal performance of this initial study.

Rapid loss of Cas9 cutting efficiency in 20.8 cells is responsible for the weak signal-to-noise ratio observed in the pilot study

Given that quality control data from CAR-T cells used in our pilot screen all indicated a healthy and functional product, we next turned our attention to our 20.8 Cas9+ clone. Previous CRISPR-Cas9 screens completed in our lab using this mouse model had not indicated that Cas9 functionality could be lost so rapidly (unpublished data, personal communication with previous lab members). However, the cells used for that screen grew significantly slower than our cells and thus were likely able to maintain high Cas9 expression over longer periods of time. Additionally, previous studies in our Eμ-Myc driven mouse model of Burkitt's lyphoma *had* shown

that that model could lose Cas9 expression in as little as 2-3 weeks (unpublished results, personal communication with previous lab members). Thus, we hypothesized that rapid loss of Cas9 functionality was responsible for the weak signals in our pilot. To begin to test this idea, we thawed 20.8 cells and immediately completed a GFP cut assay, achieving identical results as those shown in figure 3.1c. We then re-selected clone 20.8 and another back-up clone (20.12), with blasticidin for seven days. WB analysis demonstrated significantly increased levels of Cas9 expression in 20.12 cells, and a less significant increase in 20.8 cells (figure 3.25a). Re-selected cells were then cultured for four continuous weeks and GFP cut assays were repeated, demonstrating that after long term culture, Cas9 cutting efficiency was significantly diminished (figure 3.25b). Given our observation that loss of CD19 could be induced just 16 hours after a region of exon 2 is targeted by our anti-mCD19 CAR (figure 3.3b), we developed a functional cut assay where cells are monitored by flow cytometry for the loss of surface mCD19 expression using previously validated guides against mCD19 (figure 3.1e) in a lentiGuide-puro backbone. Functional cut assays set up at the same time as the GFP cut assay shown in figure 3.25b again demonstrated 20.8 cells, but not 2.12 cells, had lost most of their ability to edit after 4 weeks in culture (Figure 3.25c). In the pilot screen, 20.8 cells were thawed and recovered for 5 days to ensure robust growth before the experiment. Cut assays were then set up and after 11 days, cells were expanded for 3 days before being transduced with our libraries. Hence, loss of Cas9 functionality, on the order of 2.5-3 weeks, was responsible for weak performance of our pilot screen.

Re-establishing a more robust clone for completion of the final genome-wide CAR-T screens

To reestablish a new clone, we followed the same approach as that pursued with 20.8 cells. Kinetics experiments using the mCherry+ GFP+ hCD19+ mCD19+ Cas9+ B-ALL clone 20.12 demonstrated no delays in *in vivo* growth kinetics in the marrow, spleen or blodd (figure 3.26a). Similarly, 20.12 cells were not immunogenic, causing both immunocompetend and immunocompromised mice to succumb to disease at the same time (figure 3.26b). To determine if and when 20.12 cells also lose their Cas9 cutting abilities, we thawed the parental mCherry-GFP+ hCD19+ mCD19+ Cas9+ 20.12SP (single positive) clone from which 20.12 cells were generated and performed fluorescence-based cut assays (this time using a Tomato expressing vector) after four and ten weeks of continuous culture. After 4 weeks of culture, 20.12SP cells were finished cutting by day 3 of the assay, well within the time frame of our entire screen, and

still expressed high levels of Cas9 protein (Figure 3.26c, d). An identical cut assay performed after 10 weeks of culture demonstrated that 20.12SP cells had lost almost all of their Cas9 editing abilities (figure 3.26c). Thus, we proceeded to test this clone *in vivo*. Identical dose finding experiments completed for 20.8 cells were repeated for clone 20.12, demonstrating that 4 days after ACT, disease could be suppressed to 10-20% in the marrow and spleen using $15x10^6$ and $10x10^6$ anti-mCD19 CAR-T cells, respectively (figure 3.27a, b). Again, disease suppression was CAR-T cell dose-dependent. Blood burden also significantly suppressed at both of these doses (figure 3.27c). As before, dramatic loss of mCD19 target antigen expression on the surface of 20.12 cells resident in the BM, SP, or PB was noted (figure 3.27d-f). Finally, CAR-T engraftment was also assayed, showing high levels of the cells were present in the BM, SP, and PB (figure 3.27g-i).

We then repeated the screen with alterations noted in the methods section. Briefly, 20.12 cells were allowed to recover for a much shorter period of time after puromycin selection was completed. As 20.12 cells grow faster than 20.8 cells *in vitro*, this was not an issue. Clone 20.12 expresses hCD19. Thus, a new control CAR-T cell against hEGFRvIII was used instead of anti-hCD19. Notably, previous testing had confirmed that like all of the other CAR constructs used, this CAR had no off-targeting effects in our models (data not shown). We also more carefully titrated anti-mCD19 CAR-T dose *in vitro*, finding that at an E:T ratio of 1:10, approximately 50% of all cells lose mCD19 expression, while all cells are mCD19- at an E:T ratio of 1:2 (as before). Lastly, in our pilot screen, we sorted 20.8 cells after 24 hours of co-culture with all CAR-T cells. Although this was not an issue during our small pilot screen, completing this same step at a genome-wide scale is not feasible. Instead, we performed the *in vitro* arms of all the screens in the same way as our *in vivo* screens and did not remove CAR-T cells from co-cultures with screening cells after they were added. Instead, daily counting and splitting of our cells resulted in the rapid dilution and elimination of CAR-T cells from dishes such that by the end of the experiment, CAR-T cells represented less than 0.01% of all cells present in our cultures (data not shown). Notably, this result is expected, given the complete loss of the target epitope at both of these CAR-T cells doses after only 16 hours and the significant differences in *in vitro* growth kinetics between CAR-T cells (24hr doubling time) and 20.12 cells (8-10hr doubling time). In every *in vitro* screen completed in 20.12 cells, mCD19 expression, B-ALL cell viability, and total cell number were monitored daily. Additionally, 24hrs after initial CAR-T exposure, tissue culture supernatant was collected for future IFN-gamma measurements that can help corroborate

proper and robust CAR-T cell function. Using this approach, we were successfully able to recover the vast majority of the sgRNAs (>90%) represented in our libraries upon sequencing of amplicons from *in vitro* conditions. For the final screen, the 48 SKY pools were collapsed into 6 final libraries that were screened. (a) At about a 205-fold representation, upwards of 85-90% of our high quality library can be represented and maintained *in vitro* after CAR-T treatment at two different E:T ratios (Figure 3.28). As this data was only very recently received, our analyses are still limited and preliminary. However, as shown in figure 3.29, all guides against murine essential genes show a strong enrichment towards drop out phenotypes and guides against murine *Cd19* show strong, dose dependent responses with increasing pressure from anti-mCD19 CAR-T cells (figure 3.30 a-b). Finally, we asked whether other genes reported to either promote resistance or sensitize cells to immunotherapy scored in our screens. As with clone 20.8, guides targeting *Bid* and *Fadd* did not score in our screen (Singh et al., 2020). The gene *Ptpn2* was recently shown to sensitize cells to immunotherapy when lost and members of the IFN-g/JAK/STAT pathway (*Jak2, Ifngr1/2, Stat1*) were shown to induce resistance to immunotherapy when lost (Manguso et al., 2017; Zaretsky et al., 2017). All of these genes demonstrated robust and dose-dependent phenotypes in the expected direction (*Ptpn2* depletes while *Jak2, Ifngr1/2, Stat1* enrich) in our screen, demonstrating that to some extent, similar pathways likely dictate therapy response in checkpoint blocking and CAR-T therapy . We expect that with further filtering to reduce noise present in any and all screens, these genes will reach significance and ultimately score as hits in our screen. Genomic DNA for the *in vivo* arms is also forthcoming, but not yet available.

Discussion

In this chapter, I report our initial efforts to establish parallel *in vivo* and *in vitro* genome-wide CRISPR-Cas9 screens. To make an endeavor such as this possible, a new protocol for efficient and cheap CAR-T production had to be established. After exhausting various options reported in the literature, we were able to produce high quality CAR-T cells that could successfully suppress an extremely aggressive mouse model Ph+ B-ALL. Similar murine CAR-T doses (ACTed within 4 days of tumor cell transplantation) were previously used to suppress mouse models of B-ALL and B cell lymphoma that had a significantly longer latency than that of our model, even at higher doses than those used in our experiments. Thus, our CAR-T cells are likely even more effective than those used by other groups (Kochenderfer et al., 2010; Davila et al., 2013). Strikingly, we find that rather than specific tumor cell lysis, CAR-T treatment induces rapid, substantial loss of target antigens on the surface of these cells *in vitro*, something that we

have not seen reported with other murine CAR-T cells. Target epitope loss is also a significant finding in mice, but repeated experiments have shown that unlike what happens in a dish, CAR-T cells targeting our tumor cells *in vivo* can significantly suppress disease, leading to prolonged disease latency and in some cases, even cures (data not shown).

Emerging data from seven CAR-T trials demonstrate that antigen loss in clinical settings accounts for nearly half of all relapses (Majzner & Mackall, 2018). Thus, our murine B-ALL cells represent an ideal model in which to study this and likely, other resistance phenotypes associated with this novel and promising treatment modality. For example, significant difference in the ability of our CAR-T cells to suppress disease in the marrow versus the blood or spleen of mice is already evident from our preliminary experiments. Following up on these results will be extremely exciting in the future. Moreover, genes reported to promote resistance (*Ptpn2*) or response (*Jak2*, *Ifn1/2*, *Stat1*) to other immunotherapies that impinge on T cell functionality, also show dramatic and dose-dependent responses in predicted directions in our genome-wide *in vitro* screen (Manguso et al., 2017; Zaretsky et al., 2017). This is a particularly interesting finding, as it indicates that similarities between agents that aim to enhance T cell-based tumor killing are likely significant. Loss of members of the IFNg/JAK/STAT pathway have already been shown to be prognostic for failed checkpoint inhibitor response in melanoma patients (Zaretsky et al., 2017). Thus, in aggregate, our screens are likely to nominate clinically relevant factors that govern the response to CAR-T therapy.

As recent and growing evidence is showing that the tumor microenvironment is continuously engaged in dialogue with malignant cells, our study is particularly timely (Joyce & Fearon, 2015). Here, it will be interesting to see what hits can be identified in immunocompetent mice. Ultimately, once it is completed, this project will fill a significant gap that is currently evident in the CAR-T field. To our knowledge, no other study has investigated the effects of tumor cell changes on the effectiveness of CAR-T cells *in vivo*. Still, as exemplified by checkpoint molecules predicted by the cancer immunoediting model, the reciprocal interplay between cancer and CAR-T cells is likely to play a major role in determining therapeutic outcome (Schreiber et al., 2011; Darvin et al., 2018). Uncovering the identity of the major players involved in these processes will be a salient step forward in the rational design of highly synergistic combinations that can potentiate the effects of this promising, but expensive treatment modality.

Methods

Pooled sgRNA screening

A custom genome-wide library divided into 48 sub pools was generated in collaboration with John Doench and the Broad Institute's genomic perturbation platform (GPP). In total, 97,336 unique guides targeting the protein coding regions of 21,958 unique murine genes with 4 sgRNAs each (plus control non-targeting and intragenic cutting guides) were included. All protein coding murine genes were subdivided into 48 pools by their initial KEGG term (obtained using KEGG REST API in BioPython, biopython.org), in a non-redundant manner. All four guides targeting the protein coding region of any given gene were kept together in the same pool. Using this approach, only 36% of protein-coding genes could be classified into a KEGG pathway. Thus, the first 14 sub pools and part of sub pool 15 were filled by KEGG genes. All other genes were randomly distributed among the remaining sub pools. Mouse essential genes (defined as orthologous mouse genes for the human essential gene set from Hart et al., 2015, 1530 genes; obtained from Ensembl Biomart) were divided evenly across all pools. Guides against human *EGFRvIII*, human *CD22*, human *CD19*, and murine *Cd19* were included in the first pool. Guides against olfactory genes (1,133 total) were also distributed evenly amongst all sub pools. All 48 sub pools were cloned into a lentiviral pRDA-Crimson_170 vector (figure 3.6b). To preserve library complexity, a minimum of 1000-fold coverage of the sgRNA library was maintained at each *in vitro* step before the screen, and at a minimum of 150-fold coverage (range: 153 to 203-fold coverage *in vivo*, all *in vitro* screens performed above 500x) was maintained in all screens completed. Pool A (also the pool screened in the pilot study) consisted of the first 8 sub pools and had a total of 15,308 sgRNAs targeting the protein coding regions of 3,648 unique mouse genes. Pool B consisted of sub pools 9-16 and had a total of 15,147 sgRNAs targeting the protein coding regions of 3,648 unique mouse genes. Pool C consisted of sub pools 17-24 and had a total of 15,258 sgRNAs targeting the protein coding regions of 3,648 unique mouse genes. Pool D consisted of sub pools 25-32 and had a total of 17,335 sgRNAs targeting the protein coding regions of 3,648 unique mouse genes. Pool E consisted of sub pools 33-40 and had a total of 14,713 sgRNAs targeting the protein coding regions of 3,648 unique mouse genes. Pool F consisted of sub pools 41-48 and had a total of 19,575 sgRNAs targeting the protein coding regions of 3,718 unique mouse genes. Cloned and sequenced plasmid pools, and viral supernatant were generated by the Broad Institute's GPP.

For screens, Cas9+ cells were thawed, recovered and expanded for 5 days to ensure robust growth, and then tested for cutting efficiency using the traditional fluorescence based cut assays (GFP) or functional cut assay (sgRNAs against mCD19, track surface expression) to ensure high rates of editing efficiency (Doench et al., 2014). After cutting assays were completed (cells reached a rate of at least 75% GFP- or mCD19-; Doench et al., 2014; Doench et al., 2018) cells were expanded over three additional days and infected with sub pools. For each of the 48 sub pools, $60x10^6$ cells were spin-infected with predetermined amounts of viral supernatant (determined using titration experiments, data not shown), such that 15-30% of all cells were infected (expressed E2-Crimson, and survived puromycin selection; MOI<<1). The $60x10^6$ Cas9+ cells were placed in a total of 60mL of medium (culture medium plus viral supernatant), supplemented with 10 µg/mL polybrene (Sigma), divided into 6-well plates (4mL/well, 15 wells), and centrifuged at 1000xg and 37°C for 1.5 hrs. Cells were then pooled into large flasks and cultured overnight. Thirty-six hours later, cell density was adjusted to 10^6 cells/mL (and was never allowed to go over $3x10^6$/mL) and puromycin selection (2 µg/mL, Gibco, A1113803) was started. Cells were selected over two days and then spun out of puromycin containing medium and allowed to recover. Here, 20.8 cells were allowed to recover for 6 days and the appropriate number of infected, selected and recovered cells were sorted and combined (combined such that coverage was uniform across sub pools) into Pool A for our pilot studies. The next day, cells from Pool A were prepared for tail vein injection (methods below, in mouse studies section) or for *in vitro* screens. In this way, cutting was completed in mice or *in vitro* before CAR-T cells were administered two days later. For clone 20.12DP, cells were allowed to recover for only one day, after which the appropriate number of infected, selected and recovered cells were sorted and combined (combined such that coverage was uniform across sub pools) into Pools A-C (experiment 1) and Pools D-F (experiment 2). The next day, cells from large pools were prepared for tail vein injection into mice (methods below, in mouse studies section) or for *in vitro* screens.
In all screens: Two days later, CAR-T cells were adoptively transplanted into mice via tail vein injection (methods below, in mouse studies section) at the indicated doses. For all *in vitro* screens, $14x10^6$ library cells were seeded and treated two days later (on the same schedule as mice) with control CAR-T cells (anti-hCD19 for 20.8 or anti-hEGFRvIII for 20.12), anti-mCD19 CAR-T cells, or with no CAR-T cells, at the indicated dose. *In vitro* CAR-T screens were set up in triplicate while the no CAR-T condition was kept in a single plate. Input samples were collected just after puromycin selection had completed (Input PS) and on the day cells were injected into mice/set up for *in vitro* screens (Input or Input DOI). Six days after ACT (day 8 of disease) when

mice were becoming moribund, all animals were sacrificed and E2-Crimson+ cells were sorted from various anatomical compartments (average number sorted cells per compartment = $13.8x10^6$). For *in vitro* screens where B-ALL cells viability was above 95% and represented more than 99% of all cells present in the sample, cells were counted and $20x10^6$ cells were collected for gDNA isolation. The only condition that did not meet this cutoff was the anti-mCD19 at E:T of 1:2 for all 6 pools. Here, CAR-T cells were completely gone from culture, but B-ALL viability of cells remained low at 30-60% across replicates, necessitating sorting to isolate cells (14-$20x10^6$ sorted per replicate, per condition).

Finally, gDNA from all cells were isolated using the Machery Nagel L Midi NucleoSpin Blood Kit (Clontech, 740954.20). Modifications to the manufacturer's instructions were added. In step 1, cells were lysed in the kit's proteinase K containing lysis buffer for longer (overnight at 70°C). The next morning, lysates are allowed to cool to room temperature, 4.1µL of RNase A (20 mg/mL; Clontech, 740505) is added, and cells are incubated for 5 minutes at room temperature. The procedure then continues as indicated by the manufacturer. The concentration of the resulting gDNA is measured using the Qubit dsDNA HS assay kit (ThermoFisher, Q32854), and if necessary, diluted to 200ng/µL with elution buffer. gDNA is then submitted to the Broad Institute's GPP for Illumina sequencing.

Screen hit discovery

Sample quality control was performed by counting the number of gRNA sequences that show at least 50 reads in each sample. Samples with more than 30% of gRNA sequences that were filtered out after the above procedure were excluded from further analyses.

Guide RNA-level read counts were scaled by total read count for each sample and logarithm-transformed. Gene-level enrichment and depletion scores were computed by averaging log-normalized read counts across all gRNA sequences against each gene. Six different pooled libraries were aggregated targeting a total of 21,958 unique murine genes with a total of 88,793 sgRNAs (4 per gene + non-targeting and intergenic-cutting controls). Input samples were used as a baseline for computing scores. Specifically, every gene was first assigned an 'essentiality score' computed as the difference (i.e. log-fold change) between the average gene-level counts for the gene across replicates and that in the input sample. The CAR-T therapy enrichment/depletion score for a given gene is computed as the difference between the

essentiality scores of that gene in anti-murineCD19 CAR-T cell treated samples (treatment group) and in anti-human CD19/anti-humanEGFRvIII CAR-T cell treated samples (control group). For sample groups that have at least 2 samples retained after quality control, Student's t-tests were performed to obtain p-values for assessing significance of difference between the scores in the treatment group and the control group.

Mouse maintenance and studies

All mouse experiments were conducted under IUCAC-approved animal protocols at the Massachusetts Institute of Technology. The mouse strains used in this study included C57BL/6 (Jackson) and NOD-SCID/IL2Rg$^{-/-}$ (NSG; Jackson Laboratory). Immunocompetent recipient mice were sublethally irradiated (1 x 5 Gy [500 rads] prior to transplantation with B-ALL cells in mice later receiving ACT with CAR-T cells 2 days later, as noted in the text. For *in vivo* screens, mice were injected with 3x10^6 Cas9+ library B-ALL cells and the indicated number of CAR-T cells. Both B-ALL and CAR-T cells were prepared for transplantation by being resuspended in 200 µl Hank's balanced salt solution (Lonza) and loaded in 27.5 gauge syringes (Becton Dickinson). Cell solutions were administered via tail vein injections.

Bioluminescence studies

XenoLight D-Luciferin Potassium Salt D (PerkinElmer, 122799) was used for standard bioluminescent imaging (resuspended at 30mg/mL in saline, sterile filtered, and stored at -80°C). Mice were weighed and luciferin was loaded in 27.5 gauge syringes (Becton Dickinson) and administered via intraperitoneal injection at a dose of 165mg/kg. Mice were then anesthetized with 2.5% isoflurane (Piramal Critical Care, NDC#66794-013-25) delivered at 1 L per minute in O_2. Ten minutes from the time of luciferin injection, animals were imaged on a Xenogen IVIS system at various exposures lasting anywhere from 2 to 60 seconds with small binning. Data was analyzed using Living Image version 4.4 software (Caliper Life Sciences). Images were normalized to the same color scale for figure generation.

Cell culture

All cell lines were mycoplasma negative.

Murine B-ALL cells: Cells were cultured in RPMI with L-glutamine (Corning, 10-040-CM) medium supplemented with 10%FBS and 2-mercaptoethanol to a final concentration of 0.05mM (Gibco, 21985023).

Murine B-cell lymphoma cells (Eμ-Myc): Cells were cultured in medium composed of a 50:50 mix of IMDM with L-glutamine and 25mM HEPES (Corning, 10-016-CM) and DMEM with L-glutamine and sodium pyruvate (Corning, 10-013-CM), supplemented with 10% FBS and 2-mercaptoethanol to a final concentration of 0.05mM (Gibco, 21985023).

Murine T cells: T cells harvested from the spleens of mice were cultured in plates coated with activating antibodies (as described in CAR-T cell production methods) in T cell medium (TCM): RPMI with L-glutamine (Corning, 10-040-CM) medium supplemented with 10%FBS, recombinant human IL-2 (rhIL-2, final concentration of 20ng/mL; Peprotech, Cat# 200-02-1mg), and 2-mercaptoethanol to a final concentration of 0.05mM (Gibco, 21985023).

Human cell lines: 293T, NALM6 and Raji cells were all mycoplasma negative. 293T cells are cultured in DMEM with L-glutamine and sodium pyruvate (Corning, 10-013-CM) supplemented with 10% FBS. NALM6 and Raji cells were cultured in RPMI with L-glutamine (Corning, 10-040-CM) supplemented with 10% FBS.

Viral supernatant production

Viral supernatant is produced using standard methods. Briefly, 293T cells are transfected with retroviral or lentiviral transfer plasmid and packaging vector (retrovirus: pCL-Eco [Addgene, 12371]; lentivirus: psPAX2 (Addgene, 12260) with VSVg envelop plasmid pMD2.G [Addgene, 12259]) using Mirus TransIT-LT1 (Mirus, MIR2305) as indicated by the manufacturer. The next day, 293T cells are switched into medium composed of 60% RPMI complete and 40% DMEM complete. Viral supernatant is collected 24 and 48 hours later, spun down to remove residual 293T cells, and kept at 4°C for a maximum of 4 days.

***In vitro* killing assay**

In vitro CAR-T killing assays were performed using standard methods (examples: Posey et al., 2016; Eyquem et al., 2017). Briefly, target cells are counted and co-cultured with or without CAR-T cells at indicated E:T ratios (accounting for CAR-T infection rate) in RPMI complete supplemented with 2-mercaptoethanol and 10% FBS but no rhIL-2, as in cell culture methods above. 16-24 hours later, total cell number per well is counted, cell suspension is analyzed by flow cytometry (to assess live/dead and %mCD19+ cells), and the densities of each cell type (CAR-T, target cell, non-transduced T cell) are determined. The resulting target cell densities in CAR-T containing wells are then normalized to the resulting target cell density in control wells seeded with the same number of target cells but without CAR-T cells.

Interferon gamma ELISA release assay

Standard methods were used for enzyme-linked immunosorbent assay (ELISA). Briefly, supernatant from *in vitro* CAR-T killing assays was collected and spun down to remove any contaminating cells. IFN-gamma released into the supernatant by CAR-T cells is then measured using the DuoSet ELISA kit for mouse INF-ɣ (R&D systems, DY485) and Nunc MaxiSorp flat bottom plates (Thermo Fisher Scientific, 44-2404-21), as indicated by the manufacturer. To ensure that the assay is completed within the linear range of the kit, supernatant is initially diluted 1:10 in reagent diluent. At least six serial 4-fold dilutions are then performed. At least one standard curve for this assay is generated per plate and at least two standard curves for the entire experiment are constructed using standard solutions supplied in the mouse INF-ɣ kit. Substrate solution used is 1-Step™ Ultra TMB-ELISA (Thermo Fisher Scientific, 34028) and stop solution used is sulfuric acid 2N stop solution (VWR, BDH7500-1). Bovine serum albumin (BSA; Sigma, A8022-500G) is prepared as a sterile filtered 5% stock in PBS (Corning, 21-031-CV).

CAR-T cell production

Before collecting T cells, 6-well plates were coated overnight with activating antibodies against mCD3e (Bio X-Cell, BE0001-1) and mCD28 (Bio X-Cell, BE0015-1) at 5µg/mL each in PBS (Corning, 21-031-CV) at 4°C. The next day, 8-12 week-old male C57/BL6 mice (Jackson) were sacrificed and their spleens were collected. CD8+ T cells were isolated using Miltenyi Biotec CD8a (Ly-2) MicroBeads for mouse (positive selection kit; Miltenyi, 130-117-044) and LS columns (Miltenyi, Cat# 130-042-401) as indicated by the manufacturer. Coated plates were rinsed once with PBS and T cells were resuspended at $0.5x10^6$ to 10^6 cells/mL in T cell medium (TCM, recipe in cell culture methods). After 24 hours, activated T cells were collected (spun out of TCM containing activating antibodies and placed into fresh TCM after counting) and spin-infected at 1000xg for 1.5 hrs at 37°C in 50:50 mix of TCM medium : retroviral (RV) supernatant at a density of 10^6 cells/mL, supplemented with 10µg/mL protamine sulfate (MS Biomedicals, ICN19472910) on new rinsed antibody coated plates (as above). Before being combined with T cells in TCM, RV supernatant (viral production methods above) is supplemented with 2-mercaptoethanol to a final concentration of 0.05mM and recombinant human IL-2 to a final concentration of 20ng/mL. T cells are always cultured and infected on PBS rinsed antibody-coated 6-well plates, as described above, except during *in vitro* killing assays where no activating antibodies are ever used. The next day, T cells are collected from plates, counted, spun out of TCM medium containing activating antibodies, resuspended in fresh TCM at a cell density of $0.5x10^6$ to $1x10^6$

cells/mL, and re-plated on PBS rinsed antibody-coated plates. Twenty-four hours later, T cells are collected from antibody coated plates, counted, analyzed by flow cytometry to assess the fraction of CAR-T cells produced, spun out of TCM medium containing activating antibodies, and prepared for tail vein injection into animals or for *in vitro* kill assays/screens.

In the text, we describe early optimization steps involving Percoll (GE Healthcare, 17-0891-01) density centrifugation that were ultimately dropped from our final protocol. All Percoll experiments were completed as described (Kurachi et al., 2017).

Western Blotting

Cells were lysed with RIPA buffer (Boston BioProducts, BP-115) supplemented with 1X protease inhibitor mix (cOmplete EDTA-free, 11873580001, Roche). Protein concentration of cell lysates was determined using Pierce BCA Protein Assay (ThermoFisher Scientific, 23225). Total protein (40-60µg) was separated on 4-12% Bis-Tris gradient SDS-PAGE gels (Life Technologies) and then transferred to PVDF membranes (IPVH00010, EMD Millipore) for blotting.

Plasmids, cloning, and sgRNAs

Packaging and envelope plasmids used for viral production

Retrovirus: pCL-Eco (Addgene, 12371)

Lentivirus: psPAX2 (Addgene, 12260) with VSVg envelop plasmid pMD2.G (Addgene, 12259) or pCMV-EcoEnv (Addgene, 15802)

Chimeric Antigen Receptor (CAR) plasmids

The murine CD19 targeting second generation CAR 1D3-28Z.1-3 containing inactivating mutations in the 1st and 3rd ITAM regions of the CD3-ζ chain (Kochenderfer et al., 2010) was synthesized by Twist Bioscience and cloned into the GFP+ MP71 retroviral vector (Engels et al., 2003). The clinically used scFv sequence (heavy chain linked to light chain variable regions) against human CD19, FMC63 was provided by the Maus lab. A CD28-containing 2nd generation murine CAR targeting hCD19 protein was then constructed by switching out the scFv for 1D3-28Z.1-3 in the anti-mCD19 CAR and replacing it with the FMC63 scFv (also synthesized by Twist Bioscience). The same technique was used for the 3C10 scFv targeting human EGFRvIII, which was reported by the Rosenberg lab (Morgan et al., 2012). All CAR constructs are identical, containing a CD8a leader sequence, followed by the scFv of choice (light chain linked to heavy chain variable regions as reported for each scFv in their original papers), followed by an IgG4

hinge sequence (linker peptide), a portion of the murine CD28 molecule from amino acids IEFMY to the 3′ terminus, and finally, the cytoplasmic region of the murine CD3-ζ chain from amino acids RAKFS to the 3′ terminus with both tyrosines in ITAMs 1 and 3 mutated to phenylalanines as described (all in frame with one another; Kochenderfer et al., 2010). Tomato+ and E2-Crimson+ CARs were also generated by switching out the GFP cassette in MP71. All CAR constructs were extensively tested to ensure that they only targeted their peptide of interest. Human EGFRvIII expression was induced using pMSCV-XZ066-EGFRvIII (Addgene, plasid 20737) and murine hEGFRvIII+ B-ALL cells were generated. Retroviral supernatant to induce hCD19 expression was provided by the Maus lab and is currently proprietary. All CARs were extensively tested *in vitro* (killing assays methods) and *in vivo* (as described in text) to ensure no off target effects.

CRISPR plasmids

To generate Cas9+ murine B-ALL cell lines, lentiCas9-Blast (Addgene, 52962) was used and cells were selected with Blasticidin (Gibco, A1113903) at 20 μg/mL for 7 days and then single cell cloned and assayed for Cas9 expression via WB. Guide RNAs for murine *Cd19* were designed using the Broad Institute's sgRNA Designer (Doench et al., 2014) and cloned into lentiGuide-Puro (Addgene, 52963) for the functional cut assay (tracking loss of mCD19 on the cell surface) or pRDA-Crimson_170 to generate KOs of various test genes (vector testing, data not shown). Guide RNAs used are below (Forward/Reverse):

Murine *Cd19* sgRNAs:

sgRNA#42, targets exon 6 (5'-CACCGAATGACTGACCCCGCCAGG)/(5'-AAACCCTGGCGGGGTCAGTCATTC)

sgRNA#43, targets exon 2 (5'-CACCGCAATGTCTCAGACCATATGG)/(5'-AAACCCATATGGTCTGAGACATTGC)

Other plasmids

MSCV-mCherry (Addgene, 52114) was used to generate 20.12DP cells from mCherry- GFP+ 20.12 cells.

Antibodies

Western blotting: anti-β Actin (Cell signaling, 4967S), anti-CD19 (Abcam, ab25232), Cas9 (ActiveMotif, 61577).

Flow cytometry: anti-mCD19-BV785 (BioLegend, 115543), anti-mCD19-APC (BioLengend, 152410), anti-mCD8-APC (BioLegend, 100712), anti-hCD19-APC (BioLegend, 302212), anti-

hCD19-APC/Cy7 (BioLegend, Cat# 302218), anti-mPD-1-APC (BioLegend, 135209), anti-mCD152-PE/Cy7 (BioLegend, 106313).

Statistical analysis

Statistical analyses were performed using GraphPad Prism 7 (GraphPad Software Inc). The specific statistical tests performed are specified in figure legends. Differences are considered significant for P-values ≤ 0.05, or as indicated when adjustments for multiple hypothesis testing was required.

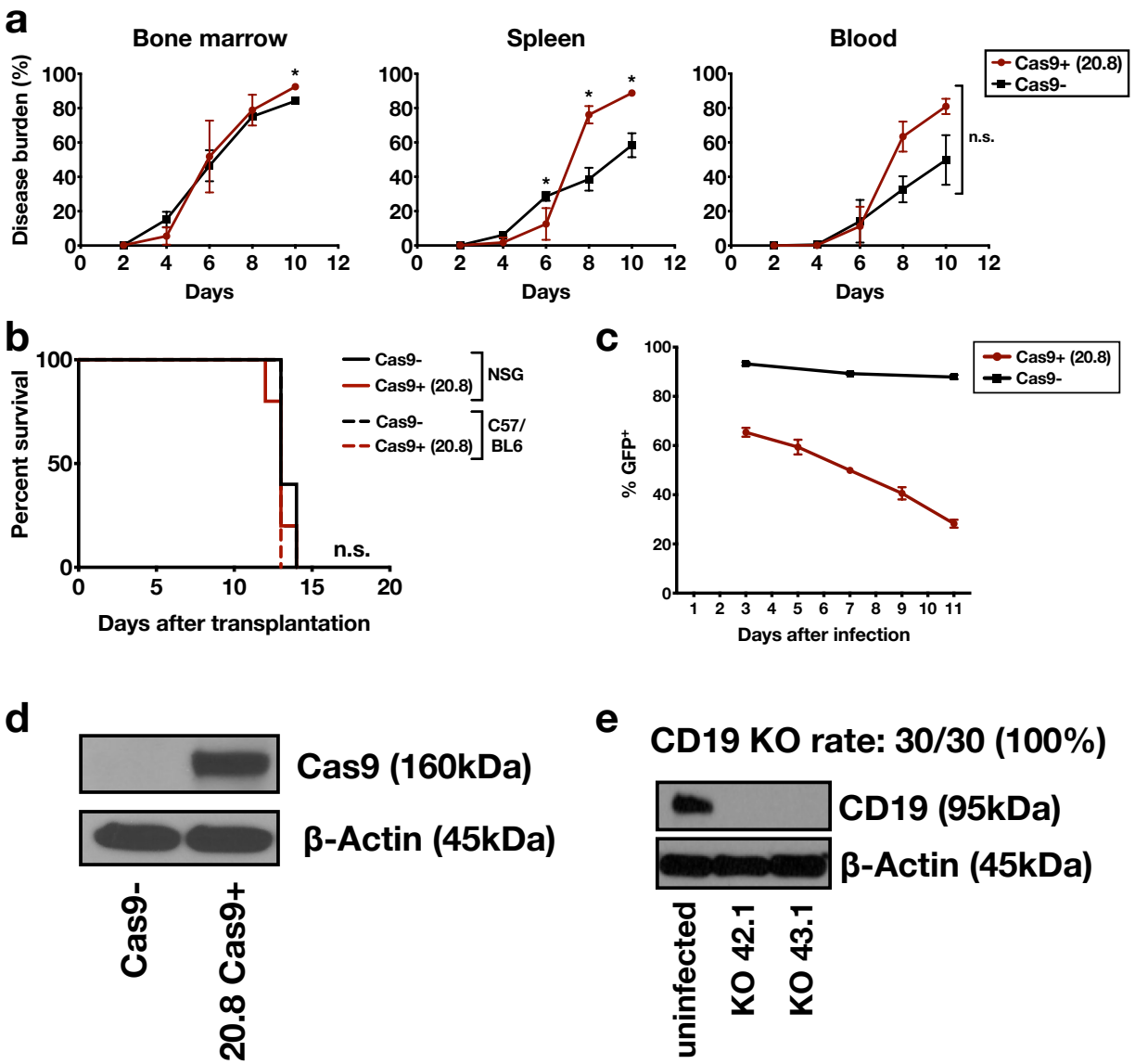

Figure 3.1. Cas9 is not additionally immunogenic in a mouse model of BCR-ABL+ B-ALL transplanted into non-irradiated immunecompetent recipient mice. (a) Tomato+ Cas9 expressing (clone 20.8) cells show highly similar growth kinetics as Tomato+ non-Cas9 expressing parental cells in hematopoietic organs, as assayed by flow cytometry on the indicated days. Non-irradiated eight week-old male C57/BL6 mice (n=6 per group) were transplanted with $6x10^5$ cells. Significance is determined using unpaired student's t-tests with Bonferroni correction for multiple comparisons. (b) Non-irradiated immunocompetent (C57/BL6) male mice and immunocompromised (NSG) mice succumbed to both Cas9- and Cas9+ (20.8) disease at the same time, indicating that Cas9 is not additionally immunogenic in our cell line. All mice (n=5 per group) were injected with $5x10^5$ cells. Significance was determined using a log-rank test. (c) An *in vitro* cut assay using an all-in-one vector expressing a fast-degradable EGFP and a validated sgRNA against EGFP (Doench et al., 2014) was used to assay Cas9 cutting efficiency in 20.8 cells, showing that cells are finished cutting at day 11. (d) Western blot (WB) for Cas9 shows that 20.8 cells express this protein. (e) Functional experiments to generate mCD19 knock out (KO) clones using two independent and non-overlapping guides show a high rate of KO in 20.8 cells. Representative data is shown. For all panels, repeated experiments displayed identical results.

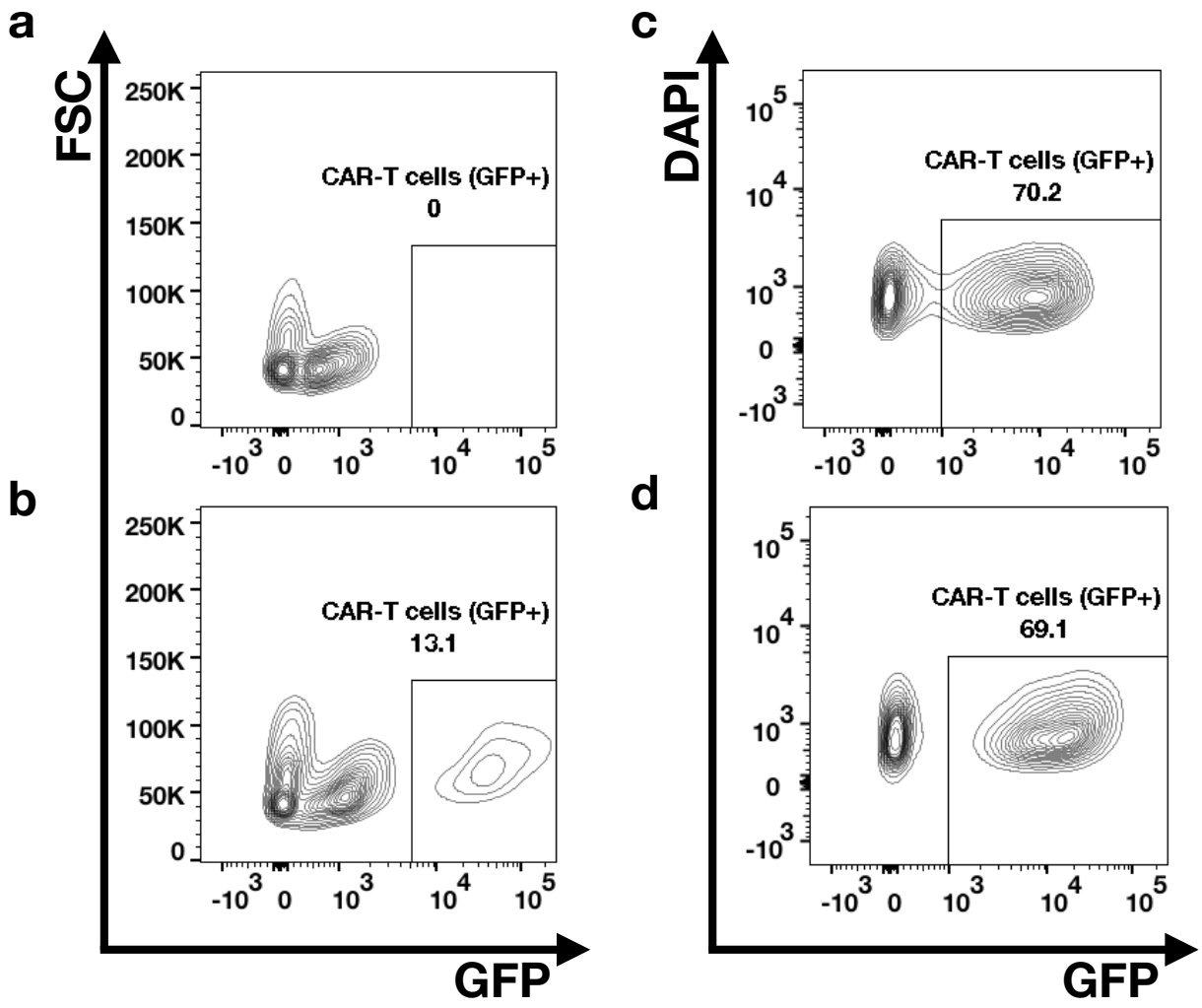

Figure 3.2. An optimized protocol efficiently produces large amounts of highly infected murine CAR-T cells. (a-b) Transduction methods using plate bound anti-mCD3e and anti-mCD28 antibodies to activate murine T-cells were inefficient (Zhong et al., 2010). Both uninfected control (a) and infected (b) T cells were only viable to 20-40% after three days in culture, on repeated experiments. (c-d) We optimized a significantly more cost effective protocol that consistently produced highly transduced (70-80% CAR-GFP+) CAR-T cells. All cells were infected with a previously reported retroviral CD28-containing 2nd generation GFP+ murine CAR-T construct against mCD19 (Kochenderfer et al., 2010). Identical constructs targeting a variety of other human and murine targets also performed the same (data not shown). Similarly, identical CAR constructs with GFP switched out for mCherry also yielded identical results (data not shown).

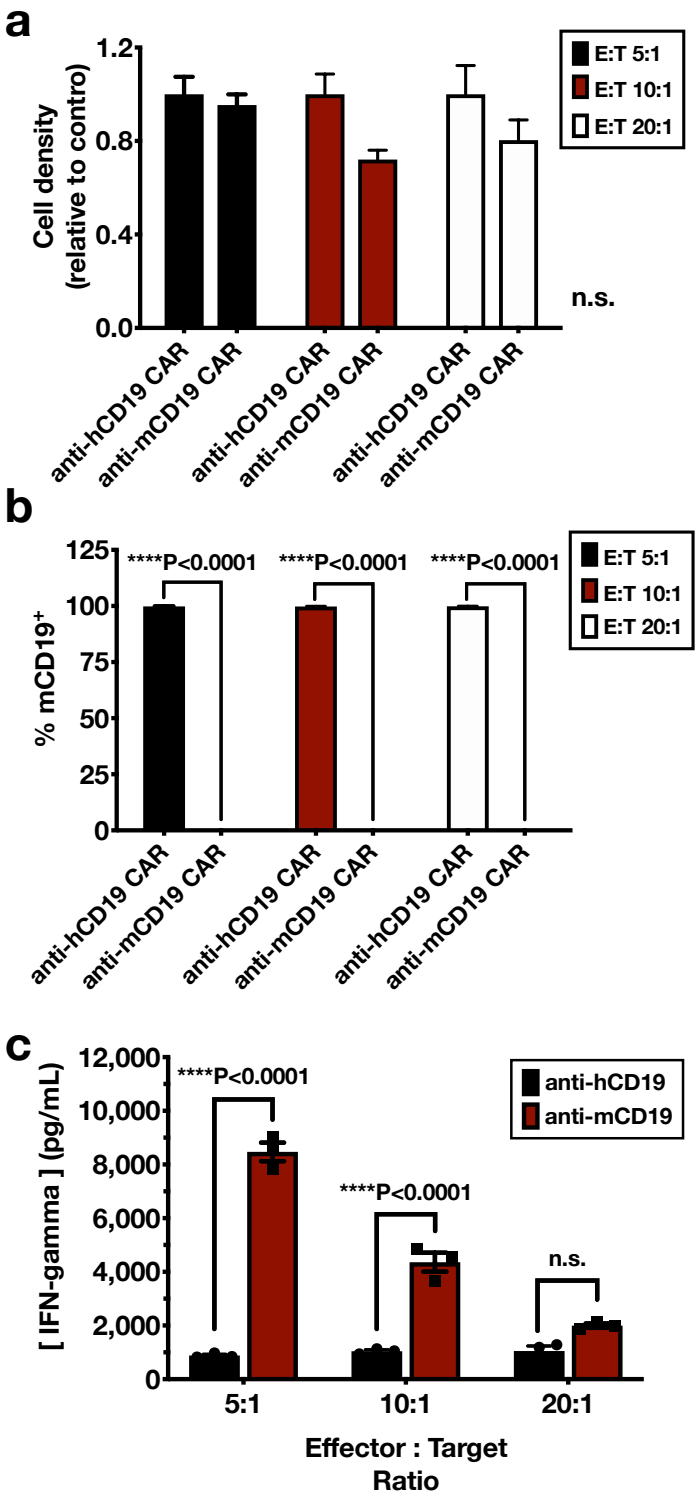

Figure 3.3. *In vitro* killing assays using mCD19+ hCD19- 20.8 target cells show that CAR-T cells are unable to suppress disease but induce dramatic antigen loss at any effector:target ratio (E:T) assayed. (a) After 24 hours of exposure to control (anti-hCD19) or anti-mCD19 CAR-T cells *in vitro*, the densities of Tomato+ mCD19+ hCD19- 20.8 cells do not change significantly. Cell density is calculated relative to wells with identical numbers of 20.8 cells seeded per E:T ratio group, but here, cells are cultured without any CAR-T cells. (b) Target 20.8 cells rapidly switch off mCD19 surface expression when exposed to anti-mCD19 CAR-T cells at any E:T ratio. (C) Enzyme-linked immunosorbent assays (ELISAs) detecting release of the proinflammatory cytokine interferon gamma (IFN-gamma) in cell culture supernatant from indicated E:T and CAR groups (from a-b). CAR-T cells against mCD19 (red) release IFN-gamma after being co-cultured with target cells that express their cognate antigen, in a graded manner. Here, more IFN-gamma is detected as the E:T ratio drops and each CAR-T cell is exposed to more B-ALL cells. Identical results are noted with all other CARs when they are exposed to their target antigen in similar experiments (data not shown). In all cases, significance is determined using a two-way ANOVA with Turkey's post-hoc test adjusted for multiple comparisons.

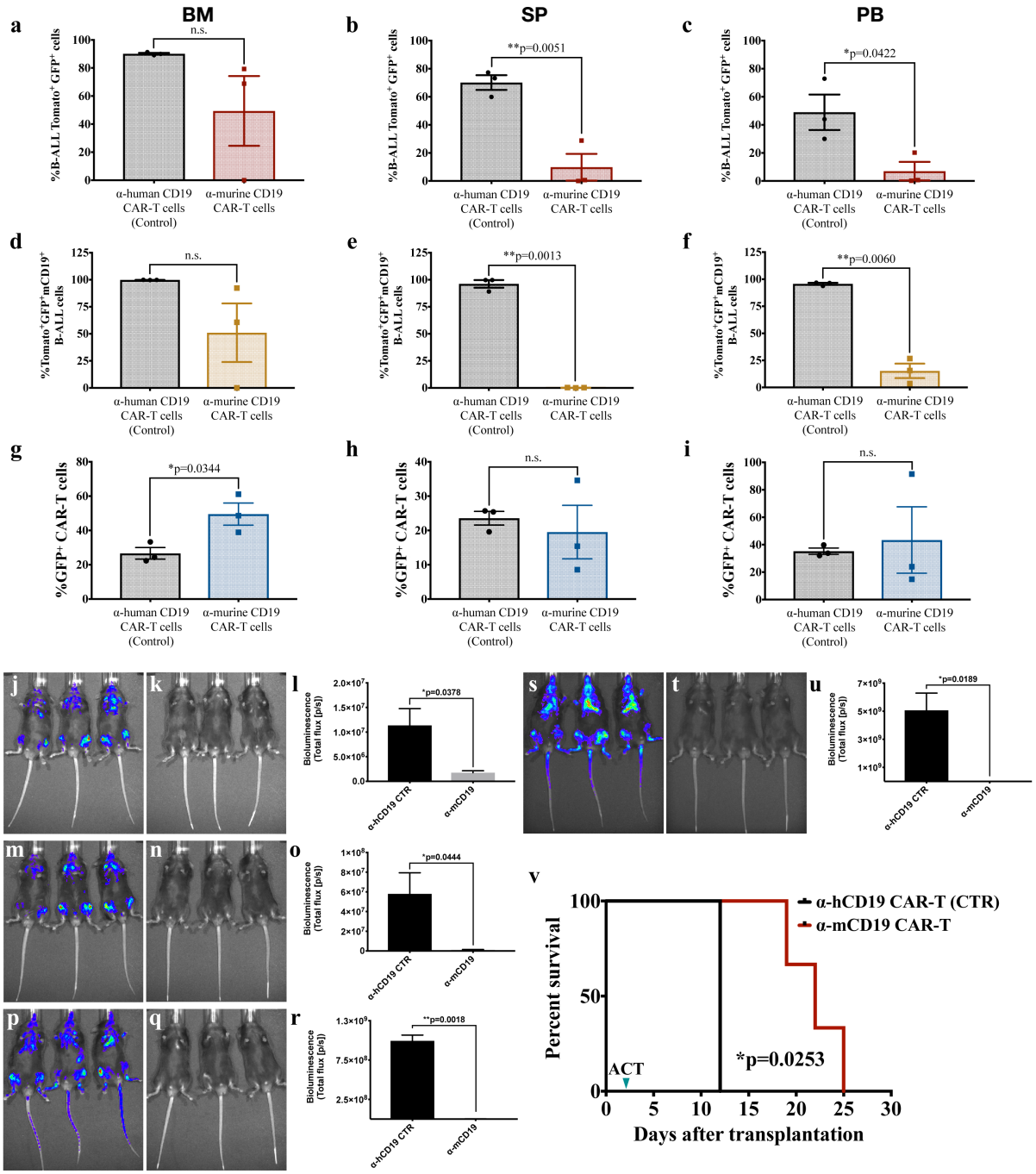

Figure 3.4. Treatment with murine CAR-T cells significantly suppresses disease and extends life in a mouse model of B-ALL. Eight-week old C57/BL6 male mice (n=3 per group) were irradiated (5 Gy) and injected with 6x10^5 mCD19+ hCD19- Cas9+ B-ALL cells (clone 20.8). Two days later, 7x10^6 CAR-T cells against either hCD19 (control) or mCD19 were adoptively transferred into mice. Moribund animals were sacrificed and tumor burden in the (a) bone marrow (BM), (b) spleen (SP), and (c) peripheral blood (PB) was quantified by flow cytometry. Significant reductions in disease burden were noted in the spleen and blood, but not in the bone marrow. Additionally, loss of the mCD19 target epitope was quantified in the bone marrow (d), spleen (e), and peripheral blood (f). Again, significant loss of the target epitope was noted in the spleen and blood, but not the bone marrow. CAR-T engraftment and expansion was most significant in the bone marrow (g), while the spleen (h) and peripheral blood (i) compartments were

not significantly different in their CAR-T engraftment from mice treated with control CAR-T cells. Disease burden was also measured by bioluminescence taken on days three (j-l), four (m-o), seven (p-r), and ten (s-u) after ACT. Here, only mice treated with control CAR-T cells (j, m, p, s) showed significant and increasing tumor burden on the days assayed. Survival analysis (v) showed that administration of $7x10^6$ CAR-T cells against mCD19 significantly extended life (red line), as compared to animals that were treated with the same dose of control CAR-T cells (black line). In all cases except panel v, significance is determined using unpaired student's t-tests. In panel v, significance is determined using a log-rank test. Results are representative of three independent experiments. The batch of CAR-T cells produced and used in this experiment were assayed *in vitro* and that matched data is shown in figure 4.3 above.

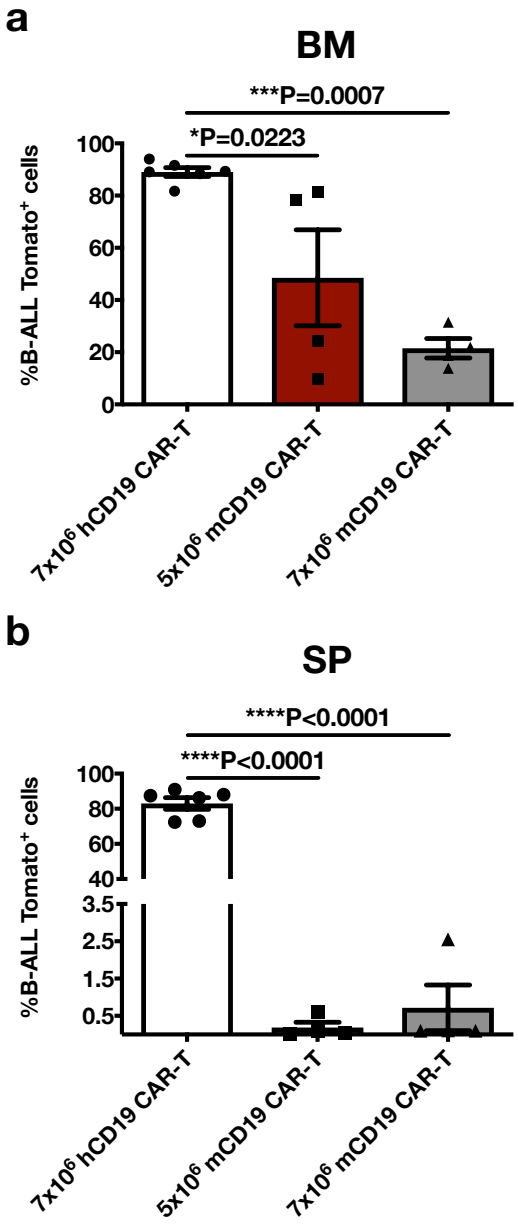

Figure 3.5. Titrating CAR-T dose *in vivo*. Experiments were conducted *in vivo* before the screen to determine the appropriate dose of CAR-T cells for either the (a) marrow (BM) or (b) spleen (SP). Male B6/C57 mice were irradiated (5 Gy) and injected with $3x10^6$ mCD19+ hCD19- Cas9+ B-ALL cells (20.8) and two days later, adoptive cell transfer (ACT) of the indicated amount and type of CAR-T cells was performed. Multiple doses ($3.5 x10^6$ to $15x10^6$) were examined and one representative experiment is shown here. (a) Four days after ACT, mice were sacrificed and organs were processed for flow cytometry analysis. Disease is successfully suppressed to 10-20% in the BM using $7x10^6$ CAR-T cells, while disease in the (b) spleen is almost completely eliminated at this dose. At a dose of $5x10^6$ CAR-T cells, BM is only suppressed to an average of about 50%, while disease in the spleen is again almost completely eliminated. Other experiments demonstrated that the appropriate dose for this organ was $3.5x10^6$ cells (data not shown). Throughout treatment, mice were monitored using bioluminescence measurements and weighed daily. Mouse weights do not significantly differ between control (anti-hCD19) and anti-mCD19 CAR-T groups and at this dose of 20.8 cells, all CAR-T doses showed little to no disease suppression (data not shown). Significance is determined using a one-way ANOVA with Turkey's post-hoc test adjusted for multiple comparisons.

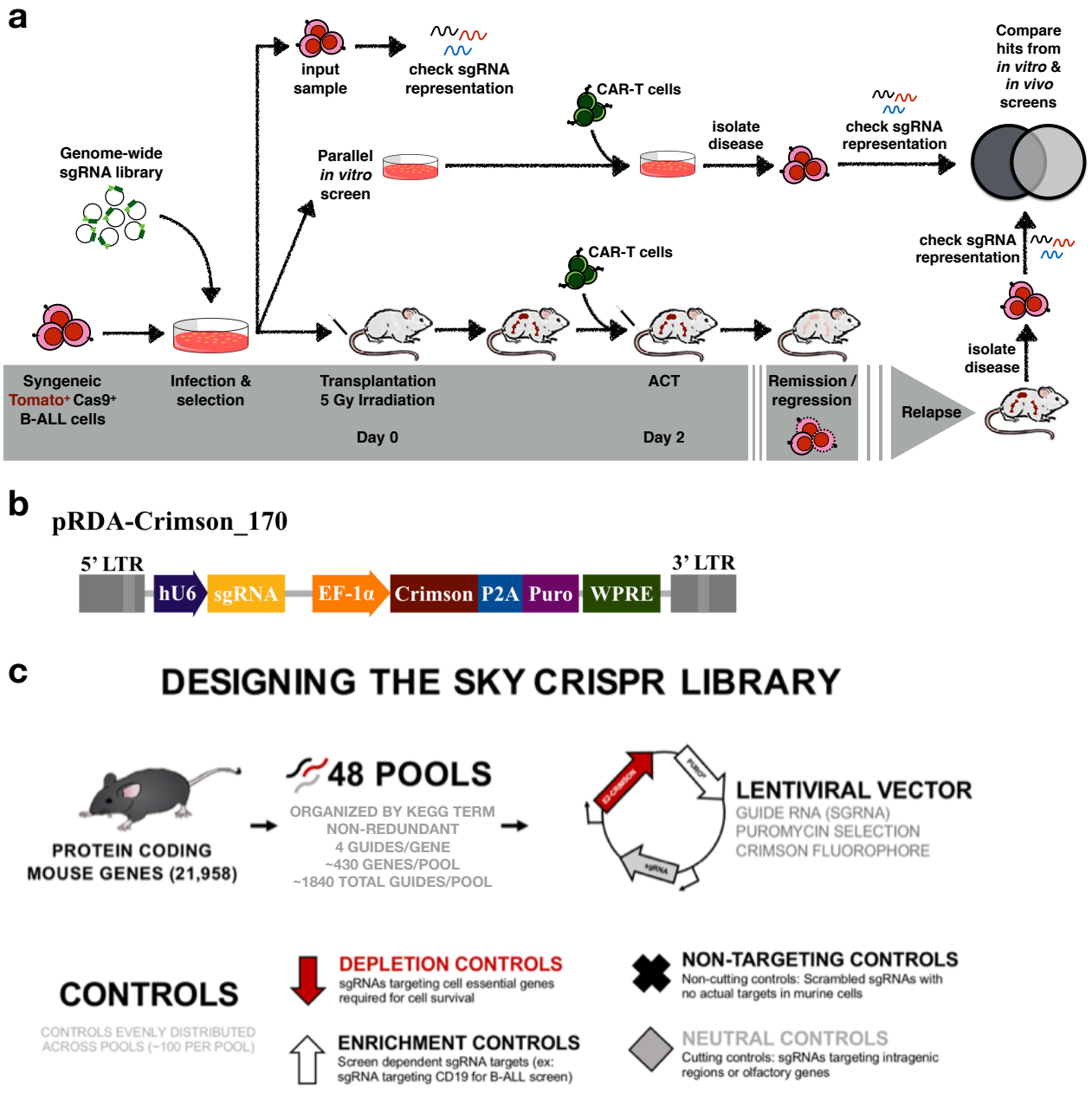

Figure 3.6. Layout of parallel *in vivo* and *in vitro* screens completed in the context of CAR-T therapy. (a) Screening layout indicating the workflow of our parallel *in vitro* and *in vivo* screens. Mice injected with $3x10^6$ Cas9+ 20.8 cells succumb to disease at day 10-11 (relapse), regardless of CAR-T type or dose. (b) Map of the lentiviral vector used to constitutively express guide RNAs off of a human U6 promoter, and Crimson and puromycin markers separated by a 2A self-cleaving peptide sequence co-expressed from an EF-1a promoter. (c) In order to facilitate this and other future *in vivo* screens in solid tumor models, we designed the SKY library, which consists of 48 pools that are each their own self-contained screening library and contain the appropriate controls (as indicated). Genes in each pool are organized by KEGG term, in a non-redundant manner. Each gene is targeted by 4 independent sgRNAs and along with about 100 control guides per pool, a total of approximately 1,840 guides are contained in each of the 48 pools.

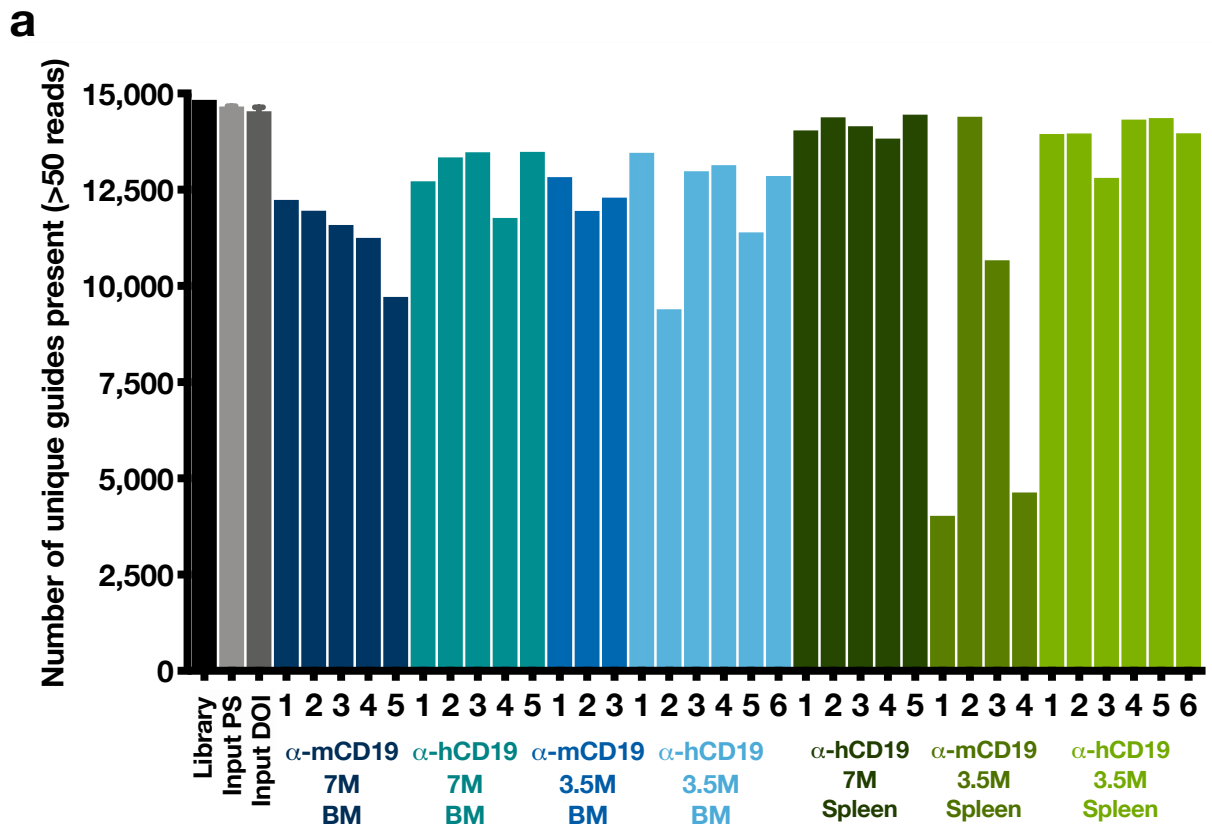

Figure 3.7. High quality sgRNA library can successfully maintain representation *in vivo*, in most organs and CAR-T doses during a small pilot screen. We are successfully able to recover the vast majority of sgRNA species upon sequencing of amplicons from *in vivo* and *in vitro* treated cells. (a) At about a 196-fold representation, upwards of 80-90% of our high-quality pilot library (first 8 pools combined, totaling 15,308 sgRNAs targeting 3,648 genes total) can be represented and maintained *in vivo* after CAR-T treatment, in all but one condition. Across 4 mice, only an average of about 50% (range: 29.9-95%) of our library could be represented in the spleens of mice treated with $3.5x10^6$ anti-mCD19 CAR-T cells. Representation is uniformly well maintained *in vitro*, with upwards of 90-95% of our library being maintained after treatment (data not shown). Input PS: input cells collected post puromycin selection (2 days before injection); Input DOI: input cells collected on the day of injection into mice.

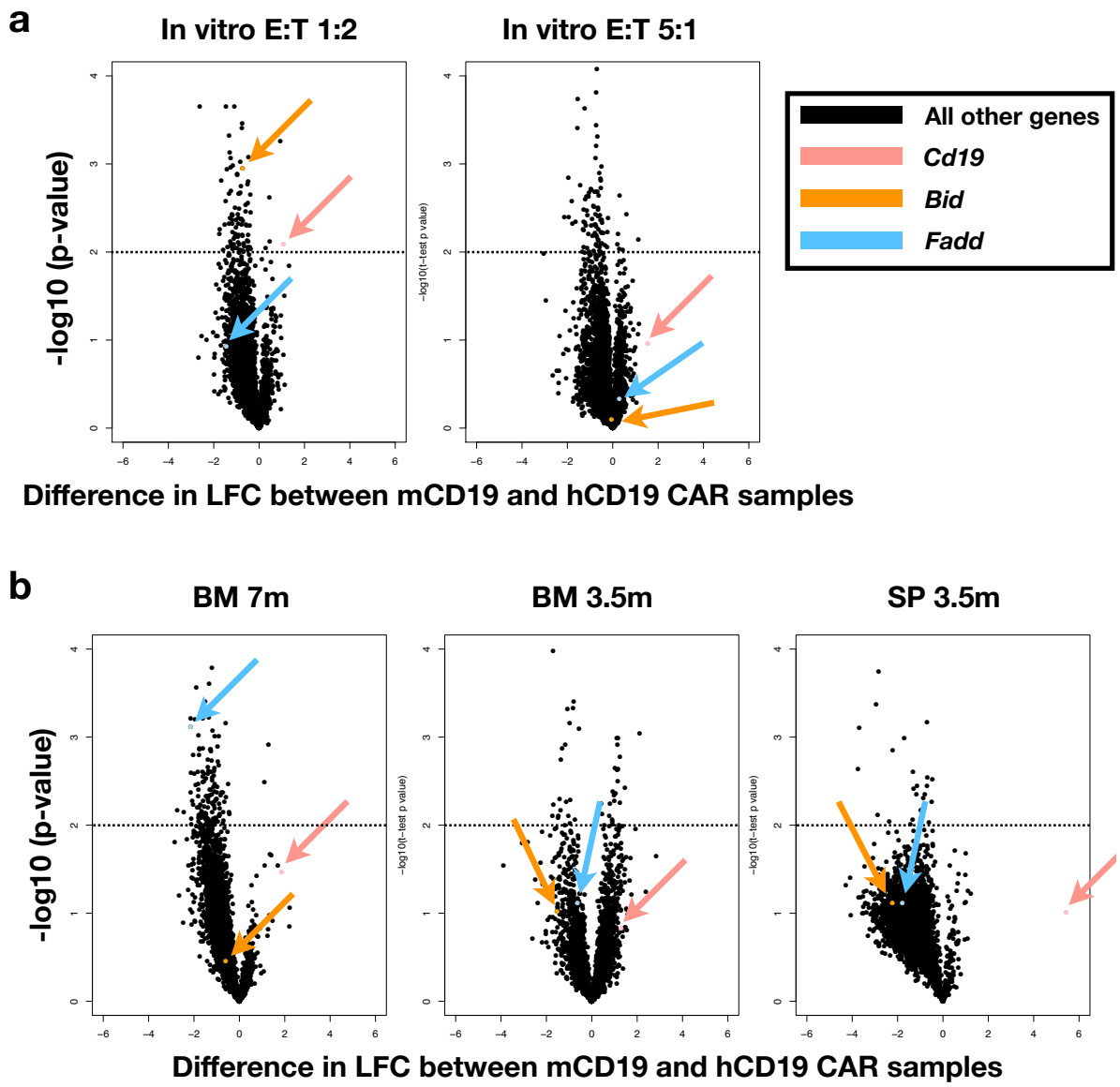

Figure 3.8. Volcano plots showing the distribution of hits in all screens. (a) In our *in vitro* arms, signals between control (hCD19) and mCD19 CAR-T conditions were low. Here, guides against *Cd19* behave as expected, enriching in cells treated with anti-mCD19 CAR-T cells. More consistent enrichment is seen in conditions where B-ALL cells are less outnumbered by CAR-T cells (E:T of 1:2, as compared to E:T of 5:1). Genes previously reported to promote resistance to CAR-T therapy in an *in vitro* screen completed in human cells (*Bid* and *Fadd*) do not consistently score in either direction in our pilot screen, either (a) *in vitro* or (b) *in vivo* (Singh et al., 2020). (b) Overall, signals for our *in vivo* 20.8 screens were also low in all conditions. Again, guides against *Cd19* enriched, but with low p-values, indicating a high amount of either mouse to mouse or guide to guide variability.

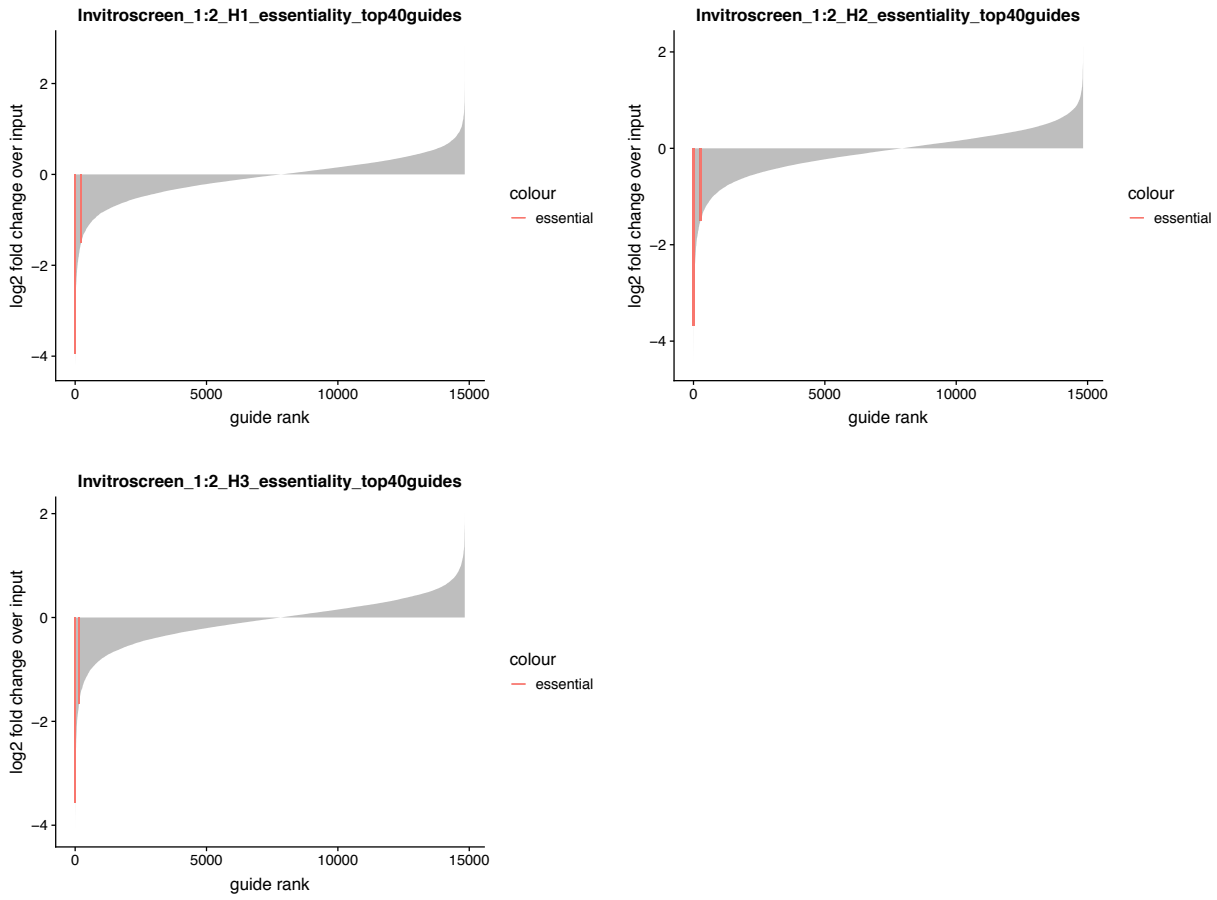

Figure 3.9. Cell essential genes consistently deplete in *in vitro* screens completed with control anti-human CD19 CAR-T cells, given at an effector to target (E:T) ratio of 1:2. To determine if guides against genes with known characteristics were behaving as expected in our *in vitro* screen (E:T of 1:2, control anti-hCD19 CAR-T cells), we examined where guides against cell essential genes (defined using the core set of consistently depleted genes across screens in the Broad Institute's Dependency Map [DepMap] project) were located globally amongst all of the guides screened in our pilot study. Consistently, guides against cell essential genes were amongst the most depleted in our screens (compared to input), as shown in the waterfall plots. For simplicity, the range of the log2 fold changes for guides against cell essential genes with the top 40 depletion scores are shown across all 3 replicates of this arm.

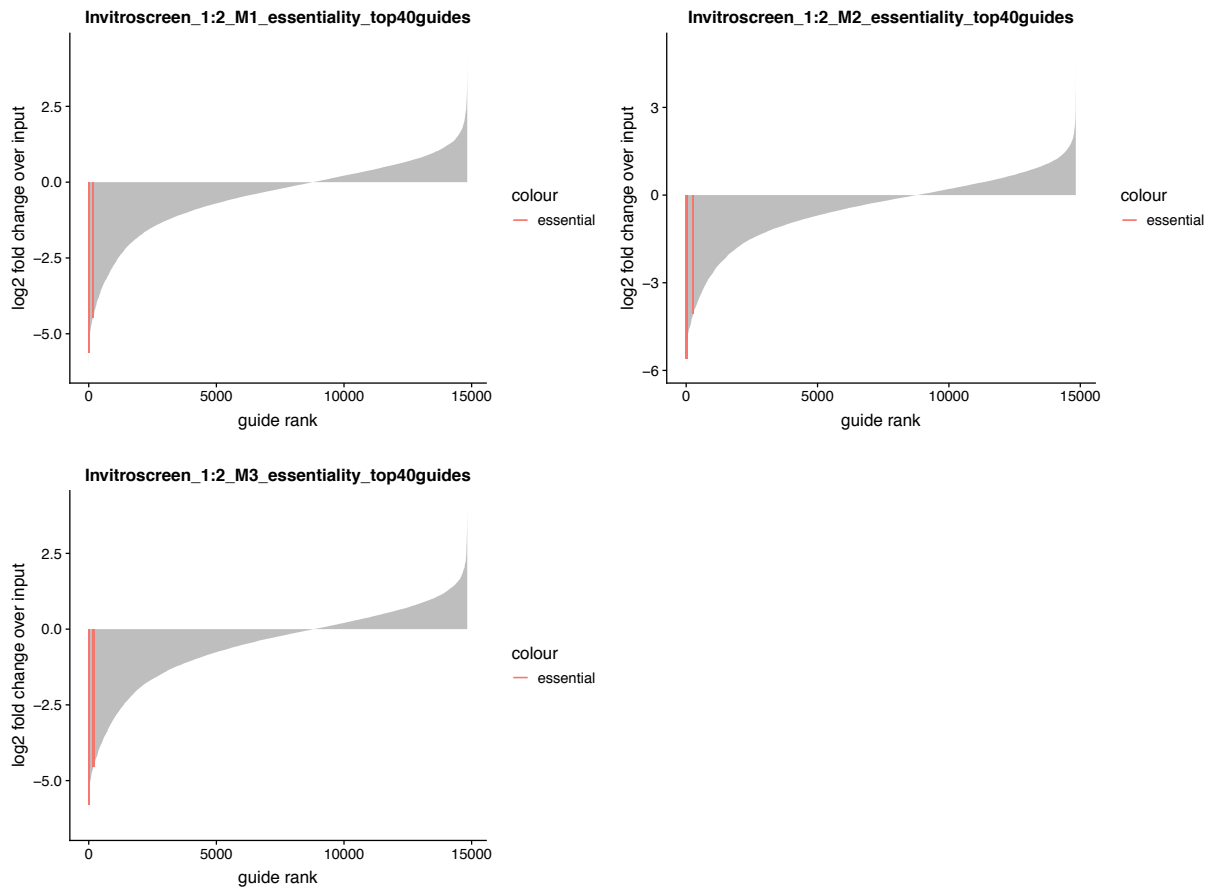

Figure 3.10. Cell essential genes consistently deplete in *in vitro* screens completed with anti-murine CD19 CAR-T cells, given at an effector to target (E:T) ratio of 1:2. To determine if guides against genes with known characteristics were behaving as expected in our *in vitro* screen (E:T of 1:2, anti-mCD19 CAR-T cells), we examined where guides against cell essential genes (defined using the core set of consistently depleted genes across screens in the Broad Institute's DepMap project) were located globally amongst all of the guides screened in our pilot study. Consistently, guides against cell essential genes were amongst the most depleted in our screens (compared to input), as shown in the waterfall plots. For simplicity, the range of the log2 fold changes guides against cell essential genes with the top 40 depletion scores are shown across all 3 replicates of this arm.

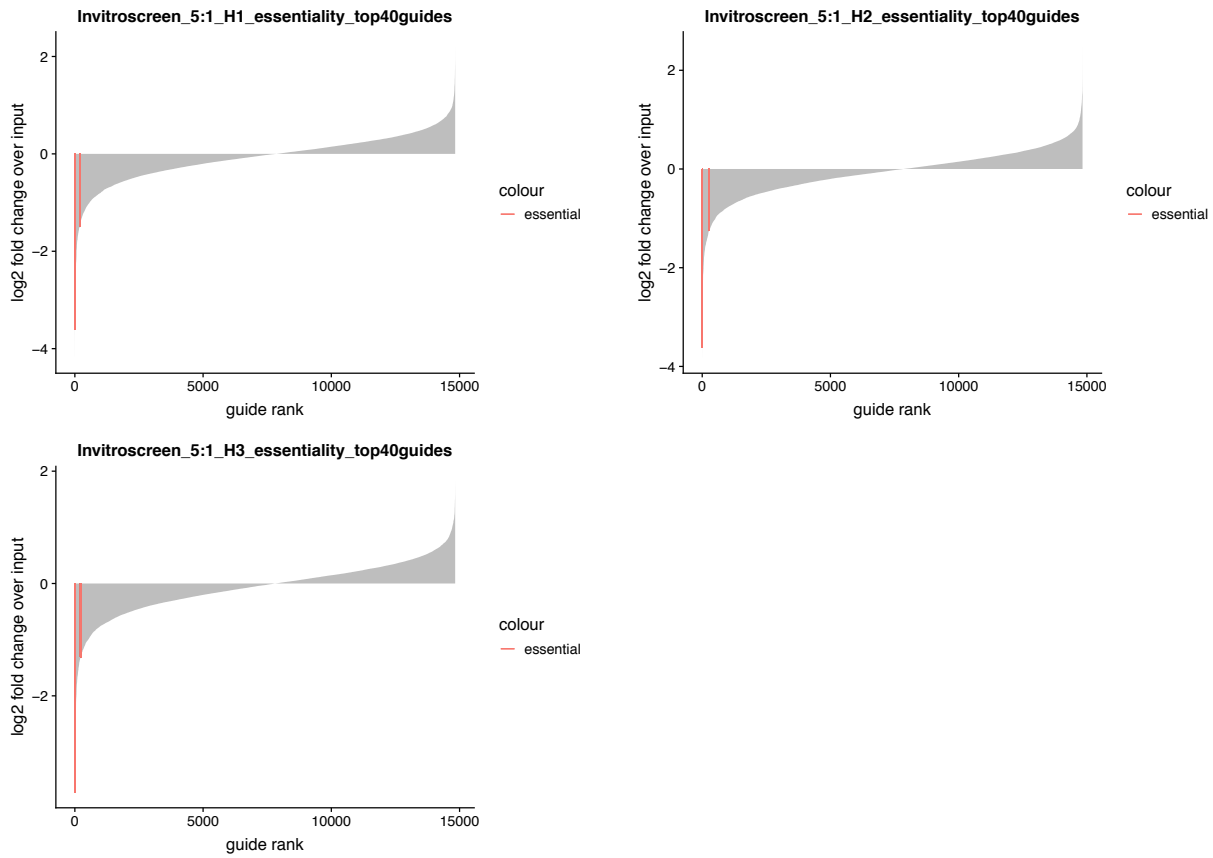

Figure 3.11. Cell essential genes consistently deplete in *in vitro* screens completed with control anti-human CD19 CAR-T cells, given at an effector to target (E:T) ratio of 5:1. To determine if guides against genes with known characteristics were behaving as expected in our *in vitro* screen (E:T of 5:1, anti-hCD19 CAR-T cells), we examined where guides against cell essential genes (defined using the core set of consistently depleted genes across screens in the Broad Institute's DepMap project) were located globally amongst all of the guides screened in our pilot study. Consistently, guides against cell essential genes were amongst the most depleted in our screens (compared to input), as shown in the waterfall plots. For simplicity, the range of the log2 fold changes for guides against cell essential genes with the top 40 depletion scores are shown across all 3 replicates of this arm.

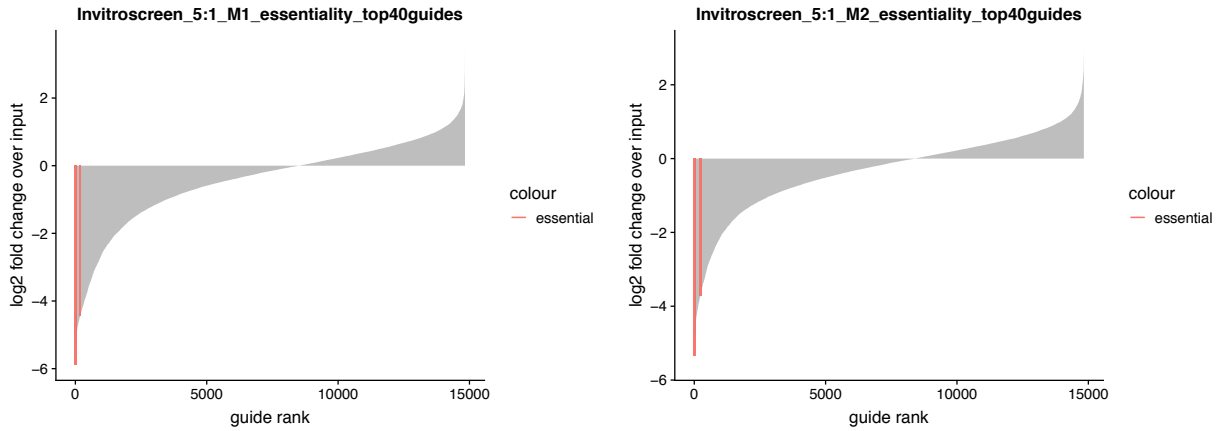

Figure 3.12. Cell essential genes consistently deplete in *in vitro* screens completed with anti-murine CD19 CAR-T cells, given at an effector to target (E:T) ratio of 5:1. To determine if guides against genes with known characteristics were behaving as expected in our *in vitro* screen (E:T of 5:1, anti-mCD19 CAR-T cells), we examined where guides against cell essential genes (defined using the core set of consistently depleted genes across screens in the Broad Institute's DepMap project) were located globally amongst all of the guides screened in our pilot study. Consistently, guides against cell essential genes were amongst the most depleted in our screens (compared to input), as shown in the waterfall plots. For simplicity, the range of the log2 fold changes for guides against cell essential genes with the top 40 depletion scores are shown across both replicates of this arm.

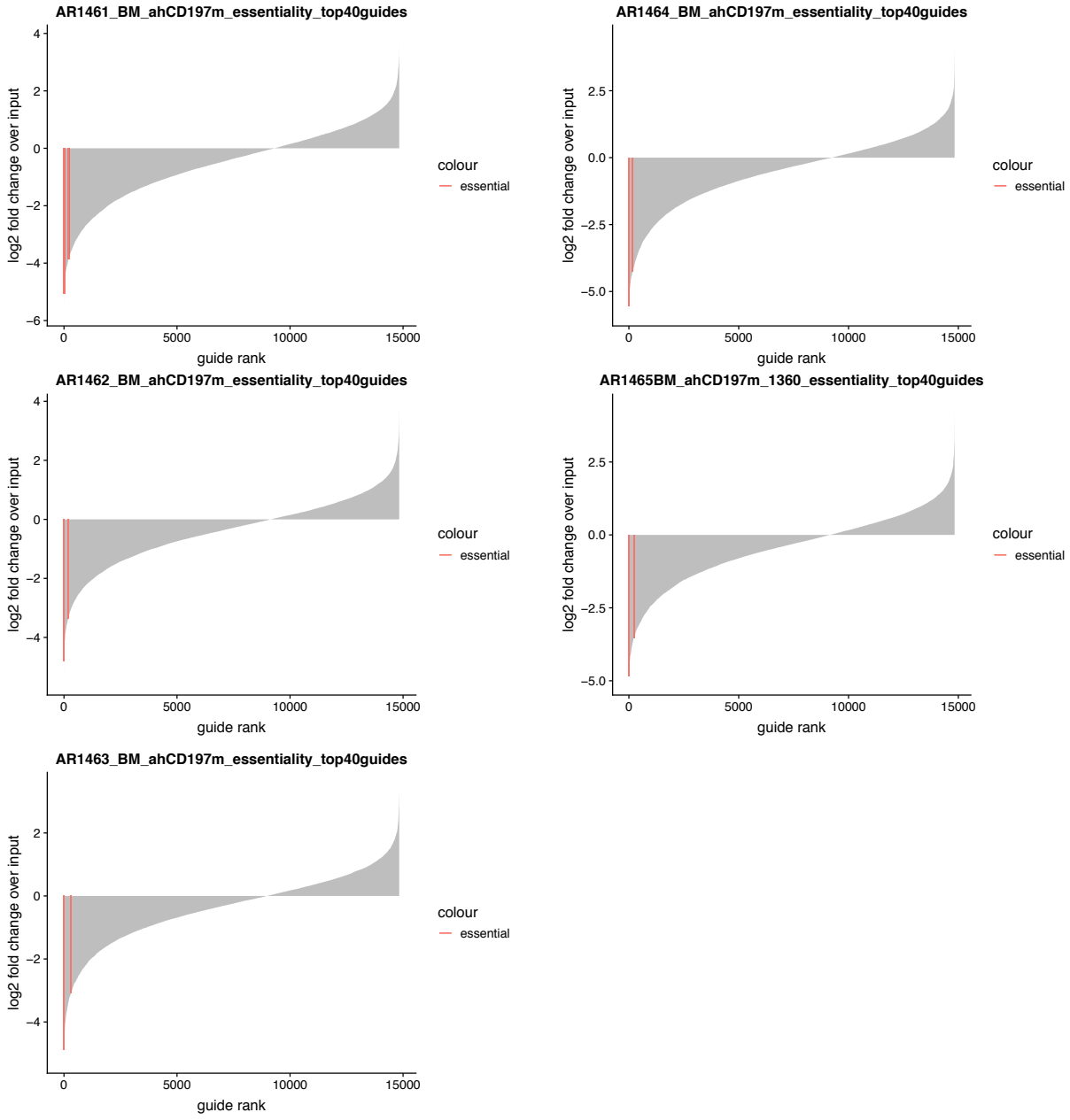

Figure 3.13. Cell essential genes consistently deplete *in vivo*, in the marrow of mice treated with 7x10^6 control anti-human CD19 CAR-T cells. To determine if guides against genes with known characteristics were behaving as expected *in vivo* (assayed in the bone marrow, 7x10^6 anti-hCD19 CAR-T cells/mouse), we examined where guides against cell essential genes (defined using the core set of consistently depleted genes across screens in the Broad Institute's DepMap project) were located globally amongst all of the guides screened in our pilot study. Consistently, guides against cell essential genes were amongst the most depleted in both this control arm, as compared to input and shown in the waterfall plots above. For simplicity, the range of the log2 fold changes for guides against cell essential genes with the top 40 depletion scores are shown across all 5 mice in this arm.

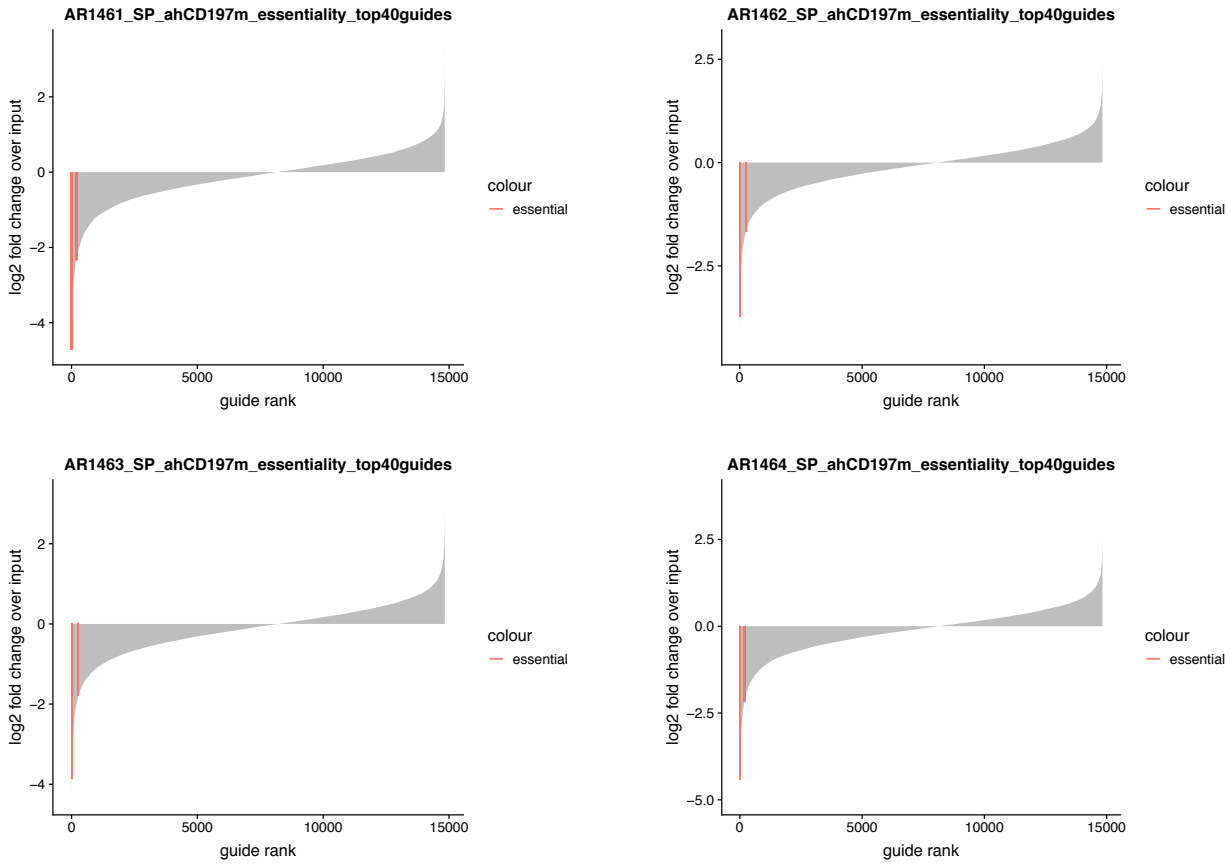

Figure 3.14. Cell essential genes consistently deplete *in vivo*, in the spleens of mice treated with 7x10^6 control anti-human CD19 CAR-T cells. To determine if guides against genes with known characteristics were behaving as expected *in vivo* (assayed in the spleen, 7x10^6 anti-hCD19 CAR-T cells/mouse), we examined where guides against cell essential genes (defined using the core set of consistently depleted genes across screens in the Broad Institute's DepMap project) were located globally amongst all of the guides screened in our pilot study. Consistently, guides against cell essential genes were amongst the most depleted in this control arm and in the spleens of mice treated with 3.5x10^6 control CAR-T cells (data not shown), as compared to input and shown in the waterfall plots above. For simplicity, the range of the log2 fold changes for guides against cell essential genes with the top 40 depletion scores are shown across all 4 mice in this arm.

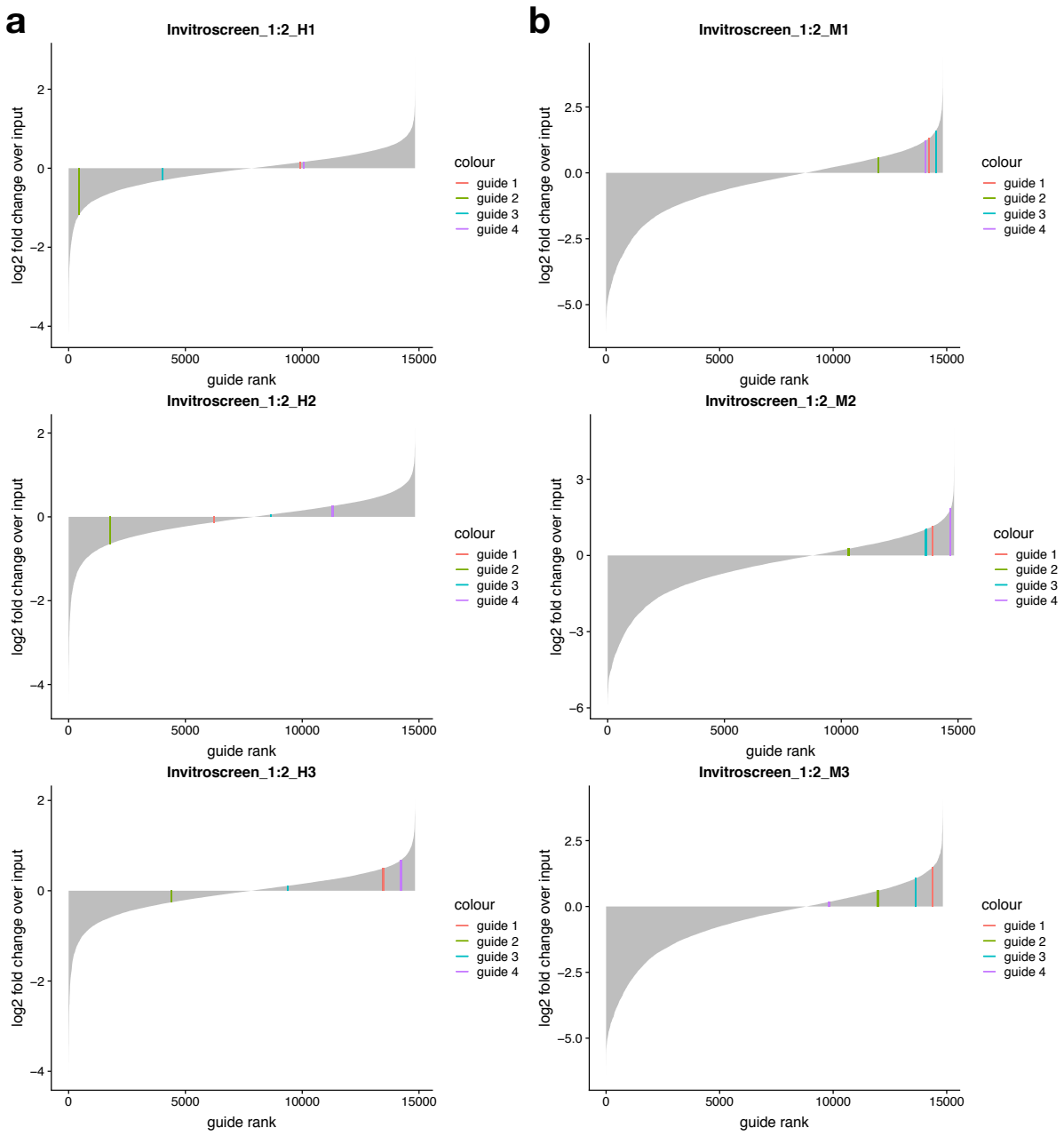

Figure 3.15. Guides against *Cd19* consistently enrich specifically when target cells are exposed to anti-murine CD19 CAR-T cells *in vitro*. Waterfall plots ordering all guides in our pilot study by their log2 fold change in the indicated experimental conditions compared to input samples. (a) *Cd19* guides are randomly distributed in 3 replicates of the *in vitro* arm completed with control (anti-hCD19) CAR-T cells at an E:T of 1:2. (b) When anti-mCD19 CAR-T cells are given at the same E:T ratio however, *Cd19* sgRNAs consistently enrich.

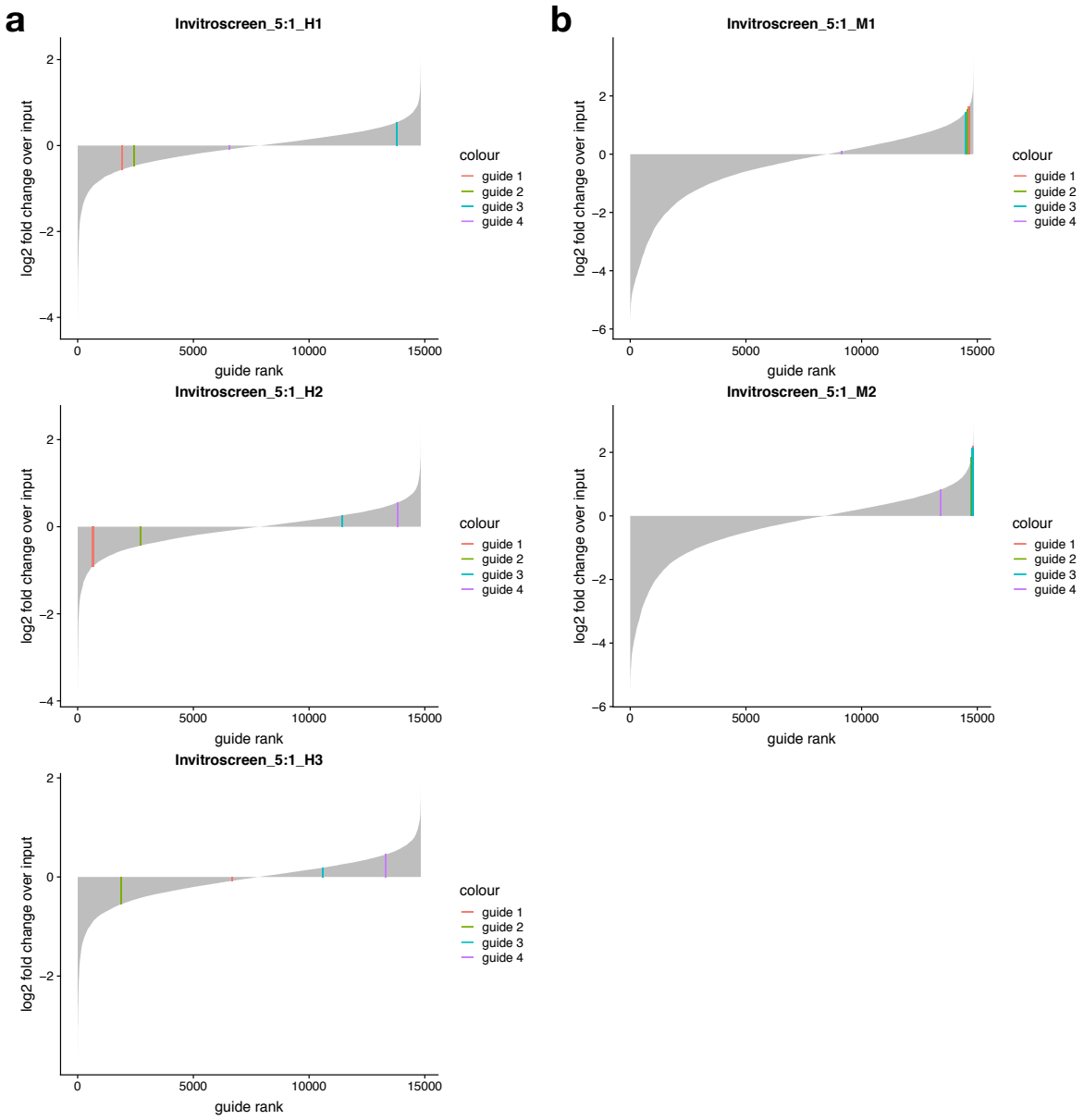

Figure 3.16. Guides against *Cd19* consistently enrich specifically when target cells are exposed to anti-murine CD19 CAR-T cells *in vitro*. Waterfall plots ordering all guides in our pilot study by their log2 fold change in the indicated experimental condition compared to input sample. (a) *Cd19* guides are randomly distributed in 3 replicates of the *in vitro* arm completed with control (anti-hCD19) CAR-T cells at an E:T of 5:1. (b) When anti-mCD19 CAR-T cells are given at the same E:T ratio however, *Cd19* sgRNAs consistently enrich. Notably, *Cd19* guide enrichment appears more consistent but less dramaric (in terms of log2 fold change values) than in screens with lower E:T ratios of 1:2 (figure 3.15b).

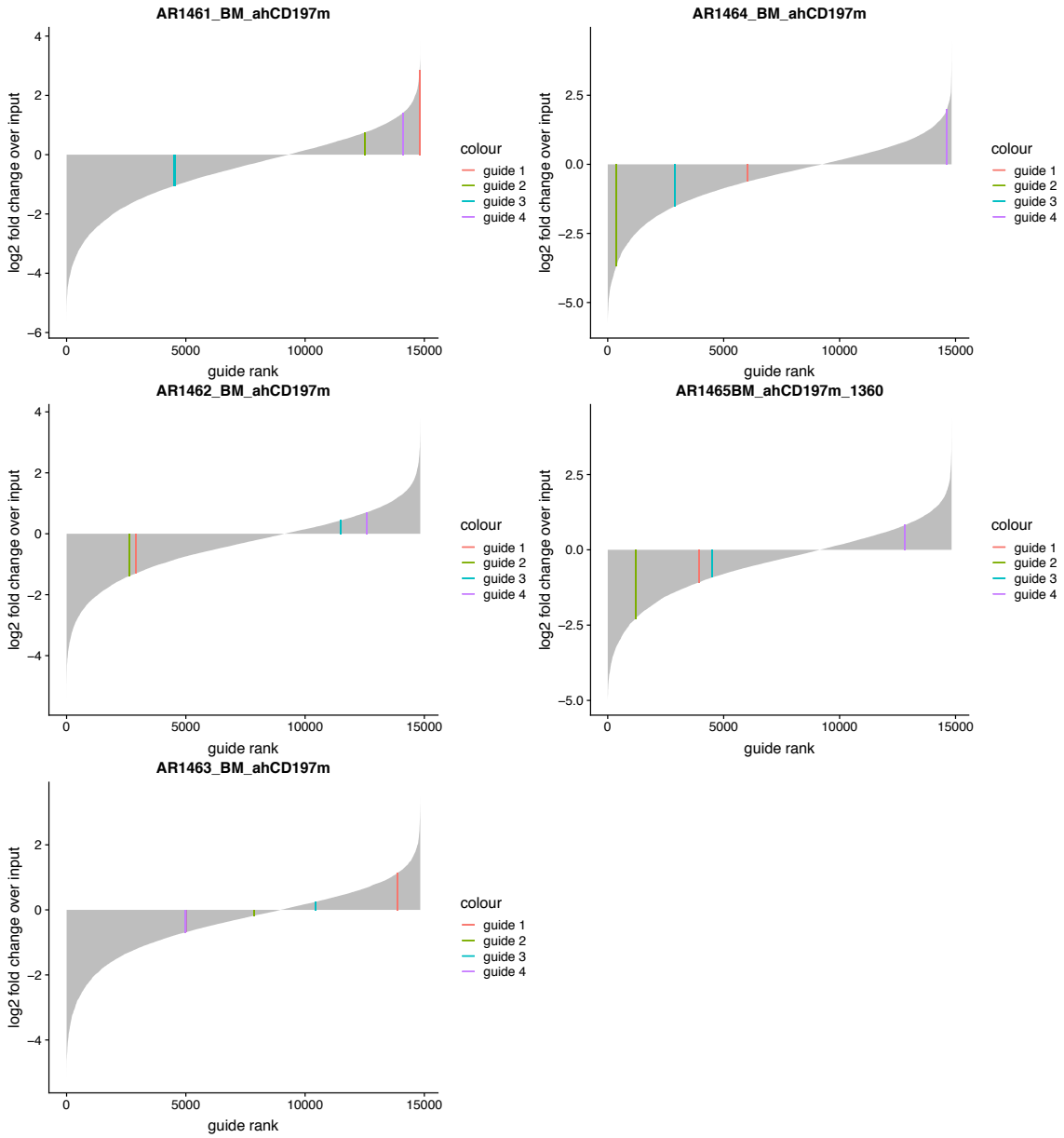

Figure 3.17. Guides against *Cd19* are randomly distributed in the marrow of mice treated with 7x10^6 control CAR-T cells *in vivo*. Waterfall plots ordering all guides in our pilot study by their log2 fold change in the indicated experimental condition compared to input sample. As expected, *Cd19* guides are randomly distributed in the marrow of 5 mice treated with 7x10^6 control (anti-hCD19) CAR-T cells.

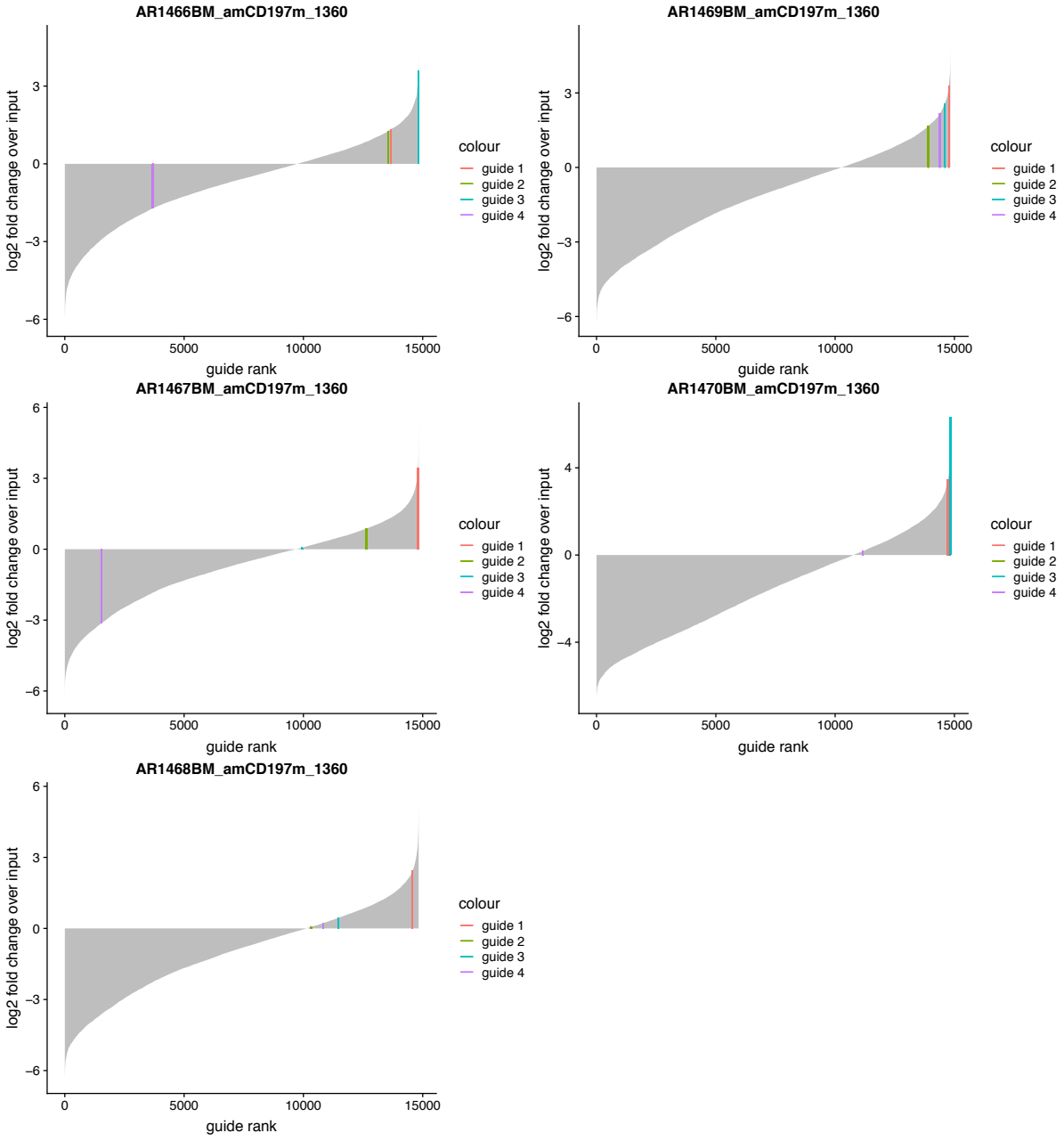

Figure 3.18. Guides against *Cd19* more consistently enrich in the marrow of mice treated with 7x10^6 anti-mCD19 CAR-T cells *in vivo*, as compared to mice treated with the same number of control CAR-T cells. Waterfall plots ordering all guides in our pilot study by their log2 fold change in the indicated experimental condition compared to input sample. As expected, *Cd19* guides more consistently show enrichment phenotypes in the marrow of 5 mice treated with 7x10^6 anti-mCD19 CAR-T cells, as compared to the marrow of mice treated with control (anti-hCD19) CAR-T cells (figure 3.17).

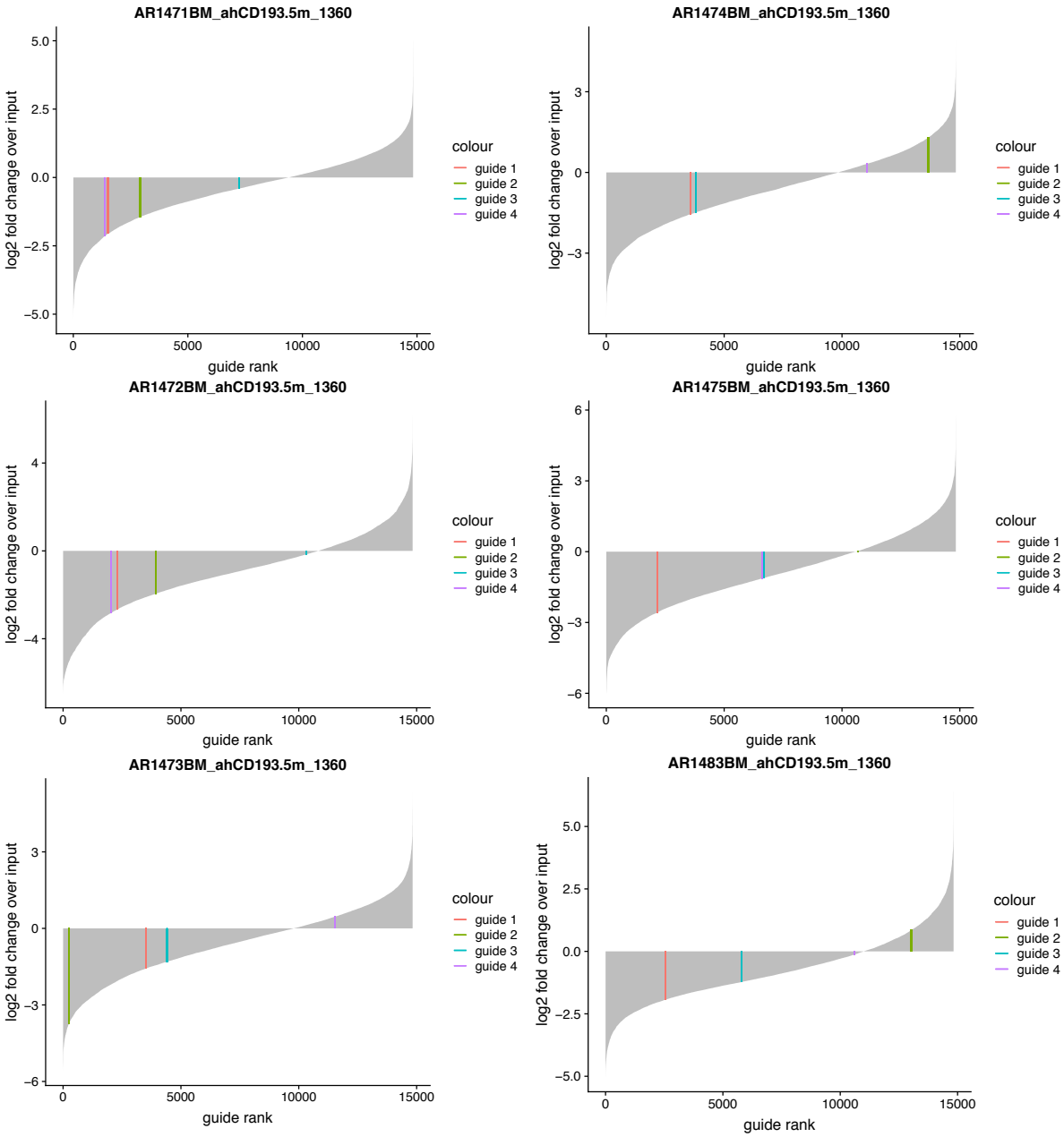

Figure 3.19. Guides against *Cd19* are randomly distributed in the marrow of mice treated with 3.5x10^6 control CAR-T cells *in vivo*. Waterfall plots ordering all guides in our pilot study by their log2 fold change in the indicated experimental condition compared to input sample. As expected, *Cd19* guides are randomly distributed in the marrow of 6 mice treated with 3.5x10^6 control (anti-hCD19) CAR-T cells.

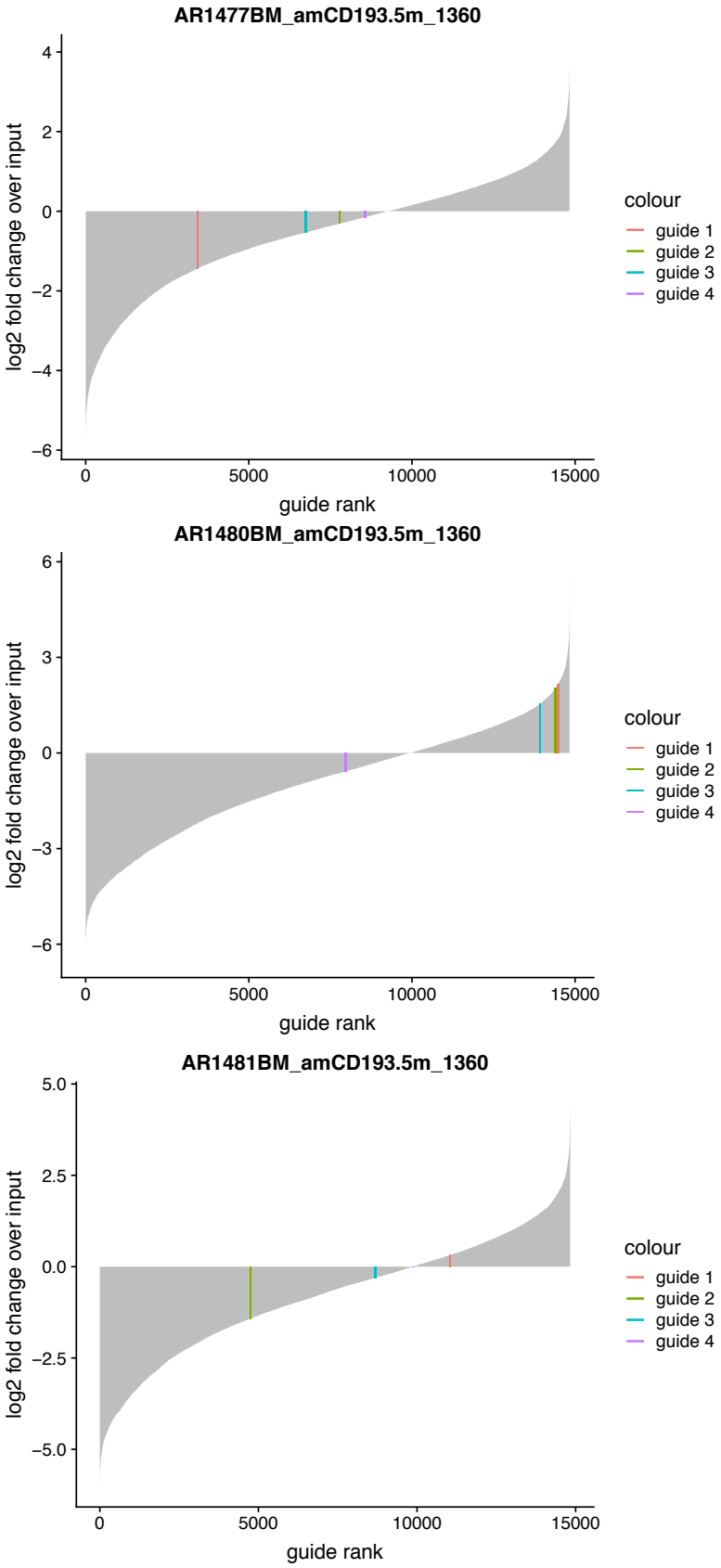

Figure 3.20. Guides against *Cd19* enrich in the marrow of one of three mice treated with $3.5x10^6$ anti-mCD19 CAR-T cells *in vivo*. Waterfall plots ordering all guides in our pilot study by their log2 fold change in the indicated experimental condition compared to input sample. *Cd19* guides consistently show enrichment phenotypes in the marrow of 1 of 3 mice treated with $3.5x10^6$ anti-mCD19 CAR-T cells, as compared to the marrow of mice treated with control (anti-hCD19) CAR-T cells (figure 3.19). This indicates that likely, the biological pressure induced by this dose of CAR-T cells was too low for this anatomical compartment.

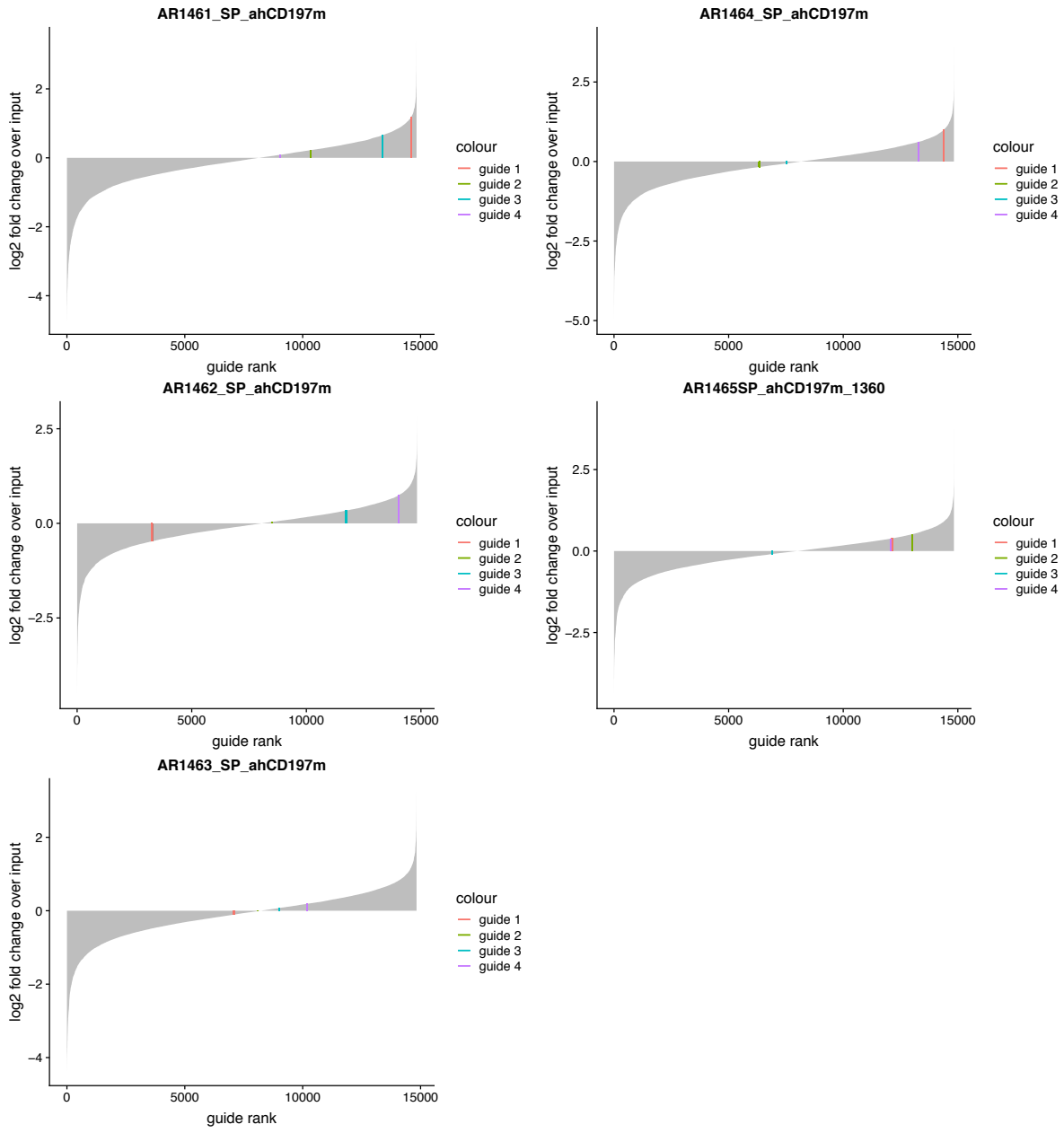

Figure 3.21. Guides against *Cd19* are randomly distributed in the spleens of mice treated with 7x10^6 control CAR-T cells *in vivo*. Waterfall plots ordering all guides in our pilot study by their log2 fold change in the indicated experimental condition compared to input sample. As expected, *Cd19* guides are randomly distributed in the spleens of 5 mice treated with 7x10^6 control (anti-hCD19) CAR-T cells.

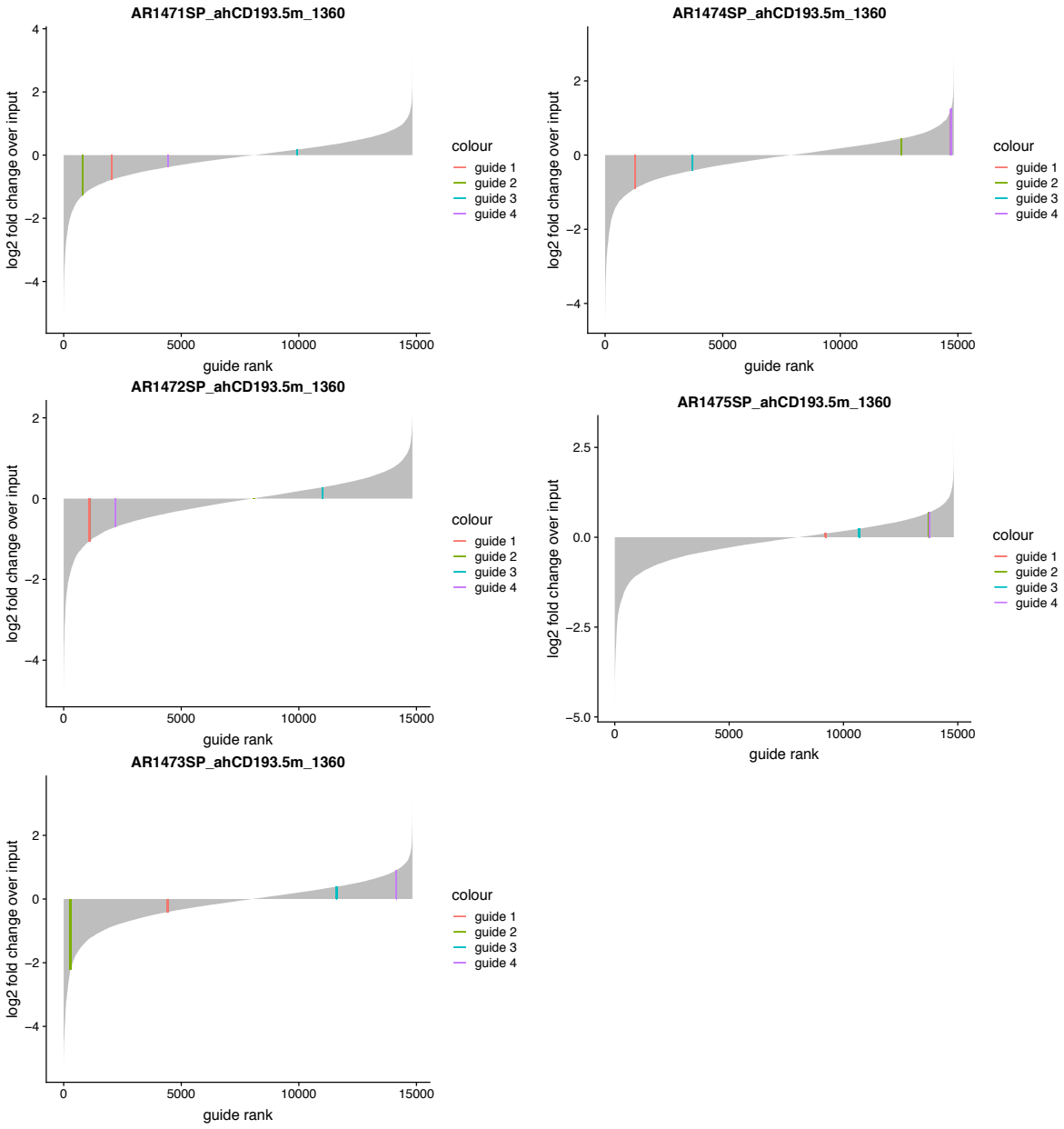

Figure 3.22. Guides against *Cd19* are randomly distributed in the spleens of mice treated with 3.5x10^6 control CAR-T cells *in vivo*. Waterfall plots ordering all guides in our pilot study by their log2 fold change in the indicated experimental condition compared to input sample. As expected, *Cd19* guides are randomly distributed in the spleens of 5 mice treated with 3.5x10^6 control (anti-hCD19) CAR-T cells.

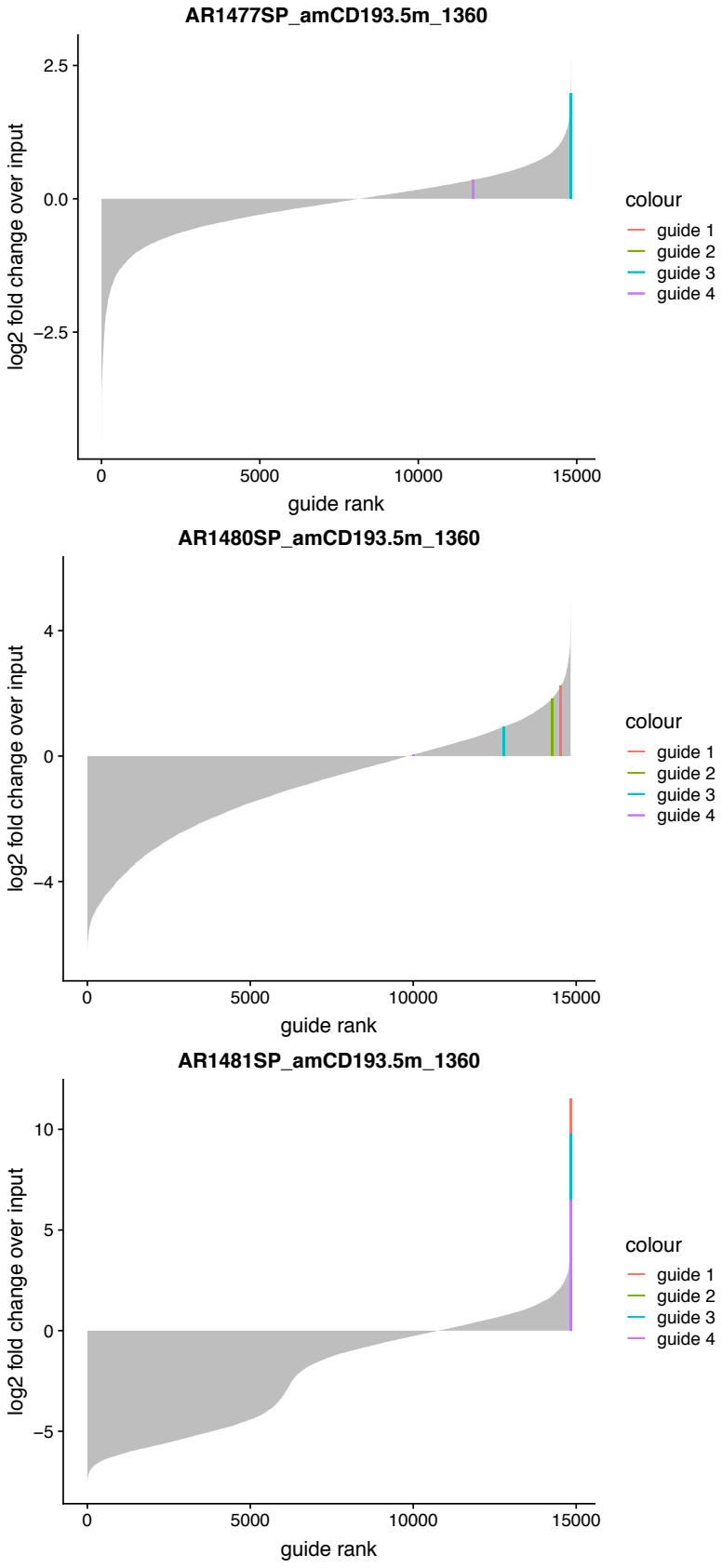

Figure 3.23. Guides against *Cd19* more consistently and dramatically enrich in the spleens of three mice treated with 3.5x10^6 anti-mCD19 CAR-T cells *in vivo*, as compared to mice treated with the same number of control CAR-T cells. Waterfall plots ordering all guides in our pilot study by their log2 fold change in the indicated experimental condition compared to input sample. As expected, *Cd19* guides more consistently show enrichment phenotypes in the spleens of all 3 mice treated with 3.5x10^6 anti-mCD19 CAR-T cells, as compared to the spleens of mice treated with the same dose of control (anti-hCD19) CAR-T cells (figure 3.22).

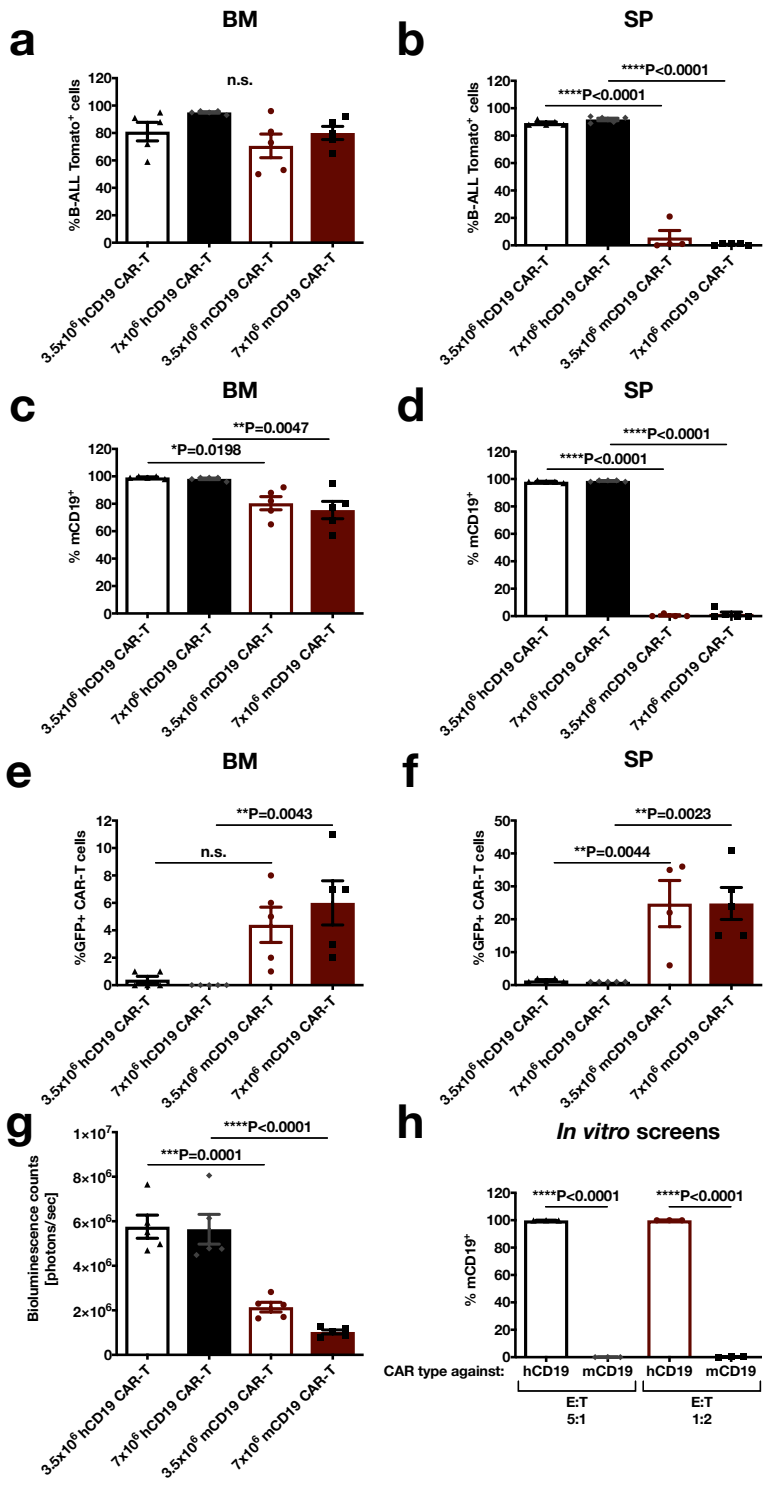

Figure 3.24. CAR-T cells used during our pilot screen were highly functional. Flow cytometric analysis of disease suppression in moribund animals, as assayed in the (a) marrow (BM) and (b) spleen (SP). (a) As expected, no dose of anti-mCD19 CAR-T cells could suppress disease in the marrow of moribund animals. (b) Conversely, as noted in previous experiments, both doses of mCD19-targeting CAR-T cells significantly and persistently suppressed disease, even in moribund animals. Stains for surface expression of mCD19 were also completed in these organs (c-d), demonstrating that the target epitope was significantly lost on cells resident in both compartments after exposure to anti-mCD19 CAR-T cells. (d) Albeit, this phenotype was considerably more pronounced in the spleen. CAR-T persistence was assayed in both the (e) BM and (f) SP. CAR-T cells could be detected in the marrow, but to a lower extent than normally observed in non-screening experiments (figure 3.4). (f) CAR-T persistence rates in the spleen matched those previously observed. (g) Results from bioluminescence imaging studies completed four days after ACT demonstrate a significant reduction in disease burden that appears to occur in an anti-mCD19 CAR-T cell dose dependent manner. (h) Cells treated with anti-mCD19 CAR-T cells at either an E:T ratio of 5:1(black) or 1:2 (red) demonstrate dramatic antigen loss. In all cases, significance is determined using a one-way ANOVA with Turkey's post-hoc test adjusted for multiple comparisons.

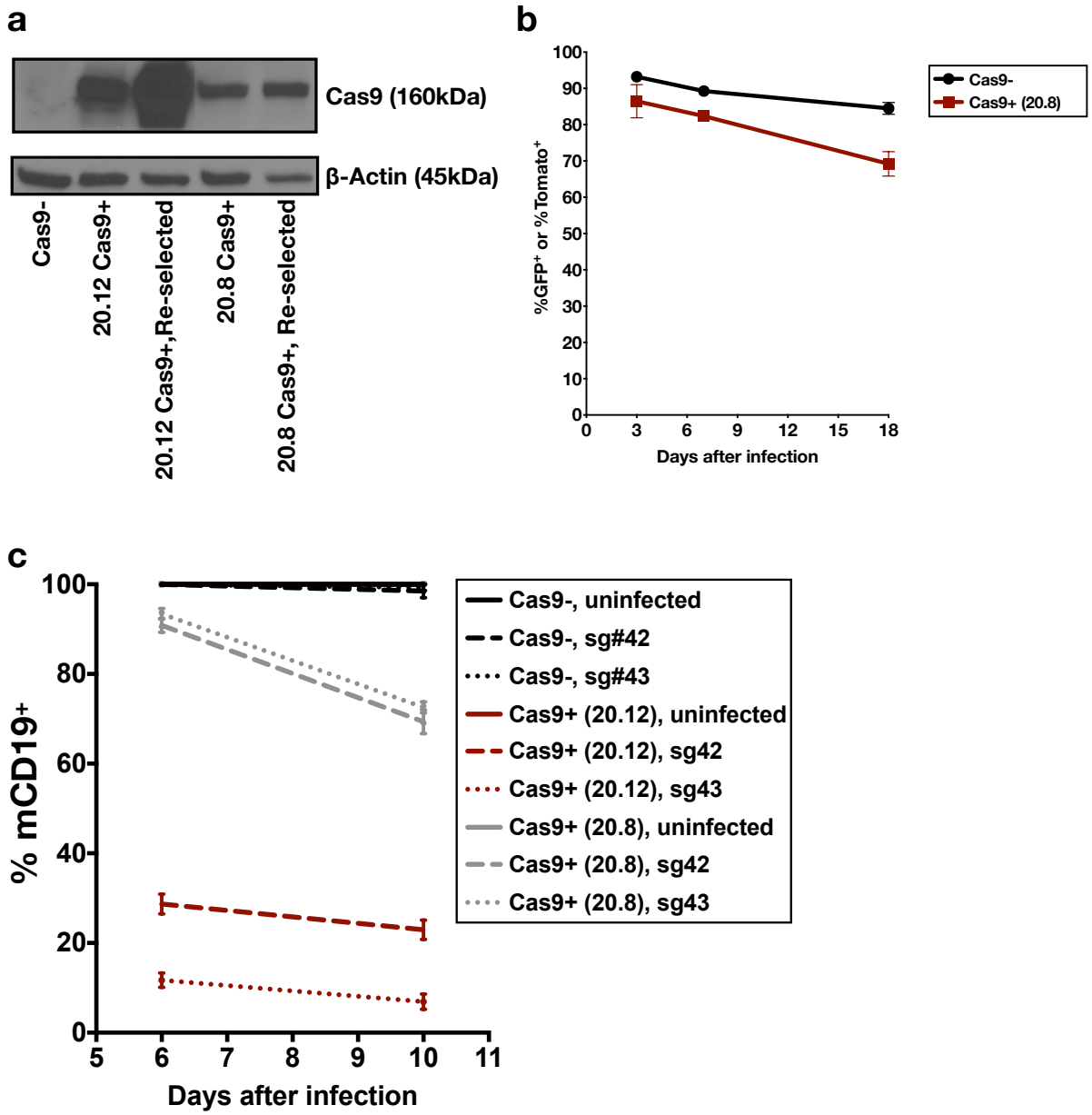

Figure 3.25. The Tomato+ Cas9+ clone 20.8 appears to lose Cas9 expression in as little as four weeks, while the mCherry+ GFP+ Cas9+ clone 20.12 continues to cut efficiently, even after four or more weeks of culture. (a) Clones 20.12 and 20.8 were thawed and cultured normally or re-selected with blasticidin (20 μg/mL) for seven days. Selected Cas9+ clones showed an increase in Cas9 protein expression, as assayed by western blot analysis. (b) Re-selected cells were cultured over longer periods and assayed for Cas9 cutting efficiency over time. After four weeks in culture, re-selected 20.8 cells could no longer efficiently induce fluorescence loss in the traditional cut assay (b) or loss of surface mCD19 expression using two independent and non-overlapping guides. mCherry+ GFP+ hCD19+ mCD19+ Cas9+ clone 20.12 was thawed, re-selected, and repeatedly tested in parallel with 20.8 cells. Unlike 20.8 cells, 20.12 cells maintain strong cutting abilities even after four weeks of culture, as shown by the significant loss of mCD19 surface expression using the same two guides. Early cultures of re-selected 20.12 cells were frozen and subsequently used for all future experiments.

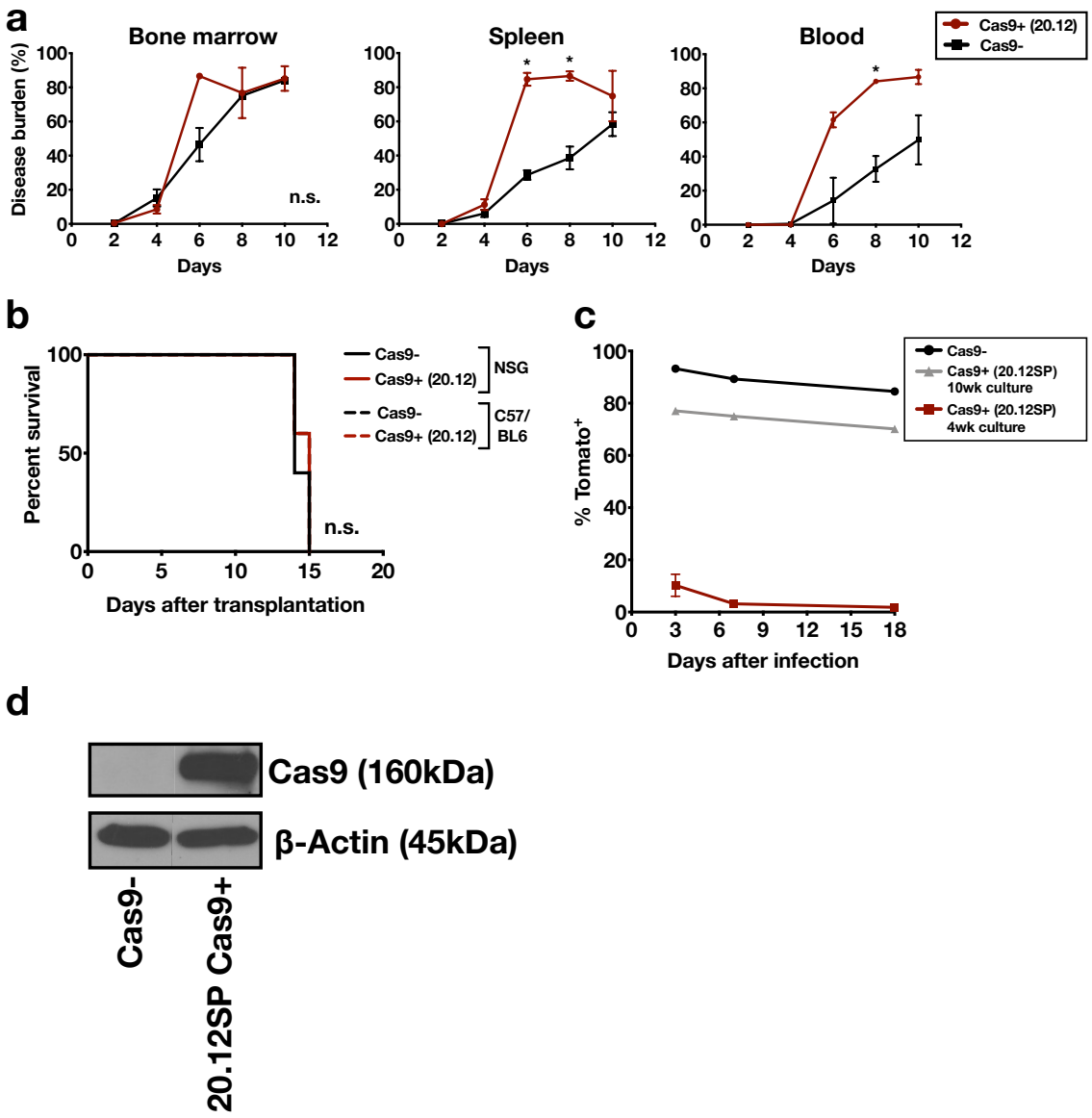

Figure 3.26. Cas9 and human CD19 are not additionally immunogenic in a mouse model of BCR-ABL+ B-ALL transplanted into non-irradiated immunecompetent recipient mice. (a) mCherry+ GFP+ hCD19+ mCD19+ Cas9 expressing (clone 20.12) cells show highly similar growth kinetics as mCherry+ GFP+ Cas9- parental cells in hematopoietic organs, as assayed by flow cytometry on the indicated days. Non-irradiated eight week-old male C57/BL6 mice (n=6 per group) were transplanted with $5x10^5$ cells. Significance is determined using unpaired student's t-tests at every time point with Bonferroni correction for multiple comparisons. (b) Non-irradiated immunocompetent (C57/BL6) male mice and immunocompromised (NSG) mice succumb to both Cas9- and Cas9+ (20.12) disease at the same time, indicating that Cas9 is not additionally immunogenic in our cell line. All mice (n=5 per group) were injected with $5x10^5$ cells. Significance is determined using a log-rank test. (c) An *in vitro* cut assay using an all-in-one vector expressing a fast-degradable Tomato cassette and a validated sgRNA against it (Doench et al., 2014) was used to assay Cas9 cutting efficiency in non-re-selected mCherry- GFP+ 20.12SP (single positive) cells over time, showing that cells are finished cutting at day 3, even after 4 weeks of long term culture. By 10 weeks in culture however, Cas9 cutting efficiency is significantly reduced and the clone is no longer "screenable". (d) Western blot (WB) showing that non-re-selected mCherry- GFP+ 20.12SP cells still express Cas9 after 4 weeks of culture. For all panels, repeated experiments displayed identical results.

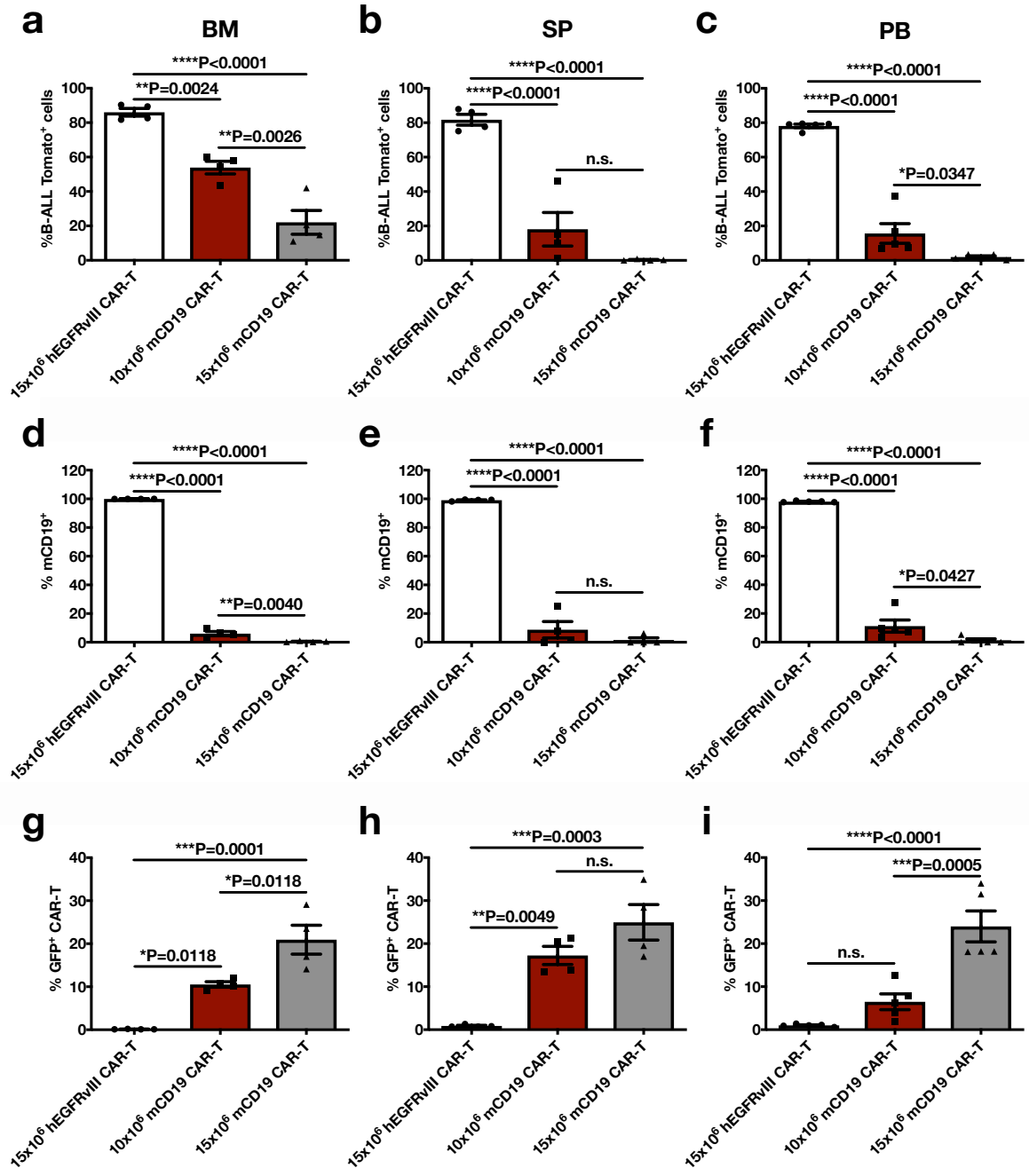

Figure 3.27. Titrating CAR-T dose for 20.12 cells. Experiments were conducted *in vivo* before the screen to determine the appropriate dose of CAR-T cells for either the (a) marrow (BM) or (b) spleen (SP). Male B6/C57 mice were irradiated (5 Gy) and injected with $3x10^6$ mCherry+ GFP+ mCD19+ hCD19+ Cas9+ B-ALL cells (20.12) and two days later, adoptive cell transfer (ACT) of the indicated amount and type of CAR-T cells was performed. Multiple doses ($3.5 x10^6$ to $15x10^6$) were examined and one representative experiment is shown here. Four days after ACT, mice were sacrificed and organs were processed for flow cytometry analysis. (a) Disease is successfully suppressed to 10-20% in the BM using $15x10^6$ CAR-T cells, while disease in the (b) spleen is almost completely eliminated at this dose. At a dose of $10x10^6$ CAR-T cells, (a) BM is only suppressed to an average of 55%, while disease in the (b) spleen is suppressed to an average of 15-20%. Throughout treatment, mice were monitored using bioluminescence measurements and weighed daily. Mouse weights do not significantly differ

among control (anti-hEGFRvIII), anti-mCD19 CAR-T groups, and mice receiving no CAR-T cells. At this dose of 20.12 cells, all CAR-T doses showed little to no life extension (data not shown). We also assessed burden in the (c) peripheral blood (PB), showing that both doses of CAR-T cells significantly reduced disease in the blood after 4 days. Surface expression of mCD19 was drastically reduced in the (d) BM, (e) SP, and (f) PB 4 days after ACT. CAR-T engraftment in all compartments and at both CAR-T cell doses is shown (g, BM; h, SP; i, PB). In all cases, significance is determined using a one-way ANOVA with Turkey's post-hoc test adjusted for multiple comparisons.

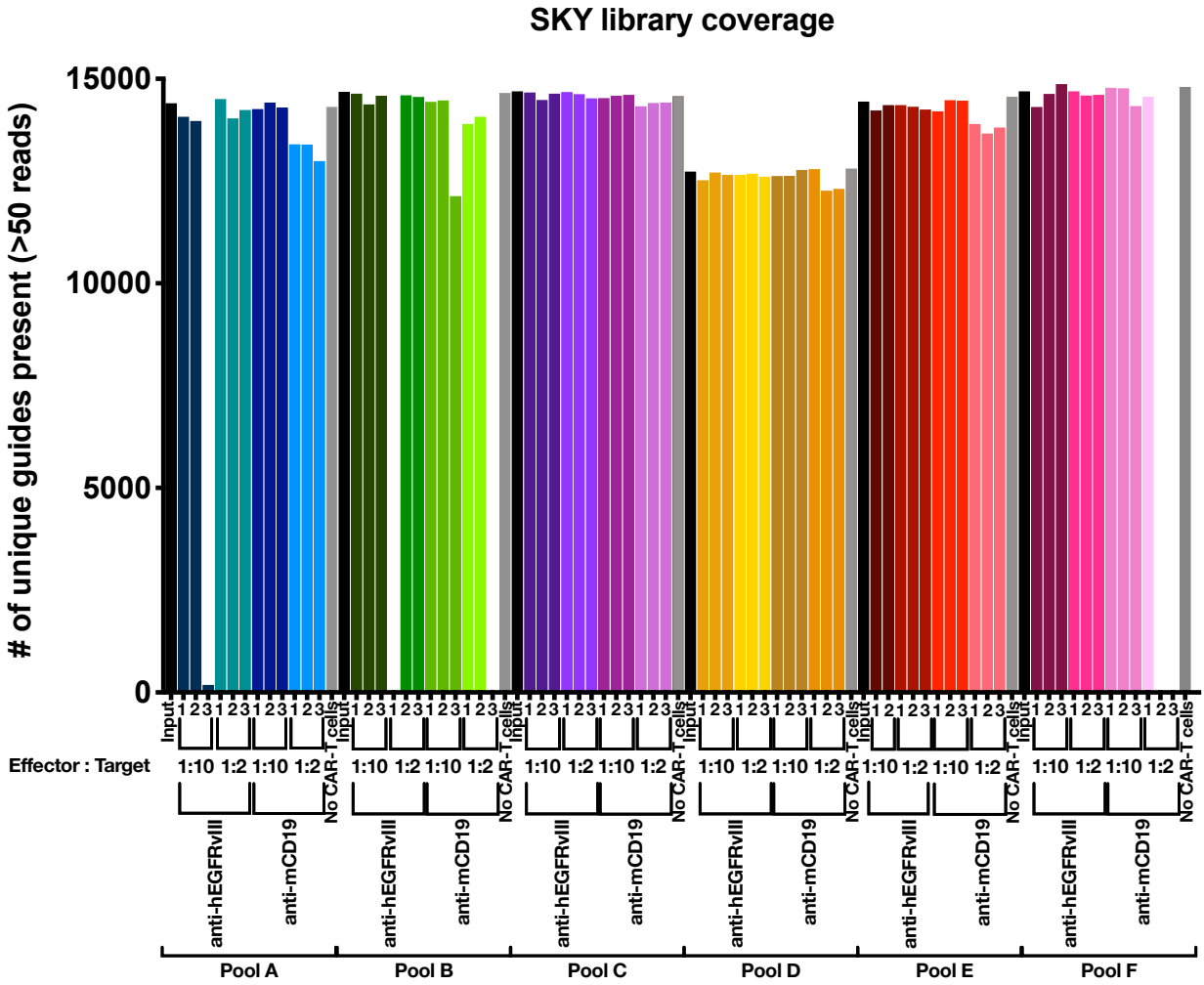

Figure 3.28. High quality sgRNA libraries can successfully maintain representation *in vitro* over two CAR-T doses in a genome-wide screen. We are successfully able to recover the vast majority of sgRNA species (>90%) upon sequencing of amplicons from *in vitro* treated conditions. The 48 SKY pools were collapsed into 6 final libraries that were screened. (a) At about a 205-fold representation, upwards of 85-90% of our high quality library can be represented and maintained *in vitro* after CAR-T treatment at two different E:T ratios (1:2 [induces complete loss of mCD19 surface antigen expression] and 1:10 [induces loss of mCD19 surface antigen expression in 50% of cells]). Each condition was completed in triplicate except Pool E, anti-hEGFRvIII, E:T of 1:10, which was completed in duplicate. Replicates dropped out of the analysis if representation (compared to input) could not be maintained, as in Pool A, anti-hEGFRvIII, E:T of 1:10, replicate 3; Pool B, anti-hEGFRvIII, E:T of 1:2, replicate 1; Pool B, anti-mCD19, E:T of 1:2, replicate 3; and Pool F, anti-mCD19, E:T of 1:2, replicates 2 and 3.

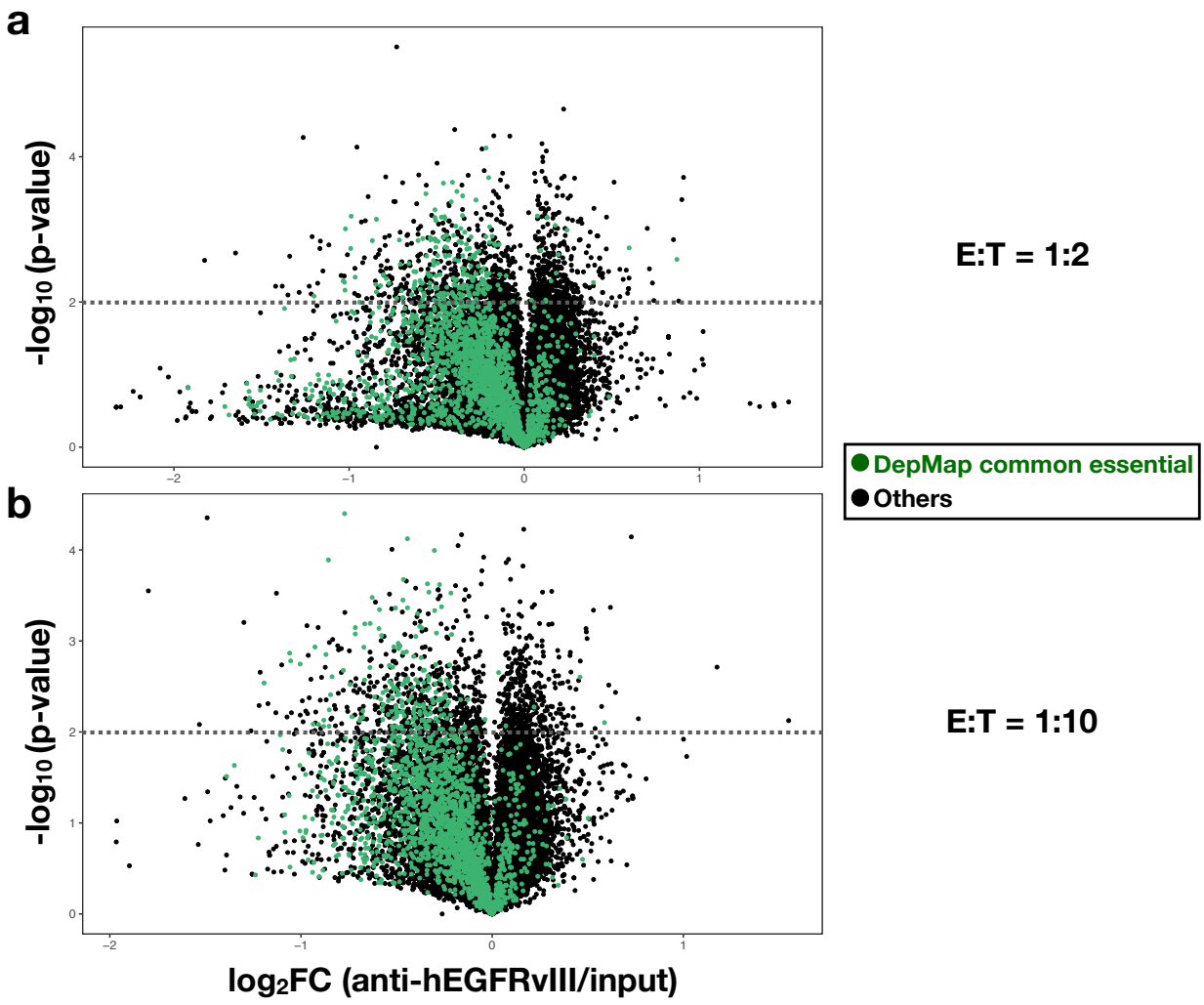

Figure 3.29. Cell essential genes display depletion phenotypes in our *in vitro* screens completed with control (anti-hEGFRvIII) CAR-T cells at both E:T ratios assayed. Preliminary quality control to check the robustness of our screen included examining the behavior of guides against cell essential genes (as defined using the Broad Institute's DepMap common essential genes) in our control CAR (anti-human EGFRvIII) conditions. Overall, at both an E:T ratio of (a) 1:2 and (b) 1:10, sgRNAs against cell essential genes show depletion phenotypes (as compared to input), as displayed using volcano plots.

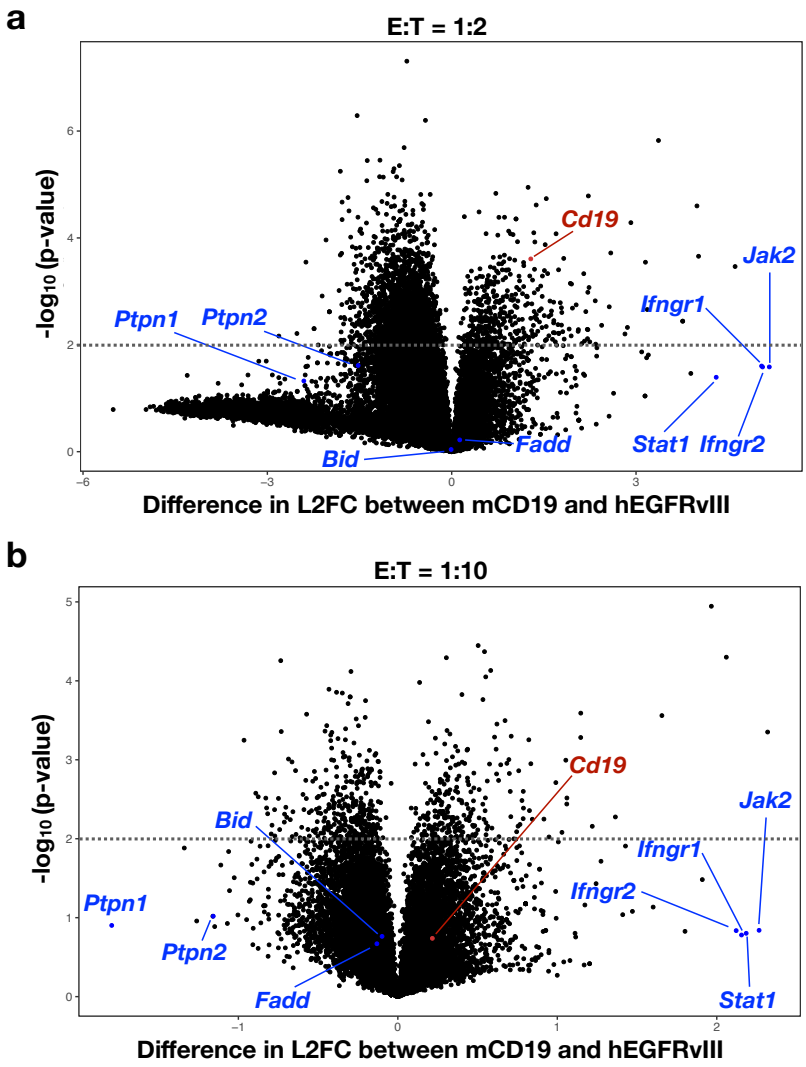

Figure 3.30. Guides against *Cd19* show a CAR-T dose dependent enrichment in our *in vitro* screens. (a-b) To assess the robustness of our screens, we examined the phenotypes of guides against the gene encoding our target antigen CD19 and guides against genes known to promote resistance or sensitization to T cell or CAR-T cell-mediated killing. As expected, CD19 guides show a dose dependent enrichment response to CAR-T cells. Cultures exposed to reduced CAR-T pressure (b) show a more weak enrichment while cultures exposed to increased CAR-T pressure (a) show a significant enrichment of guides against *Cd19*. Members of the extrinsic apoptosis pathway, *Bid* and *Fadd*, were previously identified as genes that promote resistance to CAR-T killing in an *in vitro* screen completed in human B-ALL cells (Singh et al., 2020). These genes did not score in our *in vitro* screen. Genes belonging to the interferon gamma (IFNg/JAK/STAT) pathway were previously shown to be essential for successful elimination of tumor cells by T cell mediated killing in melanoma patients treated with PD-1 blocking antibodies (Zaretsky et al., 2017). Our results agree with these findings. Here, genes from the Ifng/Jak/Stat pathway also show strong enrichment phenotypes in screens treated with E:T ratios of (a) 1:2 or (b) 1:10, indicating that loss of this pathway desensitizes tumor cells to CAR-T-based killing. Loss of the gene *Ptpn2* was recently shown to sensitize melanoma cells to T cell-based killing in an *in vivo* screen completed in the context of PD-1 blocking antibodies (Manguso et al., 2017). Our results are concordant with those findings. In our screens, guides against *Ptpn2* consistently show strong depletion phenotypes that are also dose dependent, indicating that loss of this gene sensitizes cells to CAR-T killing. Depletion of *Ptpn2* guides is more dramatic in cultures treated with (a) an E:T ratio of 1:2, as compared to those treated at (b) an E:T ratio of 1:10.

References

Darvin, P., Toor, S. M., Sasidharan Nair, V. & Elkord, E. Immune checkpoint inhibitors: recent progress and potential biomarkers. *Exp. Mol. Med.* 50, 1–11 (2018).

Davila, M. L., Kloss, C. C., Gunset, G. & Sadelain, M. CD19 CAR-Targeted T Cells Induce Long-Term Remission and B Cell Aplasia in an Immunocompetent Mouse Model of B Cell Acute Lymphoblastic Leukemia. *PLoS One* 8, 1–14 (2013).

Doench, J. G. Am i ready for CRISPR? A user's guide to genetic screens. *Nat. Rev. Genet.* 19, 67–80 (2018).

Doench, J. G. *et al.* Rational design of highly active sgRNAs for CRISPR-Cas9-mediated gene inactivation. *Nat. Biotechnol.* 32, 1262–1267 (2014).

Engels, B. *et al.* Retroviral vectors for high-level transgene expression in T lymphocytes. *Hum. Gene Ther.* 14, 1155-1168 (2003).

Eyquem, J. *et al.* Targeting a CAR to the TRAC locus with CRISPR/Cas9 enhances tumour rejection. *Nature* 543, 113–117 (2017).

Feucht, J. *et al.* Calibration of CAR activation potential directs alternative T cell fates and therapeutic potency. *Nat. Med.* 25, 82–88 (2019).

Fiedler, E. R. C., Bhutkar, A., Lawler, E., Besada, R. & Hemann, M. T. In vivo RNAi screening identifies Pafah1b3 as a target for combination therapy with TKIs in BCR-ABL11 BCP-ALL. *Blood Adv.* 2, 1229–1242 (2018).

Hart, T. *et al.* High-Resolution CRISPR Screens Reveal Fitness Genes and Genotype-Specific Cancer Liabilities. *Cell* 163, 1515–1526 (2015).

Jacoby, E. *et al.* Murine allogeneic CD19 CAR T cells harbor potent antileukemic activity but have the potential to mediate lethal GVHD. *Blood* 127, 1361–1370 (2016).

Joyce, J. A. & Fearon, D. T. T cell exclusion, immune privilege, and the tumor microenvironment. *Science* 348, 74–80 (2015).

Kochenderfer, J. N., Yu, Z., Frasheri, D., Restifo, N. P. & Rosenberg, S. A. Adoptive transfer of syngeneic T cells transduced with a chimeric antigen receptor that recognizes murine CD19 can eradicate lymphoma and normal B cells. *Blood* 116, 3875–3886 (2010).

Kurachi, M. *et al.* Optimized retroviral transduction of mouse T cells for in vivo assessment of gene function. *Nat. Protoc.* 12, 1980–1998 (2017).

Majzner, R. G. & Mackall, C. L. Tumor antigen escape from car t-cell therapy. *Cancer Discov.* 8, 1219–26 (2018).

Manguso, R. T. *et al.* In vivo CRISPR screening identifies Ptpn2 as a cancer immunotherapy target. *Nature* 547, 413–418 (2017).

Maude, S. L. *et al.* Tisagenlecleucel in children and young adults with B-cell lymphoblastic leukemia. *N. Engl. J. Med.* 378, 439–448 (2018).

Meacham, C. E. *et al.* A genome-scale in vivo loss-of-function screen identifies Phf6 as a lineage-specific regulator of leukemia cell growth. *Genes Dev.* 29, 483–488 (2015).

Morgan, R. A. *et al.* Recognition of glioma stem cells by genetically modified T cells targeting EGFRvIII and development of adoptive cell therapy for glioma. *Hum. Gene Ther.* 23, 1043–1053 (2012).

Neelapu, S. S. *et al.* Axicabtagene ciloleucel CAR T-cell therapy in refractory large B-Cell lymphoma. *N. Engl. J. Med.* 377, 2531–2544 (2017).

Paszkiewicz, P. J. *et al.* Targeted antibody-mediated depletion of murine CD19 CAR T cells permanently reverses B cell aplasia. *J. Clin. Invest.* 126, 4262–4272 (2016).

Posey, A. D. *et al.* Engineered CAR T Cells Targeting the Cancer-Associated Tn-Glycoform of the Membrane Mucin MUC1 Control Adenocarcinoma. *Immunity* 44, 1444–1454 (2016).

Restifo, N. P. *et al.* Loss of Functional Beta2-Microglobulin in Metastatic Melanomas From Five Patients Receiving Immunotherapy. *JNCI J. Natl. Cancer Inst.* 88, 100–108 (1996).

Sadelain, M., Rivière, I. & Riddell, S. Therapeutic T cell engineering. *Nature* 545, 423–431 (2017).

Schreiber, R. D., Old, L. J. & Smyth, M. J. Cancer immunoediting: Integrating immunity's roles in cancer suppression and promotion. *Science* 331, 1565–1570 (2011).

Schuster, S. J. *et al.* Tisagenlecleucel in adult relapsed or refractory diffuse large B-cell lymphoma. *N. Engl. J. Med.* 380, 45–56 (2019).

Shah, N. N. & Fry, T. J. Mechanisms of resistance to CAR T cell therapy. *Nat. Rev. Clin. Oncol.* 16, 372–385 (2019).
Singh, N. *et al.* Impaired Death Receptor Signaling in Leukemia Causes Antigen-Independent Resistance by Inducing CAR T-cell Dysfunction. *Cancer Discov.* 10, 552–567 (2020).
Williams, R. T., Besten, W. Den & Sherr, C. J. Cytokine-dependent imatinib resistance in mouse. *Genes Dev.* 21, 2283–2287 (2007).
Williams, R. T., Roussel, M. F. & Sherr, C. J. Arf gene loss enhances oncogenicity and limits imatinib response in mouse models of Bcr-Abl-induced acute lymphoblastic leukemia. *Proc. Natl. Acad. Sci. U. S. A.* 103, 6688–6693 (2006).
Zaretsky, J. M. *et al.* Mutations associated with acquired resistance to PD-1 blockade in melanoma. *N. Engl. J. Med.* 375, 819–829 (2016).
Zhong, S., Malecek, K., Perez-Garcia, A. & Krogsgaard, M. Retroviral Transduction of T-cell Receptors in Mouse T-cells. *J. Vis. Exp.* 1–5 (2010). doi:10.3791/2307

CHAPTER 4—
Discussion and future directions

Part I—AML and SUCLG2

Summary

Acute myeloid leukemia (AML) is the most common acute leukemia in adults and the deadliest of all blood cancers, killing nearly 80% of all patients diagnosed with this disease after they relapse with increasingly resistant disease (Döhner et al., 2015). One of the most striking aspects of the AML field as a whole is the discrepancy between the comprehensive knowledge we have about the genetic underpinnings of the disease and the paucity of treatment options available to patients. Unfortunately, this is a common feature amongst many difficult cancer types. In AML, this is perhaps best exemplified by persistently poor outcomes (outside of APML) and by the fact that the standard of care in AML has remained largely unchanged for more than 40 years, although this appears to be changing slowly. Here, this dissonance speaks to the continued challenge of identifying roles for malignancy-associated genes in cancer genomics, particularly after relapse. Hence, the application of more functional assays that allow researchers to investigate clinically relevant phenotypes in a massively paralleled fashion are currently necessary. Pooled *in vivo* screens offer such an approach. In this thesis, I have applied this unbiased technique in transplantable models of acute leukemias in order to investigate resistance mechanisms to various therapy modalities in clinically relevant contexts.

In terms of AML, we have completed the first *in vivo* RNAi screen in the setting of frontline combination chemotherapy and have identified SCS-G (encoded by *Suclg2*) as a novel *in vivo*-specific mediator of resistance. Depletion of SCS-G and an inability to engage its partner genes appears to be especially detrimental to LSCs, an idea supported by our analyses of previously published patient data. Here, a Suclg2 KD “chemosensitization” signature was able to stratify patients populations predicted by the context in which Suclg2 scored as a chemosensitizer. The downregulated genes from our signature predicted significantly longer survival in patients with treatment-refractory disease, AMLs that transcriptionally resemble more immature LSCs, and in AMLs profiled using BM disease, where the largest proportion of LSCs are known to reside. Our signature also predicted significantly better outcomes in patients with high SUCLA2:SUCLG2 ratios, a population predicted by the fact that these two

subunits appear to be non-redundant in mammalian cells. Extensive work by the Kibbey lab at Yale and others has shown that SCS-G regulates cataplerotic flux via the generation of mtGTP that fuels the PEPCK2 shuttle and inhibits glutamate dehydrogenase (GDH), one of the main anaplerotic (replenishing TCA cyle intermediates) entry points for amino acids to enter the TCA cycle (Kibbey et al., 2007; Jesinkey et al., 2019; Wang & Dong, 2019). Conversely, SCS-A counteracts this effect by competing with SCS-G, therefore driving down mtGTP levels. The ratio of these two subunits then determines the rate of the reaction through either node (Jesinkey et al., 2019). Hence, these proteins are non-redundant in mammalian cells. Preliminarily, our data suggest that SCS-G promotes resistance via a mechanism that likely does not involve metabolite accumulation or the upregulation of OXPHOS metabolism, as SCS-G KO/KD cells appear to have smaller mitochondria that are also more active. Additionally, depletion of other SCS members also sensitizes AML cells to therapy, indicating that proper function of this entire complex is important in AML. Overall, our data suggests a model in which an LSCs ability to switch between SCS-β isoforms is critical for survival in various contexts. In the case of chemotherapy exposure, a cell's ability to engage SCS-G-mediated pathways appears to be critical. In order to fully elucidate and confirm the mechanism by which this occurs however, key experiments remain to be completed. In this section, I will outline these experiments and highlight the open questions that our findings raise.

Key experiments

Various critical experiments remain to be completed. First, for hairpin experiments, all completed in murine AML cells, WBs assaying protein levels of all complex members should be done in order to determine whether KD of one SCS protein affects the expression of other pathway members. If knocking down one complex member decreases the expression of other SCS proteins, this could point to an alternate method by which Suclg2 KD could be sensitizing cells: by coordinating the decreased expression of the entire SCS complex, rather than affecting only Suclg2. Importantly, there is no transcriptional evidence for this, as RNAseq data from the BM of acutely treated animals shows no significant differences in the level of Sucla2 or Suclg1 expression between control (shLuc) and Suclg2 KD (sh#1660) cells (figure 4.1). Western blots will be needed to confirm this finding. This alternate mechanism is also unsubstantiated by our metabolite measurements, as SUCLG1 KD has already been shown to significantly alter intracellular succinate pools—an effect we did not observe in our experiments

(Mullen et al., 2014). Lastly, previously reported KD experiments of either β-subunit have been shown to induce rebound expression changes in other SCS complex members in some cells (pancreatic islet) but not in others (Kibbey et al., 2007). Hence, this effect appears to be context specific and it is not necessarily expected that KD experiments would induce coordinated expression changes in all other SCS genes.

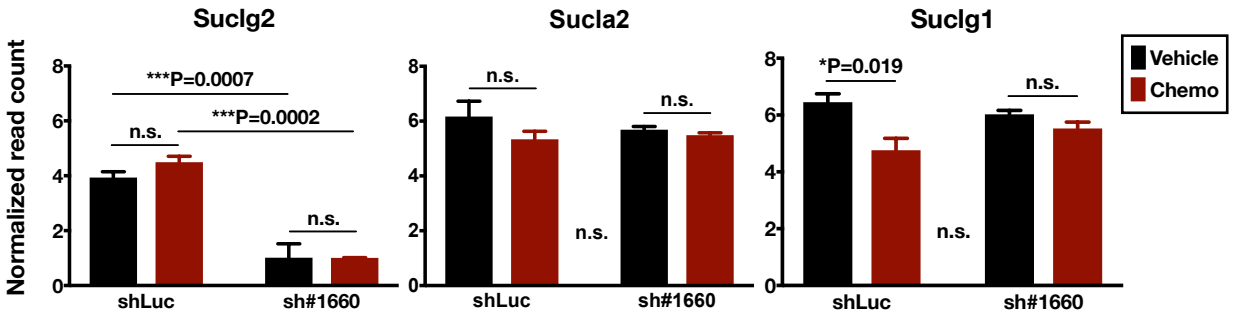

Figure 4.1. The expression levels of other SCS complex members do not significantly change upon Suclg2 KD. Expression analysis for Suclg2, Sucla2 and Suclg1 in control (shLuc) or Suclg2 KD (sh#1660) cells harvested 48 hours after *in vivo* treatment with a vehicle control (black) or combination chemotherapy (red). Data is taken from the previous RNAseq experiment described in acutely treated cells. Significance is determined by two-way ANOVA with Bonferroni's post-hoc tests adjusted for multiple comparisons.

Direct evidence showing that LSCs are specifically sensitized to therapy in response to SUCLG2 KD/KO is also critically needed and experiments to test this in both murine and human models are planned via *in vivo* competition assays. Here, Suclg2 KD/KO cells will be mixed in a 1:1 ratio with corresponding control cells, injected into animals, treated with a vehicle control or combination chemotherapy, sacrificed at various time points (2, 4, 6, 8, and 10 days after combination dosing begins), and stained to identify LSCs (CD34+CD38–). Based on our model, we hypothesize that LSCs in treated Suclg2 KD/KO animals will be eliminated more effectively than LSCs in treated control animals. If those experiments confirm our hypothesis, I will complete identical experiments with *Suclg2* cDNA expressing cells to ask if reconstituting SCS-G levels can rescue this phenotype. Preliminarily, we looked to see if a depletion of LSC transcriptional programs could be detected in treated Suclg2 KD cells harvested from the BM at 48 hours as compared to treated control cells, but no such effect could be seen. However, this could be due to two factors: 1. Transcriptional profiling was performed without separating LSCs from the bulk tumor cells that can also reside in the BM; 2. We did not perform our analysis at the appropriate time point to look for LSC depletion, as Suclg2 was shown to be critical for relapse and not acute treatment response. Accordingly, it

will also be beneficial to assay transcriptional changes at later time points, both in bulk cells and in LSCs specifically. Here, a stronger depletion signal of LSC gene expression would be expected at later timepoints after therapy exposure, based on the identification of Suclg2 in relapsed samples. It will also be critical to examine the exact cellular phenotype induced by Suclg2 KD/KO in both LSCs and bulk tumor cells, in the context of therapy. To do this, I can take advantage of the abovementioned experiments to also assess the cell cycle profiles of LSCs and bulk cells over a variety of time points. Additionally, I will stain for canonical myeloid differentiation markers and collect cells for *in vitro* colony forming assays to assess whether Suclg2 KD/KO enhances blast differentiation in response to therapy. There is some evidence from our murine RNAseq experiments that depletion of SCS-G in Suclg2 KD cells could lead to increased maturation following treatment with chemo. Here, GSEA of acutely chemo-treated BM cells shows that two of the 20 most upregulated probe sets in Suclg2 KD cells correspond to genes involved in the biosynthesis of specific granule proteins associated with myeloid maturation, including myeloperoxidase and lysozyme (one probe set shown in figure 4.2). Both direct staining and transcriptional assessment of Suclg2 KD/KO cells mentioned above should help confirm this finding.

Another prediction made by our hypothesis that Suclg2 depletion is specifically sensitizing LSCs to therapy is that venetoclax treatment will synergize with Suclg2 KD in the context of chemotherapy. Such experiments can be completed, but they are ultimately a lower priority than the other experiments listed here. Lastly, it is possible that our model is incorrect and LSCs are not specifically sensitized to therapy in the context of SCS-G depletion. As physiologic medium from mouse plasma could not recapitulate our phenotype, it is possible that the effect of Suclg2 loss is simply strongest in the BM. The Vander Heiden lab is currently in the process of generating physiologic medium that more closely resembles the BM microenvironment and experiments to dose cells in that medium will be pursued. Similarly, both single agent and combination dosing with both Ara-C and anthracycline will be repeated in mouse physiologic medium. Additionally, the experiments described below (most of which are ongoing) will also allow us to further explore alternate mechanisms.

Our TCA metabolite measurements could also be strengthened by the inclusion of a strong positive control with well-established changes in TCA intermediates, such as an *IDH*-mutant AML or venetoclax+azacitidine treated AML cells (Pollyea et al., 2018). Additionally, identical metabolite measurements in MOLM-14 cells are warranted. As MOLM-14 KO cells were generated later than the MV4-11 KOs, MV4-11 cells were characterized first. Identical *in*

vivo experiments as those set up for MOLM-14 were also pursued with MV4-11 cells but due to timing issues, data from those animals were not informative. Ultimately, getting a more complete profile of intracellular metabolite levels in human and murine models, including glycolytic intermediates, nucleotide pools, and lipids (in addition to TCA intermediates and amino acid pools) in all SUCLG2 KO/KD cells taken directly from various anatomic locations would be a better approach. Hence, we plan to complete these experiments in future studies using liquid chromatography-mass spectroscopy (LC-MS), as this technique can measure a broader set of metabolites (Lu et al., 2017). Here, it will also be important to metabolically characterize Chemo^{R} and *Suclg2* cDNA rescue cells in order to allow us to narrow in on changes that are important for resistance and on alterations that are due specifically to Suclg2 depletion. Similarly, it will also be important to repeat mitochondrial stress tests on *Suclg2* cDNA rescue cells, and to formally preform glycolysis stress tests on both human and murine cells. These experiments will help further characterize the changes induced by SCS-G depletion. Lastly, we will further characterize the mitochondrial changes induced by Sulcg2 loss via qPCR experiments in cells sorted directly from animals to quantify the ratio of mtDNA to nuclear DNA ratios, an assay that provides another measure of mitochondrial number. Staining for ROS levels will also be completed and direct imaging studies to examine mitochondrial morphology are also planned, as alterations in SUCLG2 levels have already been shown to lead to mitochondrial changes (Jesinkey et al., 2019).

Our model predicts that Suclg2 is critical in chemo-treated cells because of its ability to produce mtGTP required by Pck2 in order to continue to consume non-carbohydrate based energy sources, such as glutamine and amino acids, and support biosynthetic processes. Hence, we hypothesize that reinstating normal mtGTP levels should rescue the chemosensitization phenotype in Suclg2 KD cells. To complete this experiment, we can take advantage of the mitochondrial GTP/GDP transporter (GGC1) discovered in yeast (Vozza et al., 2004). Unlike mammalian cells, yeast do not have a GTP-specific isoform of the SCS-β subunit and their mtNDPK salvage protein is located in the intermembrane space. Thus, yeast require an alternate mechanism to supply GTP to the mitochondrial matrix. Experiments to xenotopically express GGC1 protein in Suclg2 KD cells are currently planned, and all of the requisite plasmids are cloned. To confirm that GGC1 protein is functional, we will use an established assay to measure mtGTP levels that is based on the strong allosteric inhibition of mitochondrial glutamate dehydrogenase (GDH) by mtGTP (Jesinkey et al., 2019). To this end, we have already established a collaboration with the Kibbey lab at Yale that has recently

pioneered this assay and has shown that the yeast transporter can be used to alter mtGTP levels in mammalian cells. The Kibbey lab has also developed isotope tracing probes to directly examine central carbon metabolism and the cataplerotic flux driven by mtGTP and its collaborative enzyme Pck2. Using these tracers, they have previously shown that the primary change in mitochondrial metabolism induced by increased levels of mtGTP (induced via the overexpression of SCS-G or expression of GGC1) is the diversion of carbon flux through mtPEPCK. Identical experiments in Suclg2 KD/KO cells is currently ongoing and will also be helpful in determining if our model is correct.

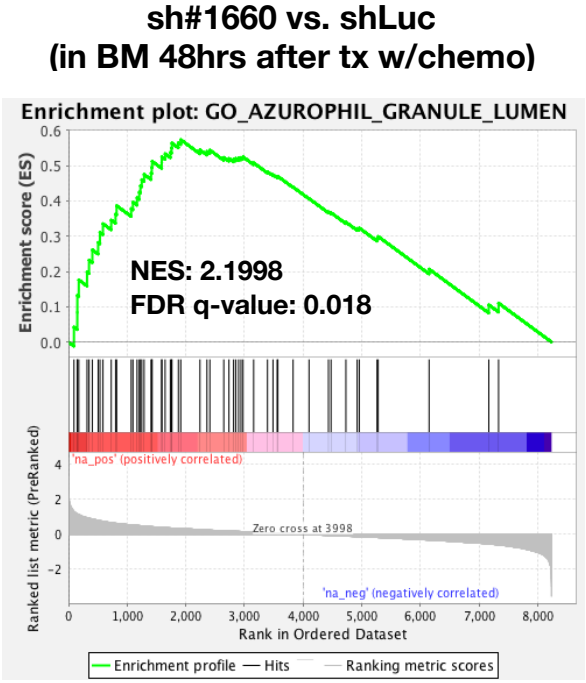

Figure 4.2. Gene sets involved in the biosynthesis of specific granule proteins are enriched in acutely treated murine Suclg2 KD cells (sh#1660) harvested from the marrow. GSEA analysis of the expression profiles of acutely treated murine AML cells (48hrs post-treatment with chemotherapy, harvested from the BM). This analysis revealed an enrichment of gene sets in Suclg2 KD cells (compared to control cells) that encode the biosynthesis of specific granule proteins associated with myeloid maturation, including myeloperoxidase and lysozyme.

Future directions

One important future direction will be to determine if normal hematopoietic cells are also sensitized to chemotherapy in the context of Suclg2 depletion or affected by it in any way. An ideal outcome would be that only AML blasts are affected by the loss of this protein, as this would indicate that a therapeutic window for SUCLG2 inhibition might exist. However, HSC properties such as stemness and quiescence have recently been shown to be exquisitely

sensitive to alterations in mitochondrial metabolism and function (Folmes & Terzic, 2016). Notably, HSCs show an increased dependence on anaerobic glycolysis and actively shuttle glycolytic metabolites away from the mitochondria by upregulating pyruvate dehydrogenase kinase (Pdk, an inhibitor of pyruvate dehydrogenase) in order to maintain stemness (Simsek et al., 2010; Takubo et al., 2013). When Pdk is lost in mice, HSCs are forced to oxidize carbons through the TCA cycle, resulting in decreased quiescence and reduce stemness, as assayed with transplantation experiments. While the energy needs of a quiescent HSC appear to be easily met through glycolysis, brisk proliferation during normal differentiation of HSCs has been shown to require a rapid metabolic switch towards increased OXPHOS metabolism (Folmes & Terzic, 2016). When mitochondrial respiration was blocked in murine HSCs by the conditional deletion of *Ptpmt1*, a PTEN-like mitochondrial phosphatase, HSCs displayed a significantly increased rate of proliferation and a complete block in differentiation (Yu et al., 2013). Hence, metabolic switches in mitochondrial metabolism have been shown to function as differentiation and self-renewal checkpoints that are activated by bioenergetic stress in HSCs. SUCLG2 and mtGTP have already been linked to the regulation of mitochondrial biology, both by our work and that of other groups (Vyas et al., 2016; Jesinkey et al., 2019). If Suclg2 is indeed promoting resistance through the engagement of gluconeogenesis, then blocking this process should not be problematic for normal HSC growth. This is because gluconeogenesis is the reverse of glycolysis and these two pathways are reciprocally regulated such that one pathways is relatively inactive while the other is highly active in a cell (Berg et al., 2015). Conversely, it could be that HSCs also rely on cataplerotic processes (specifically on SCS-G mediated pathways) to survive chemotherapy, potentially limiting the therapeutic window for Suclg2 inhibition. Still, significant differences in the metabolic properties of AML blasts/LSCs and normal HSCs *do* exist and are already being targeted clinically with venetoclax (Pollyea et al., 2018; DiNardo et al., 2018; Jones et al., 2018). Thus, it is currently impossible to predict the effects of Suclg2 inhibition on normal HSCs in the context of frontline chemotherapy *a priori*, especially given that complete loss of this or any of the other SCS complex members is embryonic lethal in mice (Kacso et al., 2016). Further exploration of this question, both in the hematopoietic compartment and in normal cells though out the body is critically important, especially given that the ultimate goal of our work is to identify therapeutically actionable drug targets that are specifically detrimental to AML.

Another future area of study will be to examine the relationship between stemness and an LSC's SUCLA2:SUCLG2 (A2:G2) ratio. As discussed above, metabolic alterations can

significantly influence various cellular properties and altering the A2:G2 ratio has already been shown to affect various aspects of pancreatic β cell biology (Kibbey et al., 2007; Jesinkey et al., 2019). Here, increasing the amount of mtGTP or decreasing the A2:G2 ratio led to β cells that were significantly more resilient to induced metabolic stress (Jesinkey et al., 2019). Specifically, islet cells challenged with excessive and sustained exposure to both glucose and lipids, a combination known to damage and exhaust β cells, naturally upregulated SUCLG2 (Poitout et al., 2010). Overall, overexpressing SUCLG2 or increasing mtGTP led to more differentiated β cells that are enhanced in their ability to synthesize insulin, function properly, and avoid apoptosis, even in the face of extreme metabolic stress. Additionally, SUCLG2 overexpression led to mitochondria that were larger, longer and more fragmented than control cells, along with expression changes in mitochondrial fission and fusion genes. Hence, it will be interesting to examine what effect, if any, altering the A2:G2 ratio has specifically on an LSC's metabolic resiliency, differentiation status, quiescence, or ability to self-renew. Ultimately, identifying if metabolic switches like those in HSCs also exist in LSCs could aid in the discovery of novel AML drug targets.

Similarly, formal examination of how A2:G2 ratios affect therapeutic outcome in patients will be important. To begin to answer this question, we can analyze multiple independent patient data sets and ask if a high A2:G2 ratio predicts better outcomes. Preliminarily, in our analyses (figure 2.18e-f), this seems likely, as patient cohorts with a high A2:G2 ratio appear to be enriched for long-term survivors. If this proves to be statistically significant over multiple patient cohorts, we can expand our results by using patient xenograft samples. Here, we can knock down SUCLG2 or overexpress SUCLA2 to increase the A2:G2 ratio and inject cells into NSG mice for xenograft experiments in the context of therapy. Increased survival in mice transplanted with AML cells bearing a high A2:G2 ratio, as compared to control will support our hypothesis.

Lastly, it will be important to follow up on the observation that Suclg2 appears to promote resistance in an *in vivo*-specific manner. As described above, we are currently collaborating with the Vander Heiden lab and will dose cells in BM physiologic medium when this formulation is ready. Another approach could be to attempt to elucidate our chemosensitization phenotype using media that is more severely depleted for specific metabolites, notably for glutamine or amino acids that can both be used to fuel the TCA cycle and cataplerosis (Owen et al., 2002; Wang & Dong, 2019). Additionally, it could be that cell-cell contacts or secreted signaling molecules that are orthogonal to nutrient availability are what

dictate the *in vivo* specific nature of this phenotype. Importantly, mechanisms like these, mediated by interactions between the TME and leukemia cells has already proven to be critical for AML chemoresistance and survival through various mechanisms (reviewed in Fiedler & Hemann, 2019). Here, co-culture dosing experiments with stromal cells from the BM or in BM conditioned medium can be performed to directly test this idea.

Alternate possible resistance mechanisms mediated by Suclg2

It is possible that Suclg2 mediates resistance through a mechanism that does not involve the rewiring of mitochondrial anabolic metabolism. Alternate possibilities are numerous, but include the upregulation of heme synthesis by Suclg2 (Fiorito et al., 2019). Previous studies in AML have already shown that heme biosynthesis pathways are upregulated in chemo-refractory cases and that they are necessary for self-renewal and proper mitochondrial function (Fukuda et al., 2017; Lin et al., 2019). The TCA cycle is an important supplier of heme synthesis precursors (e.g. succinyl-CoA) and a recent publication showed that the genes encoding the SCS complex, including SUCLG2, are amongst the most upregulated genes in MYCN-driven pediatric AML (Fukuda et al., 2017). Thus, one possibility is that Suclg2 could be promoting resistance to frontline therapy by increasing heme production. While attractive, the data reported by other groups on heme biosynthesis depletion in AML do not presently fit with our results (Fukuda et al., 2017; Lin et al., 2019). In these studies, authors showed that inhibition of heme synthesis reduced mitochondrial oxygen consumption and suppressed self-renewal of LSCs. Similar results were accomplished by Li and colleagues who showed that inhibiting heme synthesis disrupted activity through the electron transport chain and primed cells for apoptosis, again resulting in decreased oxygen consumption rates (OCR) and more depolarized mitochondria. Our results show that Suclg2 KD/KO results in smaller mitochondria that are also more active, displaying higher OCR and better coupling efficiency of respiration to ATP production and a decrease in proton leak. These data suggest that Suclg2 KD/KO cells are enhanced for their oxidative capacities and, potentially, have an increased mitochondrial membrane potential. Further, heme biosynthetic gene sets are not depleted (or enriched) in treated or untreated murine Suclg2 KD or control cells, as assessed via GSEA of our RNAseq data from acutely treated KD and control cells, or RNAseq data from treated and relapsed murine control cells. Nevertheless, mitochondrial biology does appear to be altered in the context of Suclg2 loss or depletion and examining how or if this is involved in our

chemosensitization phenotype will be an important future direction to pursue, as described above.

One metabolite that we currently cannot assay using standard LC-MS or GC-MS methods is succinyl-CoA. This coenzyme A metabolite has been shown to be particularly labile and thus is difficult to measure accurately (Tsuchiya et al., 2014; personal communications with MVH). Suclg2 KD would be predicted to increase the concentration of succinyl-CoA in normal cells (depending on the flux through SCS-A) that run their TCA cycles in the forward direction—decarboxylating citrate to succinyl-CoA and then oxidizing succinate to oxaloacetate to harvest electrons for the ETC. However, tumor and normal cells undergoing various types of physiologic stress that attenuate OXPHOS metabolism, such as hypoxia or inhibition of the electron transport chain (ETC), or tumors with defective mitochondria have been shown to run the TCA cycle in reverse (Wise et al., 2011; Metallo et al., 2012; Mullen et al., 2012). This allows cells to generate citrate and subsequently, acetyl-CoA from non-carbohydrate sources that then fuels *de novo* fatty acid and triglyceride synthesis to support cell viability. In line with this idea, GSEA analysis of acutely chemo-treated murine Suclg2 KD cells showed an upregulation of pathways involved in fatty acid and lipogenic metabolism (Figure 4.3). Similarly, increased levels of CD36 (the fatty acid translocase/receptor) were also found via direct staining of acutely treated Suclg2 KD cells, as compared to controls. Currently, fatty acid metabolism is thought to promote both AML cell survival and resistance to chemotherapy and targeted agents (Jones et al., 2019; Tabe et al., 2020). Thus, upregulation of these pathways in chemosensitized cells could indicate that counter to the currently held view, FA metabolism promotes resistance to therapy *in vivo*. Of course, this could simply represent a compensatory change that occurs due to the accumulation of succinyl-CoA when Suclg2 is depleted. Here, flux analysis to specifically examine FA metabolism would be the most helpful, along with the aforementioned LC-MS experiments we are already planning on pursuing.

Finally, we examined the set of downregulated genes that comprise our chemosensitization signature (figure 2.17) in an attempt to better understand the resistance mechanism mediated by Suclg2. The genes in this signature spanned a number of cellular processes and most were already associated with promoting various aspects of tumor biology. These include developmental genes (*Eya*, an H2Ax phosphatase that is important for proper DNA repair; Wu et al., 2013), RNA splicing and processing genes (*Clk1*, *Tra2b*, implicated in AML and other cancers, Urbanski et al., 2018), a gene encoding a chaperone protein (*Dnajc10,* Lee & Lee, 2017), an E3 ubiquitin ligase known to promote tumorigenesis (*Ube3a*, Louria-

Hayon et al., 2009; Kohli et al., 2018), a small GTPase known to promote aggressiveness and metabolic changes in cancer (*Arf6*, Li et al., 2017; Yoo et al., 2019), a poorly annotated methyltransferase (*Mettl9*), and fatty acyl-CoA reductase 2 (*Far2*), a poorly annotated FA metabolism gene. As the mechanism by which Suclg2 promotes resistance becomes more clear, it will be useful to come back to these data. Similar analyses in human KO cells would also be useful down the line. Unfortunately, for now, this list of genes does not point to an obvious or known direction downstream of Suclg2.

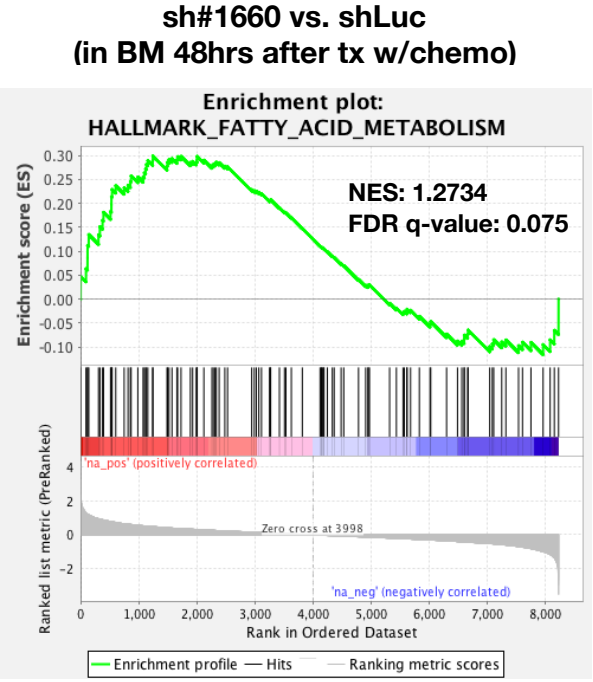

Figure 4.3. Fatty acid metabolism gene sets are enriched in acutely treated Suclg2 KD cells harvested from the bone marrow. GSEA analysis of the expression profiles of acutely treated murine AML cells (48hrs post-treatment with chemotherapy, harvested from the BM). This analysis revealed an enrichment of fatty acid metabolism gene sets in treated Suclg2 KD cells, compared to control cells.

Final perspective on AML therapy and metabolic dependencies

AML is a particularly challenging neoplasm that remains largely clinically intractable, accounting for a disproportionate amount of leukemia-related mortality (Döhner et al., 2015; Siegel et al., 2020). Adaptations in cell metabolism that favor tumorigenic growth in nutrient-poor or metabolically stressful settings (e.g. during therapy exposure) is now a well-established hallmark of many cancers, including AML (Hanahan & Weinberg, 2011). Recent studies have uncovered a number of alterations in key metabolic enzymes that allow tumor cells to rewire their metabolism and more importantly, that constitute novel dependencies that are potentially

targetable. For example, AML cells have been found to rely heavily on the metabolism of specific amino acids (AA). AMLs that are significantly impaired in their ability to synthesize arginine endogenously are sensitive to arginine deaminase that degrades arginine to citrulline, a finding that has led to clinical trials in patients (Miraki-Moud et al., 2015; Tsai et al., 2017). Similarly, other studies have also shown that AML cells are glutamine addicted and clinical trials targeting glutaminolysis are currently underway (Jacque et al., 2015; Emadi et al., 2015). Here, inhibiting glutaminase (the enzyme that catalyzes that first step in glutaminolysis by converting L-glutamine to L-glutamate and ammonium ions) reduces mitochondrial OXPHOS metabolism and significantly reduces TCA cycle intermediates. Other notable examples include mutant *IDH1/2* inhibitors to reduce oncometabolite levels in *IDH1/2* mutated AML and the OXPHOS inhibitor venetoclax (Stuani et al., 2019). From these studies it is now clear that AML, and many other cancer subtypes can also be thought of as metabolic disorders. Understanding the intricate changes in the metabolic profile of cancer cells that allows for their survival can be a powerful method to treat cancer. Indeed, some of the first successful chemotherapies developed by pioneers like Sidney Farber, Gertrude Elion, and George Hitchings were discovered based on studies examining the differential metabolic needs of cancer cells (DeVita & Chu, 2008).

One of the biggest future hurdles that the cancer metabolism field will face in coming years, specifically as it relates to therapy, is identifying patient cohorts that would benefit from metabolism targeting drugs. A salient example comes from methotrexate and 5-FU, antimetabolite chemotherapy drugs that target dihydrofolate reductase (DHFR) and thymidylate synthase (TS), respectively (Longley et al., 2003; Hagner & Joerger, 2010). The proteins targeted by these drugs are present in nearly all malignancies and yet, the efficacy of these drugs varies radically across different cancer types. This problem persists even with more targeted metabolic agents, such as mutant IDH1/2 inhibitors where sensitivity to these drugs appears to vary between *IDH1/2* mutant solid tumors and leukemias (Turcan et al., 2013; Tateishi et al., 2015). Furthermore, various studies have now clearly shown that outside of cell autonomous characteristics (e.g. mutational status, tissue lineage), environment can significantly influence cancer metabolism. One salient example comes from the glutaminase inhibitor CB839. Human non-small cell lung cancer (NSCLC) cells cultured *in vitro* rely heavily on glutamine metabolism for growth and are thus highly sensitive to this drug in this context. However, the metabolic dependency of NSCLC cells *in vivo* switches to glucose metabolism, rendering cells resistant to this inhibitor (Davidson et al., 2016; Hensley et al., 2016).

Together, these data highlight the importance of assessing tumor metabolic dependencies in physiologically relevant contexts, further validating our approach of using an *in vivo* screen to examine AML resistance. Additionally, the prospect that A2:G2 ratios could be a determinant of therapeutic outcome in patients is exciting, especially given the difficulties in determining which patient cohorts would benefit most from metabolic targeting agents. Here, this characteristic could end ultimately help inform clinicians about which patients would benefit most from therapies targeting either SCS-G or the downstream pathways it promotes (e.g. gluconeogenesis and cataplerosis). This highlights another potential utility of forward genetic screens completed in the context of chemotherapy—the identification of relevant biomarkers that can better demarcate therapy-responsive tumor types. As many cancer patients often do not benefit from a chosen regimen but still experience its side effects, the discovery of better predictive biomarkers is crucially needed. Finally, future investigations into the *in vivo* metabolic adaptations that allow cells to survive chemotherapy will certainly continue prove fruitful for the development of more potent drug combinations. As screening technology becomes increasingly precise and *in vivo* screens become more common, I suspect that more of these type of studies will be pursued. After all, some of the most powerful and effective drugs in the modern oncologist's armamentarium are, and have remained, the early chemotherapeutic agents developed based on a cancer cell's unique metabolic dependencies.

Part II— Chimeric antigen receptor therapy

Summary

Understanding how the immune system impinges on cancer initiation, development, and progression represents one of the most complex and challenging questions in immunology research. The idea that immune cells can control cancer is more than a century old and was first proposed in the 1900s by Paul Ehrlich. Given the massive body of literature and significant interdisciplinary advances on which they are founded, chimeric antigen receptors (CAR) represent a seminal breakthrough in oncoimmunology. With early groundbreaking trials demonstrating the profound power of this approach, it is no wonder that CARs have garnered as much fervent attention from basic research, biomedical, pharma, and various clinical fields today. However, the exact efficacy of any novel agent is only truly known after enough time elapses, allowing for the analysis of the long term effects induced by a given intervention. Such data for CAR-T therapy is only now emerging and it is clear that despite the promise it

represents, this new therapeutic modality is far from mastered or optimized. Significant rates of relapse undermine the ultimate utility of CAR-T cells in clinical oncology. It is clear that if we are to harness the full potency of this approach, systematic identification of the factors that influence therapeutic outcome must be completed.

To address this question directly, in a physiologically relevant context, we have completed parallel *in vitro* and *in vivo* screens in an immunocompetent mouse model of BCR-ABL+ B-ALL. Extensive experience with these murine cells in our lab has repeatedly demonstrated the powerful screening platform they represent, surpassing any other mouse model used for screening in the literature today. Additionally, we find that these B-ALL cells also demonstrate a striking loss of the target epitope after being exposed to CAR-T therapy both *in vitro* and *in vivo*. This feature makes screening for resistance to this treatment modality in our B-ALL model a clinically relevant endeavor, since this mechanism is a major contributor to CAR-T therapy failure in patients. As traditional CAR-T production methods are cost-prohibitive at the scale we pursued, we have also developed and extensively optimized a novel protocol that allows us to generate highly effective murine CAR-T cells in a cost effective manner. Further, we describe the design of a new CRISPR-Cas9 library targeting all of the genes in the murine genome. The SKY library, composed of 48 sub pools that are each self-contained screening libraries, greatly enabled this and other ongoing *in vivo* screens in our lab. I envision that these sub pools will go on to prove invaluable for other future screens completed in mice, particularly in solid tumors models where engraftment can be exceedingly low. Initial pilot studies allowed us to fully optimize our approach and the final results of the *in vivo* arm of our screen appear promising, identifying genes that are already reported to alter a tumor's response to T cell mediated killing.

Key experiments

A significant amount of experiments remain to be completed before this work can be published. Currently, there is no model in the literature for how to validate an *in vivo* specific hit from a screen such as ours. Hence, we are currently free to explore this space. In the most ideal situation, completion of out pilot screen will represent a secondary validation screen that corroborates hits identified in 20.12 cells. Thus, common genes identified between our pilot and final *in vivo* screen will represent high-confidence hits that will then be prioritized for follow up studies. Granular examination of genes from the *in vivo* arms of our pilot screens is already showing promising candidates that we can pursue in the near future. For example, one of the

most depleted genes in the spleens of mice treated with anti-mCD19 CAR-T cells (as compared to control CARs) encodes Integrin α4 (ITGA4). Notably, this appears to be an *in vivo* and spleen-specific hit, as it does not score in the *in vitro* arms of any of our screens or in the BM of mice bearing 20.8 cells. When ITGA4 associates with integrin β1 (ITGB1, also scores as a depleter in the spleen, although it is not significant in unfiltered data), they form very late antigen-4 (VLA4) (Hamidi & Ivaska, 2018). This heterodimer bids to VCAM1, fibronectin or osteopontin, and has been shown to regulate the homing, adhesion and engraftment of both normal hematopoietic progenitors and leukemia cells (Filshie et al., 1998; Matsunaga et al., 2003; Poulos et al., 2014; Behrmann et al., 2018). Further, ITGA4 is associated with TME-based therapy resistance in AML and high expression of this integrin also correlated with poor outcomes in a cohort of 415 patients with chronic lymphocytic leukemia (CLL), indicating that this gene is clinically relevant in hematopoietic malignancy (Matsunaga et al., 2003; Poulos et al., 2014; Baumann et al., 2016). As our *in vivo* experiments consistently show that CAR-T killing is most effective at the periphery (an expected result given the well described role of the marrow as a protective niche), loss of this gene in tumor cells could then sensitize them to CAR-T killing by dislodging them from the BM and forcing them to enter the spleen more readily (Fiedler & Hemann, 2019). If true, this model would then predict that pre-treatment with the anti-VLA4 antibody natalizumab, used clinically to treat autoimmune diseases, would result in the re-localization of B-ALL cells away from the BM, thus leading to a synergistic effect with CAR-T therapy, specifically *in vivo*. The half-life of natalizumab is just 11 days in human patients, but profound effects have been reported to occur as long as 6 months after therapy (Courchesne et al., 1999). This detail, and the timing of drug administration are critical to the success of the proposed experiment, as natalizumab has been shown to be effective largely though its effects on T cell homing and signaling (Waenke et al., 2014).

Another *in vivo* specific hit is *Rac2*, a Rho GTPase involved in cell growth and cytoskeletal reorganization (Durand-Onayli et al., 2018). Interestingly, our lab recently identified a role for Rac2 and other genes involved in cell migration/cytoskeletal reorganization in both lymphoma progression and resistance to frontline therapy (Meacham et al., 2009). As suppression of Rac2 was shown to be selected against at prototypical metastatic sites of disease, it could be that altering a cell's ability to migrate to, as of yet, unknown protective niches (like the marrow) could also be sensitizing them to CAR-T cells. Critically, regulators of cytoskeletal dynamics like Rac2 have been found to be significantly overexpressed or constitutively active, and associated with poor outcomes in a variety of leukemia types,

including Ph+ B-ALL (Chang et al., 2012; Durand-Onayli et al., 2018). As before, this suggests that targeting this gene could potentially have clinical value. Notably, an effective and validated inhibitor for this protein already exists (NSC23766) and has been successfully used by our own group to show that Rac2 inhibition is synergistic with frontline chemotherapy in our Burkitt lymphoma mouse model (Gao et al., 2004; Cancelas et al, 2005). Thus, an easy experiment to validate the function of this gene in CAR-T resistance would be to administer this molecule either before or concurrently with CAR-T cells, as this would be expected to potentiate their effects. The downstream mechanism for how this is working could then be worked out. Here, validation experiments used to confirm the phenotype of a gene will ultimately depend on the type and function of the protein that is encoded by any given hit.

Future directions and final perspective on CAR-T cell resistance

Although I have only described two examples of *in vivo* specific hits in the above section, our pilot screen identifies many more genes with known functions in cancer, T cell biology, and other immunological processes, along with genes that have never been associated with leukemia or therapy resistance. From these examples, it is clear that the data sets generated from this project will represent many future discoveries in the CAR-T resistance field for years to come. Similar CAR-T screens in PDAC, GBM, and lymphoma are now being pursued by various members in the lab. Hence, the resources developed by my team during the establishment of this screen will continue to contribute to significant discoveries in some of the most clinically intractable human malignancies today. Notably, establishment of the SKY library and screening platform paves the way for the discovery of genes that when targeted, can significantly boost the effectiveness of CAR-T cells in solid tumors where this therapy modality has shown especially disappointing results (Martinez et al., 2019).

Future mechanistic studies examining how alterations in cancer cells from solid tumors and leukemias impinge on CAR-T cell function can ultimately also yield more insight into the basic biology of cancer immunology. For example, one question that is still unanswered is what are the most critical aspects of the immunosuppressive microenvironment, established in part by tumor cells, that quell T, CAR-T, and other immune cell function? Other open questions that will be interesting to examine is the observation that CAR-T cells are most effective at the periphery. as the basis of this phenotype is completely unknown. Similarly, how CAR epitope loss is induced so quickly in our target cells is a highly relevant question with clinical ramifications. The speed with which this phenotype occurs suggests a mechanism in which

target proteins are rapidly endocytosed to remove them from the cell surface. If this is the case, then understanding how this process of antigen loss via endocytosis is regulated, both *in vitro* and *in vivo,* will allow us to subsequently target and potentially prevent this phenotype. Given that our screens also consistently identify genes known to promote resistance to checkpoint inhibitors, discoveries made in CAR-T cells are likely to translate to other therapies aimed at mobilizing a patient's immune system towards their tumors.

Another interesting observation that will be interesting to study in the future comes from our genome-wide *in vitro* screen. Here, 48 hrs after exposure to CAR-T cells, B-ALL cells showed a massive drop in viability not seen in our previous 24hr *in vitro* experiments. This was accompanied by the re-emergence of mCD19 expression on the cell surface. However re-expression of mCD19 was likely an effect driven by the fact that CAR-T cells had been almost completely diluted away after two days of splitting. Strikingly, the viability of cells treated with anti-mCD19 CARs at any dose remained low (as compared to B-ALL cells treated with control or no CARs) throughout the duration of the experiment, despite complete elimination of CAR-T cells from culture early on. What factors tumor cells give up on their way to becoming resistant to this treatment modality, and how those changes lead to a long-term fitness cost is a critical question that we are eager to examine. Additionally, whether this phenotype is also seen after *in vivo* treatment with CAR-T cells is currently an open question.

One limitation of our screen is the fact that we only used CD8+ T cells. Extensive literature is now showing that CD4+ CAR-T cells, given at a set ratio with CD8+ CAR-T cells is ultimately a more effective approach (Turtle et al., 2016; Golubovskaya & Wu, 2016). For the purposed of our screen, it was important to generate large amount of a uniform product in order to ensure consistency between experiments. However, low throughput follow-up studies will allow us to examine how and if the genes identified in our screen respond to a similar mix of CD4+ and CD8+ CAR-T cells. Here, we are certain that our current screen has missed critical genes that are important for the response to CD4+ CAR-T cells. Future screens completed with a 1:1 ratio of these different types of CAR-T cells, the formulation used clinically, will be critical for continuing to identify genes that control therapeutic outcome of CAR-T therapy.

With the CAR field being as vast and active as it currently is, I suspect that soon, major advancements will lead to more effective products and a better optimization of this "living therapy." One major hurdle that the CAR-T field will have to confront is the identification of tumor-associated (TAA) or tumor specific (TSA) antigens that can then be effectively targeted

without causing excessive or deadly on-target, off-tumor toxicity. One strategy that is already being deployed in the field is the use of CAR-T cells that include “and” or “if” logic gates by relying on the expression, or lack of expression of another protein outside of the CAR targeted antigen (Srivastava et al., 2019). It will be interesting to see how antigen loss phenotypes are altered when the expression of two molecules is required for CAR-T cell killing. While this will likely to represent a safer and less toxic approach, it is also likely that this will lead to less efficacious killing. Other exciting developments, like the generation of CAR-NK and CAR-macrophage cells will continue to expand the potency of this approach by further harnessing the functionality of other cells in the immune system (Wang & Wu, 2020; Wang et al., 2020). Another issue is that expanded access and more broad clinical implementation of these therapies is currently hampered by their significant costs (June et al., 2018). CAR-NK and modified CAR-T cells that limit or eliminate graft versus host disease provide a path towards off-the-shelf products that will significantly drop costs and expand access to this life saving therapy (Depil et al., 2020; Wang et al., 2020). With the safety of CRISPR-edited human CAR-T cells already established by the June group and other immunotherapies showing increasingly potent clinical effects, it is clear that we are at the precipice of a major paradigm shift in the way cancer is treated (Kruger et al., 2019; Stadtmauer et al., 2020). I believe that in all cases, the reciprocal interaction between tumor cells and the immune system cells tasked to eliminate them during immunotherapeutic applications will continue to play a major role in determining patient fate. Thus, understanding both the CAR-T/NK/Macrophage *and* the tumor cell side of this ever-present dialogue will be paramount in ultimately unleashing the full potential of this and other immunotherapies alike.

Final perspective on *in vivo* functional genomics

In the mid-2000s, the focus of the cancer research field became to leverage advances in sequencing technology to expand our understanding of tumor biology. Today, the establishment of collaborative consortia like TCGA has led to large-scale sequencing studies aimed at defining the mutational landscapes of various cancers. Notably, the coordinated execution of this work has already led to significant advances in patient care (Ding et al., 2018). For example, the molecular and genetic profiling of tumors has been clearly shown to be beneficial for clinical decision making, especially as it relates to treatment. Multiple trials have now shown that tailoring therapy based on the molecular profiling of a tumor can result in significantly better progression-free survival (PFS), as compared to PFS of alternate/traditional

treatments (Van Hoff et al., 2010; Hoefflin et al., 2018; Prager et al., 2019). Additionally, as discussed extensively in my introduction, large-scale sequencing studies have led directly to the discovery of many novel driver genes and subsequently, new agents targeting those driver mutations (Sanchez et al., 2018; Golub et al., 2019; Prahallad et al., 2019). However, while these seminal efforts to define the genes that are mutated in various tumor types has led to an intricate draft of the cancer genome and substantial progress, this approach also has major limitations. Recent sequencing studies have shown that fewer than 10% of all patients with advanced cancer have simple actionable mutations and even if they do, many new drugs appear to be limited in their ability to extend the lives of patients (Mulero-Sánchez et al., 2019). For example, one recent report assessed the benefit of new cancer drugs that entered the market between 2009 and 2013, finding that most did not show a clinical advantage in terms of overall survival (OS) or in quality of life measures after 3 years of follow-up (Davis et al., 2017). Further, many of the genes that are critical for tumor biology, including therapeutic response, are rarely amplified, deleted, or mutated (Luo et al., 2009).

The biggest weakness of the cancer genomics approach however, is ultimately its inability to functionally define how the often-complicated admixtures of genetic changes found in malignant cells conspire together to promote the emergence and development of cancer. This is especially true in the context of treatment failure. Hence, one of the biggest challenges currently still facing the cancer research field is the emergence of resistance to therapies used in the clinic (Holohan et al., 2013; Gerhards & Rottenberg, 2018; Fiedler & Hemann, 2019, Prahallad et al., 2019). As I have reviewed in my introduction and throughout my thesis, our understanding of how cancer cells avoid killing by various treatment modalities remains rudimentary. Previous efforts to explore resistance phenotypes have been hampered by the limited techniques available for the functional dissection of genetic factors that govern therapy response. The recent advent of RNAi and CRISPR-based technologies for the precise and systematic manipulation of any and all of the genes in the mammalian genome provides a path forward. Combined with the construction of better murine models of human malignancies, it is clear that cancer research is at the beginning of a promising and revolutionary time of discovery (Dow & Lowe, 2012; Sánchez-Rivera & Jacks, 2015; Zitvogel et al., 2016a; De Ruiter et al., 2018). The challenge will now be to decide how to most efficiently apply these tools for the benefit of cancer patients.

I believe that one of the most powerful applications of this technology and one of the most effective ways to advance care will be to use pooled *in vivo* screens in the context of

clinically relevant therapies. After all, tumor initiation, development, and treatment all occur *in vivo* in human patients and complex *in vivo* interactions clearly play critical roles in cancer (Joyce & Klemm, 2015; Zitvogel et al., 2016a; Fiedler & Hemann, 2019). Therefore, ensuring that the experimental contexts in which we examine the function of novel cancer genes most faithfully recapitulates the patient contexts we ultimately aim to impact, is paramount. Here, identifying novel targets that potentiate the effects of currently used chemotherapies in order to rationally design effective combination regimes is likely to be a promising area of research. Unfortunately, this is also an area that has been understudied in the last few years. Built off of the early promise of BCR-ABL inhibitors in CML, the cancer field has long been searching for the magic bullet or monotherapy that can target a cancer's Achilles heel to revolutionize the way we treat specific tumors (Horne et al., 2013). In the more than 20 years since its discovery however, it is now clear that CML and imatinib are the exception rather than the rule (Dagogo-Jack & Shaw, 2018). Still, as discussed in my introduction, the overwhelming majority of *in vivo* screens that examine resistance phenotypes have been completed using targeted therapies. These studies provide great promise for the development of combinatorial options with these agents and are critically needed, as with our CAR-T screen. However, examples of efforts to complete similar *in vivo* screens in the context of chemotherapy are much more limited. This is despite the fact that in the overwhelming majority of cases, cancer patients will be given some amount of traditional cytotoxic chemotherapy (usually in combinations) during the course of their treatment (Miller et al., 2019). Moreover, as exemplified in AML, older drug combinations are still being adjusted today, yielding significant advances in overall survivorship that are not due to the advent of novel therapies but rather to the optimization of these cytotoxic regimens and the supportive care used during their application (Fernandez et al., 2009; Löwenberg et al., 2011; Othus et al., 2014). Hence, I believe that it is now time for the cancer field to begin to reexamine how we can further potentiate the effects of traditional chemotherapy by specifically identifying genes that when altered, sensitize cells to these agents. This should allow us to design more effective combination regimens. Additionally, I believe that completing such studies *in vivo* will represent the best option for success, as it is now well accepted that a tumor's response to therapy *in vitro* commonly does not correlate with the same cell's response *in vivo*.

To clarify, my argument for *in vivo* screening approaches does not mean that I believe that there is no role for cell lines in synergistic therapy discovery. On the contrary, despite clear evidence that these experimental platforms do not adequately recapitulate complicated

organismal physiology, they have still proven extremely useful in uncovering novel genetic cancer dependencies. Some of these dependencies have ultimately validated *in vivo*, in both mouse models and in clinical trials, and have gone on to impact the way we treat cancer in the clinic. One of the best and most recent examples of this is the finding from an *in vitro* dropout screen that EGFR loss is synthetic lethal with $BRAF^{V600E}$ in colorectal cancer (CRC) (Prahallad et al., 2012). Subsequent clinical trials using a combination approach with EGFR, BRAF, and MEK or PI3K inhibitors showed significant improvement in PFS and OS, leading to FDA breakthrough designation for this triple therapy approach (van Geel et al., 2017; Corcoran et al., 2018; Kopetz et al., 2019). A powerful functional genomics technique that incorporates the use of cell lines is the completion of parallel *in vitro* and *in vivo* screens, as described in chapter 3 of this thesis. When the results from both approaches are overlapped, hits can be sorted as cell-autonomous or *in vivo*-specific, giving researchers a better idea of the types of assays that are best suited for validating candidate genes. Similarly, *in vitro* experimental platforms that are customized to assay isolated aspects of *in vivo* biology, such as secreted factors in conditioned medium experiments or cell-cell contacts in co-culture experiments, can be greatly beneficial towards identifying downstream mechanisms after candidate genes have been identified in animals. Ultimately however, as exemplified by AML chemotherapy and CAR-T therapy *in vitro* screens (reviewed in my introduction), *in vitro* systems are more often than not, insufficient for the initial detection of clinically relevant resistance genes, necessitating the use of *in vivo* approaches for screening.

While *in vivo* screens in mice have traditionally been challenging and time consuming, growing evidence suggests that this is likely to change soon. The increasing precision of mammalian genetic tools represented by CRISPR-based technologies, the mounting literature and expertise in this field, and the lessening costs associated with sequencing will greatly facilitate this approach in the future (Chow & Chen, 2018; Doench et al., 2018; Gerhards & Rottenberg, 2018; O'Loughlin & Gilbert, 2019; Prahallad et al., 2019; Schuster et al., 2019). These advancements are particularly timely, as the TME's role in therapy response becomes increasingly appreciated, both in chemo- and immunotherapy. Importantly, the notion that understanding and manipulating interactions between cancer and the TME can lead to better outcomes has already garnered direct clinical support. Here, this is perhaps best exemplified by the recent success of immune checkpoint blockers (ICB) that target either the interaction between programmed death 1 (PD1) and programmed death ligand 1 (PDL1), or cytotoxic T-lymphocyte-associated protein 4 (CTLA4)—a result that was predicted by the cancer

immunoediting model derived from research in mice more than 100 years ago (Schreiber et al., 2011; Sharma et al., 2015; Zitvogel et al., 2016a; Zou et al., 2016). Similarly, increasing evidence suggests that the long-term clinical effectiveness of traditional chemotherapy, targeted agents, and even radiotherapy can sometimes depend on the ability of the immune system to keep malignant cell growth at bay (Galluzzi et al., 2012; Galluzzi et al., 2015; Kroemer et al., 2015; Zitvogel et al., 2016b). Thus, even treatments that were once thought to target only cancer cells may actually induce therapeutically beneficial anticancer reactions from the TME.

Gaining a better understanding of how to manipulate these TME responses is critical and to this end, our lab has specifically examined this question in hematopoietic malignancies. Here, we found that low-dose chemotherapy can prime macrophages to better eliminate leukemic cells upon the subsequent administration of therapeutic antibodies (Pallasch et al., 2014). A subsequent small scale study in double hit lymphoma patients also validated this approach (unpublished results). Outside of the immune system, our lab has also defined a role for protective niches that form after the administration of chemotherapy (Gilbert & Hemann, 2011). In this thesis, I further describe our results from an *in vivo* screen where I uncovered a promising new chemoresistance gene in AML that functions cell autonomously but appears to only mediate its effects in the appropriate *in vivo* setting. Thus, mounting clinical and preclinical evidence continues to demonstrate that the dialogue between a tumor cell and the TME can determine therapeutic outcome and ultimately, patient fate. Unsurprisingly, this appears to be an especially salient concept when the therapy given to patients is itself composed of living cells, as with CAR-T therapy (Tang et al., 2016; Scarfò & Maus, 2017; Martinez & Moon, 2019). Therefore, we have also focused on elucidating genes that when lost, impact tumor response to $CD8^+$ CAR-T cells both *in vivo* and *in vitro* (Chapter 3). In this burgeoning oncoimmunology subfield, where the functionality of either $CD4^+$ or $CD8^+$ CAR-T cells cannot be adequately assessed with current *in vitro* assays (reviewed in my introduction), I expect that the greatest advances will come from the use of immunocompetent mouse models. Only in these contexts will we be more fully able to understand the ramifications of the substantial crosstalk that both cancer and CAR-T cells have with the TME. Here, future completion and validation of our screens will produce a critically needed data set that can then guide the rational addition of specific adjuvant therapies to potentiate the effects of this promising but expensive “living therapy.” Only once we clearly understand the key factors that dictate therapeutic response in this and other promising new treatment modalities can we truly expect to substantially improve

them. Enhancements that get us closer and closer to the true curative potential of CAR-T cells will improve the cost-benefit analysis of this immunotherapy, making it feasible to expand its use more broadly and critically, to solid tumors.

Lastly, as I've discussed in my introduction, I believe it is likely that many of the resistance phenotypes that emerge after treatment failure involve the cooperation of multiple genes or changes that are not readily detectable by simple sequencing approaches. Here, multiplexed CRISPR screening, potentially combined with single cell RNA-sequencing to yield deeper phenotypes beyond simple proliferation, will be invaluable for dissecting the molecular circuits that govern therapy failure (Dixit et al., 2016; Adamson et al., 2016). These multiplexed approaches will also prove invaluable in comprehensively mapping of genetic interactions in mammalian cells as they are exposed to therapy, a technique that was first pioneered in yeast and has subsequently been applied in human cells (Tong et al., 2001; Tong et al., 2004; Schuldiner et al., 2005; Bassik et al., 2013; Horlbeck et al., 2018). Clinically, the power of this pairwise approach is highlighted by the success of PARP1 inhibitors in germline mutated *BRCA* cancers (Lord & Ashworth, 2017). The promise of using functional genomics approaches to identify synthetic lethal interactions such as this (gene-gene or chemical-genetic) is especially significant. Here, synthetic lethal pairs represent a therapeutic opportunity to drug otherwise challenging targets (i.e. tumor suppressors) via alternate druggable proteins that are made specifically vulnerable by virtue of the unique genetic network of a cancer cell. Similarly, advanced epigenetic editing platforms and RNA editing (i.e. splicing) Cas enzymes can help elucidate the non-mutational changes that are already suspected to drive tumor progression and that likely also contribute resistance phenotypes (Cox et al., 2017; Konermann et al., 2018).

Given the mounting evidence highlighted here and throughout my thesis, I believe it is now obligatory to move past the cell-autonomous focus of characterizing malignant cells in isolation and instead focus on understanding how cancer cells behave when they are embedded in anatomically relevant locations. This underlies the rationale for the approach we take in the Hemann lab and the one we have taken in the studies presented here. Ultimately, we believe that continued investigations to uncover novel roles for the TME in therapeutic response will yield better treatment paradigms for patients, and to this end, pooled *in vivo* screens completed in the context of therapy is the approach we fundamentally favor.

References

Adamson, B. *et al.* A Multiplexed Single-Cell CRISPR Screening Platform Enables Systematic Dissection of the Unfolded Protein Response. *Cell* **167**, 1867-1882.e21 (2016).

Bassik, M. C. *et al.* A systematic mammalian genetic interaction map reveals pathways underlying ricin susceptibility. *Cell* **152**, 909–922 (2013).

Baumann, T. *et al.* CD49d (ITGA4) expression is a predictor of time to first treatment in patients with chronic lymphocytic leukaemia and mutated IGHV status. *Br. J. Haematol.* **172**, 48–55 (2016).

Behrmann, L., Wellbrock, J. & Fiedler, W. Acute myeloid leukemia and the bone marrow niche - Take a closer look. *Front. Oncol.* **8**, 1–13 (2018).

Berg, Jeremy, M., Tymoczko, J. L., Gatto, G. J. & Stryer, L. *Biochemistry 8th Edition*. *Biochemistry* (2015).

Chow, R. D. & Chen, S. Cancer CRISPR Screens In Vivo. *Trends in Cancer* **4**, 349–358 (2018).

Corcoran, R. B. *et al.* Research article combined BRAF, EGFR, and MEK inhibition in patients with BRAF V600E -mutant colorectal cancer. *Cancer Discov.* **8**, 428–443 (2018).

Courchesne, E., Müller, R. A. & Saitoh, O. Brain weight in autism: Normal in the majority of cases, megalencephalic in rare cases. *Neurology* **52**, 1057–1059 (1999).

Cox, D. B. T. *et al.* RNA editing with CRISPR-Cas13. *Science* **358**, 1019–1027 (2017).

Dagogo-Jack, I. & Shaw, A. T. Tumour heterogeneity and resistance to cancer therapies. *Nat. Rev. Clin. Oncol.* **15**, 81–94 (2018).

Davidson, S. M. *et al.* Environment impacts the metabolic dependencies of ras-driven non-small cell lung cancer. *Cell Metab.* **23**, 517–528 (2016).

Davis, C. *et al.* Availability of evidence of benefits on overall survival and quality of life of cancer drugs approved by European Medicines Agency: Retrospective cohort study of drug approvals 2009-13. *BMJ* **359**, (2017).

De Ruiter, J. R., Wessels, L. F. A. & Jonkers, J. Mouse models in the era of large human tumour sequencing studies. *Open Biol.* **8**, (2018).

Depil, S., Duchateau, P., Grupp, S. A., Mufti, G. & Poirot, L. 'Off-the-shelf' allogeneic CAR T cells: development and challenges. *Nat. Rev. Drug Discov.* **19**, 185–199 (2020).

DeVita, V. T. & Chu, E. A history of cancer chemotherapy. *Cancer Res.* **68**, 8643–8653 (2008).

DiNardo, C. D. *et al.* Safety and preliminary efficacy of venetoclax with decitabine or azacitidine in elderly patients with previously untreated acute myeloid leukaemia: a non-randomised, open-label, phase 1b study. *Lancet Oncol.* **19**, 216–228 (2018).

Ding, L. *et al.* Perspective on Oncogenic Processes at the End of the Beginning of Cancer Genomics. *Cell* **173**, 305-320.e10 (2018).

Dixit, A. *et al.* Perturb-Seq: Dissecting Molecular Circuits with Scalable Single-Cell RNA Profiling of Pooled Genetic Screens. *Cell* **167**, 1853-1866.e17 (2016).

Doench, J. G. Am i ready for CRISPR? A user's guide to genetic screens. *Nat. Rev. Genet.* **19**, 67–80 (2018).

Döhner, H., Weisdorf, D. J. & Bloomfield, C. D. Acute myeloid leukemia. *N. Engl. J. Med.* **373**, 1136–1152 (2015).

Dow, L. E. & Lowe, S. W. Life in the fast lane: Mammalian disease models in the genomics era. *Cell* (2012). doi:10.1016/j.cell.2012.02.023

Emadi, A. Exploiting AML vulnerability: Glutamine dependency. *Blood* **126**, 1269–1270 (2015).

Fernandez, H. F. *et al.* Anthracycline Dose Intensification in Acute Myeloid Leukemia. *N. Engl. J. Med.* **361**, 1249–1259 (2009).

Fiedler, E. C. & Hemann, M. T. Aiding and Abetting: How the Tumor Microenvironment Protects Cancer from Chemotherapy. *Annu. Rev. Cancer Biol.* **3**, 409–428 (2019).

Filshie, R., Gottlieb, D. & Bradstock, K. VLA-4 is involved in the engraftment of the human pre-B acute lymphoblastic leukaemia cell line NALM-6 in SCID mice. *Br. J. Haematol.* **102**, 1292–1300 (1998).

Fiorito, V., Chiabrando, D., Petrillo, S., Bertino, F. & Tolosano, E. The Multifaceted Role of Heme in Cancer. *Front. Oncol.* **9**, 1–15 (2020).

Folmes, C. D. L. & Terzic, A. Energy metabolism in the acquisition and maintenance of stemness. *Semin. Cell Dev. Biol.* **52**, 68–75 (2016).
Fukuda, Y. *et al.* Upregulated heme biosynthesis, an exploitable vulnerability in MYCN-driven leukemogenesis. *JCI insight* **2**, 1–12 (2017).
Galluzzi, L., Buqué, A., Kepp, O., Zitvogel, L. & Kroemer, G. Immunological Effects of Conventional Chemotherapy and Targeted Anticancer Agents. *Cancer Cell* **28**, 690–714 (2015).
Galluzzi, L., Senovilla, L., Zitvogel, L. & Kroemer, G. The secret ally: Immunostimulation by anticancer drugs. *Nat. Rev. Drug Discov.* **11**, 215–233 (2012).
Gerhards, N. M. & Rottenberg, S. New tools for old drugs: Functional genetic screens to optimize current chemotherapy. *Drug Resist. Updat.* **36**, 30–46 (2018).
Golub, D. *et al.* Mutant Isocitrate Dehydrogenase Inhibitors as Targeted Cancer Therapeutics. *Front. Oncol.* **9**, (2019).
Golubovskaya, V. & Wu, L. Different subsets of T cells, memory, effector functions, and CAR-T immunotherapy. *Cancers (Basel).* **8**, (2016).
Hagner, N. & Joerger, M. Cancer Management and Research Dovepress Cancer chemotherapy: targeting folic acid synthesis. *Cancer Manag. Res.* 2–293 (2010). doi:10.2147/CMR.S10043
Hamidi, H. & Ivaska, J. Every step of the way: integrins in cancer progression and metastasis. *Nat. Rev. Cancer* 1–16 (2018). doi:10.1038/s41568-018-0038-z
Hanahan, D. & Weinberg, R. A. Hallmarks of cancer: The next generation. *Cell* **144**, 646–674 (2011).
Hensley, C. T. *et al.* Metabolic Heterogeneity in Human Lung Tumors. *Cell* **164**, 681–694 (2016).
Hoefflin, R. *et al.* Personalized Clinical Decision Making Through Implementation of a Molecular Tumor Board: A German Single-Center Experience. *JCO Precis. Oncol.* 1–16 (2018). doi:10.1200/PO.18.00105
Holohan, C., Van Schaeybroeck, S., Longley, D. B. & Johnston, P. G. Cancer drug resistance: an evolving paradigm. *Nat. Rev. Cancer* **13**, 714–726 (2013).
Horlbeck, M. A. *et al.* Mapping the Genetic Landscape of Human Cells. *Cell* **174**, 953-967.e22 (2018).
Horne, S. D. *et al.* Why imatinib remains an exception of cancer research. *J. Cell. Physiol.* **228**, 665–670 (2013).
Jacque, N. *et al.* Targeting glutaminolysis has antileukemic activity in acute myeloid leukemia and synergizes with BCL-2 inhibition. *Blood* **126**, 1346–1356 (2015).
Jesinkey, S. R. *et al.* Mitochondrial GTP Links Nutrient Sensing to β Cell Health, Mitochondrial Morphology, and Insulin Secretion Independent of OxPhos. *Cell Rep.* **28**, 759-772.e10 (2019).
Jones, C. L. *et al.* Inhibition of Fatty Acid Metabolism Re-Sensitizes Resistant Leukemia Stem Cells to Venetoclax with Azacitidine. *Blood* **134**, 1272–1272 (2019).
Jones, C. L. *et al.* Inhibition of Amino Acid Metabolism Selectively Targets Human Leukemia Stem Cells. *Cancer Cell* **34**, 724-740.e4 (2018).
June, C. H., O'Connor, R. S., Kawalekar, O. U., Ghassemi, S. & Milone, M. C. CAR T cell immunotherapy for human cancer. *Science* **359**, 1361–1365 (2018).
Kacso, G. *et al.* Two transgenic mouse models for beta subunit components of succinate-CoA ligase yielding pleiotropic metabolic alterations. *Biochem. J.* **473**, 3463–3485 (2016).
Kersten, K., Visser, K. E., Miltenburg, M. H. & Jonkers, J. Genetically engineered mouse models in oncology research and cancer medicine. *EMBO Mol. Med.* (2017). doi:10.15252/emmm.201606857
Kibbey, R. G. *et al.* Mitochondrial GTP Regulates Glucose-Stimulated Insulin Secretion. *Cell Metab.* **5**, 253–264 (2007).
Klemm, F. & Joyce, J. A. Microenvironmental regulation of therapeutic response in cancer. *Trends Cell Biol.* **25**, 198–213 (2015).
Klichinsky, M. *et al.* Human chimeric antigen receptor macrophages for cancer immunotherapy. *Nat. Biotechnol.* (2020). doi:10.1038/s41587-020-0462-y
Kohli, S., Bhardwaj, A., Kumari, R. & Das, S. SIRT6 is a target of regulation by UBE3A that contributes to liver tumorigenesis in an ANXA2-dependent manner. *Cancer Res.* **78**, 645–658 (2018).
Konermann, S. *et al.* Transcriptome Engineering with RNA-Targeting Type VI-D CRISPR Effectors. *Cell* **173**, 665-676.e14 (2018).
Kopetz, S. *et al.* Encorafenib, binimetinib, and cetuximab in BRAF V600E–mutated colorectal cancer. *N. Engl. J. Med.* **381**, 1632–1643 (2019).

Kroemer, G., Senovilla, L., Galluzzi, L., André, F. & Zitvogel, L. Natural and therapy-induced immunosurveillance in breast cancer. *Nat. Med.* **21**, 1128–1138 (2015).
Kruger, S. *et al.* Advances in cancer immunotherapy 2019 - Latest trends. *J. Exp. Clin. Cancer Res.* **38**, 1–11 (2019).
Lee, E. & Lee, D. H. Emerging roles of protein disulfide isomerase in cancer. *BMB Rep.* **50**, 401–410 (2017).
Li, R. *et al.* Roles of Arf6 in cancer cell invasion, metastasis and proliferation. *Life Sciences* (2017). doi:10.1016/j.lfs.2017.06.008
Lin, K. H. *et al.* Systematic Dissection of the Metabolic-Apoptotic Interface in AML Reveals Heme Biosynthesis to Be a Regulator of Drug Sensitivity. *Cell Metab.* **29**, 1217-1231.e7 (2019).
Longley, D. B., Harkin, D. P. & Johnston, P. G. 5-Fluorouracil: Mechanisms of action and clinical strategies. *Nat. Rev. Cancer* **3**, 330–338 (2003).
Lord, C. J. & Ashworth, A. PARP inhibitors: Synthetic lethality in the clinic. *Science* **355**, 1152–1158 (2017).
Louria-Hayon, I. *et al.* E6AP promotes the degradation of the PML tumor suppressor. *Cell Death Differ.* **16**, 1156–1166 (2009).
Löwenberg, B. *et al.* Cytarabine Dose for Acute Myeloid Leukemia. *N. Engl. J. Med.* **364**, 1027–1036 (2011).
Lu, W. *et al.* Metabolite Measurement: Pitfalls to Avoid and Practices to Follow. *Annu. Rev. Biochem.* **86**, 277–304 (2017).
Luo, J., Solimini, N. L. & Elledge, S. J. Principles of Cancer Therapy: Oncogene and Non-oncogene Addiction. *Cell* **136**, 823–837 (2009).
Martinez, M. & Moon, E. K. CAR T cells for solid tumors: New strategies for finding, infiltrating, and surviving in the tumor microenvironment. *Front. Immunol.* **10**, 1–21 (2019).
Matsunaga, T. *et al.* Interaction between leukemic-cell VLA-4 and stromal fibronectin is a decisive factor for minimal residual disease of acute myelogenous leukemia. *Nat. Med.* **9**, 1158–1165 (2003).
Metallo, C. M. *et al.* Reductive glutamine metabolism by IDH1 mediates lipogenesis under hypoxia. *Nature* **481**, 380–384 (2012).
Miller, K. D. *et al.* Cancer treatment and survivorship statistics, 2019. *CA. Cancer J. Clin.* **69**, 363–385 (2019).
Miraki-Moud, F. *et al.* Arginine deprivation using pegylated arginine deiminase has activity against primary acute myeloid leukemia cells in vivo. *Blood* **125**, 4060–4068 (2015).
Mulero-Sánchez, A., Pogacar, Z. & Vecchione, L. Importance of genetic screens in precision oncology. *ESMO Open* **4**, 1–10 (2019).
Mullen, A. R. *et al.* Oxidation of alpha-ketoglutarate is required for reductive carboxylation in cancer cells with mitochondrial defects. *Cell Rep.* **7**, 1679–1690 (2014).
Mullen, A. R. *et al.* Reductive carboxylation supports growth in tumour cells with defective mitochondria. *Nature* **481**, 385–388 (2012).
O'Loughlin, T. A. & Gilbert, L. A. Functional Genomics for Cancer Research: Applications In Vivo and In Vitro. *Annu. Rev. Cancer Biol.* **3**, 345–363 (2019).
Othus, M. *et al.* Declining rates of treatment-related mortality in patients with newly diagnosed AML given 'intense' induction regimens: a report from SWOG and MD Anderson. *Leukemia* **28**, 289–292 (2014).
Owen, O. E., Kalhan, S. C. & Hanson, R. W. The key role of anaplerosis and cataplerosis for citric acid cycle function. *J. Biol. Chem.* **277**, 30409–30412 (2002).
Pallasch, C. P. *et al.* Sensitizing protective tumor microenvironments to antibody-mediated therapy. *Cell* **156**, 590–602 (2014).
Poitout, V. *et al.* Glucolipotoxicity of the pancreatic beta cell. *Biochim. Biophys. Acta - Mol. Cell Biol. Lipids* **1801**, 289–298 (2010).
Pollyea, D. A. *et al.* Venetoclax with azacitidine disrupts energy metabolism and targets leukemia stem cells in patients with acute myeloid leukemia. *Nat. Med.* **24**, 1859–1866 (2018).
Poulos, M. G. *et al.* Activation of the vascular niche supports leukemic progression and resistance to chemotherapy. *Exp. Hematol.* **42**, 976-986.e3 (2014).

Prager, G. W. *et al.* Results of the extended analysis for cancer treatment (EXACT) trial: A prospective translational study evaluating individualized treatment regimens in oncology. *Oncotarget* **10**, 942–952 (2019).
Prahallad, A., Jensen, M. R. & Chapeau, E. A. Deciphering mechanisms of response and resistance in large-scale mouse cancer screens. *Curr. Opin. Genet. Dev.* **54**, 48–54 (2019).
Prahallad, A. *et al.* Unresponsiveness of colon cancer to BRAF(V600E) inhibition through feedback activation of EGFR. *Nature* **483**, 100–104 (2012).
Sánchez-Rivera, F. J. & Jacks, T. Applications of the CRISPR-Cas9 system in cancer biology. *Nat. Rev. Cancer* **15**, 387–395 (2015).
Sanchez, J. N., Wang, T. & Cohen, M. S. BRAF and MEK Inhibitors: Use and Resistance in BRAF-Mutated Cancers. *Drugs* **78**, 549–566 (2018).
Scarfò, I. & Maus, M. V. Current approaches to increase CAR T cell potency in solid tumors: Targeting the tumor microenvironment. *J. Immunother. Cancer* **5**, 1–8 (2017).
Schreiber, R. D., Old, L. J. & Smyth, M. J. Cancer immunoediting: Integrating immunity's roles in cancer suppression and promotion. *Science (80-.).* **331**, 1565–1570 (2011).
Schuldiner, M. *et al.* Exploration of the function and organization of the yeast early secretory pathway through an epistatic miniarray profile. *Cell* **123**, 507–519 (2005).
Schuster, A. *et al.* RNAi/CRISPR Screens: from a Pool to a Valid Hit. *Trends Biotechnol.* **37**, 38–55 (2019).
Sharma, P. & Allison, J. P. Immune checkpoint targeting in cancer therapy: Toward combination strategies with curative potential. *Cell* **161**, 205–214 (2015).
Siegel, R. L., Miller, K. D. & Jemal, A. Cancer statistics, 2020. *CA. Cancer J. Clin.* **70**, 7–30 (2020).
Simsek, T. *et al.* The distinct metabolic profile of hematopoietic stem cells reflects their location in a hypoxic niche. *Cell Stem Cell* **7**, 380–390 (2010).
Srivastava, S. *et al.* Logic-Gated ROR1 Chimeric Antigen Receptor Expression Rescues T Cell-Mediated Toxicity to Normal Tissues and Enables Selective Tumor Targeting. *Cancer Cell* **35**, 489-503.e8 (2019).
Stadtmauer, E. A. *et al.* CRISPR-engineered T cells in patients with refractory cancer. *Science* **367**, (2020).
Stuani, L., Sabatier, M. & Sarry, J. E. Exploiting metabolic vulnerabilities for personalized therapy in acute myeloid leukemia. *BMC Biol.* **17**, 57 (2019).
Tabe, Y., Konopleva, M. & Andreeff, M. Fatty Acid Metabolism, Bone Marrow Adipocytes, and AML. *Front. Oncol.* **10**, 1–7 (2020).
Takubo, K. *et al.* Regulation of glycolysis by Pdk functions as a metabolic checkpoint for cell cycle quiescence in hematopoietic stem cells. *Cell Stem Cell* **12**, 49–61 (2013).
Tang, H., Qiao, J. & Fu, Y. X. Immunotherapy and tumor microenvironment. *Cancer Lett.* **370**, 85–90 (2016).
Tateishi, K. *et al.* Extreme Vulnerability of IDH1 Mutant Cancers to NAD+ Depletion. *Cancer Cell* **28**, 773–784 (2015).
Tong, A. H. Y. *et al.* Systematic Genetic Analysis with Ordered Arrays of Yeast Deletion Mutants. *Science* **294**, 2364–2368 (2001).
Tong, A. H. Y. *et al.* Global Mapping of the Yeast Genetic Interaction Network. *Science* **303**, 808–813 (2004).
Tsai, H. J. *et al.* A Phase II Study of Arginine Deiminase (ADI-PEG20) in Relapsed/Refractory or Poor-Risk Acute Myeloid Leukemia Patients. *Sci. Rep.* **7**, 1–10 (2017).
Tsuchiya, Y., Pham, U. & Gout, I. Methods for measuring CoA and CoA derivatives in biological samples. *Biochem. Soc. Trans.* **42**, 1107–1111 (2014).
Turcan, S. *et al.* Efficient induction of differentiation and growth inhibition in IDH1 mutant glioma cells by the DNMT Inhibitor Decitabine. *Oncotarget* **4**, 1729–1736 (2013).
Turtle, C. J. *et al.* CD19 CAR–T cells of defined CD4+:CD8+ composition in adult B cell ALL patients. *J. Clin. Invest.* **126**, 2123–2138 (2016).
Urbanski, L. M., Leclair, N. & Anczuków, O. Alternative-splicing defects in cancer: Splicing regulators and their downstream targets, guiding the way to novel cancer therapeutics. *Wiley Interdiscip. Rev. RNA* **9**, 1–36 (2018).

Van Geel, R. M. J. M. *et al.* A phase Ib dose-escalation study of encorafenib and cetuximab with or without alpelisib in metastatic BRAF-mutant colorectal cancer. *Cancer Discov.* **7**, 610–619 (2017).
Von Hoff, D. D. *et al.* Pilot study using molecular profiling of patients' tumors to find potential targets and select treatments for their refractory cancers. *J. Clin. Oncol.* **28**, 4877–4883 (2010).
Vozza, A., Blanco, E., Palmieri, L. & Palmieri, F. Identification of the mitochondrial GTP/GDP transporter in Saccharomyces cerevisiae. *J. Biol. Chem.* **279**, 20850–20857 (2004).
Vyas, S., Zaganjor, E. & Haigis, M. C. Mitochondria and Cancer. *Cell* **166**, 555–566 (2016).
Walter, R. B. *et al.* Effect of genetic profiling on prediction of therapeutic resistance and survival in adult acute myeloid leukemia. *Leukemia* **29**, 2104–7 (2015).
Wang, W., Jiang, J. & Wu, C. CAR-NK for tumor immunotherapy: Clinical transformation and future prospects. *Cancer Lett.* **472**, 175–180 (2020).
Wang, Z. & Dong, C. Gluconeogenesis in Cancer: Function and Regulation of PEPCK, FBPase, and G6Pase. *Trends in Cancer* **5**, 30–45 (2019).
Warnke, C. *et al.* Natalizumab and progressive multifocal leukoencephalopathy: What are the causal factors and can it be avoided? *Arch. Neurol.* **67**, 923–930 (2010).
Wise, D. R. *et al.* Hypoxia promotes isocitrate dehydrogenasedependent carboxylation of α-ketoglutarate to citrate to support cell growth and viability. *Proc. Natl. Acad. Sci. U. S. A.* **108**, 19611–19616 (2011).
Wu, K. *et al.* EYA1 Phosphatase Function Is Essential to Drive Breast Cancer Cell Proliferation through Cyclin D1. *Cancer Res.* **73**, 4488–4499 (2013).
Yoo, J. H. *et al.* The small GTPase ARf6 activates PI3K in melanoma to induce a prometastatic state. *Cancer Res.* **79**, 2892–2908 (2019).
Yu, W. M. *et al.* Metabolic regulation by the mitochondrial phosphatase PTPMT1 is required for hematopoietic stem cell differentiation. *Cell Stem Cell* **12**, 62–74 (2013).
Zitvogel, L., Pitt, J. M., Daillère, R., Smyth, M. J. & Kroemer, G. Mouse models in oncoimmunology. *Nat. Rev. Cancer* **16**, 759–773 (2016).
Zitvogel, L., Rusakiewicz, S., Routy, B., Ayyoub, M. & Kroemer, G. Immunological off-target effects of imatinib. *Nat. Rev. Clin. Oncol.* **13**, 431–446 (2016).
Zou, W., Wolchok, J. D. & Chen, L. PD-L1 (B7-H1) and PD-1 pathway blockade for cancer therapy: Mechanisms, response biomarkers, and combinations. *Sci. Transl. Med.* **8**, 328rv4-328rv4 (2016).